Novel Applications of Optical Analytical Techniques

by

Lalitesh Nitin Seetohul

Thesis submitted to the University of Teesside in partial fulfilment of the requirements for the degree of Doctor of Philosophy

University of Teesside

January 2009

AUTHOR’S DECLARATION

This thesis is entirely my own work and has at no time been submitted for another degree.

I certify that this statement is correct.

L. N. Seetohul

Abstract

Novel applications of optical analytical techniques have been demonstrated in three general areas, namely application of broadband cavity enhanced absorption spectroscopy (BBCEAS) to the detection of liquid phase analytes, the use of total luminescence spectroscopy to discriminate between different type of teas and the development of an optical sensor to detect ammonia gas, based on the fluorescence quenching of a dye immobilised in a sol gel matrix.

A simple BBCEAS setup has been developed with a view to perform sensitive visible wavelength measurements on liquid phase solutions. In the present work a simple low-cost experimental setup has been demonstrated for the measurement of the visible spectra of representative liquid-phase analytes in a 2 mm quartz cuvette placed at normal incidence to the cavity mirrors. Measurements on Ho^{3+} and sudan black with a white LED and the $R \geq 0.99$ mirrors covered a broad wavelength range (~250 nm) and represents the largest wavelength range covered to date in a single BBCEAS experiment. The sensitivity of the technique as determined by the best α_{min} value was 5.1 x 10^{-5} cm^{-1} and was obtained using the $R \geq 0.99$ mirrors. The best limit of detection (LOD) for the strong absorber brilliant blue-R, was approximately 620 pM.

The optical setup was then optimised for the application of BBCEAS detection to an HPLC system. A 1 cm pathlength HPLC cell with a nominal volume of 70 μl was used in this study. The cavity was formed by two $R \geq 0.99$ plano-concave mirrors with a bandwidth of ~ 420 – 670 nm. Two analytes rhodamine 6G and rhodamine B were chosen for separation by HPLC, as they were chemically similar species with distinctive visible spectra and would co-elute in an isocratic separation. The lowest value of α_{min} obtained was 1.9 x 10^{-5} cm^{-1}. The most significant advantage of the HPLC-BBCEAS study over previous studies arose from the recording of the absorption spectrum over a range of wavelengths. It was demonstrated that the spectral data collected could be represented as a contour plot which was useful in visualising analytes which nearly co-eluted. The LOD values for the two analytes studied indicated that the

developed HPLC-BBCEAS setup was between 54 and 77 times more sensitive than a commercial HPLC system.

For improved sensitivity and lower detection limits the low cost BBCEAS setup was used with a significantly longer 20 cm pathlength cell where the mirrors were in direct contact with the liquid phase analyte. This also reduced interface losses. The experiments were carried out using both $R \geq 0.99$ and $R \geq 0.999$ mirrors. The lowest α_{min} value obtained in this study was 2.8×10^{-7} cm^{-1} which is the lowest reported value to date for a liquid phase measurement, making this study the most sensitive liquid phase absorption measurement reported. The lowest LOD recorded was 4.6 pM, and was obtained for methylene blue with the $R \geq 0.999$ mirrors.

A novel application of total luminescence spectroscopy to discriminate between different types of teas objectively was also investigated. A pattern recognition technique based on principal component analysis (PCA) was applied to the data collected and resulted in discrimination between both geographically similar and dissimilar teas. This work has shown the potential of fluorescence spectroscopy to distinguish between seven types of teas from Africa, India, Sri Lanka and Japan. Geographically similar black teas from 15 different plantation estates in Sri Lanka were also studied. The visualisation technique allowed the separation of all 11 types of teas when the first two principal components were utilised.

The final part of the thesis describes the development of an optical sensor for the detection of ammonia gas. The operation of the sensor depended on the fluorescence quenching of the dye 9 amino acridine hydrochloride (9 AAH) immobilised in a sol gel matrix. It was also shown that the sensor response was not affected by the presence of acidic gases such as HCl and SO_2. The final version of the sensor made use of dual channel monitoring to improve the sensitivity of the sensor. Measurements using diluted mixtures of ammonia gas in the range 5 -70 ppm showed that the response of the sensor was nonlinear, with the sensitivity increasing at lower concentrations. The measurement of the baseline noise allowed the LOD to be estimated at ~400 ppb.

ACKNOWLEDGEMENTS

I would like to express my gratitude to my first supervisor Dr Meez Islam for all his support, patience and constant encouragement throughout my study at the University of Teesside and also for allowing me to pursue all the ideas I have had along the way.

I am also grateful to my second supervisor Prof. Zulfiqur Ali for offering me the opportunity to be part of his research group, for much precious advice and also for good values and principles he has instilled in me.

I would like to acknowledge my third supervisor Dr Steve Connolly.

Many thanks to Dr Simon Scott and Dr David James as our numerous discussions have given me the most interesting insights into various aspects of research.

Thanks to Dr Simon Bateson for his help in development of the miniaturised ammonia sensor.

Thanks to Dr Liam O'Hare my MSc project supervisor for his support.

Furthermore, I am thankful to all the staff and technicians involved, especially Helen Hodgson and Doug McLellan for their excellent technical assistance and co-operation.

Thanks to my uncle and aunt for their love, affection and continued support.

I am indebted to my brothers, sister, sister in law, niece and last but not the least my parents for all their love, encouragement and also for having always been supportive of my dreams and aspirations. Thank you for being such a wonderful family.

NITIN

TABLE OF CONTENTS

LIST OF FIGURES

LIST OF TABLES

Chapter One

1.0. Novel applications of optical analytical techniques

1.1. Introduction

Spectroscopic techniques have the ability to provide sensitive and accurate determinations of trace and ultratrace species in samples, such as environmental materials, high purity solutions, biological and medical fluids or nuclear and radioactive waste substances [1-4]. This provides the necessary information to design experimental probes for trace analysis and discrimination of complex analytes. In most quantitative application of spectroscopic techniques there is a direct relationship between the analyte concentration and the luminescence intensity.

Spectral data from spectroscopic techniques can also be used for qualitative analysis and allow characterisation of complex mixtures. Often large amounts of data are generated by spectroscopic techniques and hence there is a need for effective data analysis to identify trends and relationships in these data. Statistical chemometric techniques can be used as an indirect way to measure the properties of substances that otherwise would be very difficult to measure directly [5, 6]. Multivariate analysis techniques can be applied for visualisation and pattern recognition. One of the most commonly used visualisation technique is principal component analysis (PCA) [7].

Spectroscopy provides fundamental information about atomic and molecular properties. Much of the current knowledge of the molecular structure and dynamics of matter is based on the study of the interaction of electromagnetic radiation with matter, through processes such as absorption, emission or scattering. Figure 1.1 is a schematic energy diagram that describes some of the electronic transitions possible between the ground and excited state in a molecule (adapted from Wang *et al.* [8]).

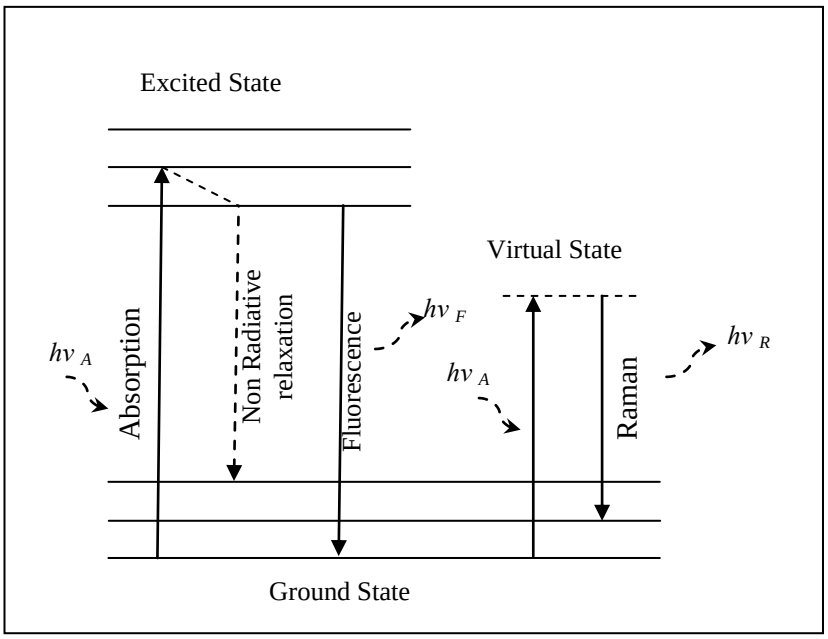

Figure 1.1: Energy diagram showing excitation and possible relaxation mechanisms.

Where hv is photon energy and the subscripts A, F and R denotes Absorption, Fluorescence and Raman scattering respectively.

During absorption spectroscopy the incident photon (hv_A) distorts the electronic distribution of absorbing molecules and results in energy being absorbed from the electric field of the photon. The experimental determination of an absorption spectrum requires the measurement of a small change in the intensity of the incident radiation against a large background and consequently the sensitivity of the technique in its standard form is poor when compared to fluorescence measurements. Although it should be noted that absorption is an absolute technique.

Fluorescence is a comparatively sensitive technique as measurements are made against essentially a zero background and consists of three main stages. The first stage being the excitation (absorption) which occurs on the femtosecond timescale. The second stage is the internal conversion (vibrational relaxation) and the final stage is the loss of excess energy (hv_F) on the time scale of 10^{-11} – 10^{-7} s [1, 9].

Raman spectroscopy is another commonly used spectroscopic technique and relies on scattering of monochromatic light. In Raman scattering the molecule is excited to a virtual state and relaxes to the ground state with emission of a photon (hv_R). Since vibrational information is specific for the chemical bonds in molecules the scattered light provides a fingerprint by which

molecules can be identified. Raman scattering is a powerful technique which provides complimentary information to infrared absorption spectroscopy.

1.2. Thesis outline

The thesis is structured as follows: Chapter two provides an introduction to absorption spectroscopy and its variants, with particular emphasis on cavity based techniques, such as cavity ring down spectroscopy (CRDS) and cavity enhanced absorption spectroscopy (CEAS). Chapter three details a new implementation of broadband cavity enhanced absorption spectroscopy (BBCEAS) to perform sensitive visible wavelength measurements on liquid-phase solutions in a 2 mm cuvette placed at normal incidence to the cavity mirrors. In Chapter four a novel application of BBCEAS to High Performance Liquid Chromatography (HPLC-BBCEAS) is described and the experimental results are compared to previous CRDS based studies. Chapter five describes sensitive liquid phase absorption measurements using the low cost BBCEAS setup from chapter three with a significantly longer 20 cm pathlength cell where the mirrors were in direct contact with the liquid phase analyte. In chapter six a novel application of total luminescence spectroscopy is used to discriminate between several types of teas. Discrimination of the teas is performed by the application of multivariate statistical techniques to the spectral data. Chapter seven details the application of a fluorescence based technique for the detection of ammonia gas. A reversible optical sensor based on the fluorescence quenching of an immobilised fluorophore in a sol gel matrix is discussed. In the final chapter the main results obtained during this Ph.D. project are summarised.

1.3. Publications related to this dissertation

Seetohul,L.N.; Islam, M.; Ali, Z. Broadband Cavity Enhanced Absorption Spectroscopy as a detector for HPLC, Analytical Chemistry, Volume 81, Issue 10, May 2009, Pages 4106-4112

Islam, M., **Seetohul, L.N**., Ali, Z. Liquid-phase broadband cavity-enhanced absorption spectroscopy measurements in a 2 mm cuvette, Applied Spectroscopy, Volume 61, Issue 6, June 2007, Pages 649-658

Seetohul, L.N., Islam, M., O'Hare, W.T., Ali, Z. Discrimination of teas based on total luminescence spectroscopy and pattern recognition, Journal of the Science of Food and Agriculture, Volume 86, Issue 13, October 2006, Pages 2092-2098

1.4. Other Publications

Andrew P. Henderson., **Lalitesh N. Seetohul**., Andrew K. Dean., Paul Russell., Stela Pruneanu and Zulfiqur Ali. A Novel Isotherm, Modeling Self-Assembled Monolayer Adsorption and Structural Changes, Langmuir, Volume 25, Issue 2, January 2009, Pages 639-1264

Novel Optical Detection in Microfluidic Device, Z. Ali; **L N Seetohul**, V Auger; M Islam; S M Scott. Pub. No: WO/2008/065455. International Application No.: PCT/GB2007/050734

1.5. Presentations

(The name of presenter is underlined)

Liquid phase BBCEAS studies in 20 cm cavity M Islam, **L Nitin Seetohul**, and Z Ali, 7th Cavity Ring-Down User Meeting Greifswald, Germany (2007)

Fluorescence quenching of dye doped sol gel by ammonia gas **L N Seetohul**, M Islam and Z Ali, University Innovation Centre for Nanotechnology Showcase Conference, UK (2007)

Broadband liquid phase cavity enhanced absorption spectroscopy Meez Islam, **Nitin Seetohul**, Zulf Ali, Cork and UCC 6th Cavity Ring-Down User Meeting (2006)

1.6. Publications in preparation

Chapter five: Liquid Phase Broadband Cavity Enhanced Absorption Spectroscopy (BBCEAS) studies in a 20 cm cell. (Submitted to Analyst).

Chapter six: Total luminescence spectroscopy and measurement procedures for geographically similar teas.

Chapter seven: An optical ammonia sensor based on fluorescence quenching of a dye immobilised in a sol gel matrix

1.7. References

[1] Schulman, G. S. (Ed.). Molecular Luminescence spectroscopy Methods and applications; John Wiley & Sons, USA, 1985, p. 826.

[2] Hollas, M. J. (Ed.), Modern Spectroscopy; Wiley, UK, 2003, p. 480.

[3] Becker, J. S. TrAC Trends in Analytical Chemistry, 24 (2005) 243.

[4] Jose, S.; Luisa, B.; Daniel, An Introduction to the Optical Spectroscopy of Inorganic Solids; J. John Wiley and Sons, England, 2005, p. 304.

[5] Miller, J.N.; Miller, J.C. An Introduction to the Optical Spectroscopy of Inorganic Solids; Pearson education limited, UK, 2000, p. 271.

[6] Otto, M. An Introduction to the Optical Spectroscopy of Inorganic Solids ;Wiley-VCH, Germany, 1999, p. 314.

[7] Gardiner, W.P. Multivariate Analysis Methods in Chemistry (1997) 293.

[8] Wang, V. L.; Wu, H. Statistical analysis methods for chemists ;Wiley-Interscience, UK, 2007, p. 362.

[9] Lakowicz, J. R. Principles of Fluorescence Spectroscopy Springer, US, 2006, p. 954.

Chapter Two

2.0. Introduction to Cavity Based Absorption Spectroscopy

Spectroscopy provides fundamental information about atomic and molecular properties. A significant fraction of present knowledge on molecular structure and dynamics of matter is based on the study of the interaction of electromagnetic radiation with matter, through processes such as absorption, emission or scattering. One of the most common spectroscopic techniques is optical absorption, which is widely used in chemical and life sciences. Absorption spectroscopy is a simple, non-invasive, in situ technique which provides quantitative information about concentration and also absolute frequency dependent absorption cross section.

2.1. Interaction of light with matter

The nature of light can be described by wave particle duality, that is, an electromagnetic wave or a stream of particles (photons). If it is considered as an oscillating electromagnetic field, physical phenomena such as reflection, refraction and diffraction can be understood. The Planck equation [1] (equation 2.1) can be used to show how if light is considered as a stream of photons, the energy of a single photon can be calculated.

$$\mathrm{E} = h\nu = \frac{hc}{\lambda} \tag{2.1}$$

Where;

E = Amount of energy per photon

h = Planck's constant (6.63×10^{-34} J s)

c = Speed of light (2.998×10^{8} m s^{-1})

λ = Wavelength of light (nm)

ν = Frequency of light (Hz)

When a beam of light is passed through a medium, several effects can result. The simplest possibility would be that the beam emerges in the same direction with the same intensity. This phenomenon is normally described as transmission. Refraction can also occur where the electromagnetic light wave would have setup transient oscillations in the electrons of the molecules of the medium and hence slowing down in transit. It should be noted that during these two phenomena no intensity is lost. Scattering of light is another observable phenomenon, but one in which some intensity is lost as photons are diverted to emerge in a direction different to the incident beam. A further possibility is that light can induce some chemical change in the molecules of the medium; an example would be the photoelectric effect, where when enough energy is provided an electron may be expelled completely from a molecule resulting in a highly reactive free radical [2, 3].

The final possibility is that of absorption of light by molecules. If the wavelength of the incident light is such that the energy per photon precisely matches the energy required for example, to excite an electronic transition, these photons do not emerge; and are absorbed in the medium [4]. Measuring the absorption of electromagnetic radiation as a function of wavelength allows the determination of the different types of energy levels present within atomic or molecular species.

The absorption of UV or visible radiation usually corresponds to the excitation of the outer electrons in atomic or molecular species. There are three types of electronic transition which can typically be considered;

(i) Transitions involving π, σ, and n electrons (mostly exhibited by large organic molecules)

(ii) Transitions involving charge-transfer electrons (mostly exhibited by inorganic species called charged transfer complexes).

(iii) Transitions involving d and f electrons (exhibited by atomic species or compounds containing the transition metals and the lanthanides and actinides).

A simple molecular electronic transition involving a π bonding to π anti-bonding transition ($\pi \rightarrow \pi^*$) is illustrated in figure 2.1.

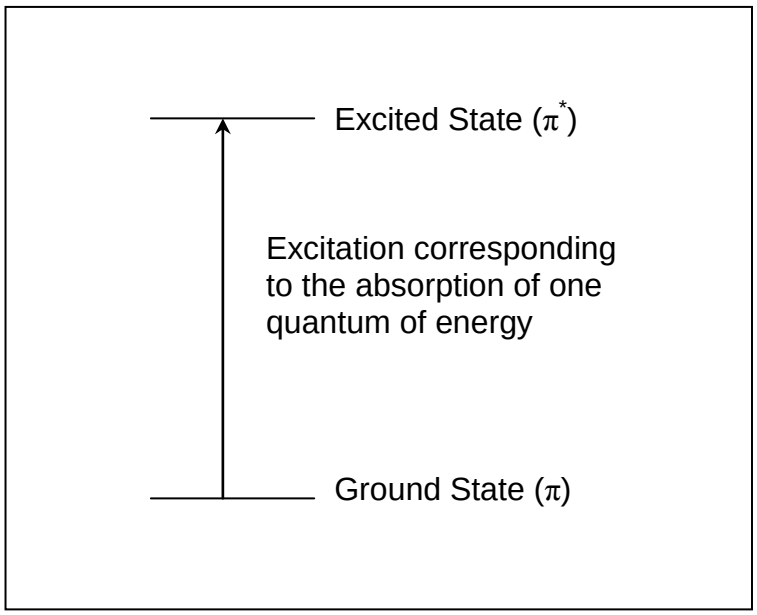

Figure 2.1: Absorption of radiation by a molecule.

Most absorption spectroscopy of organic compounds is based on transitions of *n* (non-bonding) or π electrons to the π^* excited state. This is because the absorption peaks for these transitions fall in an experimentally convenient region of the spectrum (200 - 700 nm). This variation in absorption with wavelength makes the phenomenon of light absorption a valuable tool for qualitative and quantitative analysis of chemical and biological molecules [5].

2.1.1. Absorption spectroscopy

Absorption spectroscopy is considered a universal technique as all species will display an absorption spectrum at some given wavelength in the electromagnetic spectrum. The strength of absorption is found to depend on a number of factors, namely; (i) the pathlength (*l*), (ii) the concentration (*c*) of absorbing molecules and a constant of proportionality which depends on the identity of the species.

Mathematically the phenomenon of absorption can be represented by the Beer-Lambert Law (commonly known as the Beer's Law).

$$absorbance\ (A) = -\log_{10}\left(\frac{I_0}{I}\right) = +(2.3\kappa)c\ell = \varepsilon c\ell \qquad (2.2)$$

Where I = transmitted intensity of light at distance ℓ in cm, and I_0 the respective incident initial value (when ℓ = *0),* κ is the 'decay constant', which is dependent on the type of species present. The composite proportionality constant, 2.3κ can be replaced by the symbol ε (molar absorbtivity at the wavelength and it has dimensions M^{-1} cm^{-1}), which is a property of the absorbing species. c is the molar concentration. From equation 2.2 we can directly observe that absorbance is linearly related to concentration. Hence absorbance is widely used in life sciences to measure concentration of species. In biology and biochemistry the absorbance of a solution when ℓ = 1 cm is commonly coined by the term optical density (OD) of the solution.

2.1.2. Derivation of the Beer-Lambert law

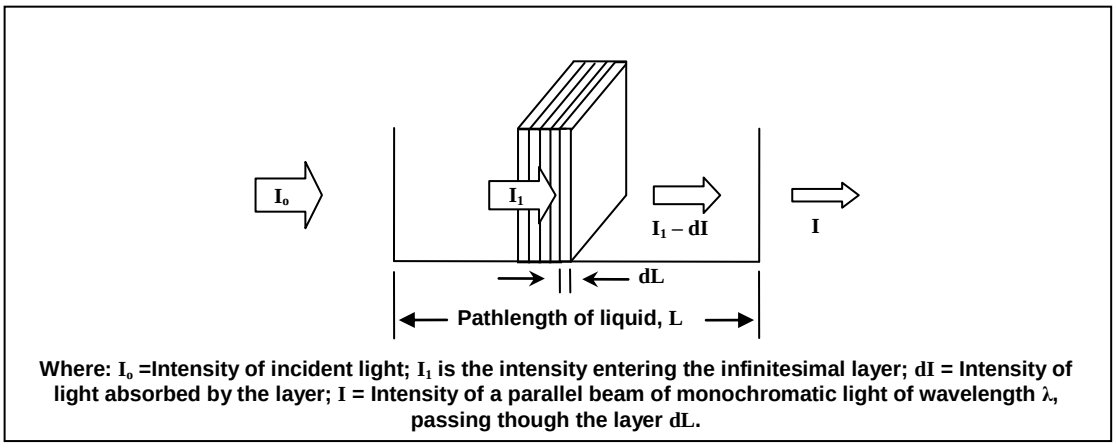

Figure 2.2: Illustration of the Beer-Lambert law

The Beer-Lambert law can be derived from the fractional amount of light absorbed (light transmitted); which is related to the thickness and concentration of a sample. The solution can be regarded as a multilayered arrangement. Each layer is equally populated by light absorbing solute molecules [6].
The change in intensity dI can be expressed as

$$dI = -k_\lambda \; I \; dL \tag{2.3}$$

Where k_λ is the wavelength dependent proportionality constant. As L increases *I* become smaller, hence a negative sign is required.
Rearranging equation 2.3

$$\frac{dI}{I} = -k_\lambda \; dL \tag{2.4}$$

Integrating this equation between limit I to I_o and for L between 0 and L gives:

$$\int_{I_o}^{I} \frac{dI}{I} = -k_\lambda \int_0^L dL$$

$$\ln \frac{I}{I_o} = -k_\lambda L \tag{2.5}$$

Since; 2.303 $\log_{10}(x) = \ln(x)$

Then,

$$\log_{10}\frac{I_o}{I} = \frac{k_\lambda L}{2.303} \tag{2.6}$$

Assuming the concentration C is an independent variable, we can write

$$dI = -k_\lambda\ I\ dC \tag{2.7}$$

Integrating equation 8 between limit I_o to I and for C between 0 and C gives:

$$\int_I^{I_o}\frac{dI}{I} = -k_\lambda\int_0^C dC$$

$$\log_{10}\frac{I_o}{I} = \frac{k'_\lambda C}{2.303} \tag{2.8}$$

The equations 6 and 8 can be combined for both L and C to give;

$$\log_{10}\frac{I_o}{I} = -\frac{k''_\lambda\ LC}{2.303} \tag{2.9}$$

$\log_{10}\frac{I_o}{I}$ is the absorbance (A), $-\frac{k''_\lambda}{2.303}$ is the molar absorbtivity (ε), when the concentration (C) is given in g mol dm^{-3}

The equation can be expressed as,

$$A = \varepsilon CL \tag{2.10}$$

2.2. Common types of instruments used for absorption measurements

Figure 2.3 highlights the basic components of a single beam spectrophotometer. Single beam spectrometers are widely used in routine laboratory measurements over a range of wavelength, most commonly in the UV-visible range.

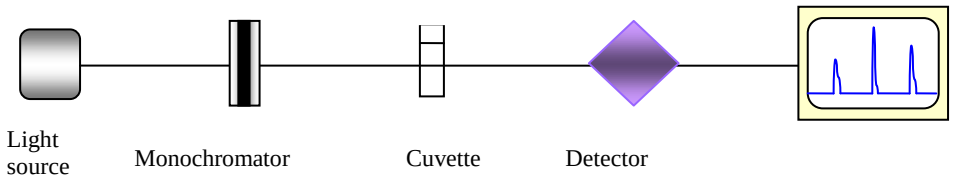

Figure 2.3: Schematic of the basic components of a single beam spectrometer

Light emitted by the light source, typically an incandescent lamp, passes through a monochromator which can be scanned to select a particular wavelength, and then through the sample cuvette and onto the detector (typically a photomultiplier tube or photodiode). The intensity reaching the detector in presence and absence of the sample is used to calculate the absorbance of the sample at a particular wavelength. The monochromator is then scanned through a range of wavelengths to obtain the absorption spectrum of the sample. The sensitivity of the instrument is limited by fluctuations in the intensity of the light source which manifests itself as noise on the absorption spectrum. Additional sources of noise arise from the detector and associated electronic components [4].

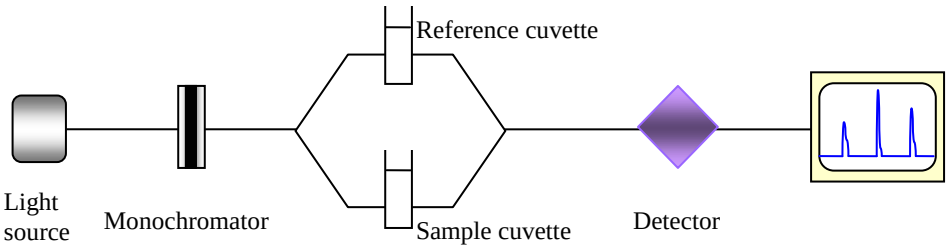

Figure 2.4: Schematic of the basic components in a double beam spectrometer

A convenient way to reduce instrumental noise from fluctuations in the intensity of the light source is to use a double beam spectrometer. Figure 2.4 shows a schematic of a double beam spectrometer (also known as a split beam spectrometer); the monochromated light is split into two, where one beam passes through the sample and the other through the reference cell. The difference in intensity between the reference and sample beam therefore represent the light absorbed by the sample [4]. The double beam configuration offers several advantages over single beam spectrometers. In the double beam configuration, fluctuations in the intensity of the light source are removed from the absorption spectrum. Hence better sensitivity is achieved.

2.2.1. Application of absorption spectroscopy

Direct absorption spectroscopy of atoms and molecules in the gas phase, yields both absolute quantitative concentrations as well as absolute frequency-dependent cross-sections, and is a very powerful tool in analytical and physical chemistry [3, 7]. Sensitive absorption spectroscopy techniques are commonly applied as diagnostic techniques. In a conventional absorption experiment, one measures the amount of light that is transmitted through a sample. A drawback of conventional absorption spectroscopy is that its sensitivity is limited compared to spectroscopic techniques which are based on the detection of phenomena induced by absorption of light, such as pressure changes in photoacoustic spectroscopy , fluorescence in laser induced fluorescence (LIF), or ion production in resonant enhanced multiphoton ionization (REMPI). The main reason is that these techniques are background free, whereas in direct absorption a small attenuation in transmitted light has to be measured on top of

a large background. A disadvantage is that these techniques do not provide an absolute measure of the concentration of a given analyte and must be first calibrated. Often the calibration process is complex and time consuming.

Several methods exist for increasing the sensitivity of absorption spectroscopy. These include frequency and wavelength modulation schemes that have been discussed in several reviews [8-11] and will not be discussed further here, and also by increasing the absorption pathlength though cavity based techniques.

2.3. Cavity based techniques

The biggest advances in improving the sensitivity of absorption measurements have occurred over the last 20 years [9, 12] as a result of the application of cavity based techniques. These have utilised optical cavities formed from two high reflectivity dielectric mirrors ($R > 0.99$) to increase the effective pathlength of measurement and have resulted in two general techniques, namely cavity ring down spectroscopy (CRDS) and cavity enhanced absorption spectroscopy (CEAS). The following sections firstly describe some of the methodology common to both techniques and then a consideration of the important characteristics of each technique in turn.

2.3.1. Cavity Mirrors

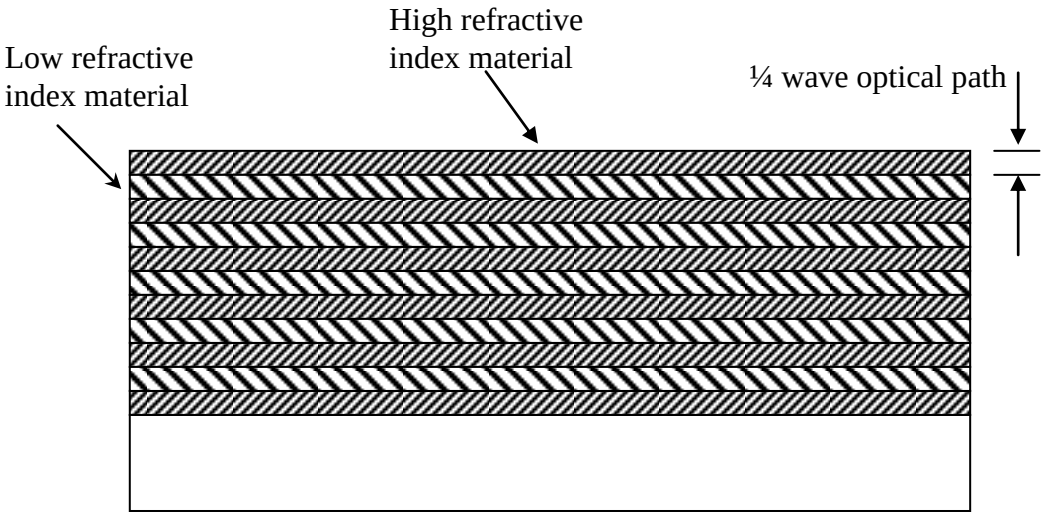

Figure 2.5: Schematic diagram of a dielectric mirror composed of alternating layers of high and low refractive index materials.

Dielectric mirrors are preferred over metallic mirrors for use in cavities as they can be constructed to have much higher reflectivities, also the transmission through dielectric mirrors can be made close to (1-*R*) even for high reflectivities and multiple layer depositions. For metallic mirrors the transmission through the mirrors falls off to zero for deposition thicknesses beyond a few hundred nanometres. Figure 2.5 as expressed by Busch *et al* [8] shows a schematic diagram of the cross-section of a multilayer dielectric mirror. These mirrors are wavelength selective and high reflectivity is obtained over a selected range of wavelengths or frequencies by constructive interference of the waves reflected at each discontinuity in refractive index. Each layer is made a quarter of a wavelength thick and of a suitable material, so as to make all the reflected waves in phase. Hence the dielectric mirrors function on the basis of constructive interference of light reflected from the different layers of the dielectric stack. Typical high reflectance mirrors may have up to forty quarter-wavelength dielectric layers that alternate between a high and low refractive index coatings. Common dielectric materials used to fabricate the layers that make up the reflecting sandwich of these mirrors include silicon dioxide (SiO_2), titanium dioxide (TiO_2), zirconia (ZrO_2) and thorium fluoride (ThF_4) [9]. The multilayer dielectric mirrors have characteristics such as resistance to abrasion

and resistance to chemical attack that makes them ideal for cavity based spectroscopy. State of the art dielectric mirrors can be fabricated to have ultra-high reflectivities of $R \geq 0.99999$ over a narrow range of wavelengths (typically ~50 nm in the visible part of the spectrum) by depositing several hundred dielectric layers [9]. Alternatively, they can be fabricated to have moderately high reflectivity ($R \geq 0.995$) but over a much wider wavelength range e.g. the entire visible spectrum (400 – 700 nm). This is achieved by depositing multiple dielectric stacks with slightly different central wavelength. One practical consequence is that the variation of the reflectivity profile with wavelength is no longer smooth as is the case for single wavelength dielectric stacks and instead contains 'spikes' in the profile where the reflectivity abruptly changes.

2.3.2. Types of optical cavities

Optical cavities can be produced by arranging at least two mirrors facing each other and placed at some distance from each other so that light is reflected back and forth between the mirrors. The three possible optical arrangements that produce linear cavities are shown in figure 2.6.

(a) plano-plano (b) plano-concave (c) plano-concave

Figure 2.6: Configurations of linear optical cavities

Optical cavities can be classified into two categories; stable or unstable according to their losses. A cavity is geometrically stable if a paraxial ray bundle is refocused within the cavity after successive reflection off the mirrors so that the optical energy is trapped within the cavity. On the other hand if the optical energy escapes the cavity after several reflections then it is said to have an unstable geometry. A stable cavity can be achieved when at least one of the cavity mirrors is concave.

2.3.3. Cavity mirrors arrangements

By varying the distance between a pair of concave mirrors different types of cavities can be produced. Figure 2.7 shows some of the configurations that can be achieved.

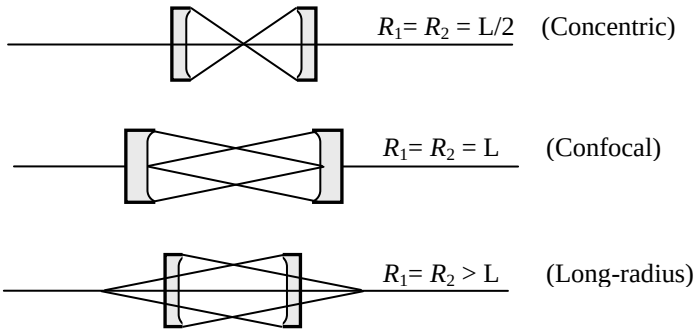

Figure 2.7: Cavity mirror arrangements.

The cavities show different properties in terms of spot size and sensitivity with regard to misalignment. For application in cavity based experiments the preferred configuration is one which shows insensitivity towards misalignment whilst the optimum spot size generally depends on the application. When $R_1 = R_2 = L/2$, the cavity is referred to as a concentric cavity. When $R_1 = R_2 = L$, the focal points of both mirrors coincides halfway between mirror separation and it is referred to as a confocal cavity. A confocal cavity is relatively insensitive to misalignment, but produces a rather small spot size. A long-radius cavity (variation of a Fabry-Perot cavity) is produced when $R_1 = R_2 > L$. This cavity produces a large spot size, but requires careful alignment procedures to achieve a stable cavity. For any given experimental setup, the wavelength range that can be covered depends on the reflectivity characteristics of the mirrors used in the cavity [9, 13].

2.3.4. Mode structures of cavities

Interference occurs between pulse fragments propagating in the same direction inside the cavity for laser pulses whose length exceeds the round-trip length of a cavity. These interference effects can be explained by the Fabry–Perot theory of resonators [14]. The Fabry–Perot resonant cavity is essentially a pair of highly reflective mirrors. When a monochromatic laser source is incident on the cavity such that the distance between the two mirrors is an integer multiple of the laser wavelength, the light experiences constructive interference as it bounces back and forth inside the cavity. Under such conditions, the light intensity builds inside the cavity to an equilibrium value, and a small portion of the signal escapes through each mirror. Therefore the interference pattern formed in a cavity shows resonance enhancement of intensity for the frequencies interfering ‘‘in phase,’’ and quenching of intensity for the frequencies interfering ‘‘out of phase’’ [15] .

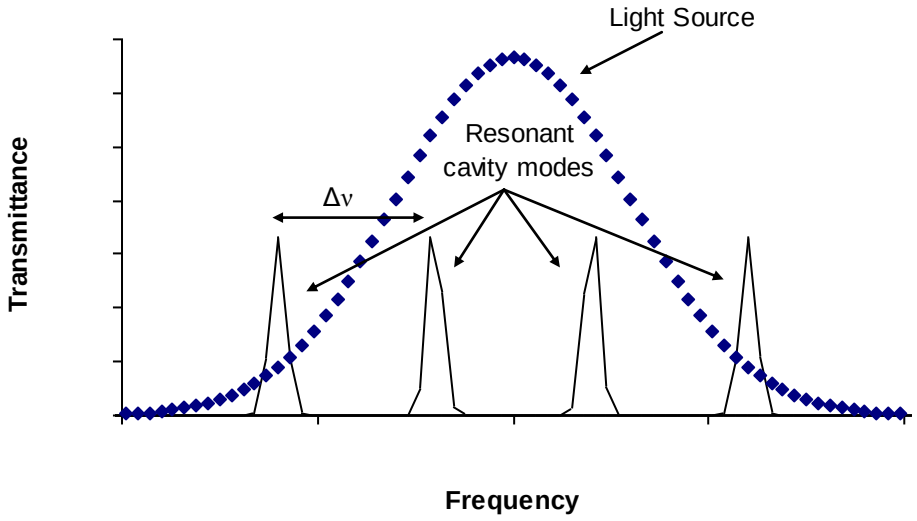

Figure 2.8: Cavity modes structures

The cavity modes are shown in figure 2.8 and the frequency interval between two modes, the free spectral range (FSR), can be expressed as [15]:

$$\Delta \nu = \frac{c}{2\,L} \tag{2.11}$$

Where, c = speed of light, L is the cavity length

It is this interference pattern that is the source of etalon effects that cause variation of the intensity of light transmitted through a cavity as a function of frequency. The optical frequencies for which the intensity of light inside the cavity is resonantly enhanced give rise to the longitudinal modes of the cavity [13, 14, 16]. The gap between resonant frequencies of the Fabry-Perot etalon is the Free Spectral Range (FSR), and it can be described by the following equation [15]

$$FSR = \frac{c}{2nL} \tag{2.12}$$

Where, c – is the speed of light, n – is the refractive index of the medium and L – is the length of the cavity

The mode structure of optical cavities introduces experimental consequences for CRDS and CEAS setups, where the linewidth of the laser source is less or comparable to the FSR of the cavity. For these setups, the transmission of the cavity can be zero unless the laser wavelength is in resonance with the cavity modes and consequently it is common practice to rapidly change the length of the cavity by placing one of the cavity mirrors on a piezoelectric transducer (PZT). This allows the laser wavelength to be partly in resonance with one or more of the cavity modes during the timescale of the experiment. For setups using broadband light sources such as BBCEAS, the mode structure of the cavity is normally not an issue as several thousand cavity modes will typically be accessible by the light source, ensuring substantial transmission through the cavity.

2.3.5. Types of detectors

Despite the large number of detectors available, they can be classified under two major groups namely: thermal and photoelectric (quantum) detectors. The thermal detectors respond to heat energy gained by the absorption of photons. The intensity of the incident light can therefore be determined by monitoring a temperature dependent physical magnitude of the material (i.e. change in electrical resistance). As thermal detectors depends on the total amount of heat energy reaching the detector, their response is independent of wavelength [4, 5]. Since the detector is based on heating a thermocouple, the time response is slow. One advantage of these detectors is the flat response towards incoming radiation. Examples of common thermal detectors used in spectroscopy are thermopiles and pyroelectric detectors [3].

In photoelectric detectors a change in physical magnitude occurs when quanta of light energy interact with electrons in the detector material generating free electrons. Therefore theoretically single photons could be detected. When light of an adequate wavelength reaches a photoelectric detector and is absorbed, the carrier density changes, causing a change in electrical conductivity of the semiconductor. The change in conductivity is proportional to the intensity of incident light. The main limitation of this kind of detector is the noise caused by thermal excitation. If there is a large current generated by the detector in the absence of incident light (dark current/noise), the sensitivity of the photoelectric detector becomes poor. Hence they are sometimes cooled during operation in order to reduce the dark current/noise. Commonly used photoelectric detectors include photoconduction detectors, photodiodes and photomultipliers. Even in the absence of incident light, these detectors generate output signals that are usually randomly distributed in intensity and time and these signals are due to noise. The two main type of noise in photoelectric detectors are dark noise, which has been described above, and shot noise.

Shot noise is the inherent noise in counting a finite number of photons per unit time. Photons reaching the detector are statistically independent and uncorrelated events. Although the mean number of photons arriving per unit

time is constant on average at each measured time interval, the number of detected photons may vary. The major source of shot noise in semiconductors is due to the random variations in the rate at which charge carriers are generated and recombine [5]. Table 2.1 describes basic parameters such as the spectral range and time constant of different types of detectors [17].

Table 2.1: Basic parameters of different detectors.

Detector	Spectral range (nm)	Time constant
Thermopile	100 – 4000	20 ms
Pyroelectric	100 – 4000	10 ns – 100 ps
Photomultiplier	100 – 1500	0.5 – 5 ns
Photodiodes	200 – 4000	10 – 100 ns
Avalanche photodiodes	200 – 1000	10ps – 1 ns
Photoconduction	1000 – 20000	~ µs

The thermal detectors have a large spectral range from ultraviolet to mid-infrared region of the electromagnetic spectrum and the pyroelectric detectors shows faster time constant compared to thermopile detectors. Photoelectric detectors mainly have a working range from the UV region of the electromagnetic spectrum to the mid infrared. The working range of photomultipliers span from the ultraviolet to the near-infrared. The intensity of light involved in cavity enhanced spectroscopy tends to be very low. Under these conditions the noise produced by the detector can be greater than the detected signal. The simplest method to minimise the level of noise is through signal averaging by performing consecutive measurements and then calculating the average signal. If the source of noise is randomly distributed in time, then the signal to noise ratio (S/N) should improve by $\sqrt{n}$ (where n is the number of measurements).

2.4. The development of CRDS

Herbelin *et al.* [18] were the first to propose the use of an optical cavity for measuring the reflectance of mirror coatings. The reflection losses are in a way the absorption of the optical cavity. The reflectance of their mirrors was accurately determined by modulating the intensity of a continuous wave (CW) light beam and measuring the phase shift introduced by the optical cavity. The phase shift was inversely related to the sum of the reflected losses in the cavity. There were major limitations to the precision of their technique due to the noisy character of the transmitted laser intensity.

Anderson *et al.* [19] in 1984 unaware of previous work carried out by Kastler [14] demonstrated that the high reflectance of mirrors could be measured with higher accuracy by suddenly switching off the CW light source when the intracavity field exceeded a certain threshold value and recording the subsequent intensity decay of the light in the optical cavity.

O'Keefe and Deacon [20] in 1988 showed that the problems associated with mode coincidences could be bypassed by using a pulsed laser and achieved sensitivity greater than that attained by using stabilised continuous wave light sources. Furthermore they were the first to propose that a simple experimental design for measuring cavity losses could be achieved as no electronics were needed for monitoring the intracavity power or switching off the laser, before observing the decay transient. They also demonstrated the sensitivity by measuring the Cavity Ring Down (CRD) absorption spectrum of the weak bands of molecular oxygen. They reported the first minimum detectable loss which was 2×10^{-8} cm^{-1} for a cavity of 25 cm with cavity mirrors of $R \geq 0.9999$ [20]. Their study is generally acknowledged as the first experimental demonstration of CRDS.

2.4.1. Experimental implementations of CRDS

CRDS is a sensitive absorption technique in which the rate of absorption rather than the magnitude of the absorption of a light pulse confined in an optical cavity are measured [21]. A schematic of the experimental setup of a conventional CRDS system is shown in figure 8 (a). Typically a tuneable, pulsed laser having pulse duration of ~ 15 ns is used as the light source [10]. The radiation from the laser is introduced into the cavity with the appropriate mode-matching optics required as there is a need to match the field distribution of the incident laser source to that of the recipient cavity mode. CRDS cavities generally consist of two identical plano-concave high reflectivity mirrors ($R \geq 0.999$) with radius of curvature between 25 cm and 1 m separated by a distance such that the cavity is optically stable [10]. The sample is placed inside the high-finesse optical cavity consisting of the two mirrors. The short laser pulse that is coupled into the cavity is reflected back and forth inside the cavity and, every time the light pulse is reflected off one of the mirrors a small fraction of the light leaks out of the cavity. Instead of measuring the total intensity of light exiting the cavity, one determines the decay time by measuring the time dependence of the light leaking out of the cavity. Hence, the rate of absorption can be obtained; the more the sample absorbs, the shorter is the measured decay time [9].

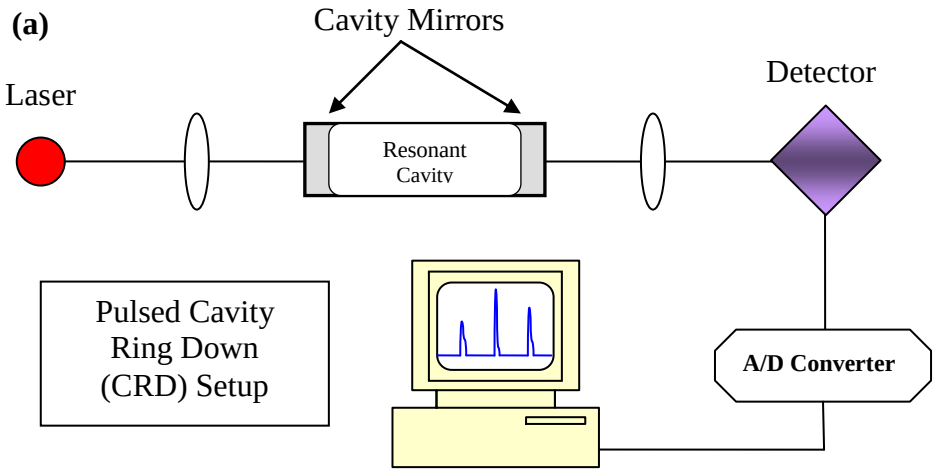

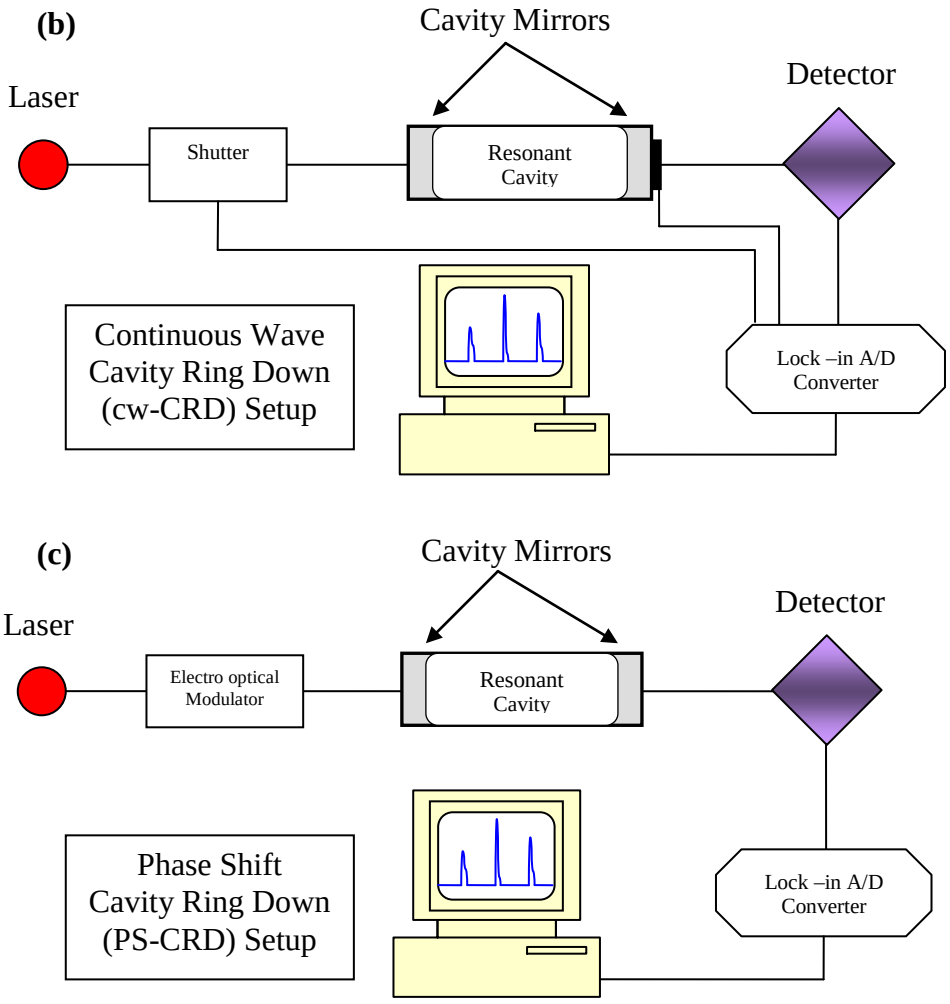

Figure 2.9: Schematic diagram of typical CRDS setups

Figure 2.9 (b) represent a schematic for Continuous Wave Cavity Ring Down Spectroscopy (cw-CRDS). A tuneable continuous Wave (cw) laser which has to be switched off in order to be able to observe the ring down time is used instead of a pulsed laser. When compared to pulsed CRDS, cw-CRDS allows higher data acquisition rates and higher spectral resolution [22].

In phase shift cavity ring down (PS-CRD) spectroscopy as shown in figure 8(c), the output of a cw laser is passed though an electro-optical modulator that sinusoidally modulates the light source. The modulated light is coupled into cavity and the light that leaked out of the cavity is detected and the phase shift of the signal is determined with a fast lock-in amplifier. The sensitivity of this technique is comparable to cw-CRDS and since no fit of the

ring down transient is required, PS-CRDS can easily be performed with analogue detection electronics [8, 11, 18, 20, 23].

2.4.2. Advantages of CRDS

Since the absorption is determined from the time dependent behaviour of the signal, it is independent of pulse to pulse fluctuations of the laser. The effective absorption pathlength, which depends on the reflectivity of the cavity mirrors, can be very long (up to several kilometres), while the sample volume can be kept rather small. The main advantage of CRDS is that the absorption coefficient can be calculated directly from the measured ringdown time constant and thus the concentration of species can be determined absolutely if the absorption cross section is known [10].

2.4.3. Disadvantages of CRDS

Cavity ring down spectroscopy cannot be applied effectively to liquids. The large scattering losses in liquids coupled with short cavity lengths results in a very short ring down time that is difficult to accurately measure. Most liquid cells, especially those used in HPLC and CE, have pathlengths on the order of 1 – 10 mm. Even with high reflectivity mirrors, the ringdown time of these cells is less than 100 nanoseconds, which require highly specialised experimental setups with short pulsewidth (< 1 ns) light sources and fast response detection systems with instrumental response times of less than 1 ns [11, 24]. CRDS is an order of magnitude more expensive than some alternative spectroscopic techniques, due to the experimental complexity, requirement for laser systems, fast detection system and high reflectivity mirrors.

2.5. Basic theoretical aspects of Cavity Ring Down Spectroscopy (CRDS) based on Pulsed Laser Cavity Ring Down Spectroscopy (PL-CRDS)

In a typical CRDS experiment, a light pulse with a spectral intensity distribution $I(\nu)$ and a duration which is shorter than the CRD time τ is coupled into a non-confocal optical cavity consisting of two highly reflecting mirrors. The fraction of the light that is successfully coupled into the cavity bounces back and forth between the mirrors. The intensity of the light inside the cavity decays as a function of time, since at each reflection off a mirror a small fraction of the light is coupled out of the cavity. The time dependence of the intensity inside the cavity is easily monitored by measuring the intensity of the light exiting the cavity. In an empty cavity, this ring down time is a single-exponentially decaying function of time with a $1/e$ CRD time τ which is solely determined by the reflectivity R of the mirrors and the optical pathlength d between the mirrors. The presence of absorbing species in the cavity gives an additional loss channel for the light cavity and will still decay exponentially, resulting in a decrease in the CRD time τ .The intensity of light exiting the cavity is given by [11]

$$I(t) = I_o \exp\left(\frac{\alpha\, d + |\ln R|}{d} c\, t \right) \tag{2.13}$$

Where the reciprocal ring-down time (decay time for non exponential decay) is given by

$$\tau_{CRD}{}^{-1} = \alpha\, c + |\ln R| \frac{c}{d} \tag{2.14}$$

The absorption coefficient α can be represented by

$$\alpha = \frac{1}{c}\left(\tau_{CRD}^{-1}\ (filled\ \ cavity) - \tau_{CRD}^{-1}\ (empty\ cavity) \right) \tag{2.15}$$

2.6. Cavity enhanced absorption spectroscopy

The quantitative measurement of absorbing species using cw-CRDS measurements can be carried out without the performing independent calibration and offers great sensitivity. Nevertheless such performance is not always required from a sensitive absorption technique.[11]. The complexity and cost of cw-CRDS experiments can be high especially in systems where a high speed data acquisition scheme is required. The weak signals leaking out of the cavity is captured by fast response expensive detectors, then amplified and digitised without degradation of the time resolution in order to be able to fit the low noise ring down decays. In order to simplify CRDS, Cavity enhanced absorption spectroscopy (CEAS) was developed to eliminate the constraint of digitalisation of the low noise ring down decays [12]. In CEAS the steady state transmission though the cavity is dependent upon the attenuation of the light trapped within the cavity by an absorbing species [25, 26]. Therefore rather than looking at the cavity ring down time, this technique is based on the detection of the time integrated intensity of the light passing through the cavity and uses the properties of high finesse passive optical resonator to enhance the effective pathlength. The technique associated with this process has been coined with different terminologies either CEAS (Cavity Enhanced Absorption Spectroscopy) [25] or ICOS (Integrated cavity output Spectroscopy) [26]. This technique will henceforth be referred to by the more commonly used abbreviation CEAS. Although standard implementation of CRDS is about 50 times more sensitive than CEAS as showed from comparable studies from Murtz *et al.* [27] and Peeters *et al.* [28] CEAS does show some obvious advantages.

CEAS allows cheaper, simpler experimental setups and alignment procedures. It is much less demanding on the speed associated with the detection system and also has lower requirements for the mechanical stability of the cavity when compared to CRDS. Work has been carried out to make CEAS more sensitive by using phase sensitive detection [30], although this does impact on one of the main advantages of CEAS due to the associated complicated and expensive experimental setup.

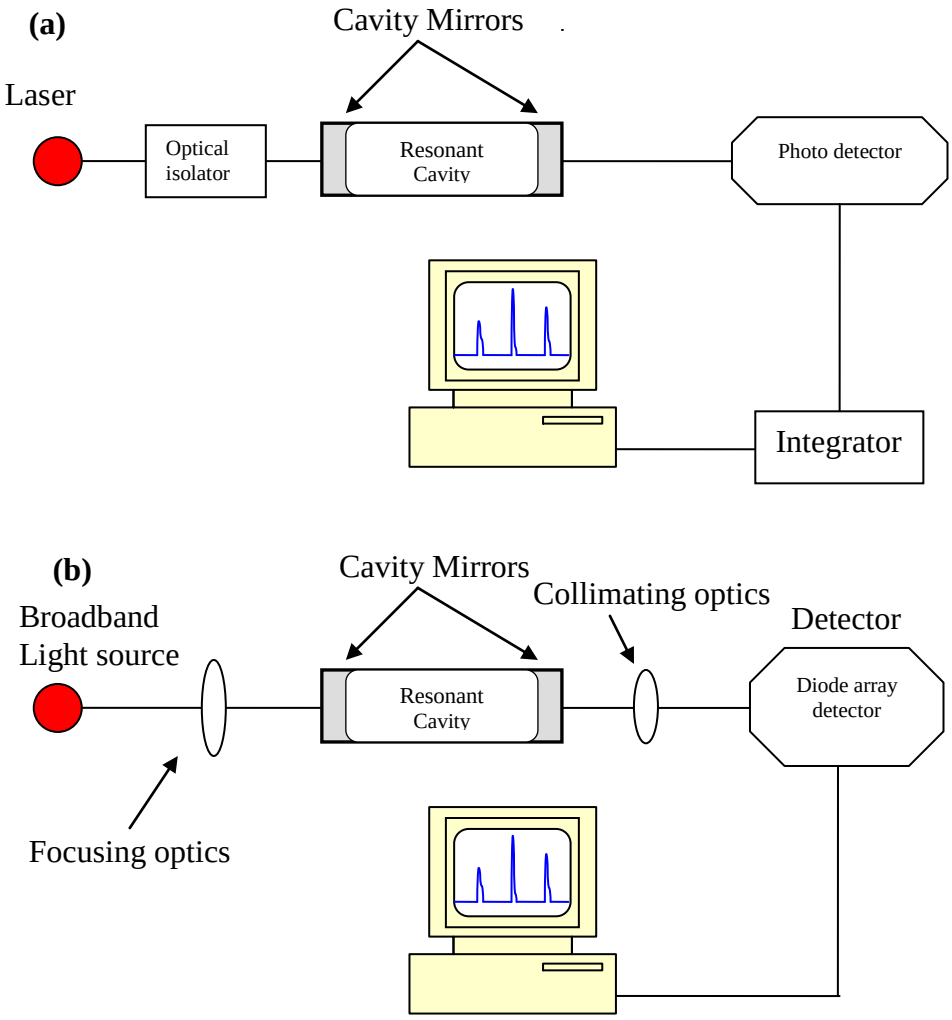

Figure 2.10: Schematic diagram of CEAS experimental setups.

As shown in the schematic in figure 2.10 (a) no modulator, shutter or switch is used in CEAS. The laser light is coupled directly into the cavity and the time integrated intensity of the light leaking out is measured with a detector placed behind the cavity of the end mirror. CEAS spectra can generally be obtained in various ways depending on the scanning speed of the laser [30]. As the rate at which light is coupled into the cavity depends on the mode structures of the cavity. For a laser that can be scanned several times at a high repetitive rate, the signal is recorded as a function of time, which is proportional to the wavelength of the laser. When a laser that can be scanned slowly is used, the cavity modes are reduced using a piezoelectric transducer mounted on one of the mirrors [8]. A further simplification of CEAS can be achieved through Broadband Cavity Enhanced Absorption Spectroscopy (BBCEAS), which is a

technique that allows sensitive measurement of absorptions over a broad wavelength range. Figure 2.9 (b) shows a schematic of a BBCEAS setup and consist of a broadband light source (i.e. Xenon arc lamp or high intensity LED). Light leaking from the cavity is dispersed by a polychromator and detected by a charge coupled detector (CCD). BBCEAS does not suffer from the mode structures problem associated with narrow linewidth light sources as a broadband light source excites a large number of transverse electromagnetic modes and modes with off-axis intensity distribution. Therefore the light exiting the cavity represents a superposition of all the excited modes [11, 31].

2.6.1. CEAS – Theoretical Background

The number of passes in the cavity experiments depends on mirror spacing and radii of curvature and angle of incidence of the beam with respect to the cavity axis. CEAS detects the light leaking out of the high finesse cavity. The measured absorption is a function of the different intensities passing through the cavities with and without an absorbing medium [32]. For cavity illuminated by an incoherent, broadband light source, the cavity mode structures of the cavity intensity may be neglected [33, 34]. In the case of broadband CEAS (modeless linear cavity), the cavity transmission is determined only by the reflectivity of the mirrors and the one pass absorption by the medium inside the cavity. Figure 2.11 as described by Mazurenka *et al.* [11] illustrates the propagation of a beam of light in a cavity of length L formed from two mirrors of reflectivity *R*. I_{in} denotes the incident intensity and I_{out} representing the light leaking out of the cavity.

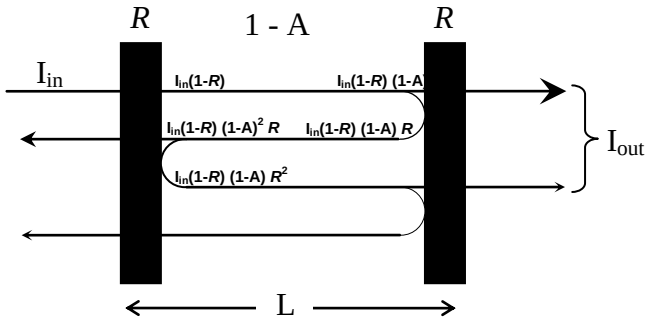

Figure 2.11: Schematic of beam propagation within a CEAS setup

Mazurenka *et al*. [11] derived the transmission for R < 1 and A < 1, as the sum of a geometrical progression and the following derivations (equation 2.16 to 2.19) are as described in the review.

$$I_{out} = I_{in} \frac{(1-R)^2(1-A)}{1-R^2(1-A)^2} \tag{2.16}$$

Where:

I_{in} - Incident light; R - Mirror reflectivity; I_{out} - Transmitted light;

A – One-pass absorption by the medium inside the cavity

Considering an empty cavity with loss A = 0 and same mirror reflectivity R the time integrated transmitted intensity of light I_o is given by the following equation;

$$I_o = I_{in} \frac{(1-R)}{(1+R)} = I_{in} \frac{(1-R)}{2} \tag{2.17}$$

The fractional losses at each round trip in the cavity can be expressed as a function of the ratio of intensities measured with and without absorption losses i.e. $\frac{I_o}{I_{out}}$;

$$1-A = \pm\sqrt{\frac{1}{4}\left(\frac{I_o}{I_{out}}\frac{\left(1-R^2\right)}{R^2}\right)^2 + \frac{1}{R^2} - \frac{1}{2} - \frac{I_o}{I_{out}}\frac{\left(1-R^2\right)}{R^2}} \tag{2.18}$$

With substitution of the one-pass fractional intensity change caused by absorption, (1-A) = $e^{-\alpha L}$ (according to Beer-Lambert law), the absorption coefficient, α, can be denoted as

$$\alpha = \frac{1}{L}\left|\ln\left(\left(\frac{1}{2R^2}\left(\sqrt{4R^2 + \left(\frac{I_0}{I_{out}}\left(1-R^2\right)\right)^2} - \frac{I_o}{I_{out}}\left(1-R^2\right)\right)\right)\right)\right| \tag{2.19}$$

Equation 2.19 is valid for large absorptions and small reflectivities as no approximation of the reflectivity R or the absorption cross section α was carried out.

2.6.2. Sensitivity of CEAS and CRDS

CEAS is not as sensitive as comparable CRDS measurements, because it relies on an intensity measurement rather than a time domain measurement. A major source of noise in CEAS measurements is due to residual mode structures that are not completely removed. Limitations arises as for CEAS it is necessary to measure the ratio of the light intensities as precisely as possible, and also working with mirrors reflectivity as close as possible to $R = 1$. This depends on the mirror coatings, calibration of the mirrors by CRDS and also intensity of the light source available.

A serious limitation to the sensitivity when using very high reflectivity mirrors is the limited amount of light reaching the detector. The accuracy of CEAS measurements tends to be affected two major factors, the mirrors reflectivity and the uncertainty in absorption coefficient [25, 35, 36]. If the calibration of the CEAS setup is made by measurements of the absorption of well known concentrations of molecules with accurately determined absorption cross sections, the accuracy and sensitivity will be limited by the noise levels or fluctuation of light reaching the detector and also the sensitivity of detector. The limiting noise source is generally the statistical fluctuation, commonly known as the shot noise of the photon stream exiting the cavity. With high reflectivity mirrors the shot noise increases due to the low cavity transmission, hence resulting in poorer sensitivity.

2.7. References

[1] Ellis, A.; Feher, M.; Wright, T. Electronic and photoelectron spectroscopy: Fundamentals and case studies; Cambridge University Press, UK, 2005, p. 286.

[2] Eland, J. H. D. Photoelectron spectrscopy: An introduction to ultraviolet photoelectron spectroscopy; Butterworth & Co Ltd, UK, 1984, p. 271.

[3] Hollas, M. J. Modern spectroscopy; John Wiley & Sons Ltd, UK, 2007, p. 452.

[4] Harris, A. D. Light spectroscopy; Bios scientific publishers Ltd, UK, 1996, p. 182.

[5] Knowles, A.; Burgess, C. (Eds.). Practical Absorption Spectroscopy: Ultraviolet spectrometry group; Chapman & Hall Ltd, London, 1984, p. 234.

[6] Skoog, A.D.; West, M.D.; Holler, J.F. Fundamentals of analytical chemistry ; Harcourt Asia PTE Ltd, India, 2001, p. 870.

[7] Sole, G.J.; Bausa, E.L.; Jaque, D. An introduction to the optical spectroscopy of inorganic solids; John Wiley & Sons Ltd, England, 2005, p. 282.

[8] Busch, K. W.; Busch, M. A. in: K.W. Busch and M.A. Busch (Eds.), cavity-ringdown spectroscopy An ultratrace-Absorption measurement technique, Oxford University Press, USA, 1999, p. 7.

[9] Busch, K. W.; Busch, M. A. (Eds.), An introduction to the optical spectroscopy of inorganic solids; Oxford University Press, USA, 1999, p. 269.

[10] Berden, G.; Peeters, R.; Meijer, G. International reviews in physical chemistry, 19 (2000) 565.

[11] Mazurenka, M. Annual reports on the progress of chemistry. Section C, Physical chemistry, 101 (2005) 100.

[12] Paldus, B. A. Canadian journal of physics, 83 (2005) 975.

[13] Hernandez, G. Applied Optics, 9 (1970) 1591.

[14] Kastler, A. Nouvelle Revue d'Optique, 5 (1974) 133.

[15] Ingle, D.J.; Crouch, R.S. Prentice-Hall, Inc, US, 1988, p. 590.

[16] Zalicki, P.; Zare, R.N. The Journal of Chemical Physics, 102 (1995) 2708.

[17] Jose, S.; Luisa, B.; Daniel, J. An Introduction to the Optical Spectroscopy of Inorganic Solids; John Wiley and Sons, England, 2005, p. 304.

[18] Herbelin, J. M. Applied optics, 19 (1980) 144.

[19] Anderson, D. Z.; Frisch, J.C.; Masser, C. S. Applied Optics, 23 (1984) 1238.

[20] O'Keefe, A.; Deacon, D. A. G. Rev. Sci. Instrum., 59 (1988) 2544.

[21] Fidric, B. G. Optics and photonics news, 14 (2003) 24.

[22] He, Y. Chemical Physics Letters, 319 (2000) 131.

[23] Brown, S. S. Chemical reviews, 103 (2003) 5219.

[24] Paldus, B. A.; Zare, R. N. in: Busch, M. A. and Busch, K. W. (Eds.), Cavity-ringdown spectroscopy An ultratrace-absorption measurement technique, Oxford University press, USA, 1999, p. 1.

[25] Engeln, R.; Berden, G.; Peeters, R.; Meijer, G. Review of scientific instruments, 69 (1998) 3763.

[26] O'Keefe, A. Chemical Physics Letters, 293 (1998) 331.

[27] Mu¨rtz, M.; Frech, v.; Urban, W. Applied Physics B: Lasers and Optics, 68 (1999) 243.

[28] Peeters, R.; Berden, G.; Ólafsson, A.; Laarhoven, L. J. J.; Meijer, G. Chemical Physics Letters, 337 (2001) 231.

[29] Chan, M.; Yeung, S. Chemical Physics Letters, 373 (2003) 100.

[30] Bakowski, B. Applied physics. B, Lasers and optics, 75 (2002) 745.

[31] He, Y. Journal of the Chinese Chemical Society, 48 (2001) 591.

[32] Paldus, B.; Provencal, R.; Katchanov, A. Cavity enhanced optical detector - US patent 7154595 (2006) .

[33] Bakhirkin, Y. A.; Kosterev, A. A.; Roller, C.; Curl, R. F.; Tittel, F. K. Applied Optics, 43 (2004) 2257.

[34] Fiedler, S. E.; Hese, A.; Ruth, A. A. Chemical Physics Letters, 371 (2003) 284.

[35] Gianfrani, L. Proceedings of SPIE--the international society for optical engineering, 3821 (1999) 90.

[36] Mazurenka, M. Analytical chemistry, 78 (2006) 6833.

Chapter Three

3.0. Broadband Cavity Enhanced Absorption Spectroscopy (BBCEAS) measurements in a 2 mm cuvette

Conventional absorption measurements are a common means for detecting analytes in solution, but typically lack sensitivity. It is known that for example, UV-visible absorption spectroscopy, suffers from comparatively poor sensitivity as an absorbance measurement relies on small differences between two relatively large signals being measured. Recently, the sensitivity of absorption measurements in the gas phase has been greatly increased by several orders of magnitude. This gain in sensitivity has been achieved by using CRDS, CEAS and variants of these techniques [1-5]. Simpler variations on CEAS have been demonstrated and applied successfully to spectroscopy on different wavelength region in the visible [1, 6-8], near infrared [9, 10], and mid infrared [11].

The aim of this study was to demonstrate a novel implementation of broadband cavity enhanced absorption spectroscopy (BBCEAS) to perform sensitive visible wavelength measurements on liquid-phase solutions, in a 2 mm cuvette placed at normal incidence to the cavity mirrors. Previous studies have placed optical components in the cavity at Brewster's angle in order to minimize loss due to reflection. Where the Brewster's angle is the angle of incidence at which light with a particular polarisation is perfectly transmitted through a surface, with no reflection (i.e. angle at which least losses is observed). Xu *et al* [12] were the first to demonstrate this idea experimentally by inserting a UV-Visible cuvette oriented at Brewster's angle into a ring-down cavity to study the C-H stretching fifth vibration overtone of benzene [12]. A similar approach was also used by Alexander [13] to study the reaction kinetics of nitrate radicals with terpenes in solution. Xu's technique was rather limited because the refractive index of the liquid sample needed to be close to that of the fused-silica cuvette used. Synder and Zare [14] resolved these limitations by designing a flowcell with wedged angles that could be used for liquid samples of any given refractive

index. This technique was also used by Bechtel and co-workers [15]. Fielder *et al*. [1] showed that a similar local minimum in the reflectivity also existed at 0 degrees angle of incidence. Even though there was a 4% reflection loss per surface at 0 degrees, in a cavity this reflected light was in theory recycled into the cavity. This local minimum varied more sharply than the minimum at Brewster's angle [1,16] but allowed easier alignment of the optical component and was also present for unpolarized light, unlike the Brewster's angle minimum, which required p-polarized light.

3.1. Optical setup and measurement procedures

The experimental setup for liquid-phase BBCEAS consisted of three major components: the broadband light source, the cavity, and the multiplex detector.

3.1.1. Light Source

Recently, high intensity LEDs have become available. Although significantly less powerful than a Xenon arc lamp, these are available at a range of visible wavelengths with power outputs greater than 200 mW, low power consumption, long lifetimes, and very low cost.

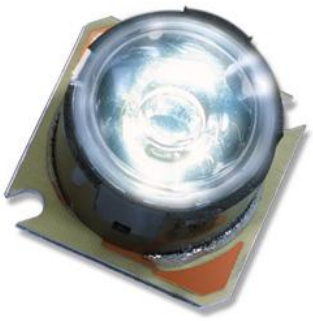

Figure 3.1: White Luxeon 'O star' LED.

The LEDs used for this study were from the 'O star' range of Luxeon 1 W devices (Lumileds, San Jose, CA). They consisted of a Luxeon emitter and integrated collimator (lens) moulded from optical grade acrylic and mounted to a

square aluminium sub-mount that included 2 slotted mounting holes. The O star produced a narrow collimated beam due to the inclusion of the collimating optics. The divergence of the output was reduced to 10 degrees. The LEDs were powered with a DC forward current of 350 mA. The central emission wavelength of the red, green, and blue LEDs were 630, 535, and 455 nm, respectively, whilst the bandwidths were approximately 20, 35, and 20 nm respectively, as shown in figure 3.2. A white LED covering the range 450–700 nm was also used for some of the measurements as shown in figure 3.3.

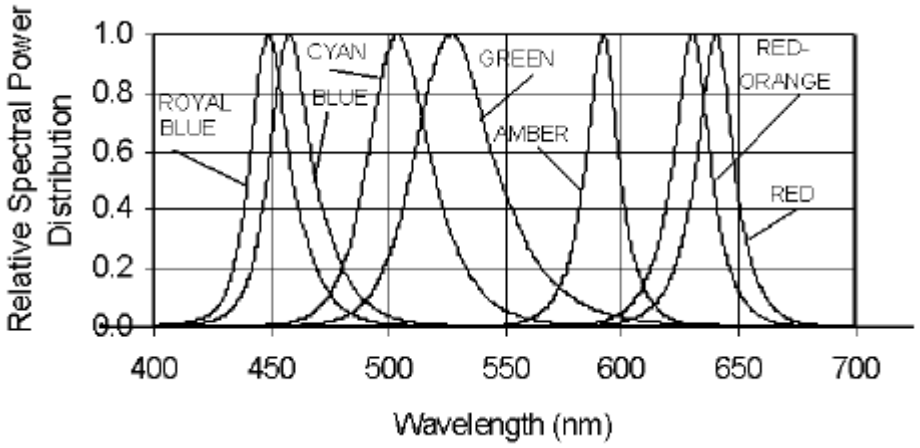

Figure 3.2: Relative intensity versus wavelength spectra for Luxeon LEDs
(Technical data sheet DS23 (03/06) **http://www.lumileds.com/pdfs/DS23.pdf** accessed 2008)

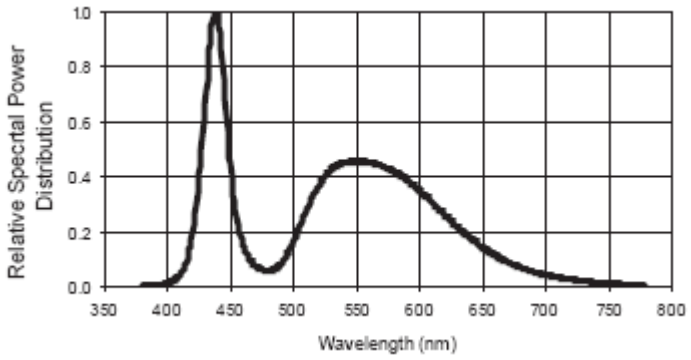

Figure 3.3: Luxeon white LED spectrum
(Technical data sheet DS23 (03/06) **http://www.lumileds.com/pdfs/DS23.pdf** accessed 2008)

3.1.2. The Cavity

The cavity was formed by two high reflectivity concave mirrors separated by 5 cm. A near confocal arrangement which is normally insensitive to misalignment was not used as the intensity of light detected after the cavity was found to be too low. Therefore a near long radius arrangement was adopted. A quartz cuvette with a 2 mm path (Optiglass Ltd, UK) was mounted on a rotation stage (Thorlabs, UK) and placed in the cavity at 0 degrees angle of incidence.

The choice of high reflectivity mirrors for BBCEAS experiments was not straightforward. Initially, the requirement was for high reflectivity mirrors ($R \geq 0.999$) with a bandwidth of 300 nm covering the visible range of the spectrum. Although such dielectric mirrors can be fabricated, the large bandwidth requires multistack designs that result in significant ripples in the reflectivity curve as a function of wavelength. At certain points the reflectivity can vary by more than a factor of 10. This introduces problems when the output from the cavity is detected with a CCD spectrograph because the variation of intensity as a function of wavelength can result in saturation at certain pixels and low counts at others. As a result of this information it was decided to instead obtain ‘‘standard’’ design high reflectivity mirrors, which have a bandwidth of; 100 nm and a relatively flat variation of reflectivity with wavelength.

Three mirror sets nominally of blue, green, and red wavelengths were obtained (Laseroptik, Germany), covering the range 400 – 700 nm with $R \geq 0.999$, a diameter of 25 mm, and a radius of curvature of ~1500 mm. Initial experiments, however, revealed that aside from the red LED and red mirror set, insufficient light intensity after the cavity could be detected with the CCD spectrograph once the cuvette was inserted into the cavity.

Consequently, a set of lower reflectivity mirrors ($R \geq 0.99$) was obtained (Layertec, Germany). These had an effective range from 420 to 670 nm, and although there were ripples in the reflectivity curve as a function of wavelength at this lower reflectivity, their effect on the variation of the intensity of the cavity light as a function of wavelength was significantly smaller and did not limit detection with a CCD spectrograph. In addition to the high reflectivity and low

reflectivity mirror sets, an intermediate reflectivity mirror set could be created by combining the mirror sets;

$$R = \sqrt{R_1 \times R_2} \tag{3.1}$$

$$= \sqrt{0.99\text{x}0.999} \geq 0.9945$$

These mirror reflectivities assumed the minimum manufacturer's specification and were not verified by independent CRDS measurements.

3.1.3. Charge-Coupled Device Spectrograph

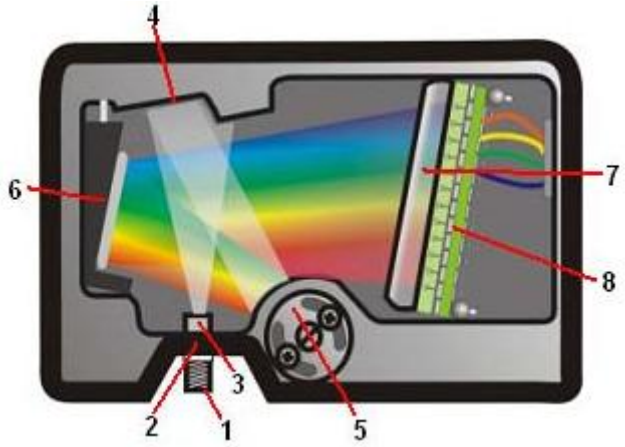

Figure 3.4: Schematic of Avantes AVS2000 spectrometer.

(1-SMA Connector; 2-Slit; 3- Filter; 4-Collimating Mirror; 5-Grating; 6-Focusing Mirror; 7-L2 Detector Collection Lens; 8-CCD Detector)

Figure 3.4 shows a schematic of the Avantes AVS2000 spectrometer. The light exiting the cavity was detected by the compact CCD spectrograph. This low-cost device consisted of a factory-sealed unit that contained an f/4, 42 mm focal length asymmetrically crossed Czerny–Turner design spectrograph bench. The detector was an uncooled 2048 element linear silicon CCD array (Sony ILX511). A 600 lines/mm grating with a blaze wavelength of 400 nm provided a spectral range of 200 to 850 nm and in combination with a 25 µm entrance slit resulted in a spectral resolution of 1.5 nm. Light was coupled into the spectrometer through an SMA905 fibre-optic connector.

The device was powered through a USB port, which also allowed data transfer. The software package Avasoft (Avantes, The Netherlands) was used

to control the spectrometer and record spectra. The lack of thermoelectric cooling of the CCD sensor resulted in relatively high levels of dark noise and restricted the use of long integration time. The maximum integration time that could be used with acceptable noise was three seconds.

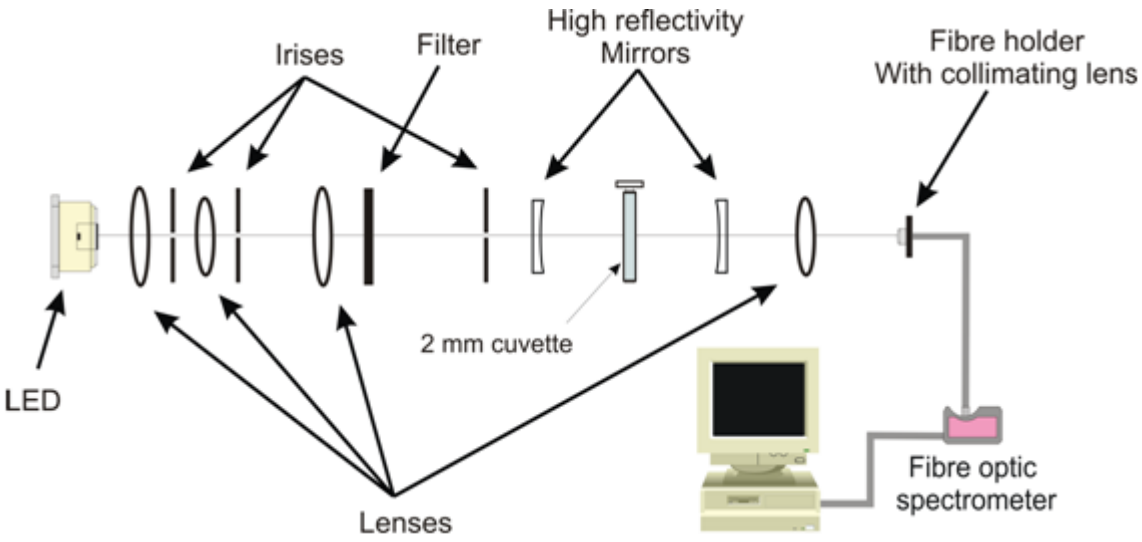

Figure 3.5: A scheme of the experimental setup for liquid-phase BBCEAS measurements.

A schematic of the experimental setup is shown in figure 3.5. The red O star LED exhibited a lambertian beam pattern and hence a higher luminous output compared to the other LEDs used in this study. The blue, green and white LED had a more divergent 'batwing' beam pattern. Although all the O star Luxeon LEDs were quoted to have the same divergence, within the experimental setup it was found that the red LED was better collimated than either the blue, green or white LEDs. The output from the LED was partially collimated by the integrated optic to a divergence angle of ~10 degrees; however, this was insufficient for alignment through the cavity. A series of lenses and irises were used to further collimate the beam. This resulted in only a small fraction of the initial output from the LED reaching the first mirror of the cavity. The optimum geometry of the lenses was quite complex to calculate from first principles therefore the optical setup was empirically assessed by trial and error to achieve maximum light leaking out of the cavity. At best only about 1% of the LED output remained after collimation and this remains a disadvantage of using astigmatic light sources such as LEDs which are

inherently difficult to collimate sufficiently. By contrast laser light sources are generally well collimated and most of the output can be used. The narrow beam from the LED was coupled in the optical cavity formed by two plano-concave mirrors with a diameter of 25 mm and a radius of curvature of 1.5 m. The higher luminous power and better collimation of the red LED resulted in experiments with two $R \geq 0.999$ mirrors being possible, whilst this was not possible with the other LEDs as insufficient light reached the detector with this mirror reflectivity combination.

The quartz cuvette was mounted on a rotation stage and placed equidistant between the two high finesse cavity mirrors, which were separated by 5 cm. The typical alignment procedure for the cavity involved firstly alignment of the cavity without the cuvette by maximising the amount of light that leaked out, hence maximising the output from the LED reaching the spectrograph at a given integration time, by iterative adjustment of the front and back cavity mirrors. The cuvette was then placed in the cavity with a blank solvent solution (typically acetonitrile). This resulted in a large decrease in the intensity of light reaching the spectrograph due to interface losses at the cuvette windows and the solvent. The integration time was increased appropriately to ensure the signal from the LED was significantly above the dark noise level, but not high enough to saturate the detector. Typical integration times for the 3 mirror sets with the red LED were ~10 ms for the $R \geq 0.99$ set, ~150 ms for the $R \geq 0.9945$ set and ~2 s for the $R \geq 0.999$ set. As mentioned earlier the use of the green and blue LEDs resulted in lower light intensities reaching the detector and thus longer integration times for the $R \geq 0.99$ and 0.9945 mirror sets had to be used, whilst insufficient intensity was present for use with the $R \geq 0.999$ mirror set. Likewise the white LED produced even lower intensities and could only be used with the $R \geq 0.99$ mirror set. The cuvette was then rotated to maximise the intensity reaching the detector and the rotation stage was locked. The front and back cavity mirrors were then further adjusted iteratively to maximize the output reaching the detector. The cuvette was subsequently filled and emptied with a syringe, ensuring minimum disturbance to the optimum alignment. The light leaking out of the cavity was focussed by a 50 mm focal length lens onto the entrance of a 600 μm diameter, 1 m length, 0.22 numerical aperture quartz fibre

(Thorlabs U.K). This was connected to the entrance slit of the spectrograph by an SMA905 fibre connection.

The experimental setup in principle allowed the measurement of the absorption spectrum of liquid or solution phase analytes at selected wavelengths in the range 400 - 700 nm depending on the output of the LED light source used. Many species are known to absorb in this region so the choice of potential analytes was large. In general most liquid phase absorption spectra are broad (linewidths > 50 nm) and featureless. Exceptions to this include the solution phase spectra of lanthanide ions which have relatively sharp features (~5 nm linewidths) in their absorption spectrum. Holmium chloride which produces Ho^{3+} ions in aqueous solution was chosen as a species for study as some of the absorption features were coincident with the output of the red, green and blue LEDs and thus this species could be studied at 3 separate wavelengths regions. The use of a white LED with the $R \geq 0.99$ mirrors allowed the simultaneous measurement of all 3 absorption features.

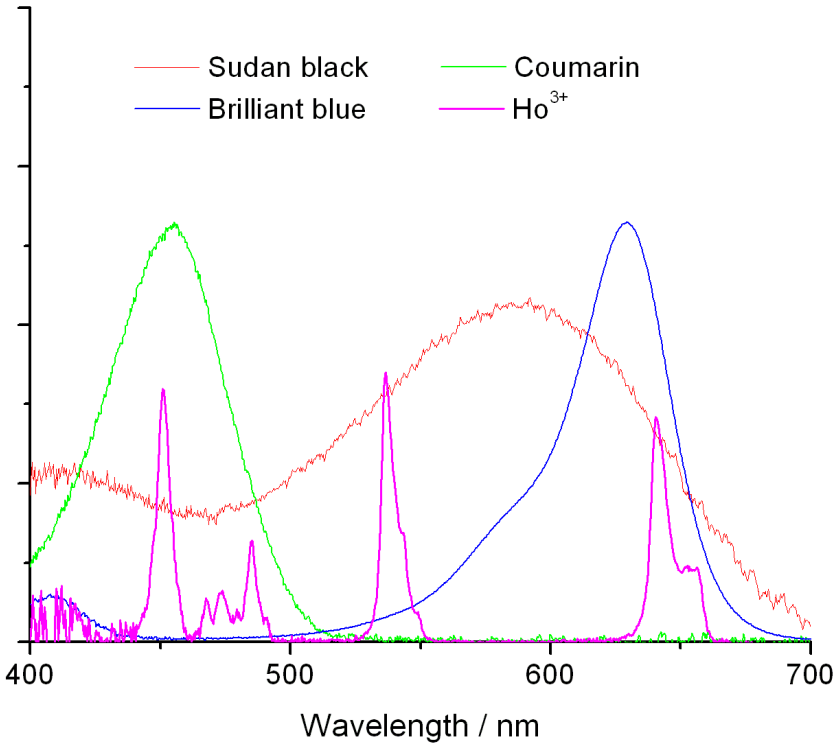

Figure 3.6: Scaled single pass absorption spectra of brilliant blue, sudan black, coumarin 334 and Ho^{3+}

As shown by the scaled absorption profile (figure 3.6) the other species chosen for study were the water soluble food dye brilliant blue-R, (Sigma – Aldrich, UK) which had a broad absorption peaking at ~630 nm. The staining dye sudan black (Sigma – Aldrich, UK) which had a broad absorption peaking at ~570 nm and which was soluble in non polar solvents such as hexane. The fluorescent dye coumarin 334 (Sigma – Aldrich, UK) which was soluble in polar solvents such as ethanol and had a broad absorption peaking at ~450 nm was also chosen for study. All the dyes had large molar extinction coefficients (10^4 – 10^5 M^{-1} cm^{-1}) whilst that of Ho^{3+} was much smaller (~4 M^{-1} cm^{-1}).

The choice of solvents required some consideration as previous studies had noted problems with the use of hydrogen bonded solvents such as water and methanol in the red part of the spectrum [15] .This was due to the presence of background solvent absorption as a result the 4^{th} overtone of the O-H stretch at ~640 nm. Preliminary experiments were performed with brilliant blue-R dissolved in water and non hydrogen bonded polar solvents such as acetonitrile. For measurements in our 2 mm cell no difference in the maximum number of passes possible at around 640 nm could be discerned. It should be noted that the previous study where this issue was raised involved measurements in a much longer 21 cm cell with higher reflectivity mirrors than used in this study. Consequently 18 MΩ.cm ultra pure water (Millipore, USA) was used as the solvent for the Ho^{3+} and brilliant blue-R measurements. For the other analytes spectrophotometric grade solvents were used. Hexane (Fisher Scientific, UK) was used as the solvent for sudan black whilst ethanol (Fisher Scientific, UK) was used as the solvent for coumarin 334.

3.2. Experimental Methodology

As noted earlier, one of the main disadvantages of CEAS based techniques is that unlike CRDS experiments, the absorption coefficient (ε) cannot be directly calculated and instead must be obtained through a separate calibration. In order to calculate absorption coefficients either the mirror reflectivities must be known or calibration with molecules of known cross section and number density must be undertaken. For the liquid phase BBCEAS experiments reported in this study the calibration and the experimental methodology could be performed in a straightforward manner and were very similar to the experimental methodology for conventional UV-visible absorption spectroscopy. The calibration could be used to obtain in the first instance the cavity enhancement factor (*CEF*) or the number of passes made within the cavity. Once the effective pathlength had been calculated, the minimum detectable change in the absorption coefficient, α_{min}, could also be calculated.

The first step in the calibration was to obtain a single-pass spectrum of the analyte to be studied. This was performed in a standard 1 cm pathlength cuvette with a tungsten halogen light source and the same Avantes AVS2000 spectrometer. The concentration of the solution was typically a factor of ten higher than in the 2 mm cuvette in the cavity. An absorption spectrum was obtained by recording a background spectrum with just the solvent in the cuvette, I_0, followed by the sample spectrum, I, and then the calculation of the absorbance from the equation below.

$$ABS = \log_{10}\left(\frac{I_0}{I}\right) \tag{3.2}$$

The Beer–Lambert law was then used to scale the peak of the absorption spectrum to the concentration used in the cavity and the 2 mm cuvette pathlength. This gave the single-pass absorbance under cavity conditions, ABS_{sp}. The cavity enhanced absorption spectrum was obtained by first recording a background solvent only spectrum with the 2 mm cuvette inside the cavity. A sample spectrum was then recorded and the absorbance spectrum calculated. The value of the cavity-enhanced absorbance at the peak

wavelength of the single-pass spectrum was measured for an analyte. This gave the cavity absorbance, ABS_{cav}. The number of passes within the cavity or the cavity enhancement factor (*CEF)* could be calculated as the ratio of ABS_{cav} to ABS_{sp}.

$$CEF = \frac{ABS_{cav}}{ABS_{sp}} \tag{3.3}$$

Let's consider the ABS_{cav} to ABS_{sp} values for sudan black collected at a wavelength of 564 nm. When substituted in equation 3.3;

$$CEF = \frac{0.189}{0.00365} = 51.8 \approx 52$$

The *CEF* could be calculated for the whole wavelength range using the same equation and a representative graph of the *CEF* for sudan black is shown in figure 3.7.

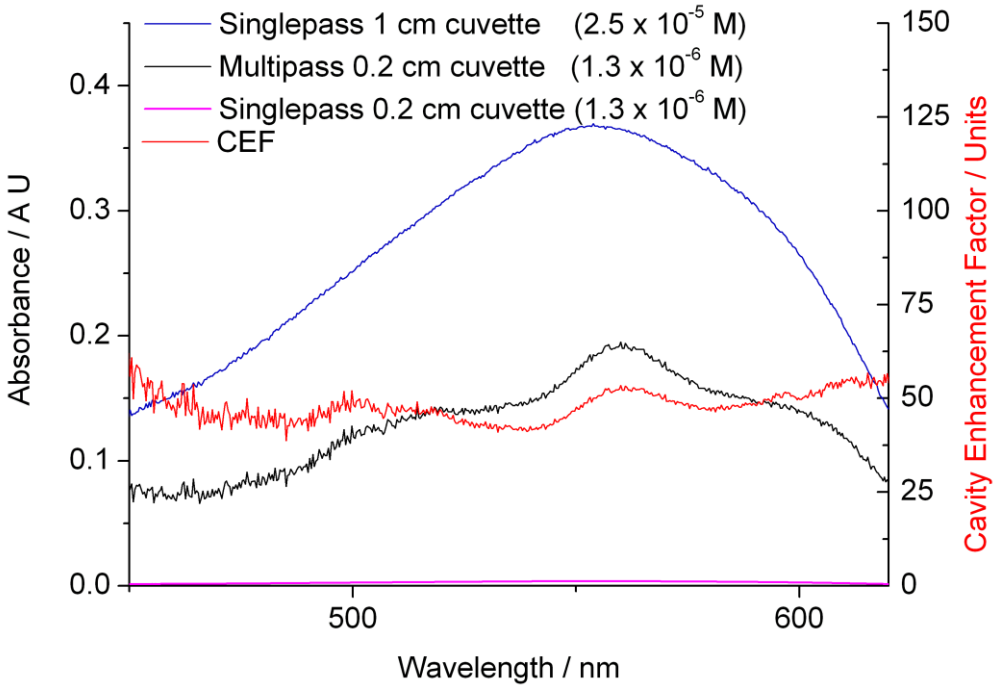

Figure 3.7: Absorption spectrum for sudan black and calculated cavity enhancement factor. (singlepass absorbance in 1 cm cuvette, conc. of 2.5 x 10^{-5} M; Multipass absorbance in 0.2 cm cuvette, conc. of 1.3 x 10^{-6} M; Scaled singlepass absorbance for 0.2 cm cuvette and conc. 1.3 x 10^{-6} M)

The effective pathlength of the measurement (l_{eff}) could also be calculated by the following equation

$$l_{eff} = CEF \times width\ of\ cuvette \tag{3.4}$$

Given that the base pathlength was 2 mm

$$l_{eff} = CEF \times 0.2\ cm \tag{3.5}$$

For the *CEF* value calculated for sudan black (wavelength = 564 nm) above, the effective pathlength was

$$l_{eff} = 52 \times 0.2 = 10.4 \text{ cm}$$

Determination of the sensitivity of the measurement required the calculation of α_{min}. For each measurement to obtain a *CEF* value, ten replicate measurements were also performed. The standard deviation in the absorbance value as a function of wavelength was calculated using a spreadsheet program (Microsoft Excel). The mean of the standard deviation values corresponded to the minimum detectable absorbance change ΔABS_{min}. The value of α_{min} could be obtained by dividing ΔABS_{min} by l_{eff} in cm. A factor of 2.303 was required to convert the absorbance values from $\log_{10}$ units to $\log_e$ (ln) units, which are the typical units of measurement for α_{min}. The calculated value of α_{min} was essentially the minimum detectable change in the absorption coefficient:

$$\Delta\alpha_{\min} = \frac{2.303\ \Delta ABS_{\min}}{l_{eff}} \tag{3.6}$$

The limit of detection (LOD) of an analyte is usually calculated from the 99%, three standard deviations (3σ), confidence limit of the noise on the baseline of an absorption spectrum. Therefore the LOD could be calculated by using the equation below

$$LOD = \frac{3\,\alpha_{\min}}{2.303\varepsilon} \tag{3.7}$$

Where, ε is the value of the molar extinction coefficient for the analyte under study at the wavelength of measurement. The ε values were experimentally determined using conventional UV-visible spectroscopy in a 1 cm cuvette, from plots of absorbance versus concentration data for the analytes at the wavelength of measurement. The mean values obtained from ten replicate measurements are listed in Table 3.1, along with the wavelength of measurement.

3.2.1. Precautionary measures taken to avoid contamination

To avoid contamination and ensure accuracy during preparation of very dilute solutions, special cleaning procedures of glassware and other precautions were adopted.

The following cleaning procedure consisting of a number of wash/ dry steps was used to clean glassware for the low concentration work (< 10^{-6} M). As an initial step all glassware were washed with detergent (Decon 90 (Fisher Scientific, UK)), triple rinsed with deionised water followed by rinses with analytical grade methanol and dried in an oven at 110 ^{o}C prior to acid rinse. Note: Volumetric flasks were not dried in an oven as they were either air dried or blow dried with nitrogen after the methanol rinse. If the glassware was not clean the above step was repeated and physical abrasion was applied using a bottle brush. The glassware was then cleaned with 50 % Nitric acid solution (Fisher Scientific, UK), rinsed three times with deionised water and dried prior to use. Some glassware required cleaning with acid peroxide solution consisting of equal volume of concentrated sulphuric acid and 3% hydrogen peroxide and was tripled rinses with deionised water prior to the Nitric acid cleaning step.

All solutions were prepared at room temperature in calibrated grade A glassware's, using calibrated Gilson pipettes (Anachem Ltd, UK) for volumetric solution transfer. Transfer devices were never placed into standard solutions to avoid possible contamination. Instead, aliquots from the standard solution were transferred in a suitable container. Standard stock solutions were weighed before storage in a darkened cupboard. If there was any significant change in the weight before the next use the solution was discarded.

3.3. RESULTS

Table 3.1: A summary of the results obtained in terms of analyte, the LED used, the wavelength of measurement, the reflectivity of the mirrors, the *CEF* value, the minimum detectable change in absorption α_{min}, the molar extinction coefficient ε at the wavelength of measurement, and the LOD of the analyte.

Analyte	LED	Wavelength (nm)	Reflectivity	*CEF*	α_{min} (cm^{-1})	ε (M^{-1} cm^{-1})	LOD (M)
Ho^{3+}	Red	641	0.99	46 ± 0.2	6.7×10^{-5}	3.35	2.6×10^{-5}
Ho^{3+}	Red	641	0.9945	64 ± 1.1	3.9×10^{-4}	3.35	1.5×10^{-4}
Ho^{3+}	Red	641	0.999	104 ± 2.1	4.8×10^{-4}	3.35	1.9×10^{-4}
Ho^{3+}	Green	537	0.99	40 ± 0.2	1.6×10^{-4}	4.67	4.4×10^{-5}
Ho^{3+}	Green	537	0.9945	58 ± 1.2	6.4×10^{-4}	4.67	1.8×10^{-4}
Ho^{3+}	Blue	452	0.99	44 ± 0.5	1.8×10^{-4}	3.61	6.3×10^{-5}
Ho^{3+}	Blue	452	0.9945	65 ± 2.2	8.5×10^{-4}	3.61	3.1×10^{-4}
Ho^{3+}	White	641	0.99	47 ± 0.4	2.1×10^{-4}	3.35	8.1×10^{-5}
Ho^{3+}	White	537	0.99	40 ± 0.3	2.0×10^{-4}	4.67	5.5×10^{-5}
Ho^{3+}	White	452	0.99	44 ± 0.8	4.1×10^{-4}	3.61	1.5×10^{-4}
Brilliant blue- R	Red	630	0.99	51 ± 0.1	5.1×10^{-5}	1.06×10^{5}	6.2×10^{-10}
Brilliant blue- R	Red	630	0.9945	60 ± 0.9	3.0×10^{-4}	1.06×10^{5}	3.7×10^{-9}
Brilliant blue- R	Red	630	0.999	104 ± 3.1	6.0×10^{-4}	1.06×10^{5}	7.4×10^{-9}
Sudan black	Red	620	0.99	59 ± 0.4	5.3×10^{-5}	1.76×10^{3}	3.9×10^{-8}
Sudan black	Red	620	0.9945	74 ± 0.8	1.8×10^{-4}	1.76×10^{3}	1.3×10^{-7}
Sudan black	Red	620	0.999	93 ± 2.7	3.9×10^{-4}	1.76×10^{3}	2.9×10^{-7}
Sudan black	White	564	0.99	52 ± 0.3	1.9×10^{-4}	4.72×10^{3}	5.1×10^{-8}
Coumarin 334	Blue	456	0.99	45 ± 0.5	2.0×10^{-4}	5.07×10^{4}	5.2×10^{-9}
Coumarin 334	Blue	456	0.9945	53 ± 2.4	1.2×10^{-3}	5.07×10^{4}	3.1×10^{-8}

Liquid-phase BBCEAS measurements have been carried out in a 2 mm cuvette for four different analytes mostly at the peak absorption wavelength, using appropriate LEDs and high reflectivity mirror sets. Table 3.1 summarizes the measurements made in terms of the analyte studied, the LED used, the wavelength of measurement, the reflectivity of the mirror set used, the *CEF* or number of passes obtained for each analyte (the 1σ error limit on the measurement is also shown), the calculated α_{min} values for each measurement, the molar extinction coefficient ε of the analyte at the wavelength of measurement, and an estimation of the LOD for each analyte.

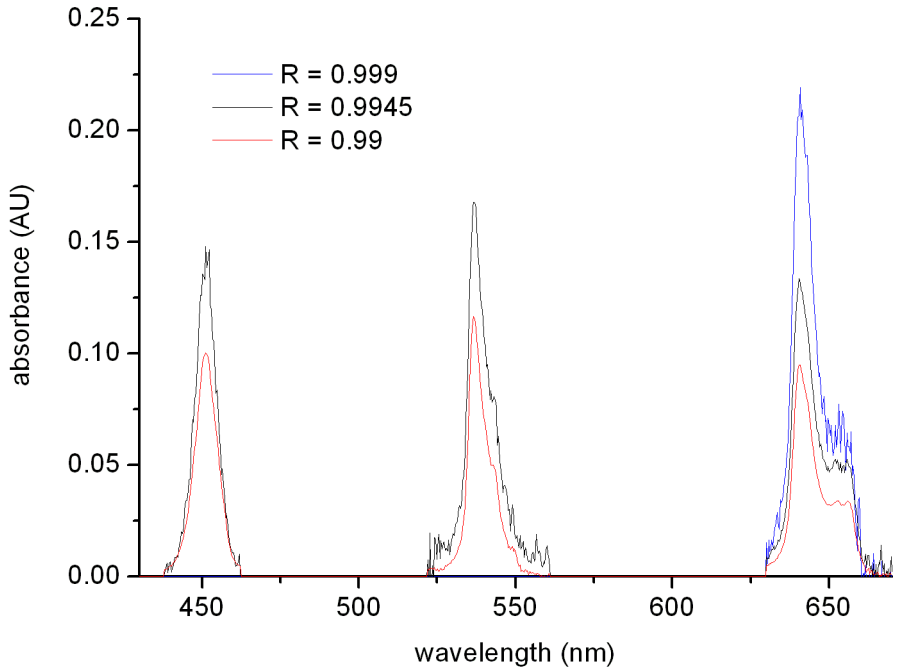

Figure 3.8: BBCEAS spectra of 3.1 x 10^{-3} M Ho^{3+} in water
(Obtained using the red, green, and blue LEDs and the *R* ≥ 0.99, 0.9945, and 0.999 mirror sets for the red LED and the *R* ≥ 0.99 and 0.9945 mirror sets for the green and blue LEDs)

Figure 3.8 shows representative absorption spectra of Ho^{3+} collected with the *R* ≥ 0.99 and 0.9945 mirror sets for the green and blue LEDs and the *R* ≥ 0.99, 0.9945, and 0.999 mirror sets for the red LED.

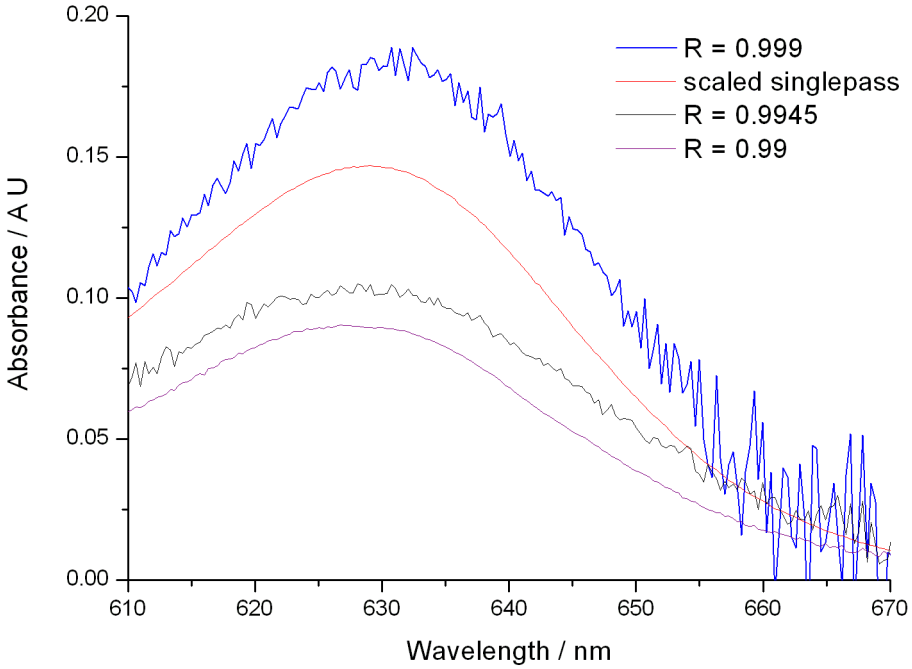

Figure 3.9: BBCEAS spectra of 7.9 x 10^{-8} M brilliant blue-R in water
(Obtained using the red LED and the *R* ≥ 0.99, 0.9945, and 0.999 mirror sets. A scaled single-pass spectrum is also shown)

Figure 3.9 shows representative absorption spectra of brilliant blue-R recorded with the red LED and the R ≥ 0.99, 0.9945, and 0.999 mirror sets, between 610 and 670 nm.

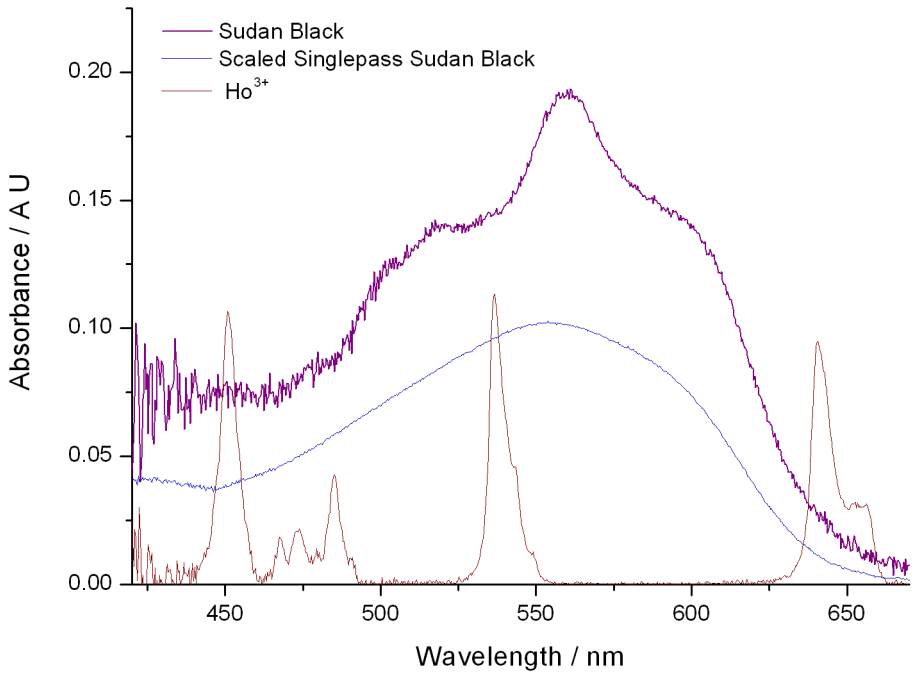

Figure 3.10: BBCEAS spectrum of 4.0 x 10^{-6} M sudan black in hexane and 3.1x 10^{-3}M Ho^{3+} in water, in the range 420–670 nm, obtained with the white LED and the $R \geq 0.99$ mirror set. A scaled single-pass spectrum of sudan black is also shown.

Figure 3.10 shows representative absorption spectra recorded over a ~250 nm wavelength range in a single measurement for Ho^{3+} and sudan black using the white LED and the $R \geq 0.99$ mirror set.

3.3.1. Measurement of the dynamic range of the technique.

To investigate the suitability of liquid-phase BBCEAS as an analytical tool, measurements were made on a selected analyte over a range of concentrations to determine the dynamic range of the technique and also provide an independent measurement of the LOD of the selected analyte. The analyte chosen was the dye brilliant blue-R, which was studied with the red LED and the $R \geq 0.99$ mirror set, as previous measurements with this combination of LED and mirror set yielded the lowest α_{min} value and LOD.

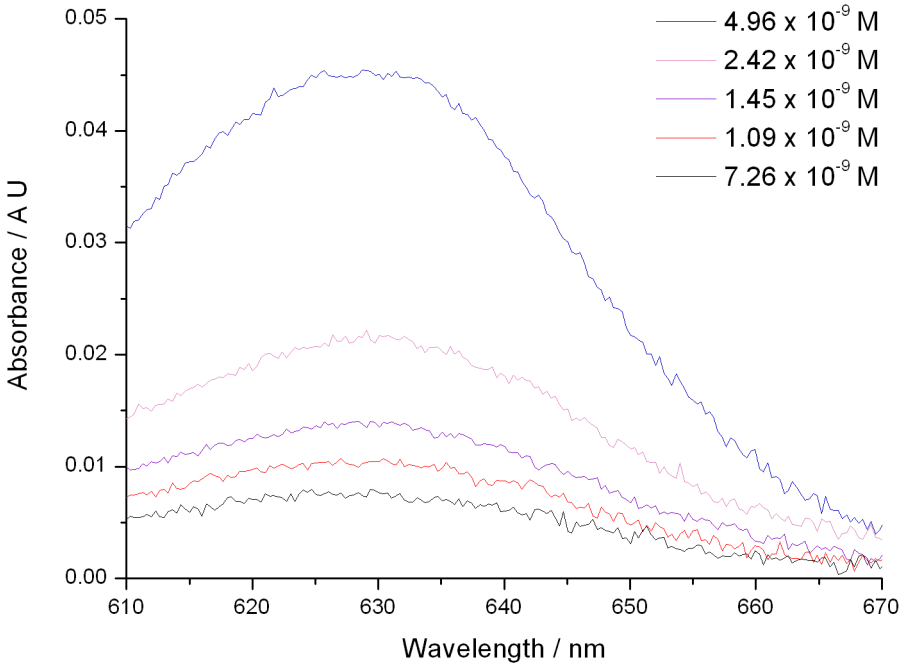

Figure 3.11: BBCEAS spectra of brilliant blue-R, for a range of low concentrations from ~7 nM to ~50 nM, obtained using the red LED and the $R \geq 0.99$ mirror set.

Figure 3.11 shows spectra of brilliant blue-R at a range of low concentrations from ~7 nM to ~50 nM, recorded between 610 and 670 nm with the $R \geq 0.99$ mirror set.

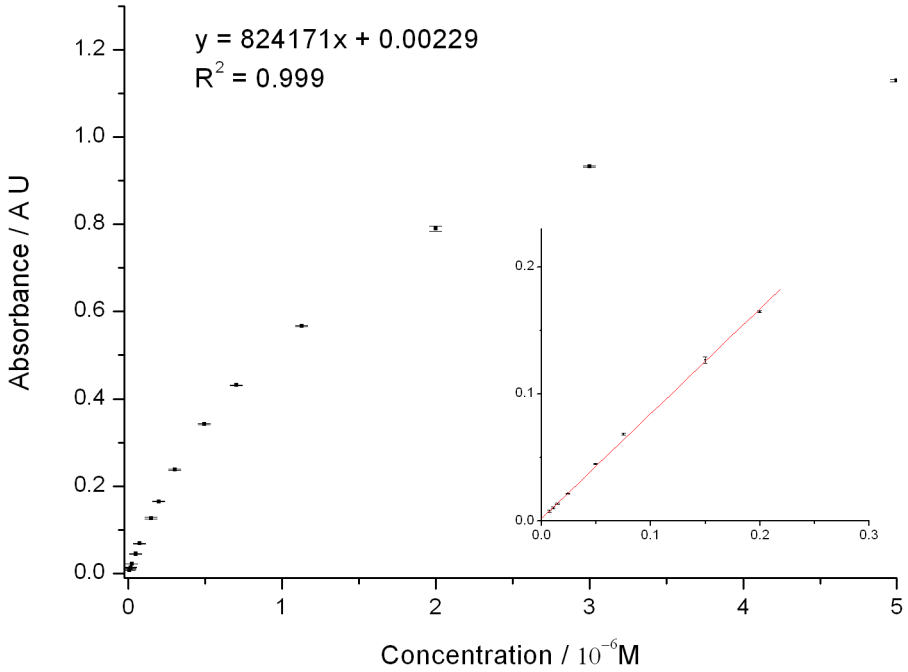

Figure 3.12: An absorbance versus concentration plot of brilliant blue-R, in the range ~7 nM to ~5 µM, obtained using the red LED and the *R* ≥ 0.99 mirror set. The inset shows the measurements in the linear range from ~7 nM to ~200 nM. The error bars represent the 1σ error limit of three replicate measurements at each concentration. The equation on the diagram refers to an error-weighted linear fit to the measurements of the linear region.

Figure 3.12 shows plots of absorbance versus concentration for brilliant blue-R. The brilliant blue-R measurements were made at 630 nm and a range of concentrations from ~7 nM to ~5 µM. Three replicate measurements were made at each concentration and the error bars for each concentration represent the standard deviation of the measurements. The plot can be broken into two parts. The insert shows measurements in the range ~7 nM to ~200 nM, which show a linear dependence of the absorbance on the concentration. The measurements at higher concentrations, up to ~5 µM are nonlinear. An error-weighted regression through the linear part of the plot yields a straight line (equation of the line is given in figure 3.12) with the correlation coefficient R^2 = 0.999 and a 1σ error limit for the intercept of 3 x 10^{-4}. The LOD can be calculated from the value of the 3σ error limit on the intercept, which produces a concentration of 1.1 nM. This value is similar to the 620 pM LOD that was obtained from previous measurements with the red LED and the *R* ≥ 0.99 mirror

set, using the standard deviation of the noise on the absorbance measurement to determine the LOD. The limit of quantification (LOQ) can also be determined from the 10σ error limit on the intercept and yields a concentration of 3.6 nM. At absorbance values above ~0.25 the plot in figure 3.12 is no longer linear with respect to increasing concentration, but measurements of absorbance values of up to ~1.2 were made without significantly visible increases in the 1σ error limit on three replicate measurements.

3.4. DISCUSSION

For each analyte, results have been obtained for values of the *CEF*, the α_{min}, and also the LOD. These values are discussed in turn. The *CEF* values show the expected general trend of increasing for each analyte as the reflectivity of the cavity mirrors increases. The values of the *CEF* are, however, lower than would be expected in comparison with gas-phase measurements, for which in the limit of very high mirror reflectivity ($R \rightarrow 1$) and low absorption ($\alpha \rightarrow 0$) it can be shown that [3]:

$$\frac{I_0}{I} = 1 + \frac{\alpha l}{1 - R} \tag{3.8}$$

A conventional single-pass experiment can be expressed as

$$\frac{I_0}{I} = 1 + \alpha l \tag{3.9}$$

That is, the increase in the number of passes and sensitivity for a cavity-based experiment is given by $(1 - R)^{-1}$. This assumes that absorption and scattering losses by the mirrors are low and that scattering losses by the gas-phase sample are insignificant and the absorption is small. For most gas-phase measurements all these conditions are satisfied. For the liquid-phase measurements in this study apart from the losses due to imperfect mirror reflectivities, the cavity is subject to additional losses due to scattering and absorption by the solvent as well as the cuvette windows. These losses could be measured for the system in this study by recording the intensity of light

exiting the cavity in the absence and presence of the cuvette and solvent and from the knowledge of the number of passes for a given mirror set.

Measurements with the $R \geq 0.99$ mirror set showed that the combined cuvette and solvent losses were ~1 x 10^{-2} per pass, which is consistent with the lower than expected increase of the *CEF* values with increasing mirror reflectivity. This value is, however, rather high compared with the only other liquid-phase BBCEAS study, of Fielder *et al* [1]. . They reported cuvette losses of ~10^{-3} per pass and solvent losses of ~10^{-3} cm^{-1}. Single-pass measurements on the solvents in a 1 cm cuvette indicated losses of ~10^{-3} cm^{-1} across the 450 to 650 nm range and so suggest that the solvents are unlikely to be responsible for the higher than expected loss. Possible explanations for the higher than expected loss include the lack of fine adjustment for the vertical alignment of the cuvette in the cavity, lack of co-planarity of the cuvette windows, and less than optimal polishing of cuvette windows, leading to increased scattering from the optical surfaces.

One advantage of the BBCEAS experiment was that measurements could be made over a wide wavelength range usually limited by the bandwidth of the cavity mirrors used or the bandwidth of the light source. The measurements on Ho^{3+} and sudan black with the white LED and the $R \geq 0.99$ mirrors covered a wavelength range of ~250 nm and represents the largest wavelength range covered to date in a single BBCEAS experiment. As demonstrated by the Ho^{3+} measurements, coverage of a broad wavelength range allowed in principle several transitions to be measured in a single experiment.

The separate measurement of the Ho^{3+} transitions with the white LED as well as the red, green, and blue LEDs and the $R \geq 0.99$ mirror set allowed the reproducibility and robustness of the technique to be assessed. The independent *CEF* values for the red, green, and blue transitions obtained using the two separate light sources were almost identical within the error limits of the measurement, thus indicating that the *CEF* values were highly reproducible. The variation in the *CEF* values between the red, green, and blue transitions was most likely due to variations in the reflectivity profile of the $R \geq 0.99$ mirror set as a function of wavelength. For the other analytes, the *CEF* values showed the general trend of increasing with mirror reflectivity. For a given mirror

reflectivity the differences in values between the analytes were again most likely due to variations in the reflectivity profile of the mirror sets. The ripples in the reflectivity versus wavelength profile were most significant for the $R \geq 0.99$ mirror set due to the nature of their design. The ripples occurred over ~50 nm and for narrow linewidths spectra such as Ho^{3+} resulted in no visible distortion of the shape of the spectral features. Even for moderately broad absorptions such as that of brilliant blue-R in figure 3.9 the spectral distortion, at least visually, was marginal. For broad absorptions such as that of sudan black in figure 3.10, the spectral distortion was more significant. The single-pass spectrum of sudan black was by comparison broad and featureless.

The spectral distortion could be corrected by knowledge of the form of the reflectivity profile either from the manufacturer's data sheet or from independent CRDS measurements. A simpler procedure could be to obtain the form of the reflectivity profile by taking the ratio of the BBCEAS spectrum of a broad absorber to the single-pass spectrum and using that data to correct all other spectra. The sensitivity of most cavity-based experiments is determined from the minimum detectable change in the absorption coefficient, α_{min}. This typically refers to the standard deviation of the noise on the baseline of the measurement. From Table 3.1 it can be seen that the values obtained in this study range from 5.1×10^{-5} cm^{-1} to 1.2×10^{-3} cm^{-1}. Standard gas-phase cavity measurements typically report α_{min} values of, 10^{-7} cm^{-1} [2]. In comparison, the values from this study are significantly higher; however, this is not surprising because the α_{min} values are inversely proportional to the total pathlength and hence are affected by both the short base pathlength of 2 mm and also the relatively low number of passes. In gas-phase studies a base pathlength of ~1 m and more than a 1000 passes through the sample are common. It is consequently more appropriate to make comparisons with other liquid-phase cavity-based studies.

3.4.1. Comparison with Previous Liquid-Phase Cavity Studies.

Table 3.2: A comparison between this study and previous liquid-phase cavity studies as a function of technique, the mirror reflectivity, base pathlength, the wavelength of measurement, the lowest value of α_{min}, the minimum LOD for an analyte, and the molar extinction coefficient ε for that analyte.

Study	Technique	Mirror reflectivity	Base path length (cm)	Wavelength (nm)	α_{min} (cm^{-1})	LOD (M)	ε (M^{-1} cm^{-1})
This work	BBCEAS	0.99	0.2	630	5.1×10^{-5}	6.2×10^{-10}	1.06×10^{5}
Xu *et al.*[13]	CRDS	0.9997	1	607	1×10^{-5}	-	-
Van der Sneppen *et al*.[18]	CRDS	0.99993	0.2	457	1.0×10^{-5}	1.2×10^{-8}	3.6×10^{4}
Fiedler *et al.*[1]	BBCEAS	0.99	1	607	2×10^{-5}	-	-
Fiedler *et al.*[2]	BBCEAS	0.99	0.1	607	3×10^{-5}	-	-
McGarvey *et al.*[19]	CEAS	0.99998	0.175	783	3×10^{-6}	2×10^{-10}	6×10^{4}
Alexander [14]	CRDS	0.9998	2.32×10^{-3}	628	5.4×10^{-3}	7.1×10^{-8}	1×10^{5}

Table 3.2 summarizes some of the figures of merit obtained from this study such as the lowest value of α_{min} obtained, the lowest LOD obtained, and the molar absorption coefficient for the analyte in question. These are compared with corresponding data, where available, from the small number of previous liquid-phase cavity studies. Table 3.2 also lists the base pathlength of the measurement, the wavelength of measurement, and the reflectivity of the cavity mirrors used in the studies. A discussion of the α_{min} values and the LOD values is undertaken in the paragraphs below. The CRDS studies related to HPLC detection have typically quoted the baseline noise in absorbance units (AU), but these can be converted to α_{min} values by multiplying by 2.303 to convert from $\log_{10}$ units to ln ($\log_e$) units and then dividing by the pathlength of the cell in cm. Care must be taken that the comparison is made with the root mean squared (rms) 1σ noise value rather than the peak-to-peak 3σ noise value, which is often stated. For example, van der Sneppen *et al.* [18] reported the baseline noise in their study to be 2.7 x 10^{-6} AU, peak to peak, in a 2 mm pathlength cell. This corresponds to an rms value of ~9 x 10^{-7} AU, which produces an α_{min} value of 1.0 x 10^{-5} cm^{-1}.

Comparing with the results from this study, it can be seen that the mirror reflectivities used in the previous liquid-phase studies are generally much higher. The lowest α_{min} value obtained in this study, 5.1 x 10^{-5} cm^{-1}, was obtained using $R \geq 0.99$ mirrors. The base pathlength of 2 mm is in the middle of the range of those used in the previous studies. The values of α_{min} obtained consequently compare surprisingly favourably with the previous studies given the simplicity of the experimental setup and the data analysis. The study carried out by Fiedler *et al*. [1] is the most similar to the current one. Their measurements using a modified double-beam UV-visible spectrometer and a 1 cm cell, with $R \geq 0.99$ mirrors, yielded similar values of α_{min} of ~2 x 10^{-5} cm^{-1}, albeit with a five times longer base pathlength and a double beam setup. Separate measurements in a 1 mm cell using a high intensity Xe arc lamp as the light source and a CCD spectrograph detector produced an α_{min} of ~3 x 10^{-5} cm^{-1}, which is similar to our values but using a significantly more expensive light source.

The values of α_{min} in Table 3.1 are generally seen to increase as the reflectivity of the mirrors increases. This counterintuitive trend is attributable to the decrease in the intensity of light reaching the detector as the reflectivity of the mirrors increases. This required the integration time on the CCD array to be increased to enhance the signal, but due to the lack of thermoelectric cooling of the CCD array, integration times longer than ~100 ms resulted in nonlinear increases in the dark noise. This manifested itself in increased noise on the absorbance measurement and consequently higher values of α_{min}. Aside from the $R \geq 0.99$ mirror sets, all the other mirror sets required the use of integration times in excess of 100 ms. Thus, even though the effective pathlength increased with the use of higher reflectivity mirror sets, the increase in noise due to increased dark noise from longer integration times usually resulted in poorer values of α_{min}. Table 3.1 also lists the LOD values for the analytes studied based on the calculated value of α_{min} and ε of the analyte. For the strong absorber brilliant blue-R (ε ~1.06 x 10^5 M^{-1} cm^{-1} at 630 nm), it has been shown that the minimum LOD is approximately 620 pM. The value of the LOD of an analyte will depend on both ε and the pathlength of the measurement.

In general, longer pathlengths and larger values of ε will produce lower LODs. The most appropriate comparison is with the CEAS study carried out by McGarvey *et al*.[18] which reported an LOD for bacteriochlorophyll a (ε ~ 6 x 10^4 M^{-1} cm^{-1} at 783 nm) of approximately 200 pM using much higher reflectivity $R \geq 0.99998$ mirrors and a significantly more complex and expensive experimental setup. Comparisons of the LOD values obtained in this study can also be made with the previous studies related to CRDS measurements on HPLC systems, as these typically report LOD measurements on strong absorbers such as dye molecules. It should be noted that in general the HPLC studies report LODs based on the injected concentration before LC separation. Chromatographic broadening results in the concentration in the detection cell being significantly lower.

Taking into account differences in the base pathlength, as well as the molar extinction coefficients of the analytes studied, the LOD values from this study compare very favourably with the previous studies, especially given the simplicity of the experimental setup and the data analysis. For BBCEAS measurements, a linear dynamic range of measurement of about two orders of

magnitude, from the LOD of ~1 x 10^{-3} AU to 0.2 AU, has been shown. For larger absorbance values, up to the maximum measured value of 1.2, where the response becomes nonlinear, and the concentration can in principle still be quantified using a calibration curve. The nonlinear behaviour at higher concentrations is attributed to the increasing absorbance due to the analyte, resulting in a reduction in the number of passes in the cavity and consequently a reduction in the effective pathlength. The multiplex nature of detection used in BBCEAS also offers the advantage of detecting simultaneously over a range of wavelengths and thus does not require the analytes to all absorb at a single wavelength.

The sensitivity of the experimental setup could be improved in a number of ways. The simplest improvement would be to increase the pathlength of the cuvette. Most conventional implementations of liquid-phase UV-visible spectroscopy tend to use 1 cm cuvettes, and this would in principle decrease the α_{min} values by a factor of five without increasing the experimental difficulty or the applicability of the technique. It has been shown that the use of $R \geq 0.999$ mirrors increases the effective pathlength by a factor of approximately 2.5 compared to $R \geq 0.99$ mirrors, but there is not a corresponding improvement in the sensitivity due to increased noise from the uncooled CCD detector at longer integration times. This could be addressed by using either a cooled detector, which would allow the use of longer integration times without the associated increase in dark noise, or a higher intensity light source, which would allow shorter integration times to be used.

Given that at best only about 1% of the output of the LED could be effectively used, a more efficient method of coupling the LED output into the cavity would also allow the use of shorter integration times for the higher reflectivity mirrors. These changes would in principle improve the sensitivity of the technique such that an α_{min} of ~ 2 x 10^{-6} cm^{-1} could be achieved, allowing the detection of strong absorbers (ε ~1 x 10^{5} M^{-1} cm^{-1}) down to the 50 pM level. Further improvements could be made by reducing the reflection and scattering losses in the cavity, which would lead to greater effective pathlengths with the higher reflectivity mirrors. This could be achieved by better fine control of the vertical alignment of the cuvette in the cavity, polishing the cuvette windows,

and also ensuring that the cuvette windows are as parallel as possible during manufacture.

3.5. CONCLUSION

A simple low-cost BBCEAS experimental setup has been demonstrated for the measurement of four representative liquid-phase analytes in a 2 mm quartz cuvette at a range of wavelengths in the visible part of the electromagnetic spectrum and using mirror sets with three different reflectivities. The methodology for the measurement of the absorption spectrum required a simple calibration and is conceptually similar to standard UV-visible absorption spectroscopy. The results yielded the number of passes through the sample or the *CEF*, as well as the sensitivity of the measurement through the minimum detectable change in absorbance, α_{min}. The limit of detection for each analyte was also calculated. The use of a white LED and $R \geq 0.99$ mirrors allowed measurements in the range; 420 – 670 nm to be made in a single experiment.

The *CEF* values were found to generally increase with higher mirror reflectivities, although the increase was significantly less than expected in comparison with gas-phase measurements. This was attributed to relatively large scattering and absorption losses from the cuvette windows. The α_{min} values tended to increase with increasing mirror reflectivities due to lower levels of light reaching the detector and, consequently, increasing amounts of dark noise from the detector at the longer integration times needed to make the measurements. Consequently, for the current experimental setup the most sensitive measurements were made with the lowest reflectivity $R \geq 0.99$ mirror set. In comparison with previous cavity based studies on liquids, the lowest α_{min} values from this study were found to offer similar levels of sensitivities to the best previous measurements, using in general much lower reflectivity mirrors and a simpler experimental setup and data analysis. Finally, some suggestions to improve the sensitivity of the experimental setup were made and some technical challenges that need to be overcome to make BBCEAS a widely applicable analytical technique were identified.

3.6. References

[1] Fiedler, S. E. Review of scientific instruments, 76 (2005) 023107-1-023107.

[2] Paldus, B. A.; Kachanov, A. A. Canadian Journal of Physics, 83 (2005) 975.

[3] Mazurenka, M. Annual reports on the progress of chemistry. Section C, Physical chemistry, 101 (2005) 100.

[4] Berden, G.; Peeters, R.; Meijer, G. International reviews in physical chemistry, 19 (2000) 565.

[5] Busch, K. W; Busch, M. A (Eds.), Cavity-Ringdown Spectroscopy An untratrace-Absorption measurement technique; Oxford University Press, USA, 1999, p. 269.

[6] Engeln, R.; Berden, G.; Peeters, R.; Meijer, G. Review of scientific instruments, 69 (1998) 3763.

[7] Ball, S. M.; Langridge, J. M.; Jones, R. L. Chemical Physics Letters, 398 (2004) 68.

[8] Langridge, J. M.; Ball, S. M.; Jones, R. L. The Analyst, 131 (2006) 916.

[9] Berden, G; Peeters, R; Meijer, G. Chemical Physics Letters, 307 (1999) 131.

[10] Barry, H. R.; Corner, L.; Hancock, G.; Peverall, R.; Ritchie, G. A. D. Chemical Physics Letters, 333 (2001) 285.

[11] Peeters, R.; Berden, G.; Ólafsson, A.; Laarhoven, L. J. J.; Meijer, G. Chemical Physics Letters, 337 (2001) 231.

[12] Xu, S; Sha, G; Xie, J; Xu, S.Review of scientific instruments, 73 (2002) 255.

[13] Alexander, A. J.Chemical Physics Letters, 393 (2004) 138.

[14] Snyder, K. L.; Zare, R. N. Analytical Chemistry, 75 (2003) 3086.

[15] Bechtel, K. L.; Zare, R. N.; Kachanov, A. A.; Sanders, S. S.; Paldus, B. A. Analytical Chemistry, 77 (2005) 1177.

[16] Fiedler, S. E.; Hese, A.; Ruth, A. A. Chemical Physics Letters,371(2003) 284.

[17] van der Sneppen, L.; Wiskerke, A.; Ariese, F.; Gooijer, C.; Ubachs, W. Analytica Chimica Acta, 558 (2006) 2.

[18] McGarvey, T.; Conjusteau, A.; Mabuchi, H. Optics express, 14 (2006) 10441.

Chapter Quatre

4.0. Application of Broadband Cavity Enhanced Absorption Spectroscopy (BBCEAS) to High Performance Liquid Chromatography (HPLC)

High pressure, or high performance liquid chromatography (HPLC), is one of the most important analytical methods for the separation of a mixture of compounds. Its many uses include, checking the purity of compounds, monitoring changes during scale up, revision of synthetic procedures, evaluating new formulations, and running control/assurance of the final product in numerous area of research and industry [1].

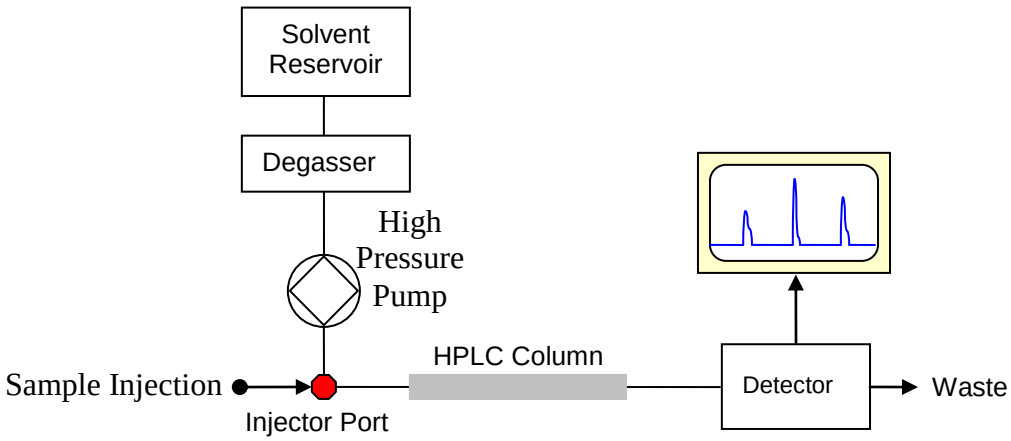

Figure 4.1: Schematic of a typical HPLC setup

A simplified schematic of a typical HPLC setup is shown in figure 4.1. Briefly, a solvent is degassed and pumped through the system using a high pressure pump. Typical flow rates in conventional columns are 1 ml min^{-1} [2]. The liquid sample mixture is usually injected into the LC column though the injection valve of the injection port using a syringe. The sample is carried by the flowing solvent through the column where the separation occurs as the sample flows across the stationary phase. The analytes can be detected by a variety of techniques based on physical characteristics such as absorption, fluorescence,

conductivity and refractive index. The major components in an HPLC setup; solvent (mobile phase), column (stationary phase) and detectors are discussed in turn below.

Before discussing the major parts, it should be noted that there are two main variants in use in HPLC namely, ‘Normal phase HPLC’ and ‘Reversed phase HPLC’ and they depend on the relative polarity of the solvent and the stationary phase. The mobile phase in HPLC refers to the solvent which is continuously applied to the stationary phase (column). When a sample solution is injected into the mobile phase of an assay through the injector port, the mobile phase acts as a carrier for the sample solution. As the sample solution flows through the column with the mobile phase, the components of that solution migrate according to the non-covalent interactions of the compound with the column [1, 3]. The chemical interactions of the mobile phase and sample, with the column, determine the degree of migration and separation of components contained in the sample. Samples which have stronger interactions with the mobile phase tend to elute from the column faster and thus have a shorter retention time, while those that show stronger interactions with the stationary phase elute more slowly. The mobile phase can be altered in order to manipulate the interactions of the sample and the stationary phase. The two most commonly used type of elution are isocratic and gradient.

In isocratic chromatography all conditions and settings of the separation are held constant. That is, the compounds are eluted using a constant mobile phase. This type of chromatography is both simple and inexpensive, but with poor resolution of some compounds and also separation may not be achieved in a reasonable amount of time. In gradient chromatography one or more of the parameters is varied. The most typical gradient is a continuous variation of the mobile phase composition from low elution to high elution strength [3].

There are several equations that can be use to describe isocratic and gradient elution [1-3]:

Table 4.1: Equations for isocratic and gradient elution

Where: t_g – Retention time; t_o – Column hold up time; k' – Capacity or retention factor; σ_g – Bandwidth; N – Number of theoretical plates; V_m – column hold up volume; R_s – Resolution; F – phase ratio; α – Separation factor; Φ – Volume fraction; S – gradient elution constant; t_G – gradient time; $\bar{k}$ - gradient retention factor; k_o – value of k at the start of gradient elution.

	Equations for isocratic elution	Equations for gradient elution
Retention Time (s)	$t_g = t_0 k' + t_0$	$t_g = t_0 \bar{k} \log\left(\frac{2.3k_0}{\bar{k}}\right)$
Bandwidth (ml)	$\sigma_g = V_m\left(1+k'\right)N^{-\frac{1}{2}}$	$\sigma_g = \frac{V_m(1+\bar{k})N^{-\frac{1}{2}}}{2}$
Resolution ($\Delta t_R/4\sigma$ or $\Delta t_g/4\sigma_g$)	$R_s = \left[(1/4)(\alpha-1)N^{\frac{1}{2}}\right]\left[\frac{k'}{\left(1+k'\right)}\right]$	$R_s = \left[(1/4)(\alpha-1)N^{\frac{1}{2}}\right]\left[\frac{\bar{k}}{\left(1+\bar{k}\right)}\right]$
Capacity Factor	$k' = \frac{(t_R - t_0)}{t_0}$	$\bar{k} = \frac{t_G}{\Delta\Phi S t_0} = \frac{t_G F}{\Delta\Phi S V_m}$

The stationary phase (column) is one of the most important components of the HPLC because the separation of the sample components is achieved when the components pass through the column. Several types of column are available and they are generally classified according to their function.

i) Normal phase column

The retention in this type of column is governed by the interaction of the polar parts of the stationary phase and solute. The packing must be more polar than the mobile phase with respect to the sample for retention to occur in the normal phase. Therefore, the stationary phase is usually silica. Typical mobile phases are relatively non polar solvents such as hexane, methylene chloride, chloroform and diethyl ether.

ii) Reverse phase column

The packing material in this type of column is relatively nonpolar and the solvent is more polar when compared to the sample. Retention is due to the interaction of the nonpolar components of the solutes and the nonpolar stationary phase. Typical stationary phases are nonpolar hydrocarbons, waxy liquids, or bonded hydrocarbons. The stationary phase is generally made up of hydrophobic alkyl chains ($-CH_2-CH_2-CH_2-CH_3$) that interact with the analyte. There are three common chain lengths, C4, C8, and C18 and the solvents are usually polar aqueous-organic mixtures such as methanol-water or acetonitrile-water [1, 2, 4].

iii) Size exclusion column

Molecules are separated according to their size in this type of column. Small molecules penetrate into the pores within the packing while larger molecules only partially penetrate the pores. Hence larger molecules elute before the smaller once.

iv) Ion exchange column

In this type of column the components are separated based upon the attractive ionic forces between molecules carrying charged groups of opposite charge to those charges on the stationary phase. Separations are made between a polar mobile phase, usually water containing salts or small amounts of alcohols, and a stationary phase containing either acidic or basic fixed sites.

A large number of detection methods are available for identifying the separated solutes. Some of the conventional detection methods include UV-visible absorption, fluorescence and conductivity detection. More recent detection methods include, Fourier transform infrared (FTIR), mass spectrometry and laser induced fluorescence [2, 4]. The most widely used detection technique for HLPC is UV-visible absorption spectroscopy. This is probably because many compounds have an absorption spectrum in this part of the electromagnetic spectrum; also the technique is relatively simple and reasonably sensitive. However, the sensitivity is poor when compared to detection techniques such as fluorescence or mass spectrometry which have detection limits several orders of magnitude lower but are either not as widely applicable (fluorescence) or are considerably more expensive (mass spectrometry). As has been described in chapter 2, cavity techniques based on CRDS and CEAS have lead to a considerable improvement in the sensitivity of

absorption spectroscopy through an increase in the effective pathlength of measurement. Most previous cavity based studies have reported measurements on gas phase species [5-10], as the scattering and absorption losses are significantly lower than measurements for liquid and solid phase species, and thus greater number of passes through the sample can be achieved. In principle however, there are more species of interest for study in the liquid phase. Given the importance of HPLC as an analytical tool, the application of cavity based techniques to potentially enhance the sensitivity of UV-visible detection is a logical test case for the technique. Consequently, of the few liquid phase cavity studies reported to date, a large fraction have involved the application of liquid phase CRDS to high performance liquid chromatography (HPLC) systems [5, 11-15]. Snyder *et al*. [11] constructed a custom built flow cell which had the correct Brewster's angle at both the air / glass and glass / liquid interfaces to minimise reflection losses. The system developed by Snyder *et al*.[11] used a Nd:YAG laser operating at 10 Hz with nanosecond timescale pulse duration as the light source, whilst a photomultiplier tube was used for detection. Their analyte was studied at a wavelength of 470 nm. Bechtel *et al*. [12] in a follow up study employed a compact doubled-diode cw-laser operating at 488 nm as light source with the Brewster's angle flow cell. The output was monitored by a photodiode. van der Sneppen *et al*.[13] exploited the advantage of a liquid only cavity in which mirrors were clamped leak tight around a 2 mm silicon rubber spacer such that surfaces or Brewster's angles inside the cavity needed not to be considered. The light source used in this study was a Nd:YAG laser operated at a wavelength of 532 nm with a repetition rate of 10 Hz and 5 ns pulse duration. The detection system consisted of a photodiode coupled to an amplifier. The system also required an auxiliary photodiode to trigger the detection system. van der Sneppen *et al*.[14] in a later study, also explored using a 1 cm cuvette placed inside a ring down cavity at normal incidence geometry for LC-CRDS measurements in the ultraviolet region. This system had a Nd:YAG laser as the light source, but it was operated at 355 nm with a photodiode detector. Further measurements at 273 nm were also made using a frequency doubled dye laser as the light source. It should be noted that all the previous studies have used CRDS as the technique of choice for measurement. As discussed previously,

CRDS allows the absorption coefficient of the analyte to be directly measured whilst CEAS measurements first require a calibration, also in the gas phase CRDS measurements tend to be more sensitive than comparable CEAS measurements. However CRDS suffers from the disadvantages that the detection scheme is complex and expensive compared to CEAS due to the requirement to measure ringdown events on the μs to high ns timescale [10, 16]. This requirement is pushed to even shorter timescales by experimental schemes which have short cavity lengths such as that used by van der Sneppen *et al*.[15] and the inherent high losses present in liquid phase studies. These limit the range of analyte concentrations which can be studied before the ringdown time becomes too short to measure. In addition all the previous HPLC studies with CRDS detection have made measurements at a single wavelength. This was to emulate HPLC UV-visible detectors which operated at a single wavelength such as those based on a mercury lamp operating at 254 nm. However, this type of detection scheme suffers from a number of disadvantages, namely that the analyte under study can only be detected if it has an absorbance at the detection wavelength, also co-eluting analytes which absorb at the detection wavelength cannot be distinguished. These problems have been largely addressed by modern UV-visible detection schemes in commercial HPLC systems. These are based on multiplex detection at a range of wavelengths using a broadband UV-visible light source (typically a combination of a deuterium lamp and a tungsten halogen lamp) and a diode array detector, coupled to a spectrograph. Using this approach an analyte can be detected provided it has an absorbance in the range 200 – 1000 nm (usually limited by the output range of the light source and the sensitivity/working range of the spectrograph and diode array detector). Even analytes which co-elute can be distinguished provided they have sufficiently different UV-visible absorption spectra.

It became apparent during the course of our liquid phase BBCEAS studies that BBCEAS detection applied to a HPLC system would be analogous to the modern day UV-visible detection scheme used in HPLC systems. It would overcome the problems associated with single wavelength detection mentioned above and also address some of the problems inherent with CRDS measurements such as the requirement for complex, fast and expensive

detection schemes, a laser light source and experimental problems with short cavity lengths. The aims of our study were to demonstrate the application of BBCEAS detection to an HPLC system, measure the sensitivity of the setup, which would allow comparison with the previous CRDS based detection studies and also make a direct comparison with a modern commercial HPLC system which used UV-visible detection.

4.1. Experimental setup and methodology for HPLC-BBCEAS

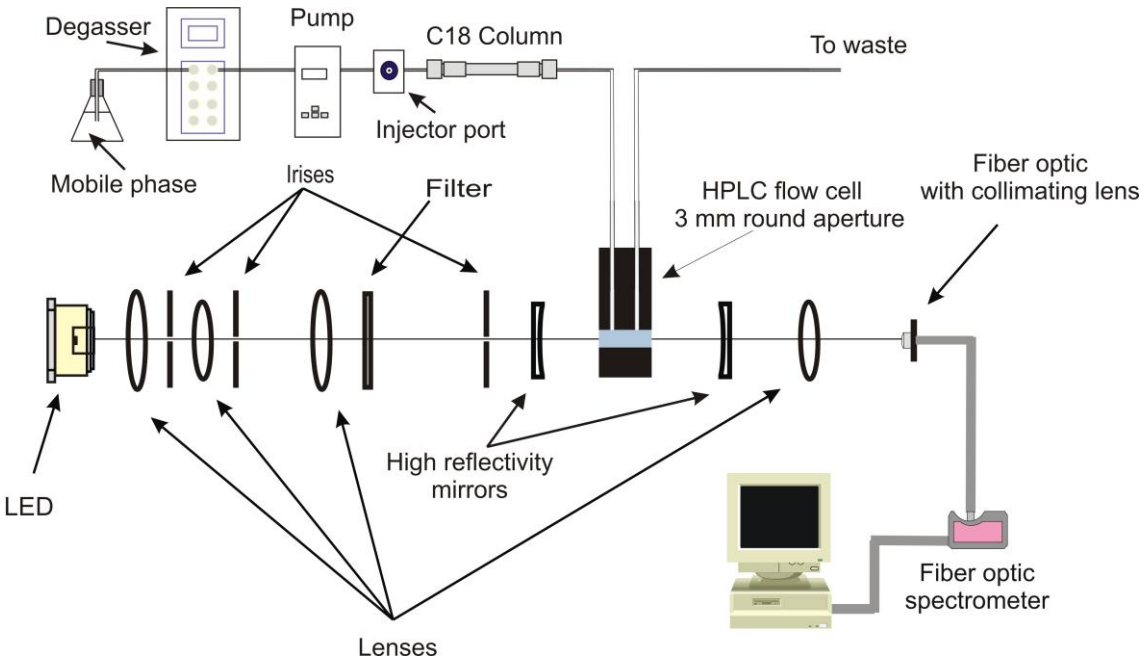

Figure 4.2: A scheme of the experimental setup for liquid-phase HPLC-BBCEAS measurements

A schematic of the experimental setup is shown in figure 4.2. The optimum geometry of the lenses was difficult to calculate and so the optical setup was empirically determined by trial and error to achieve the maximum light intensity exiting the cavity. At best ~1% of the LED output remained after collimation. The narrow beam from the white LED (Luxeon O star) was coupled into the 5 cm optical cavity formed by two plano-concave $R \geq 0.99$ mirrors with a diameter of 25 mm, radius of curvature (roc) = -50 cm, with a bandwidth ~420 – 670 nm (Layertec, Germany). The 1 cm pathlength HPLC cell (Starna UK) had

quartz windows with a 3 mm diameter circular aperture and a nominal volume of 70 μl.

The typical alignment procedure for the cavity involved firstly alignment of the cavity without the HPLC cell by maximising the amount of light which leaked out, hence maximising the output of the LED reaching the spectrograph at a given integration time by iterative adjustment of the front and back cavity mirrors. The HPLC cell which was mounted on a modified standard 1 inch mirror mount was then placed in the cavity with a blank solvent solution (typically acetonitrile). This resulted in a large decrease in the intensity of light reaching the spectrograph due to interface losses at the 3 mm windows and also from the solvent. The integration time was increased appropriately to ensure the signal from the LED was significantly above the dark noise level, but not high enough to saturate the detector. Typical integration times for the $R \geq 0.99$ mirror set with the white LED were ~240 ms. The HPLC cell was then rotated about both the horizontal and vertical plane to maximise the intensity reaching the detector. The front and back cavity mirrors were then further adjusted iteratively to maximize the output reaching the detector. The HPLC cell was coupled to a Genesis C18 (4 μm particle size 150mm x 4.6 mm; Alltech Associates, Inc) column which was attached to a pump and degasser (Knauer) and injection port with a 20 μl loop. The mobile phase used was 85% acetonitrile (CH_3CN) HPLC grade (Fisher Scientific, UK), 14.9% HPLC water (H_2O) (Fisher Scientific, UK) and 0.1 % formic acid (HCOOH) (Fisher Scientific, UK), under isocratic elution at a flow rate of 1 ml min^{-1}. The test samples were injected through the injector port, ensuring minimum disturbance to the optimum alignment. The light leaking out of the cavity was focussed by a 50 mm focal length lens onto the entrance of a 600 μm diameter, 1 m length, 0.22 numerical aperture quartz fibre (Thorlabs U.K). This was connected to the entrance slit of the spectrograph by an SMA905 fibre connection. The output of the cavity was monitored by the same spectrograph described in chapter 3 section 3.13 and spectral data was acquired using the Avasoft software. After introduction of the analyte through the injection port, data acquisition was manually started for each run. These data were then continuously acquired at a sampling rate of approximately one sample point every 3 seconds and streamed to the PC for 3 minutes for each run on the system. The sampling rate arose from a

combination the spectral integration time of ~240 ms and the 10 consecutive spectra recorded for each point. Performance limitation on data throughput was introduced by the hard disk buffer on the PC and resulted in a timing error of about ±0.2 s between each spectrum. These data were then processed using a custom built Excel™ macro (Appendix A). Figure 3 shows representative data collected and processed using Excel™. Each chromatogram consisted of up to 75 data points. These data points represent the peak absorbance of the analyte, which were extracted manually from the full wavelength profile of the given analyte. The inset in figure 4.3 shows representative absorbance profiles for rhodamine 6G collected at their respective sampling time over the wavelength range 450 – 600 nm.

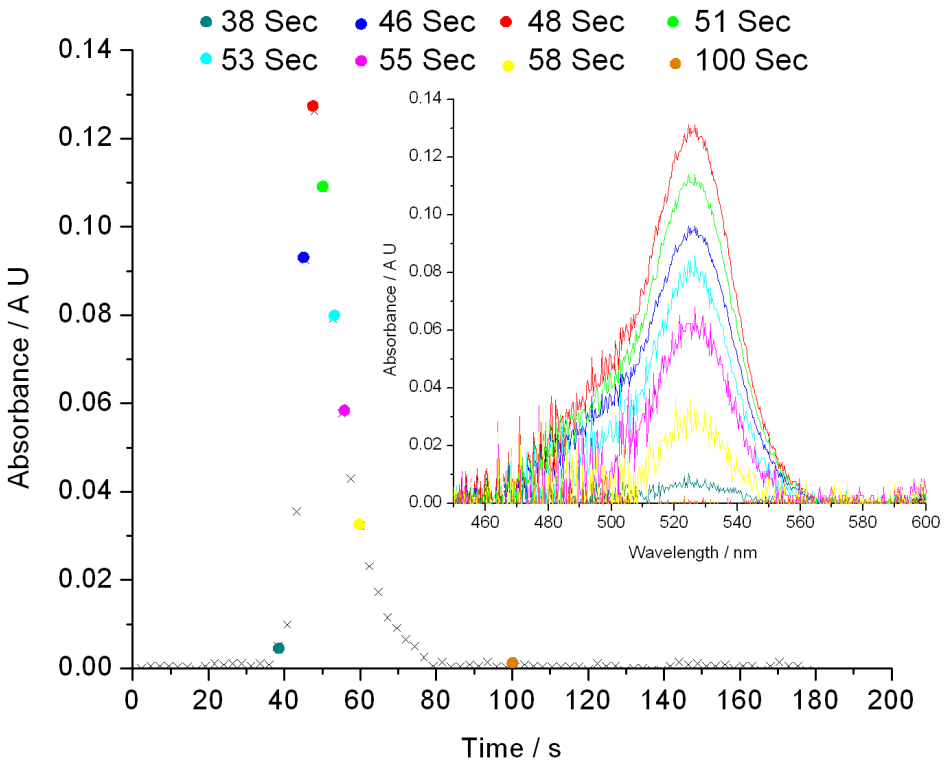

Figure 4.3: Representative chromatogram of rhodamine 6G obtained using the HPLC-BBCEAS setup. The inset shows full absorption profiles at selected times.

4.2. Choice of analytes

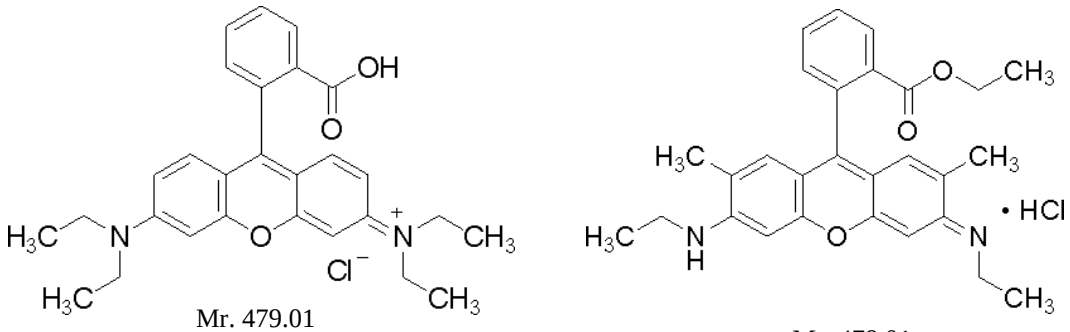

Figure 4.4: Structural formulae of rhodamine 6G and rhodamine B

The two analytes chosen for separation by HPLC were the water tracer laser dye rhodamine 6G (Sigma – Aldrich, UK) and the staining fluorescent dye rhodamine B (Sigma – Aldrich, UK). Figure 4.4 shows the chemical structure of the two analytes whilst figure 4.5 shows the visible spectra of the two analytes in the solvent mixture used for the mobile phase.

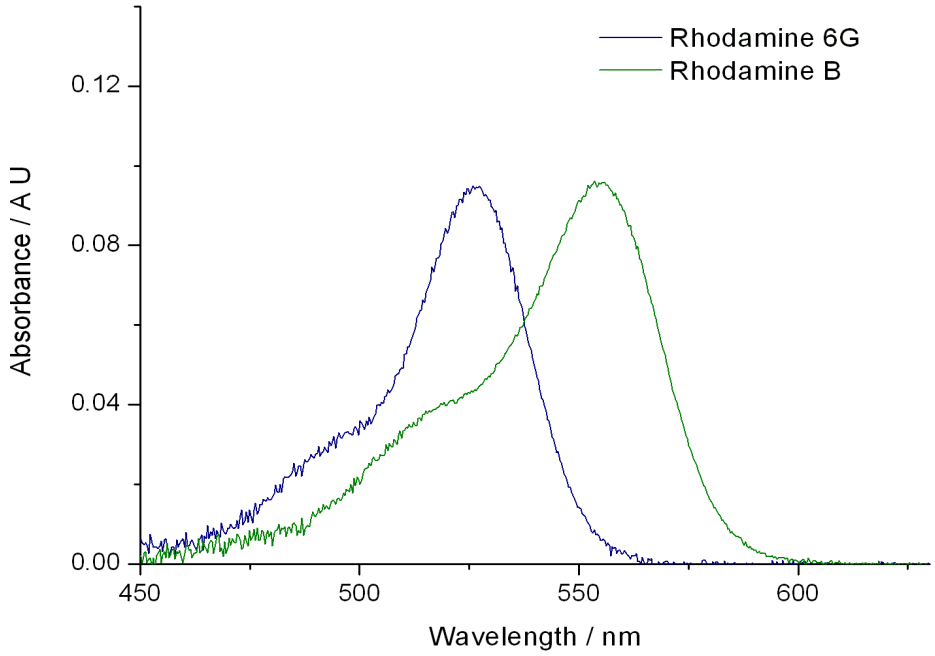

Figure 4.5: Visible spectrum of rhodamine 6G and rhodamine B dissolved in the mobile phase solvent mixture.

It can be seen that the two species have distinctive visible spectra with rhodamine 6G showing a peak absorption at 527 nm whilst that for rhodamine B is at 556 nm (these peaks are shifted from 530 nm and 543 nm respectively when dissolved in ethanol [10]. The rationale for the choice of the two analytes was twofold. Firstly both species had high molar extinction coefficients at their peak absorption wavelengths (see table 4.2) and thus were good test case molecules to obtain the best possible LOD for HPLC-BBCEAS experiments. Secondly both were chemically similar species but had distinctive visible spectra which would mean that they would likely co-elute in an isocratic separation. However, in principle they could be distinguished by their visible spectra. This would allow the construction of an experiment where the advantage of multiplex detection following HPLC could be tested. The mobile phase used was 85% acetonitrile (CH_3CN) HPLC grade (Fisher Scientific, UK), 14.9% HPLC water (H_2O) (Fisher Scientific, UK) and 0.1 % formic acid (HCOOH) (Fisher Scientific, UK).

4.3. Experimental setup and methodology for the commercial HPLC system

Figure 4.6: Photograph of the Perkin Elmer 200 series instrument used in this study

The commercial HPLC system used for comparative measurements was a Perkin Elmer series 200 HPLC instrument as shown in figure 4.6. The unit consisted of an auto sampler with dual syringe system (sample syringe and the

flush syringe). The sample syringe drew up the sample through the needle into the sample loop which had a volume of 20 µl. The sample was then injected into the injection valve port. The flush syringe flushed the sample loop, needle and sample tubing between injections. A Perkin Elmer pump (PE 200 Quaternary Pump) was use to propel the reagent solution through the system. HPLC separations were performed with the same Genesis C18 (4 µm particle size 150mm x 4.6 mm) column (Alltech Associates, Inc), used for the HPLC-BBCEAS experiments.

Samples were chromatographed with a (85% CH_3CN: 14.9% H_2O: 0.1% HCOOH) mobile phase with an isocratic elution for 5 min at a flow rate of 1 ml min^{-1}. 20 µl of the sample solution was analysed under the conditions mentioned above. After separation of the rhodamine dyes by the column, analysis by UV-visible absorption spectroscopy, in the range 200 – 900 nm in a 1 cm pathlength HPLC cuvette was performed using a series 200EP photodiode array detector. Spectral data were collected at a sample rate of 1 s^{-1}.The operation of the HPLC system was controlled by PerkinElmer's TotalChrom® Chromatography Data Systems software, whilst these spectral data generated by the Series 200EP PDA Detector were processed by the IRIS® Spectral Processing Software.

4.4. Results

HPLC-BBCEAS measurements have been performed in a 1 cm cuvette for the dyes rhodamine 6G and rhodamine B, at their peak absorption wavelength, using a white LED and a cavity formed by two high reflectivity $R \geq 0.99$ mirrors. The first series of measurements were made on each dye passing individually through the HPLC-BBCEAS system, to test the performance of the setup. These measurements are summarised in table 4.2 which lists important figures of merit obtained from these data such as the cavity enhancement factor (*CEF*), the LOD obtained both from a linear regression through a plot of concentration versus absorbance and also the standard deviation of noise on a spectrum. The LOD values refer to injected concentrations. Chromatographic broadening by the column means the actual detected concentrations in the cuvette are significantly lower. The sensitivity of the measurement is given by the listed α_{min}

values. The methodology for obtaining these parameters from raw spectral data has been described in detail in chapter 3 section 3.2. The LOD values obtained from the HPLC-BBCEAS measurements are compared with single pass measurements in the HPLC-BBCEAS setup where one of the cavity mirrors had been removed and also the LOD values obtained from measurements in the commercial Perkin Elmer HPLC system. The following section shows representative data used to obtain the LOD values for rhodamine 6G and rhodamine B. This in turn is followed by a description of the results obtained from separation of a mixture of the two dyes using HPLC-BBCEAS.

Table 4.2: A summary of the results obtained in terms of analyte used, the wavelength of measurement, the *CEF* value, the minimum detectable change in absorption α_{min}, the molar extinction coefficient ε at the wavelength of measurement, and the LOD of the analyte.

	Rhodamine 6G (527nm)	**Rhodamine B (556nm)**
Number of passes (*CEF*)	40	45
LOD BBCEAS (nM) Regression method	2.1	2.1
LOD BBCEAS (pM) Spectral method	426	271
α_{min} (cm^{-1})	2.9×10^{-5}	1.9×10^{-5}
LOD Singlepass (nM) Regression method	14	13
LOD Perkin Elmer (nM)	23	21
ε (M^{-1} cm^{-1})	90558	92676

4.4.1. Rhodamine 6G

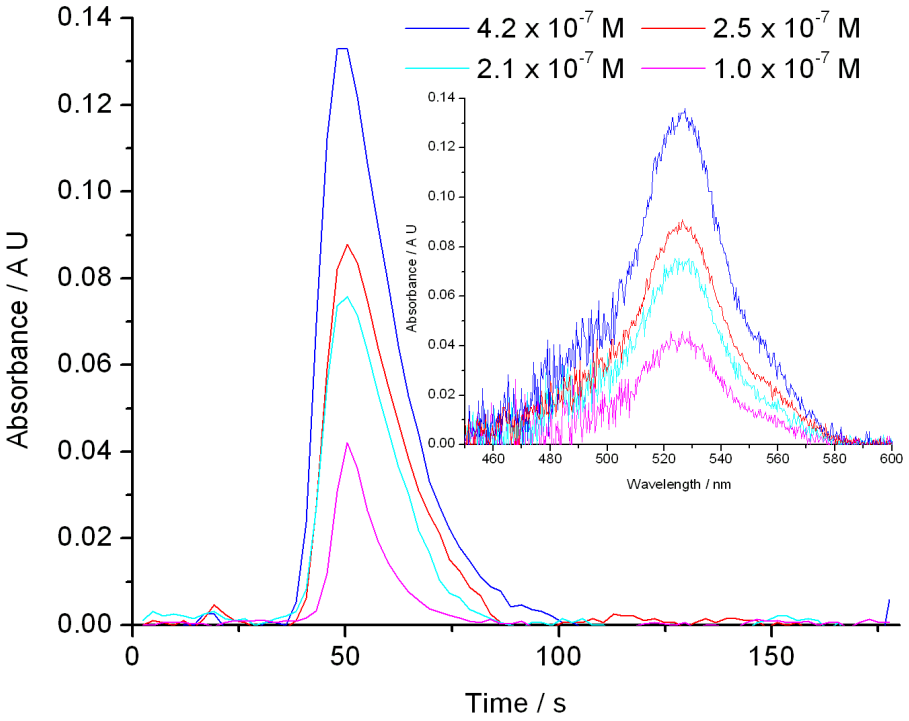

Figure 4.7: Chromatograms of rhodamine 6G measured at 527 nm.
(HPLC-BBCEAS setup, at selected injected concentrations. The inset shows the full absorption spectra of rhodamine 6G at the chromatogram maxima)

The determination of the LOD for rhodamine 6G and rhodamine B required plots of maximum absorbance versus injected concentrations. As described in section 4.1., individual chromatograms for a given injected concentration of analyte were stitched together using an Excel™ macro to extract the absorbance at the peak wavelength for a spectral time series. Figure 4.7 shows a series of chromatograms obtained for injected concentrations of rhodamine 6G, between 1.0×10^{-7} M and 4.2×10^{-7} M. These were obtained by recording the absorbance at the peak wavelength of 527 nm as a function of time. The inset shows the full absorption spectrum recorded between 450 and 600 nm for the peak maximum of each chromatogram. The value of the peak absorbance for each chromatogram was then used in an absorbance versus injected concentration plot to determine the LOD for the given analyte.

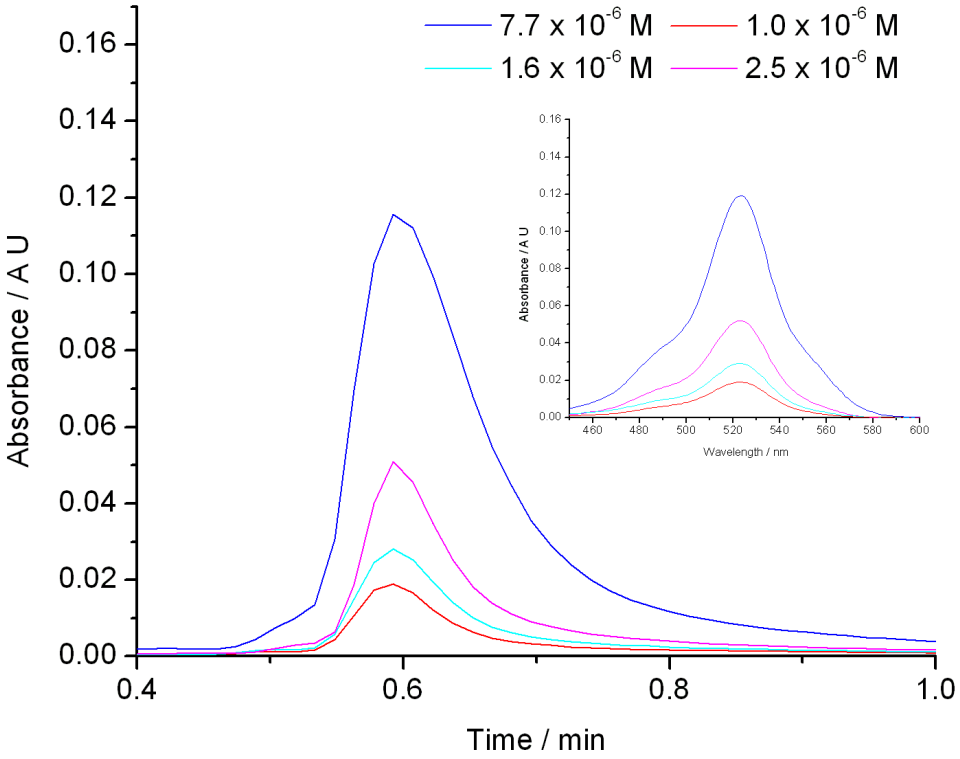

Figure 4.8: Chromatograms of rhodamine 6G measured at 527 nm.
(Using the Perkin Elmer HPLC system, at selected injected concentrations. The inset shows the full absorption spectra of rhodamine 6G at the chromatogram maxima)

Individual chromatograms for a given injected concentration of analyte were obtained from the Perkin Elmer HPLC software and the absorbance at the peak wavelength was extracted from the chromatograms. Figure 4.8 shows a series of chromatograms obtained for injected concentrations of rhodamine 6G, between 1.6×10^{-6} M and 7.7×10^{-6} M. These were obtained by recording the absorbance at the peak wavelength of 527 nm as a function of time. The inset shows the full absorption spectrum recorded between 450 and 600 nm for the peak maximum of each chromatogram. The value of the peak absorbance which represents the peak of the chromatogram was then used in an absorbance versus injected concentration plot to determine the LOD for the given analyte.

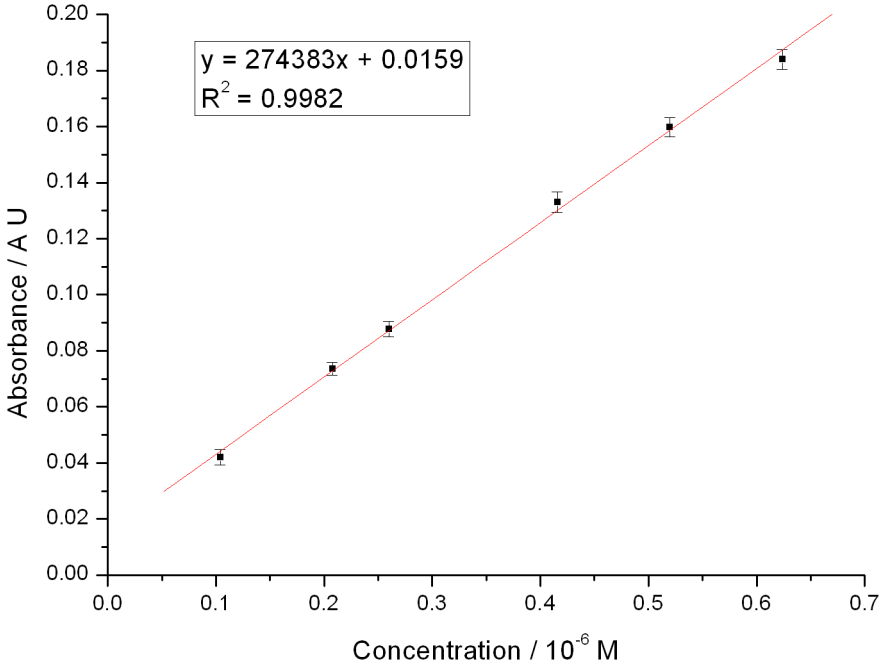

Figure 4.9: Absorbance versus concentration plot for rhodamine 6G.
(Injected concentration range ~0.1 µM to ~0.6 µM, obtained using the white LED and the R ≥ 0.99 mirror set. The line shows the measurements in the linear range from ~0.1 µM to ~0.6 µM. The error bars represent the 1σ error limit of three replicate measurements at each concentration. The equation on the diagram refers to an error-weighted linear fit to the measurements)

Figure 4.9 show the plot of absorbance versus concentration for rhodamine 6G. The rhodamine 6G measurements were made at 527 nm and a range of ~0.1 µM to ~2 µM for the injected concentration of the dye. Three replicate measurements were made at each concentration and the error bars for each concentration represents the standard deviation of the measurements.
The plot shows measurements in the range ~0.1 µM to ~0.6 µM, which exhibit a linear dependence of the absorbance on the concentration. The measurements at higher concentrations, up to ~2 µM were nonlinear. An error-weighted regression through the linear part of the plot yields a straight line (equation of the line is given in figure 4.9) with a correlation coefficient R^2 = 0.9982 and a 1σ error limit for the intercept of 2.48 x 10^{-3}. The LOD can be calculated from the value of the 3σ error limit on the intercept, which produces a concentration of 2.1 nM. The limit of quantification (LOQ) can also be determined from the 10σ

error limit on the intercept and yields a concentration of 6.8 nM. At absorbance values above ~0.2 the plot in figure 4.9 is no longer linear with respect to increasing concentration, but measurements of absorbance values of up to ~0.35 were made without significantly visible increases in the 1σ error limit on three replicate measurements.

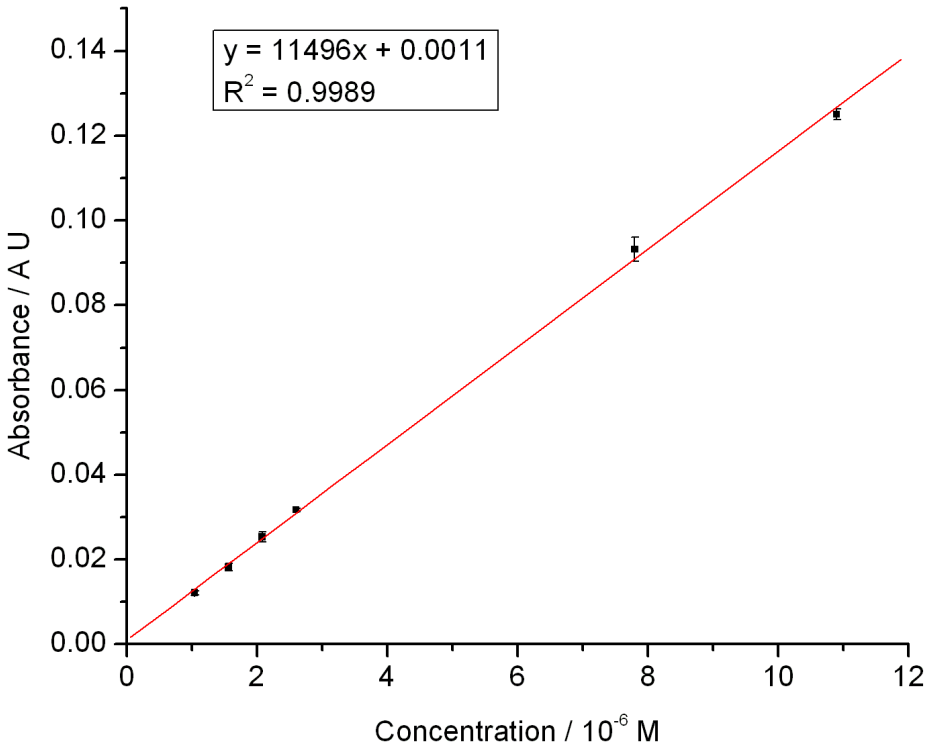

Figure 4.10: Absorbance versus concentration plot for rhodamine 6G.
(Injected concentration range ~1 µM to ~10 µM, obtained using the white LED and with one of the cavity mirrors removed. The error bars represent the 1σ error limit of three replicate measurements at each concentration. The equation on the diagram refers to an error-weighted linear fit to the measurements)

Figure 4.10 show the plot of absorbance versus concentration for rhodamine 6G made in a single-pass measurement where one of the cavity mirrors had been removed. The rhodamine 6G measurements were made at 527 nm and a range of ~1 µM to ~10 µM for the injected concentration of the dye. Three replicate measurements were made at each concentration and the error bars for each concentration represents the standard deviation of the measurements. The line shows a linear dependence of the absorbance on the concentration. An error-weighted regression through the linear part of the plot

yields a straight line (equation of the line is given in figure 4.10) with a correlation coefficient R^2 = 0.9989 and a 1σ error limit for the intercept of 4.2 x 10^{-4}. The LOD can be calculated from the value of the 3σ error limit on the intercept, which produces a concentration of 14 nM. The limit of quantification (LOQ) can also be determined from the 10σ error limit on the intercept and yields a concentration of 46 nM. Absorbance measurements were only taken within the range where there was a linear dependence between absorbance and concentration.

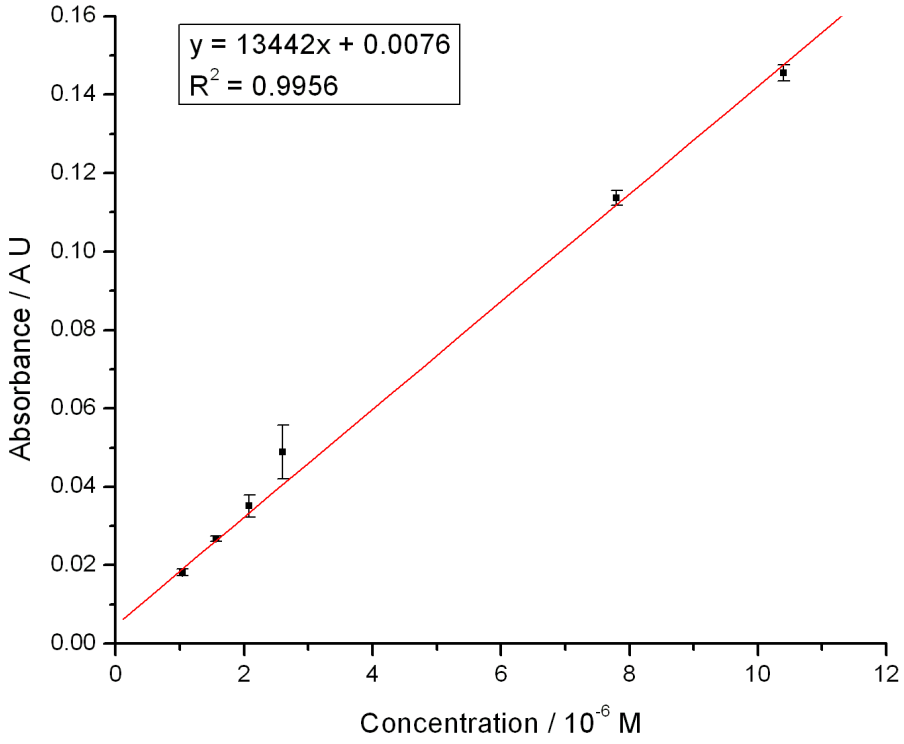

Figure 4.11: Absorbance versus concentration plot for rhodamine 6G.
(Injected concentration range ~1 µM to ~10 µM, obtained using a Perkin Elmer series 200 HPLC system. The error bars represent the 1σ error limit of three replicate measurements at each concentration. The equation on the diagram refers to an error-weighted linear fit to the measurements)

Figure 4.11 show the plot of absorbance versus concentration for rhodamine 6G made using an HPLC (Perkin Elmer 200 series). The rhodamine 6G measurements were made at 527 nm and a range of ~1 µM to ~10 µM injected concentration. Three replicate measurements were made at each concentration and the error bars for each concentration represents the standard

deviation of the measurements. The plot shows a linear dependence of the absorbance on the concentration. An error-weighted regression through the linear part of the plot yields a straight line (equation of the line is given in figure 4.11) with a correlation coefficient R^2 = 0.9956 and a 1σ error limit for the intercept of 6.9 x 10^{-4}. The LOD can be calculated from the value of the 3σ error limit on the intercept, which produces a concentration of 23 nM. The limit of quantification (LOQ) can also be determined from the 10σ error limit on the intercept and yields a concentration of 77 nM. Absorbance measurements were only taken within the range where there was a linear dependence between absorbance and concentration.

4.4.2. Rhodamine B

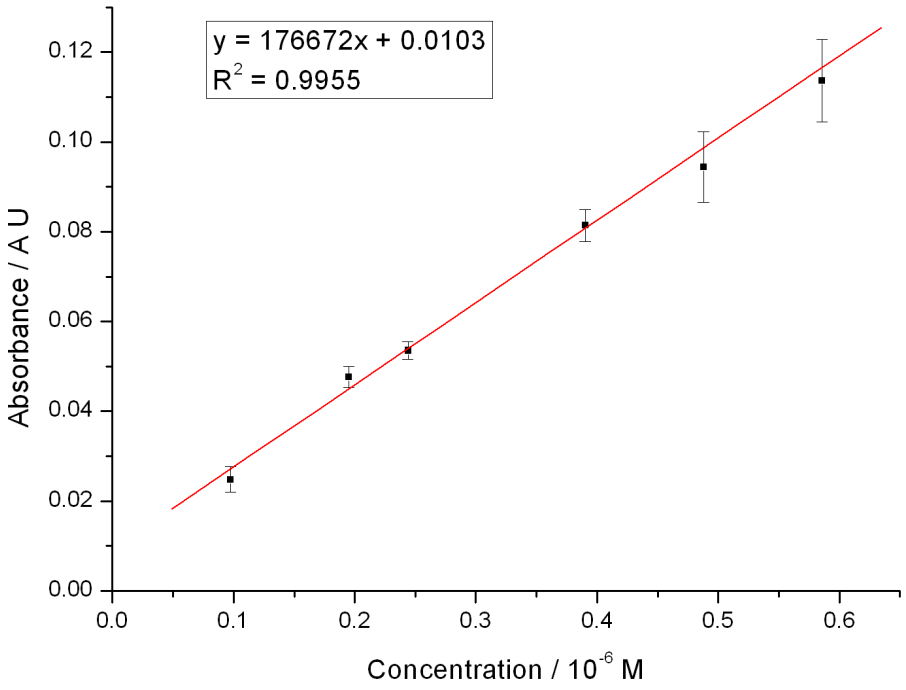

Figure 4.12: Absorbance versus concentration plot for rhodamine B in the BBCEAS setup. (Injected concentration range ~0.1 µM to ~0.6 µM, obtained using the white LED and R ≥ 0.99 mirror set. The line shows the measurements in the linear range from ~0.1 µM to ~0.6 µM. The error bars represent the 1σ error limit of three replicate measurements at each concentration. The equation on the diagram refers to an error-weighted linear fit to the measurements)

Figure 4.12 show the plot of absorbance versus concentration for rhodamine B in the BBCEAS setup. The rhodamine B measurements were

made at 556 nm and a range of ~0.1 µM to ~0.6 µM injected concentration. Three replicate measurements were made at each concentration and the error bars for each concentration represents the standard deviation of the measurements. The plot shows measurements in the range ~0.1 µM to ~0.6 µM, which exhibit a linear dependence of the absorbance on the concentration. The measurements at higher concentrations, up to ~2 µM were nonlinear. An error-weighted regression through the linear part of the plot yields a straight line (equation of the line is given in figure 4.12) with a correlation coefficient R^2 = 0.9955 and a 1σ error limit for the intercept of ~3 x 10^{-3}. The LOD can be calculated from the value of the 3σ error limit on the intercept, which produces a concentration of 2.2 nM. The limit of quantification (LOQ) can also be determined from the 10σ error limit on the intercept and yields a concentration of 7.2 nM. Absorbance measurements were only taken within the range where there was a linear dependence between absorbance and concentration.

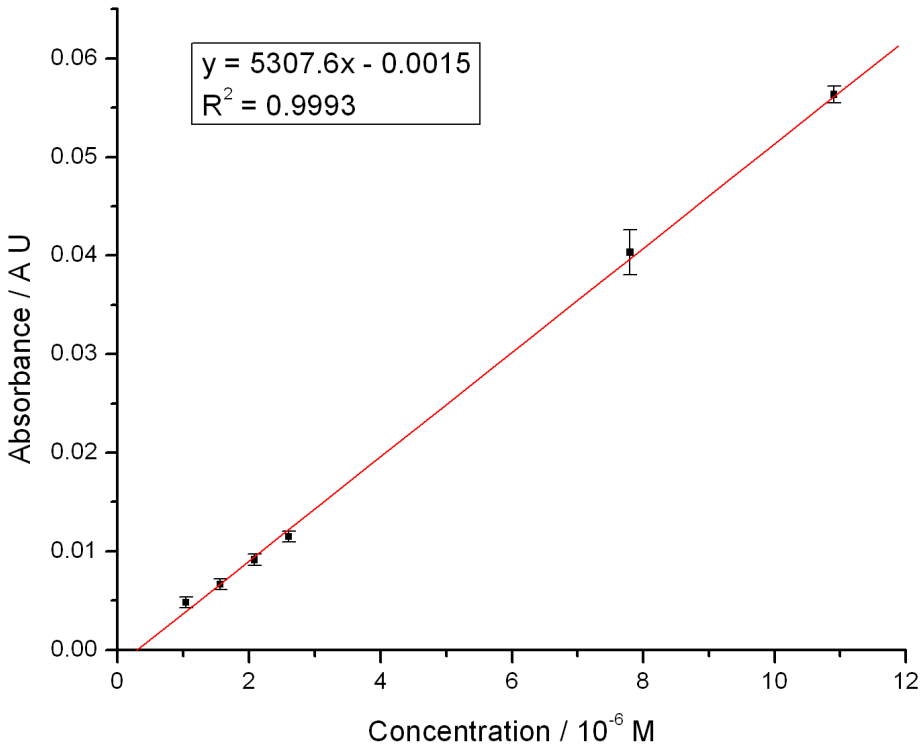

Figure 4.13: Absorbance versus concentration plot for rhodamine B.
(Injected concentration range ~1 µM to ~10 µM, obtained using the white LED and with one of the cavity mirrors removed. The error bars represent the 1σ error limit of three replicate measurements at each concentration. The equation on the diagram refers to an error-weighted linear fit to the measurements)

Figure 4.13 show the plot of absorbance versus concentration for rhodamine B made in a single-pass measurement where one of the cavity mirrors had been removed. The rhodamine B measurements were made at 556 nm and a range of ~1 µM to ~10 µM injected concentration. Three replicate measurements were made at each concentration and the error bars for each concentration represents the standard deviation of the measurements. The plot shows a linear dependence of the absorbance on the concentration. An error-weighted regression through the linear part of the plot yields a straight line (equation of the line is given in figure 4.13) with a correlation coefficient R^2 = 0.9993 and a 1σ error limit for the intercept of 4 x 10^{-4}. The LOD can be calculated from the value of the 3σ error limit on the intercept, which produces a concentration of 13 nM. The limit of quantification (LOQ) can also be determined from the 10σ error limit on the intercept and yields a concentration

of 43 nM. Absorbance measurements were only taken within the range where there was a linear dependence between absorbance and concentration.

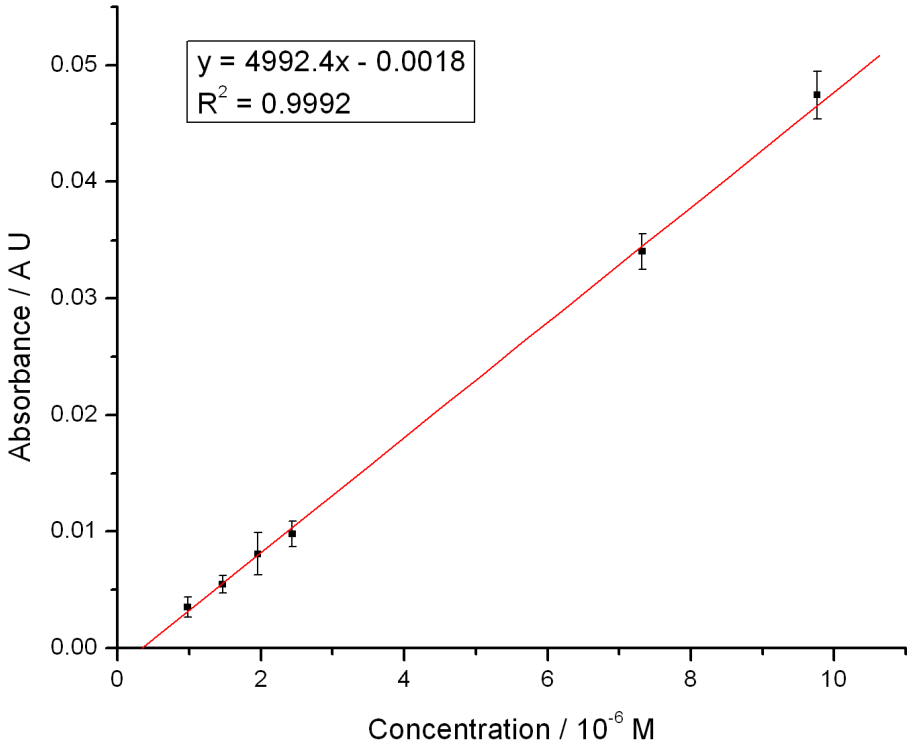

Figure 4.14: Absorbance versus concentration plot for rhodamine B.
(Injected concentration range ~1 µM to ~10 µM, obtained using a Perkin Elmer series 200 HPLC system. The error bars represent the 1σ error limit of three replicate measurements at each concentration. The equation on the diagram refers to an error-weighted linear fit to the measurements)

Figure 4.14 show the plot of absorbance versus concentration for rhodamine B made using an HPLC (Perkin Elmer 200 series). The rhodamine B measurements were made at 556 nm and a range of ~1 µM to ~10 µM injected concentration. Three replicate measurements were made at each concentration and the error bars for each concentration represents the standard deviation of the measurements. The plot shows a linear dependence of the absorbance on the concentration. An error-weighted regression through the linear part of the plot yields a straight line (equation of the line is given in figure 4.14) with a correlation coefficient R^2 = 0.9992 and a 1σ error limit for the intercept of 6.46 x 10^{-4}. The LOD can be calculated from the value of the 3σ error limit on the intercept, which produces a concentration of 21 nM. The limit of quantification

(LOQ) can also be determined from the 10σ error limit on the intercept and yields a concentration of 70 nM. Absorbance measurements were only taken within the range where there was a linear dependence between absorbance and concentration.

4.4.3. Discrimination of co-eluting substances using HPLC-BBCEAS

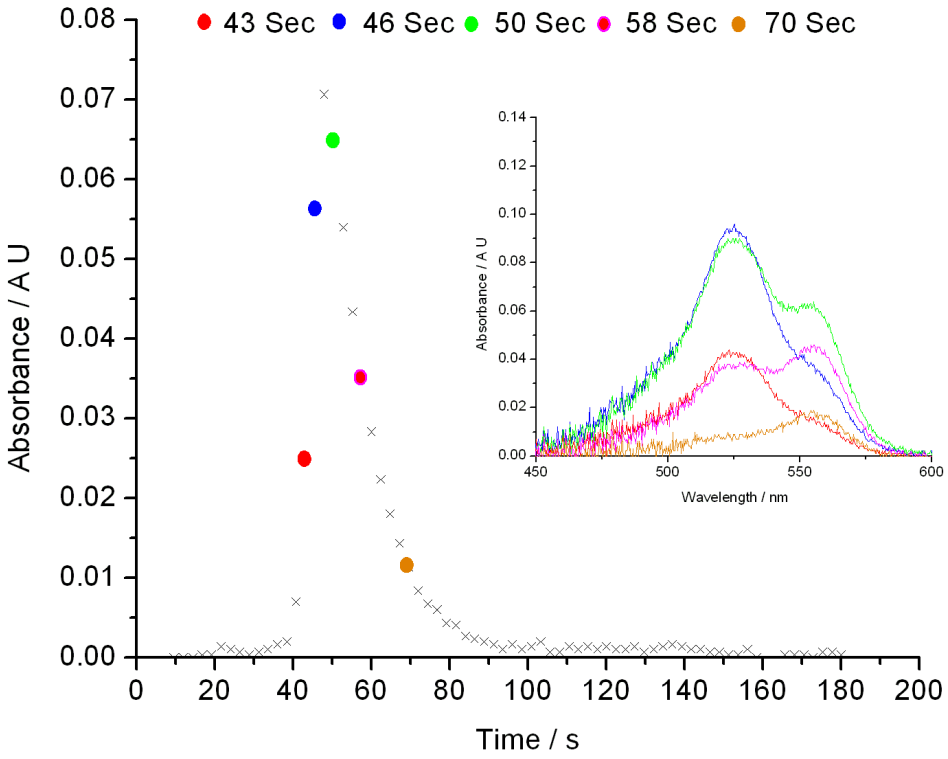

Figure 4.15: Chromatogram compiled from BBCEAS data collected at 541 nm for rhodamine 6G and rhodamine B.

To simulate conditions under which multiplex detection offers a clear advantage over single wavelength detection, a dye mixture of rhodamine 6G and rhodamine B was analysed using the BBCEAS setup. The injected concentrations of the two dyes were 2.6×10^{-7} M and 2.4×10^{-7} M respectively. Under the isocratic conditions applied for the HPLC-BBCEAS experiment, the dyes nearly co-eluted. Figure 4.15 shows the chromatogram plot of absorbance versus time for rhodamine B and rhodamine 6G made in a multipass

measurement with $R \geq 0.99$ cavity mirrors. Absorbance spectra were recorded for ~180 s at a sample rate of approximately one sample point every three seconds using the spectrometer software. The chromatogram was then complied using Excel™ and the absorbance data at 541nm wavelength, as described in section 4.1.

541 nm was chosen as the wavelength for constructing the chromatogram as it was approximately the midpoint between the peak absorption wavelengths of the two analytes. The inset shows representative absorption spectra at 43, 46, 50, 58 and 70 seconds recorded between 450 and 600 nm. A similar comparative experiment was performed on the commercial Perkin Elmer HPLC system.

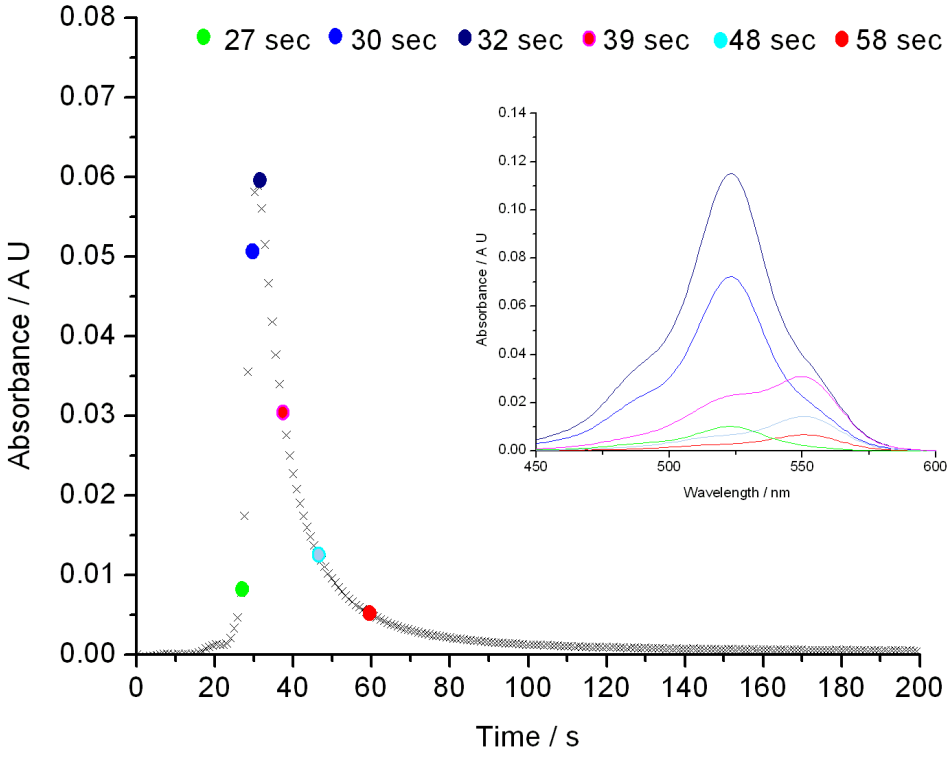

Figure 4.16: Chromatogram compiled from Perkin Elmer HPLC data collected at 541 nm for rhodamine 6G and rhodamine B.

A dye mixture of rhodamine 6G and rhodamine B was analysed using the detection system of the Perkin Elmer HPLC setup. The injected concentrations of the two dyes were in the same ratio to that used for the HPLC-BBCEAS set - up. Under the isocratic conditions applied for the HPLC experiment, the dyes

nearly co-eluted. Figure 4.16 shows the chromatogram plot of absorbance versus time for rhodamine B and rhodamine 6G. The data for the chromatogram was obtained from the HPLC software. As for the HPLC-BBCEAS setup 541 nm was chosen as the wavelength for recording the chromatogram as it was approximately the midpoint between the peak absorption wavelengths of the two analytes. The inset shows representative absorption spectra at 27, 30, 32, 39, 48 and 58 seconds recorded between 450 and 600 nm.

These spectral data can also be represented in the form of a contour plot, where the x axis represents time, the y axis represents wavelength and a colour code is used to represent absorbance intensity. This type of plot can be useful in the visualisation of analytes which nearly co-elute.

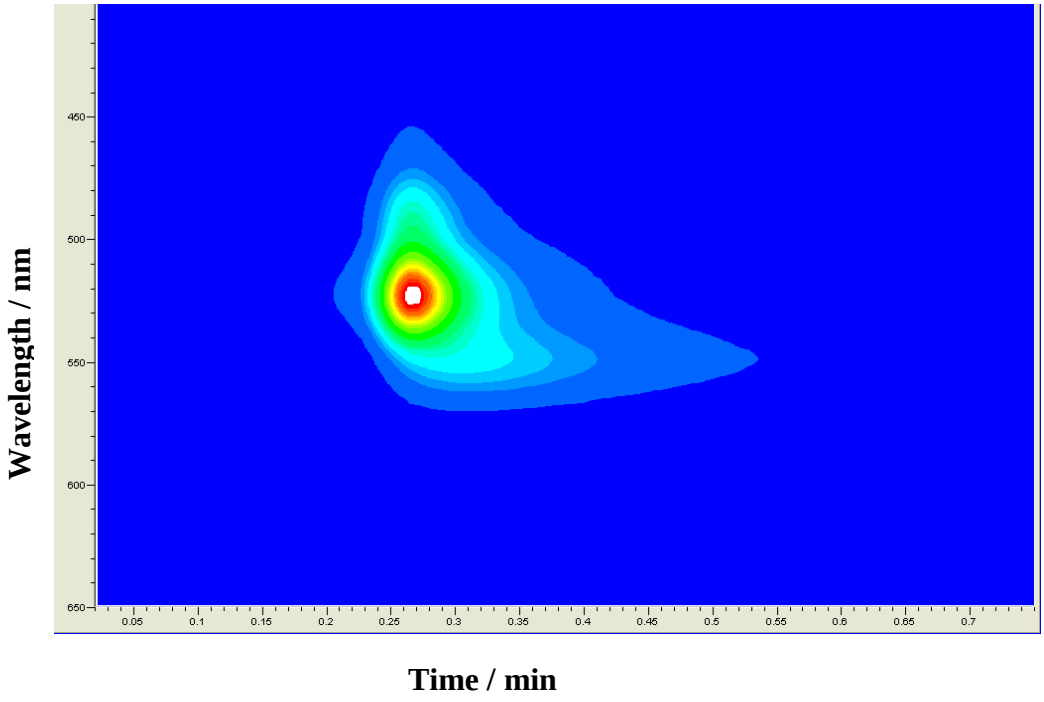

Figure 4.17: Contour plot for rhodamine B and rhodamine 6G dye mixture.

Figure 4.17 shows a contour plot for a mixture of rhodamine 6G and rhodamine B, which was chromatographed using the commercial Perkin Elmer HPLC system.

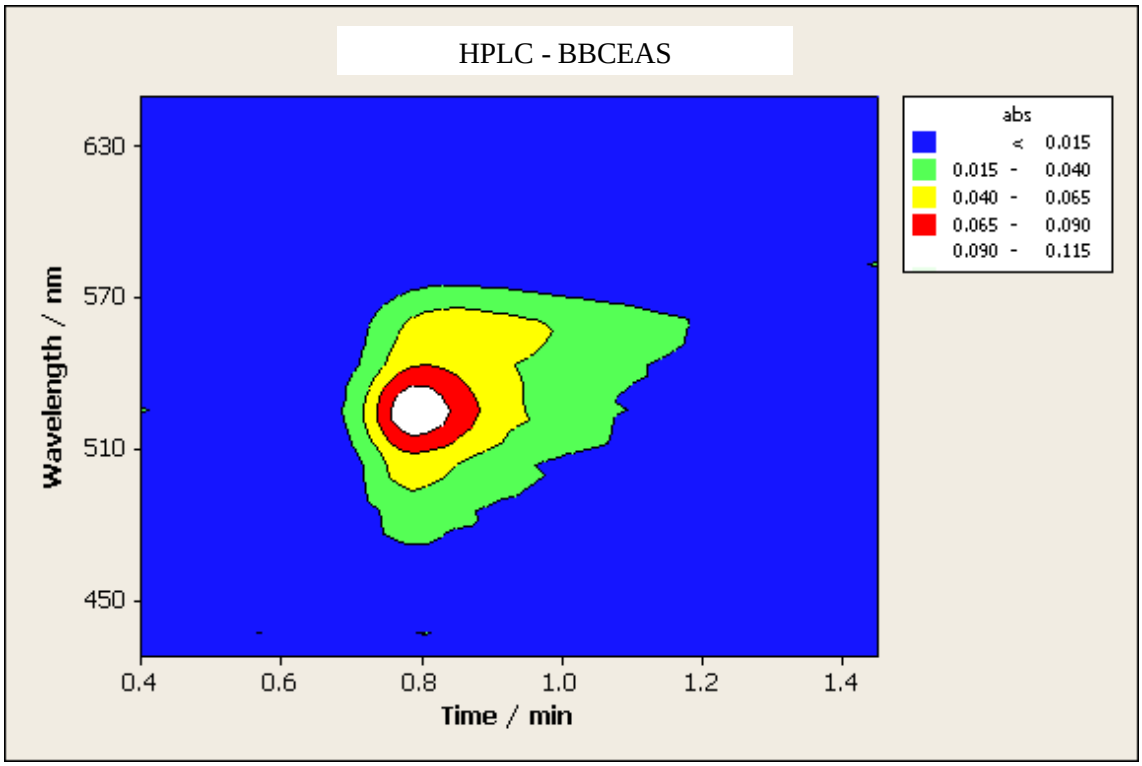

Figure 4.18: Contour plot for rhodamine B and rhodamine 6G dye mixture for data obtain by the HPLC- BBCEAS system.

Figure 4.18 shows a contour plot obtained from spectral data collected from the HPLC- BBCEAS system when a dye mixture of rhodamine 6G and rhodamine B was injected though the system.

4.5. Discussion

The first reported application of BBCEAS detection to an HPLC system has been demonstrated by this study. Furthermore the application of BBCEAS has allowed the identification of co-eluting analytes to be shown, which again represents the first time this has been reported for the application of cavity based techniques to HPLC. It is pertinent to firstly discuss some of the figures of merit obtained from this study and then make a detailed comparison with the previous HPLC-CRDS studies and finally conclude with some suggestions on how the experimental setup could be improved.

4.5.1. Comparison of figures of merit obtained from this study

The main figures of merit obtained were the *CEF* value, α_{min} and the LOD for the 2 analytes, as listed in table 4.2. Comparative LOD values for a single pass measurement and also a commercial HPLC system were also obtained. The *CEF* values of 40 and 45 for rhodamine 6G and rhodamine B respectively are consistent with the values obtained previously from our studies on a 2 mm cuvette placed in a cavity with $R \geq 0.99$ mirrors chapter 3 (section 3.3). Given that the setup of the optical detection is essentially the same aside from a longer 1 cm pathlength cuvette; these values are to be expected. The slight difference in *CEF* values between rhodamine 6G and rhodamine B probably arises as a result of the variation in reflectivity of the cavity mirrors with wavelength as has been discussed previously in chapter 3 (section 3.4.), in relation to some of the results obtained with the 2 mm cuvette. The *CEF* values are limited by scattering losses from the cuvette of ~1×10^{-2} per pass. This value implies that the *CEF* values for the current experimental setup cannot be improved significantly by simply using higher reflectivity mirrors and that the $R \geq 0.99$ mirrors used in this study are close to the optimum mirror reflectivity for maximising the *CEF* value whilst also allowing sufficient transmission through the cavity. The scattering losses from the cuvette could be reduced by 'superpolishing' the surfaces [14] . This would allow the *CEF* to be improved by

about a factor of ten when using appropriate higher reflectivity mirrors, but would also add extra expense to the experimental setup which in its present incarnation benefits from the use of standard off the shelf HPLC cuvettes.

The α_{min} value is a measure of the sensitivity of the experiment and figures of 2.9×10^{-5} cm^{-1} and 1.9×10^{-5} cm^{-1} were obtained for the measurements on rhodamine 6G and rhodamine B, respectively. The difference between the two analytes arises from the variation in the intensity output of the white LED as a function of wavelength (figure 2.3). The photon flux at 556 nm is significantly higher than that at 527 nm (the wavelength of measurement for the two analytes). Thus to maintain approximately the same photon count level for the two analytes at their peak absorption wavelengths the integration time on the CCD spectrometer has to be increased for the rhodamine 6G measurements relative to those for rhodamine B. As discussed in chapter 3 (section 3.4) this results in an increase in dark noise from the uncooled CCD detector which manifests itself in increased baseline noise in the absorption spectrum and hence a higher α_{min} value relative to rhodamine B, as this is determined from the 1σ noise on the absorption spectrum. The α_{min} values can also be compared with our earlier measurements in a 2 mm cell using essentially the same experimental setup chapter 3 (section 3.1.). The lowest α_{min} value obtained was 5.1×10^{-5} cm^{-1} for measurements on brilliant blue-R at 630 nm using a red LED and the $R \geq 0.99$ mirror set. Given the base pathlength for the current study is five times longer, one would expect based on simple scaling, for the α_{min} value to be five times smaller, i.e. $\sim 1 \times 10^{-5}$ cm^{-1}. The best value obtained for the HPLC-BBCEAS measurements is however, 1.9×10^{-5} cm^{-1}. The reason for the discrepancy is most probably because a red LED was used for the measurements on the 2 mm cuvette. These have a significantly higher photon flux per nanometre than the white LED and thus could be used with a shorter integration time on the CCD detector which led to lower levels of dark noise on the absorption spectrum and consequently a smaller α_{min} value.

The LOD values for the two analytes have been measured by two means, firstly from the calculated α_{min} value and also from an error weighted linear regression through a plot of absorbance versus concentration. There are significant differences between the LOD values obtained by the two methods. The LOD value for rhodamine 6G obtained by the regression method was

approximately five times higher than the value obtained by the spectral method, whilst that for rhodamine B was approximately eight times higher. One would expect the LOD values obtained by the regression method to be approximately two times lower, as the regression method involves three replicate measurements at each concentration, with each measurement resulting from the average of 10 successive spectra recorded for each sample point, whilst the spectral method involves just one measurement arising from the average standard deviation between 10 successive spectra. Initially this discrepancy appeared puzzling but further investigation revealed the source to be the timing error between successive sample points on the chromatogram, introduced by the limitations of the hard disk buffer on the PC. As mentioned previously this results in an error of approximately ±0.2 s between successive sample points. This means for replicate measurements, the peak absorbance will differ for each measurement as a result of the timing jitter between sample points. By comparison, these data collected from the commercial Perkin Elmer HPLC instrument, which sampled at a faster rate of around 1 sample per second and showed no detectable timing jitter between sample points. Consequently the LODs obtained by the spectral method are probably a more accurate reflection of what is possible with the HPLC-BBCEAS setup, whilst the LODs obtained by the regression method highlight what is obtainable for replicate measurements with the current experimental limitations. The LOD determined by the regression method was also obtained for a single pass measurement in the HPLC-BBCEAS setup and also from a commercial Perkin Elmer HPLC instrument. When compared to the single pass measurement, the LOD for the BBCEAS measurement is approximately seven times lower for both analytes. At first glance this is surprising given that the *CEF* value for the two analytes is between 40 and 45 and one would assume a similar improvement in the LOD values. However, this difference can be explained by the method for making the single pass measurement, which involved removing one of the cavity mirrors. This led to a large increase in the intensity of light reaching the detector and consequently a much shorter integration time could be used to record the absorption spectrum. As a result much lower levels of dark noise from the CCD detector were present on the absorption spectrum leading to less variation between replicate measurements and thus a lower LOD than might have been

expected. Comparing the HPLC-BBCEAS LODs obtained by the regression method with those from the commercial Perkin Elmer instrument, it can be seen that our values are between 10 and 11 times lower. This is a significant improvement over the commercial instrument achieved using an experimental setup which is simple and low cost and with the potential for considerable further improvement if issues such as the timing jitter between sample points can be addressed. If the LODs from the spectral method are seen as a fairer indication of what is obtainable from HPLC-BBCEAS, then the values from the current study are between 54 and 77 times better.

4.5.2. Comparison with previous studies

Comparison with the previous HPLC-CRDS measurements can also be made. Table 4.3 summarises some of the figures of merit from these studies and compares them with those obtained from this study. The sensitivity of the HPLC-CRDS measurements is usually quoted in terms of the baseline noise on the measurement in absorbance units. However, for our measurements we cannot determine the sensitivity in these units and quote the sensitivity in terms of α_{min} in cm^{-1} units. Instead it is possible to convert the absorbance unit values of the HPLC-CRDS to α_{min} values by multiplying by 2.303 to convert from $\log_{10}$ units to ln ($\log_e$) units and then dividing by the pathlength of the cell in cm. Care is taken that the comparison is made with the root mean squared (rms) 1σ noise value rather than the peak-to-peak 3σ noise value, which is often stated. Table 4.3 also lists the base pathlength of the measurement, the wavelength of measurement, and the reflectivity of the cavity mirrors used in the studies.

Table 4.3: A comparison between this study and previous liquid-phase cavity studies as a function of technique, the mirror reflectivity, base pathlength, the wavelength of measurement, the lowest value of α_{min}, the minimum LOD for an analyte, and the molar extinction coefficient ε for that analyte.

Study	Technique	Mirror reflectivity	Flow cell volume (µL)	Base path length (cm)	Wavelength (nm)	α_{min} (cm^{-1})	LOD (M)	ε (M^{-1} cm^{-1})
This work	BBCEAS	0.99	70	1	450 - 600	1.9×10^{-5}	2.1×10^{-9}	9.3×10^{4}
Bechtel *et al.*[12]	CRDS	-	10	0.03	488	2.6×10^{-6}	1×10^{-7}	-
Snyder *et al.* [11]	CRDS	0.9993	10	0.03	470	2.5×10^{-4}	9.2×10^{-8}	9×10^{3}
Bahnev *et al.*[5]	CRDS	0.9998	12	0.2	532	1.6×10^{-4}	2.5×10^{-9}	5.4×10^{4}
van der Sneppen *et al.*[13]	CRDS	0.99996	12	0.2	532	1.0×10^{-5}	1.5×10^{-8}	1.4×10^{4}
van der Sneppen *et al.*[13]	CRDS	0.99993	12	0.2	457	1.0×10^{-5}	1.2×10^{-8}	3.6×10^{4}
van der Sneppen *et al.*[13]	CRDS	0.9995	12	0.2	355	5.0×10^{-5}	7.5×10^{-8}	1.02×10^{4}
van der Sneppen *et al.*[14]	CRDS	0.9995	80	1	355	3.0×10^{-5}	4×10^{-8}	1.02×10^{4}
van der Sneppen *et al.*[14]	CRDS	0.9991	80	1	273	1.0×10^{-3}	5×10^{-7}	-

The earliest HPLC-CRDS studies were performed in the research group of Professor Richard Zare at Stanford University, U.S.A.[11]. These utilised a custom built HPLC cell which had the cell windows at the correct Brewster's angle at both the air / glass and glass / liquid interfaces to minimise reflection losses. The base pathlength of the cell was only 300 μm which allowed very small cell volumes to be used. High reflectivity ($R \geq 0.999$) mirrors were used to form the optical cavity (although the actual reflectivity of the mirrors in Bechtel *et al.*[12] is not stated). P-polarised light from a dye laser at 470 nm and a compact argon ion laser at 488 nm were used as the CRDS light sources [11, 12]. The sensitivity of the experiments were very high considering the short base pathlength, reflecting the extremely low losses at the cell interfaces. However, it can be argued that the experimental complexity was also high given the requirement for the expensive custom built HPLC cell. The remaining four previous HPLC-CRDS studies have all been performed in the research group of Professor Freek Ariese at Vrije University, The Netherlands. The first three experiments utilised a simple 2 mm pathlength HPLC cell which had been constructed by using a rubber spacer with a 12 μL elliptical hole to separate compact high reflectivity cavity mirrors which were in direct contact with the analyte. The first two studies were performed at 532 nm whilst the last study made measurements at 457 and 355 nm. The use of high reflectivity mirrors and the lack of interface losses resulted in low values of α_{min} for the measurement at 532 and 457 nm (1.0×10^{-5} cm^{-1}). The measurement at 355 nm had a significantly worse α_{min} value of 5.0×10^{-5} cm^{-1} as the fabrication of high reflectivity mirrors becomes increasingly more difficult at UV wavelengths. However, the applicability and usefulness of the technique also increases the further into the UV measurements can be made, as a large fraction of potential analytes have strong absorptions in the 200 – 300 nm range. The final study is the one most similar to ours as it utilised a 1 cm pathlength HPLC cell. This cell however, was not a standard item and had been 'superpolished' to reduce scattering losses when placed in the cavity. This allowed ~500 passes at 355 nm when the cuvette, filled with a blank eluent, was placed in the cavity with $R \geq 0.9995$ mirrors. Measurements were made in the UV at 355 and 273 nm. The α_{min} value at 355 nm was slightly better than the previous measurement in the 2

mm cell (3.0×10^{-5} cm^{-1}) whilst that at 273 nm was relatively poor (1.0×10^{-3} cm^{-1}) as a result of lower performance high reflectivity mirrors and the instrumental response being significantly longer.

The results obtained in this study compare surprisingly well with the previous measurements. The sensitivity of the technique as determined by the best α_{min} value of 1.9×10^{-5} cm^{-1} is towards the lower end of the values obtained from the six previous HPLC-CRDS. It should be pointed out that the value of α_{min} is proportional to the base pathlength and at 1 cm the pathlength used in this study is the joint longest. However, this is the standard pathlength for cells used in most commercial HPLC systems and consequently there is no major disadvantage in using such a cell. These α_{min} values have been obtained using relatively low reflectivity $R \geq 0.99$ mirrors and only 45 passes. The previous studies have all used $R > 0.999$ mirrors and typically in excess of 1000 passes. The flow cell volume of 70 μL is amongst the highest when compared to the previous studies and in general smaller flow cell volumes will result in less chromatographic broadening. However, the cell used is a standard HPLC cell and thus its impact on performance should be negligible if comparison is made with commercial HPLC instruments.

The novelty of this study lies in the demonstration of the first application of CEAS detection to an HPLC system and in particular a variant of BBCEAS. The major advantages of the technique include the low cost of the experimental setup. The LED light source cost ~£3 compared to the ~£10000+ of the pulsed laser light sources used in the HPLC-CRDS studies. The cavity mirrors are off the shelf items from Layertec (Germany) which are normally used as an output coupler for a dye laser. These cost ~£400 for a pair of mirrors. The high reflectivity $R > 0.999$ mirrors used in the previous studies typically require custom coating runs for production, where the price of the coating run can be on the order of £2000 - £3000. The HPLC cell was a standard item which cost ~£150, unlike the custom built cells used in some of the previous studies which cost considerably more. The CCD spectrograph was the most expensive item in the experimental setup and cost ~£1500. This however, is still considerably cheaper than the detection system for CRDS measurements which typically use high bandwidth sampling oscilloscopes which can cost ~£10000. Given that a typical commercial HPLC system costs ~£30000 the addition of BBCEAS

detection might only add ~10% to the system cost whilst CRDS detection would at least double the cost.

The simplicity of the experimental methodology and data analysis is another advantage of the HPLC-BBCEAS technique. The experimental complexity of CRDS based measurements arises from the need for fast detection techniques to measure ringdown times on the order of nanoseconds to microseconds, whereas BBCEAS measurements only require relative intensities to be recorded on the timescale of several seconds. Also HPLC-CRDS requires the extraction of ringdown times from exponential decays in the intensity of light exiting the cavity, followed by further data manipulation to obtain an absorption spectrum. The methodology for BBCEAS measurements on the other hand is very similar to conventional UV-visible absorption spectroscopy and the calibration to calculate the *CEF* value is straightforward.

The most significant advantage of the current HPLC-BBCEAS study over the previous HPLC-CRDS studies arises from the recording of the absorption spectrum over a range of wavelengths in each measurement. The measurements on rhodamine 6G and rhodamine B were all recorded between 450 and 600 nm, whilst the previous HPLC-CRDS studies only made a measurement at a single wavelength. As discussed earlier there are important advantages in having the ability to record the absorption spectrum of the analyte over a range of wavelengths. Namely any analyte which absorbs in the detection range of the measurement can be studied rather than only those which absorb at the single wavelength of measurement of the HPLC-CRDS studies. In addition analytes that co-elute or nearly co-elute can be distinguished provided they have sufficient differences in their UV-visible spectrums. The measurements in this study cover a significant part of the visible spectrum (450 – 600 nm), in fact usable data was collected up to 700 nm. These spectra are only displayed to 600 nm as both rhodamine 6G and rhodamine B have negligible absorption beyond 600 nm. The wavelength range of measurement meant that data at the peak absorption of both analytes could be used to obtain the best possible LOD value, whereas with a single wavelength measurement the determination of the LOD would be restricted to one wavelength which may be quite far removed from the peak absorption of the analyte.

The experiments outlined in section 4.4.3., demonstrate the case where HPLC-BBCEAS can be used to distinguish between two nearly co-eluting analytes. This type of experiment would be difficult if not impossible to tackle using single wavelength detection as the only information regarding the separation of analytes would arise from the chromatogram which would show a single peak indicating the presence of only one analyte. HPLC-BBCEAS adds an extra dimension of spectral data such that every point on the chromatogram also contains a visible spectrum between 450 and 600 nm. The two analytes chosen for this experiment (rhodamine 6G and rhodamine B) are chemically similar and hence would be expected to have very similar retention times in an HPLC separation. The shapes of the visible spectra are also very similar but the peak absorption of rhodamine B (λ_{max} = 556 nm) is red shifted by 29 nm relative to rhodamine 6G (λ_{max} = 527 nm). If the two analytes co-eluted, one would expect the visible spectrum of each point around the peak of the chromatogram to have the same shape and show two maxima corresponding to the peak absorption of the two dyes. Even in the case of an unknown mixture, if the identity of the analytes could not be easily determined by comparison with reference spectra, it could nevertheless be stated unambiguously, that the single peak on the chromatogram is in fact a mixture of co-eluting dyes. Provided the reference spectra of the components in the mixture are known. The studies on a mixture of rhodamine 6G and rhodamine B show that they nearly co-elute under the experimental conditions used. Figure 4.15 shows the chromatogram obtained from plotting the absorbance at 541 nm as a function of time. This shows a single peak which given the absence of any other information would indicate the presence of a single compound. HPLC-BBCEAS however, provides an absorption spectrum for each chromatogram point and the inset to figure 4.15 shows the absorption spectrum between 450 and 600 nm for selected time points on the chromatogram. From this one can see that the shape of the absorption spectrum changes markedly across the chromatogram peak. If this was a true unknown mixture this information would provide unambiguous proof that the chromatogram peak was indeed due to a nearly co-eluting mixture, even if the reference spectra of the components in the mixture did not exist. Given that the reference spectra of the two analytes are known in this case, the time evolution of the absorption spectra allows the order

of elution for the 2 analytes to be determined. The earliest time point at 43 s shows a single peak in the absorption spectrum at 527 nm which indicates that rhodamine 6G is the major analyte at this point. There is a minor protuberance at 556 nm compared to the rhodamine 6G reference spectrum, indicating the presence of a small amount of rhodamine B. By 50 s this protuberance has become a secondary peak at 556 nm which suggests that similar amounts of rhodamine 6G and rhodamine B are eluting at this point. At 58 s the peak at 556 nm has become the major peak whilst the relative intensity of the peak at 527 nm is diminishing and by 70 s it has all but disappeared. This behaviour is consistent with rhodamine 6G eluting slightly faster than rhodamine B. These data can also be represented in the form of a contour plot as shown in figures 4.17 and 4.18. The y axis shows the wavelength scale whilst the x axis represents the timescale. The intensity of any x,y point is represented by a colour coded scale. This type of plot also allows nearly co-eluting analytes to be discriminated. If the two dyes co-eluted then the peak intensity decrease would be parallel to the x axis. In figure 4.18 however, at increasing times the peak intensity shifts to slightly longer wavelengths indicating the presence of a more slowly eluting analyte.

4.6. Further work

Although the performance of our HPLC-BBCEAS system compares favourably with the commercial Perkin Elmer system and also the previous HPLC-CRDS studies, the sensitivity could be improved by a number of modifications. The discrepancy between LODs obtained by the spectral method and the regression method highlighted the problem of excessive timing jitter between sample points limiting the precision of replicate measurements. This could be addressed simply by using a faster PC with a larger hard disk buffer. The experimental sensitivity is mainly limited by the dark noise produced by the uncooled CCD detector, as was the case for our earlier BBCEAS experiments. The dark noise could be reduced by using a spectrograph with a thermoelectrically cooled detector although this would significantly increase the cost of the experimental setup. Typical spectrograph systems with thermoelectrically cooled CCD detectors cost ~£15000. Alternatively a more powerful light source could be

used as this would shorten the integration times needed, resulting in lower levels of dark noise from the CCD detector. More powerful white LED sources are now available (5W devices versus the 1W devices used in this study, at little extra cost) and it is likely that the power output will continue to increase in the future as a primary motivation for the development of these devices is to replace conventional light bulbs. Therefore this would represent a cost effective improvement to the experimental setup provided the extra light intensity could be efficiently coupled into the optical cavity. If the integration time for measurement could be reduced from 200 ms to 20 ms then the dark noise level and also the sensitivity of the experiment could be improved by a factor of ~3. If a cooled CCD detector was also used then further improvement would be achieved.

The current measurements have been made in the wavelength range 450 – 600 nm and in fact usable spectral data to 700 nm has been recorded. The applicability of the technique would however, be greatly increased if measurements could be extended to shorter wavelengths into the UV as most common analytes have strong absorptions in the UV region from 200 to 400 nm. The technical challenges involve finding suitable high intensity broadband light sources which operate in the UV and also broadband high reflectivity dielectric mirrors which function in the UV. Recent advances have resulted in high intensity LEDs which operate at wavelengths as short as 240 nm, these however, only have typical bandwidths of 10 – 20 nm, which means that several different LEDs would be needed to cover the UV wavelength range. High intensity xenon arc lamps similar to the one used by Fielder *et al*. in their studies, offer a source of broadband radiation down to about 200 nm, whilst the long wavelength output extends into the near infrared. Their main disadvantages compared to LED sources, is a much larger size and power consumption and also a much greater cost (typically > £1000). High reflectivity mirrors tend to be more difficult to manufacture for operation in the UV as the quarter wave stacks require thinner depositions to be made for each layer and thus tighter control of manufacturing tolerances. In addition the materials used for the dielectric layers tend to show greater scattering and absorption losses at UV wavelengths. The bandwidth of the mirror also narrows at UV wavelengths. Nevertheless leading mirrors manufacturers are currently able to produce

custom broadband UV mirrors which would cover the range 250 – 400 nm with $R \geq 0.99$ reflectivity. Consequently the application of BBCEAS to HPLC detection at UV wavelengths looks both feasible and promising.

4.7. Conclusion

The first reported application of a CEAS based detection method, attached to an HPLC system has been demonstrated by this study. Furthermore the use of HPLC-BBCEAS has allowed the absorption spectrum of the analyte in the range 450 – 600 nm to be recorded for every point on the chromatogram. The experimental methodology is very similar to that used in commercial HPLC systems and offers a number of advantages over the previous single wavelength HPLC-CRDS studies. The overall cost of the experimental setup is also very low when compared to the HPLC-CRDS studies. Experiments have been performed on the dyes rhodamine 6G and rhodamine B and comparisons have been made with single pass measurements, a commercial Perkin Elmer HPLC system as well as the previous HPLC-CRDS studies. The *CEF* values were limited by scattering and absorption losses from the cuvette and suggest that the $R \geq 0.99$ mirrors used have almost the optimum reflectivity. The LOD values for the two analytes obtained by the regression method indicate that our HPLC-BBCEAS setup is an order of magnitude more sensitive than the commercial HPLC system. This is presently limited by errors introduced by a timing jitter between sample points. A comparison of the α_{min} values with the previous HPLC-CRDS studies showed that our measurements were amongst the most sensitive, whilst using a low cost experimental setup and a simple experimental methodology, which would be relatively easy to implement onto existing commercial HPLC systems. Finally experiments were performed on a mixture of the two dyes, which nearly co-eluted under the conditions used. The use of BBCEAS detection allowed the presence of the two dyes to be determined even though the chromatogram consisted of a single peak.

4.8. References

[1] Neue, U. D. HPLC Columns: Theory, Technology, and Practice Wiley-VCH, New York, 1997.

[2] Colins, H.; Guiochon, M.; Martin, M. in: Engelhardt, H. (Ed.), Practice of high performance liquid chromatography : applications, equipment, and quantitative analysis, Springer-Verlag, Berlin, 1986, p. 4.

[3] Snyder, L. R.; Stadalius, M. A.; Quarry, M. A.; Analytical Chemistry, 55 (1983) .

[4] Majors, R. E. American Laboratory, 35 (2003) 46.

[5] Bahnev, B.; van der Sneppen, L.; Wiskerke, A. E.; Ariese, F.; Gooijer, C.; Ubachs, W. Analytical Chemistry, 77 (2005) 1188.

[6] Brown, S. S. Chemical reviews, 103 (2003) 5219.

[7] Berden, G.; Peeters, R.; Meijer, G. International reviews in physical chemistry, 19 (2000) 565.

[8] Pei, S. Spectroscopy and Spectral Analysis, 25 (2005) 1908.

[9] Zalicki, P.; Zare, R. N. Journal of Chemical Physics, 102 (1995) 2708.

[10] Mazurenka, M. Annual reports on the progress of chemistry. Section C, Physical chemistry, 101 (2005) 100.

[11] Snyder, K. L.; Zare, R. N. Analytical Chemistry, 75 (2003) 3086.

[12] Bechtel, K. L.; Zare, R. N.; Kachanov, A. A.; Sanders, S. S.; Paldus, B. A. Analytical Chemistry, 77 (2005) 1177.

[13] van der Sneppen, L.; Wiskerke, A.; Ariese, F.; Gooijer, C.; Ubachs, W. Analytica Chimica Acta, 558 (2006) 2.

[14] van der Sneppen, L.; Ariese, F.; Gooijer, C.; Ubachs, W. Journal of Chromatography A, 1148 (2007) 184.

[15] van der Sneppen, L.; Wiskerke, A. E.; Ariese, F.; Goouer, C.; Ubachs, W. Applied Spectroscopy, 60 (2006) 931.

[16] Paldus, B. A.; Kachanov, A. A. Canadian Journal of Physics, 83 (2005) 975.

.

Chapter Five

5.0. Liquid Phase Broadband Cavity Enhanced Absorption Spectroscopy (BBCEAS) studies in a 20 cm cell

The quest for greater sensitivity for absorption based measurements has made great progress in the gas phase through the introduction of CRDS and CEAS techniques, such that detection of certain species at the sub part per trillion (ppt) level is now possible [1, 2]. In the liquid phase, as mentioned in chapter 3, the number of cavity based studies reported to date is fairly small and most of these have not been geared towards obtaining the highest sensitivity possible. Traditionally absorption based measurements in the liquid phase have been considered a very useful but relatively insensitive technique with LODs in the nanomolar range for strongly absorbing species and standard experimental setups. Higher sensitivity spectroscopic measurements in the pico – femto molar range require the use of fluorescence based techniques, which often are not applicable to many common analytes.

The aim was to demonstrate sensitive liquid phase absorption measurements using the low cost BBCEAS setup from our previous study, however instead of using a 2 mm cuvette, a 20 cm pathlength cell where the mirrors were in direct contact with the liquid phase analyte was used. In principle this should allow more sensitive measurements to be made due to the longer base pathlength, also the previous BBCEAS on 2 mm cuvette measurements (chapter three) suffered from rather high cavity losses from the use of a cuvette in the cavity, leading to only small improvements in the number of passes when higher reflectivity mirrors were used. The lack of additional optical components in the cavity should lead to lower cavity losses and a greater number of passes with higher reflectivity mirrors [3, 4].

Most of the cavity studies have reported measurements on gas phase species as the scattering and absorption losses are significantly lower than measurements for liquid and solid phase species and thus greater number of

passes through the sample can be achieved. Of the few previous liquid phase cavity based studies, the most directly relevant are the ones which have made measurements in cavities where the liquid under study is in direct contact with the cavity mirrors. The earliest of these studies and also the ones most similar to the present study were the CRDS based measurements of Hallock *et al*. [5, 6] Their first study [6] was made in a 21 cm cell, where the cavity was formed by one flat and one concave $R \geq 0.9998$ (between 620 – 670 nm) mirror which were in direct contact with the liquid phase analytes. The light source was a tuneable pulsed Nd:YAG pumped dye laser which was operated at selected wavelengths between 620 and 670 nm. A photomultiplier tube connected to an oscilloscope formed the detection system. They noted that careful choice of solvent had to be made as many of the common ones showed strong absorptions in the 620 – 670 nm regions. Spectrophotometric grade cyclohexane, hexane, toluene and acetonitrile were identified as suitable solvents. They stated that measurements had been made on a range of inorganic and organic compounds although only very general measurements of sensitivity and LODs were given. In a later study, Hallock *et al*. [5] reported kinetic measurements on methylene blue in a 23 cm cavity formed by two $R \geq 0.9998$ (at 655 nm) mirrors. A simpler experimental setup was used, based on cw-CRDS. This utilised a cheap laser diode operating at 655 nm as the light source. An acousto optic modulator (AOM) was used to chop the laser beam on the Hz to MHz timescale. As before a photomultiplier tube connected to an oscilloscope was used as the detection system.

The more recent studies of Bahnev *et al*. [7] and van der Sneppen *et al*. [3] are all related to the application of CRDS to HPLC detection and have consequently used a much shorter 2 mm base pathlength cell. This was formed by squeezing two 5 mm diameter high reflectivity mirrors onto a 2 mm thick silicon rubber spacer which had a 12 μL hole in the middle to allow the passage of light. Capillary tubes inserted into the top and bottom of the spacer allowed the flow of analyte through the cell. The light source in all three studies was short pulse length Nd:YAG lasers, although the laser wavelength used varied between the studies. The first two studies used laser radiation at 532 nm whilst the latter study also made measurements at 355 nm [3, 7]. The detection

system used in all three studies was a fast photomultiplier tube connected to a high bandwidth oscilloscope.

Only one previous study where the liquid phase analyte was in direct contact with the cavity mirrors has used CEAS. McGarvey *et al.*, [8]reported CEAS measurements on the biomolecule bacteriochlorophyll *a* made at 783 nm using a Titanium Sapphire laser system locked to a cavity resonance and high reflectivity mirrors in direct contact with the liquid sample in a 1.75 mm cavity.

5.1. Optical setup and measurement procedures

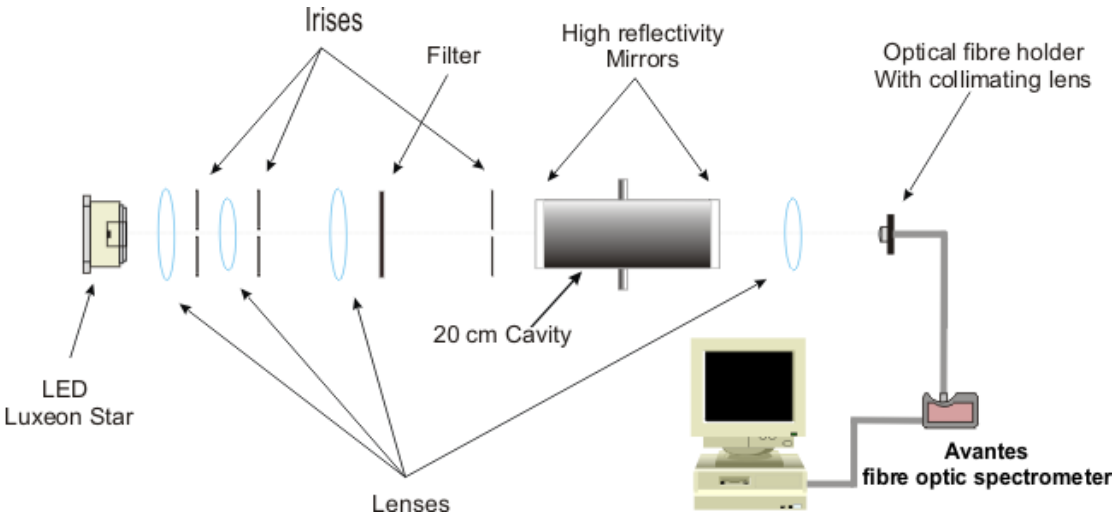

Figure 5.1: A schematic of the experimental setup for liquid-phase BBCEAS measurements in a 20 cm cell.

A schematic of the experimental setup is shown in figure 5.1. The optimum geometry of the lenses was difficult to calculate; therefore the optical setup was empirically assessed by trial and error to achieve maximum light leaking out of the 20 cm cavity. The high intensity LED light source, the high reflectivity cavity mirrors and the CCD spectrograph detector are the same as used in our previous study, reported in chapter 3. The experimental methodology is also largely similar. To avoid unnecessary repetition, only brief descriptions of these items is made here and the reader is referred to the relevant parts of chapter 3 for more details.

The output from a high intensity 1W LED (Luxeon O star, white or red) was collimated into a 20 cm liquid tight cavity formed by two high reflectivity mirrors which were in direct contact with the liquid phase analytes. The body of the cavity was constructed from 2mm thick stainless steel tubing which had an internal diameter of 25 mm. The volume of the cavity was 98 cm^3. Stoppered ports on the top and bottom of the stainless steel tubing allowed the cavity to be filled and emptied. Some of the experiments required the use of $R \geq 0.99$ mirrors, 25 mm diameter, radius of curvature (roc) = -50 cm, with a bandwidth ~420 – 670 nm (Layertec, Germany). Other experiments utilised higher reflectivity, $R \geq 0.999$ mirrors, 25 mm diameter, roc = -1.5 m (Laseroptik, Germany). These had a narrower bandwidth of ~100 nm and covered the range 600 – 700 nm. For measurements with the $R \geq 0.999$ mirrors a red Luxeon O star 1W LED was used, as the intensity from the white LED at the detector was insufficient for use with this mirror reflectivity combination. The light exiting the cavity was focussed into a 600 μm diameter, 1m length fibre optic cable (Thorlabs, UK) which was connected to a compact CCD spectrograph (Avantes AVS2000, The Netherlands). The spectrometer operated over the range 200 – 850 nm with a spectral resolution of ~1.5 nm. The lack of thermoelectric cooling of the CCD sensor resulted in relatively high levels of dark noise and restricted the use of long integration time. The maximum integration time that could be used with acceptable noise was ~3 seconds.

The typical alignment procedure for the cavity was though the iterative adjustments of the front and back mirrors to maximise the amount of light that leaks out, hence maximising the output of the LED reaching the spectrograph at a given integration time. The 20 cm cell was then filled with a blank solvent solution (typically acetonitrile). This resulted in a large decrease in the intensity of light reaching the spectrograph due to absorption and scattering by the solvent. The integration time was increased appropriately to ensure the signal from the LED was significantly above the dark noise level, but not high enough to saturate the detector. Typical integration times for the $R \geq 0.99$ mirror set with the white LED were ~30 ms, whilst those with the $R \geq 0.999$ mirrors and the red LED needed higher integration times of ~ 2.5 s. The front and back cavity mirrors were then further adjusted iteratively to maximize the output reaching

the detector. The spectrometer was connected to a personal computer via a USB cable and spectral data were recorded using the Avasoft program.

5.1.1. Experimental methodology

As noted in chapter 3, one of the main disadvantages of CEAS based techniques is that unlike CRDS experiments the absorption coefficient (α) cannot be directly calculated and instead must be obtained through a separate calibration. For the liquid phase BBCEAS experiments reported in this study the calibration and the experimental methodology could be performed in a straightforward manner similar to the experimental methodology for conventional UV-visible absorption spectroscopy as described earlier in chapter 3 (section 3.1.). The calibration could be used to obtain in the first instance the cavity enhancement factor (*CEF*) or the number of passes made within the cavity. Once the effective pathlength had been calculated, the minimum detectable change in the absorption coefficient α_{min} could also be calculated. The first step in the calibration was to obtain a single pass spectrum of the analyte to be studied. This could be performed in a standard 1cm pathlength cuvette with a tungsten halogen light source and the same Avantes AVS2000 spectrometer. The concentration of the solution was typically a factor of 1000 higher than in the 20 cm cavity. The number of passes within the cavity (*CEF*), the effective pathlength and the sensitivity α_{min} for each measurement were calculated as described in chapter 3, as was the limit of detection (LOD) for the analytes under study.

The linear dynamic range of measurement could be determined by making absorbance measurements for a series of different concentrations in the cavity. Three separate measurements at each concentration were made. An error weighted regression through the linear part of the plot also allowed an independent determination of the LOD from the 3σ error limit on the intercept divided by the product of the effective pathlength and the molar extinction coefficient. The mechanical stability of the system could also be estimated as the three replicate measurements required the cavity to be emptied and refilled for each measurement.

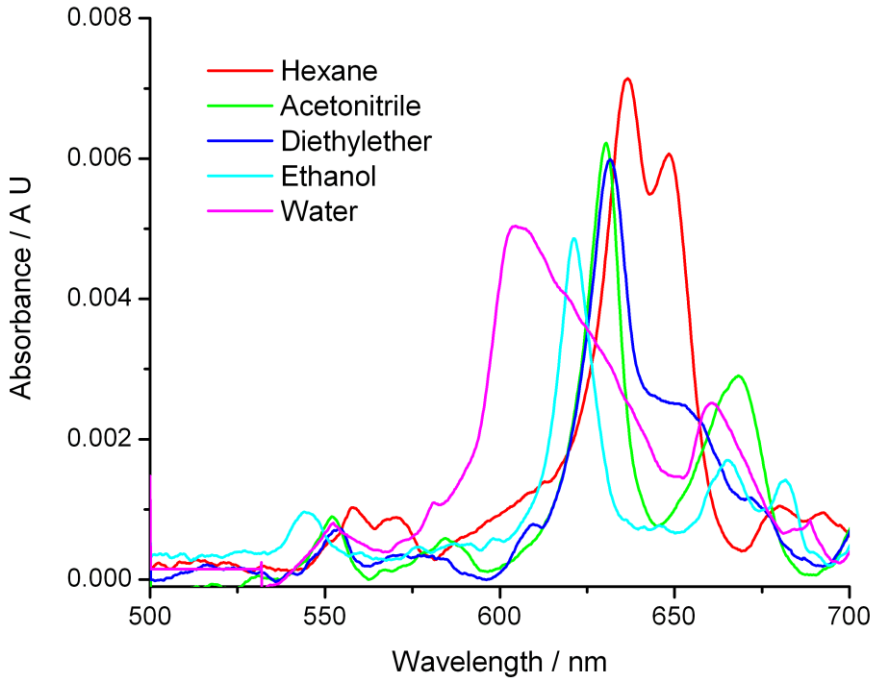

Figure 5.2: Single pass absorption spectra of hexane, acetonitrile, diethylether, ethanol and water, recorded in a 10 cm pathlength cell with a double beam spectrometer.

Some new experimental challenges arose as a result of the hundredfold increase in the base pathlength from our previous measurements in a 2 mm cuvette. It was noticed early on that the background absorption from the solvents used was far more significant than in the 2 mm cuvette. The background absorptions were due to high CH and OH overtone vibrations found in most common solvents. Single pass absorption measurements on a range of common solvents in a 10 cm pathlength cell were recorded with a commercial double beam spectrometer (Jasco V630), between 500 and 700 nm, at 1.5 nm resolution, to identify the location of these overtone vibrations. The reference background was air. These spectra are shown in figure 5.2. Although the absolute values of the absorbances were small in the 10 cm cell, the use of the double beam spectrometer allowed the absorption features to be clearly seen. Water had the broadest absorption, presumably due to the 4^{th} overtone of the OH stretch. The other solvents displayed clear absorption features above ~610 nm, due to the 5^{th} overtone of the CH stretch. It was even possible to see the

absorption due to the weaker 6th overtone of the CH stretch at ~550 nm. The presence of the absorption features meant that the maximum number of passes at these wavelengths would be greatly reduced, especially for higher reflectivity mirrors.

Consequently additional preliminary cavity measurements were performed on the staining dye sudan black with the $R \geq 0.99$ mirror set and spectrophotometric grade hexane, acetonitrile, diethyl ether and ethanol, in an attempt to identify the most suitable solvent. These absorption spectra are shown in figure 5.3. It can be seen by comparing with the single pass spectrum of sudan black, that significant spectral distortion occurs at ~620 nm and 550 nm as a result of the 5th and 6th overtone CH vibration limiting the cavity enhancement at these wavelengths. Additional distortions arose from the ripples in reflectivity profile of the $R \geq 0.99$ mirror set.

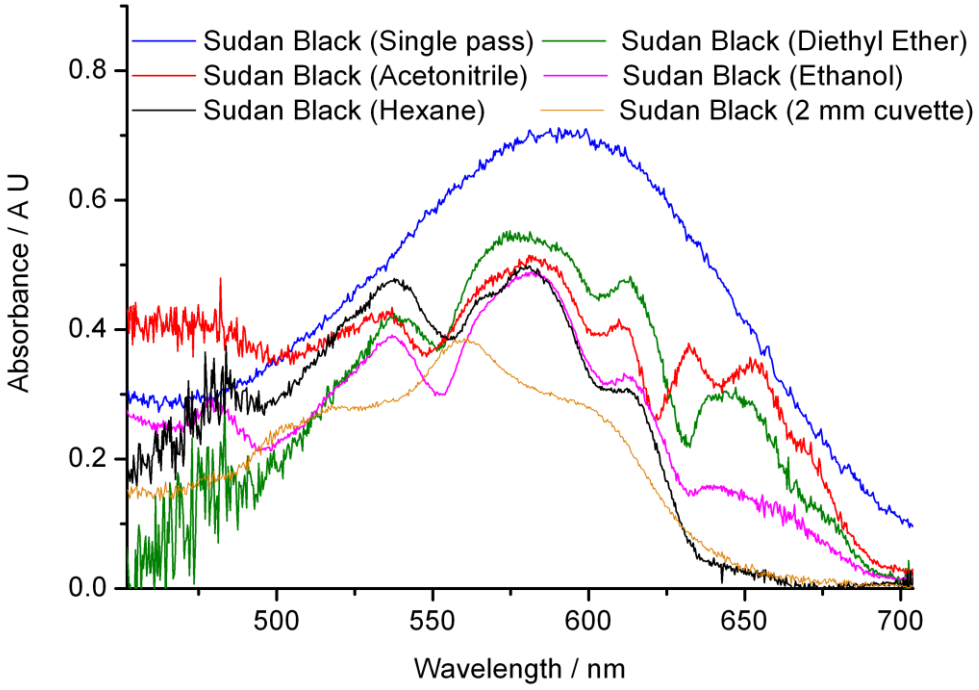

Figure 5.3: Scaled absorption spectra of sudan black dissolved in acetonitrile, hexane, diethylether and ethanol, recorded in the 20 cm cavity with the $R \geq 0.99$ mirror set.

By comparing with a single pass spectrum of a known concentration of sudan black, the *CEF* as a function of wavelength could be calculated for each solvent between 450 and 670 nm. It was found that acetonitrile (spectrophotometric grade, Fisher Scientific, UK) offered the highest *CEF* value, that is the greatest transparency over the largest wavelength range with the $R \geq 0.99$ mirrors, and consequently it was chosen as the solvent for subsequent measurements. Use of diethyl ether, which had similar transmission properties, was ruled out as a result of its high volatility, which caused condensation of the solvent on the external face of the cavity mirrors.

5.1.2. Choice of analytes

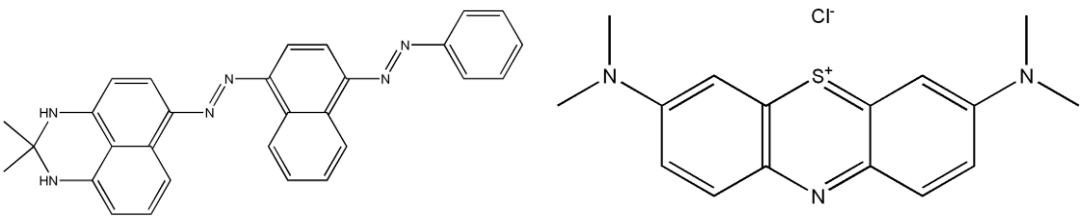

Sudan black Methylene blue

Figure 5.4: Structural formulae of sudan black and methylene blue

The two analytes chosen for study were the dye molecules, sudan black and methylene blue, as shown in figure 5.4. Sudan black had already been studied in the 2 mm cuvette and was chosen as it had a very broad absorption spectrum covering most of the visible spectrum and thus could be used to demonstrate the wavelength coverage of BBCEAS in the 20 cm cell. The second analyte needed to have a high molar extinction coefficient so that the measured LOD would be as low as possible, also its peak wavelength of absorption needed to coincide with the output of the red LED, so that it could be studied with the higher reflectivity $R \geq 0.999$ mirror set. Our initial choice was brilliant blue-R which had been also studied in the 2 mm cuvette. Unfortunately its peak absorption wavelength coincided with the 5^{th} overtone of the CH stretch in acetonitrile, which would have greatly restricted the *CEF* value at this wavelength. After some experimentation with a number of other strongly

absorbing dyes, methylene blue was identified as the most suitable candidate for study as it was sufficiently soluble in acetonitrile and also it peak absorption wavelength of 655 nm was far enough removed from the background solvent absorption peak of acetonitrile.

5.2. Results

Liquid-phase BBCEAS measurements have been carried out in a 20 cm cavity for two different analytes dissolved in acetonitrile, at the peak absorption wavelength, using appropriate LEDs and high reflectivity mirror sets.

Table 5.1: A summary of the results obtained in terms of analyte, the wavelength of measurement, the reflectivity of the mirrors, the *CEF* value, the minimum detectable change in absorption α_{min}, the LOD of the analyte calculated by both the spectral method (LOD_s) and the regression method (LOD_r) and the molar extinction coefficient ε at the wavelength of measurement.

Analyte	***R*** **≥**	***CEF***	**Wavelength / nm**	α_{min} **/ cm^{-1}**	**Conc. / M**	**LOD_s / M**	**LOD_r / M**	ε **/ M^{-1} cm^{-1}**
Methylene Blue	0.99	78	655	4.4×10^{-7}	4.2×10^{-10}	7.1×10^{-12}	3.2×10^{-11}	7.9×10^{4}
Methylene Blue	0.999	429	655	2.8×10^{-7}	6.0×10^{-10}	4.6×10^{-12}	1.2×10^{-11}	7.9×10^{4}
Sudan Black	0.99	82	584	3.4×10^{-7}	1.1×10^{-9}	1.8×10^{-11}	1.6×10^{-10}	2.5×10^{4}

Table 5.1 summarizes the measurements made in terms of the analyte studied, the wavelength of measurement, the reflectivity of the mirror set used, the *CEF* or number of passes obtained for each analyte, the calculated α_{min} values for each measurement, an estimation of the LOD for each analyte, obtained by two independent means, namely a spectral method (LOD_s) and a regression method (LOD_r), and finally the molar extinction coefficient ε of the analyte at the wavelength of measurement.

5.2.1. Methylene Blue

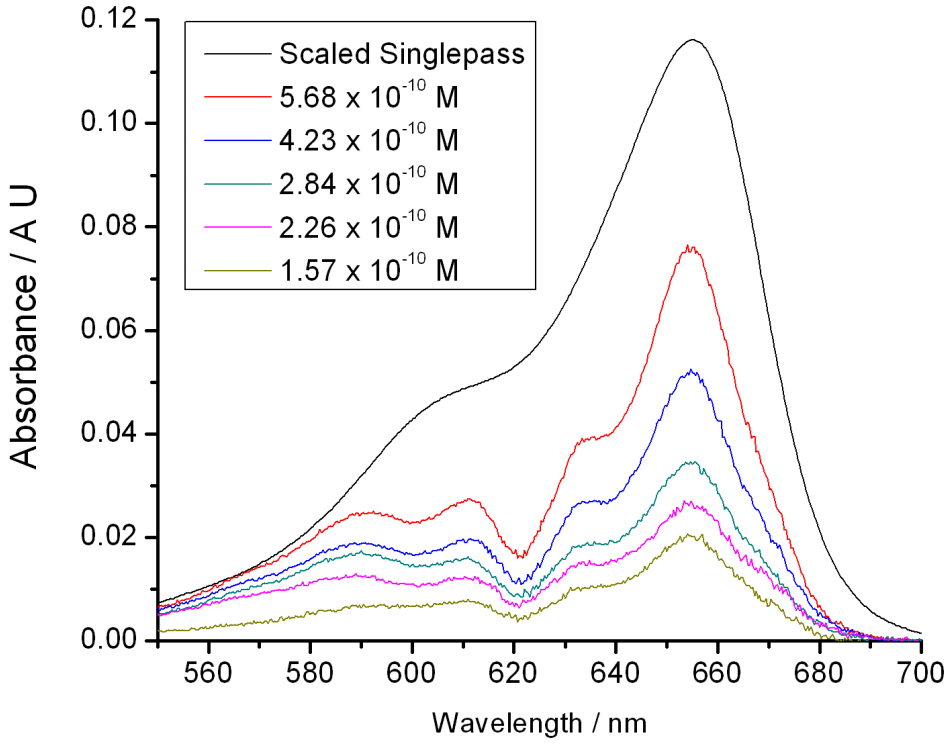

Figure 5.5: The BBCEAS spectrum of methylene blue in acetonitrile in the range 550–700 nm, obtained with the white LED and the $R \geq 0.99$ mirror set. A scaled single-pass spectrum of methylene blue is also shown.

Figure 5.5 shows representative absorption spectra recorded over a ~150 nm wavelength range in a single measurement for methylene blue using the white LED and the $R \geq 0.99$ mirror set. When compared to the scaled single pass measurement, the absorption effect due to the solvent can be observed at ~ 620 nm.

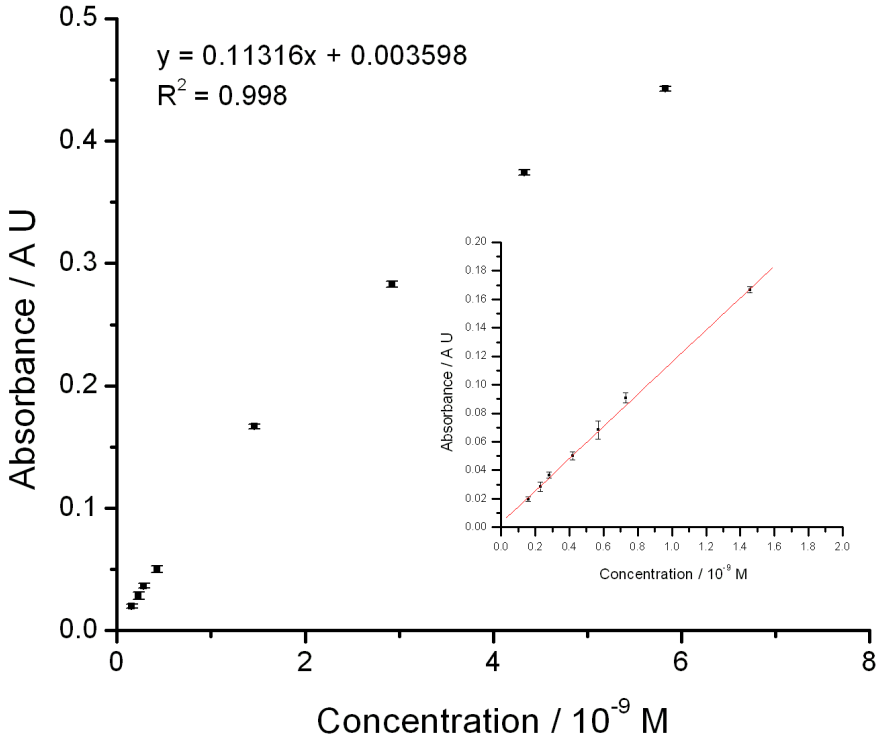

Figure 5.6: An absorbance versus concentration plot for methylene blue.
(Injected concentration range ~0.1 nM to ~ 6 nM, obtained using the white LED and the R ≥ 0.99 mirror set. The inset shows the measurements in the linear range from ~0.1 nM to ~1.5 nM. The error bars represent the 1σ error limit of three replicate measurements at each concentration. The equation on the diagram refers to an error-weighted linear fit to the measurements shown in the insert)

Figure 5.6 shows plots of absorbance versus concentration for methylene blue. The methylene blue measurements were made at 655 nm and a range of concentrations from ~0.1 nM to ~ 5 nM. Three replicate measurements were made at each concentration and the error bars for each concentration represent the standard deviation of the measurements. The plot can be broken into two parts. These data in the inset show measurements in the range ~ 0.1 nM to ~1.5 nM, which show a linear dependence of the absorbance on the concentration. The measurements at higher concentrations, up to ~ 6 nM are nonlinear. An error-weighted regression through the linear part of the plot yields a straight line (equation of the line is given in fig. 5.6) with the correlation coefficient R^2 = 0.998 and a 1σ error limit for the intercept of 1.3 x 10^{-3}. The LOD can be calculated from the value of the 3σ error limit on the

intercept, which produces a concentration of 32 pM. The limit of quantification (LOQ) can also be determined from the 10σ error limit on the intercept and yields a concentration of 109 pM. At absorbance values above ~0.2 the plot in fig. 5.6 is no longer linear with respect to increasing concentration, but measurements of absorbance values of up to ~0.45 were made without significantly visible increases in the 1σ error limit on three replicate measurements.

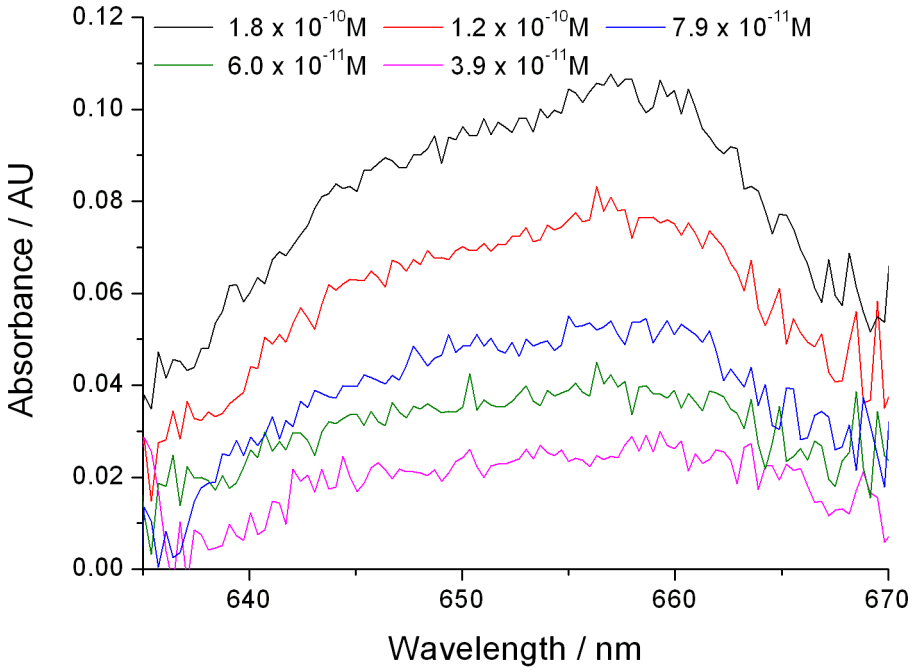

Figure 5.7: The BBCEAS spectrum of methylene blue in acetonitrile in the range 630–660 nm, obtained with the red LED and the $R \geq 0.999$ mirror set.

Figure 5.7 shows representative absorption spectra recorded over a ~30 nm wavelength range in a single measurement for methylene blue using the red LED and the $R \geq 0.999$ mirror set. The transmission through the cavity was much lower than with the $R \geq 0.99$ mirrors, consequently the use of much longer integration times (~2.5 s) resulted in the visible effects of dark noise on these absorption spectra.

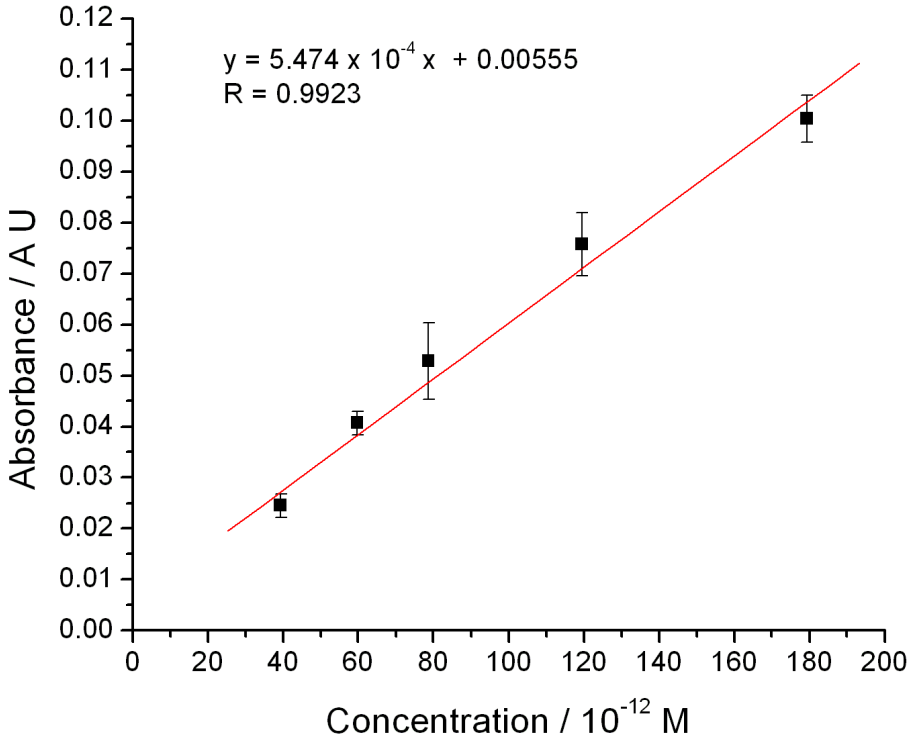

Figure 5.8: An absorbance versus concentration plot for methylene blue.
(Injected concentration range ~40 pM to ~ 200 pM, obtained using the red LED and the R ≥ 0.999 mirror set. The error bars represent the 1σ error limit of three replicate measurements at each concentration. The equation on the diagram refers to an error-weighted linear fit to the measurements)

Figure 5.8 shows plots of absorbance versus concentration for methylene blue obtained with the red LED and the $R \geq 0.999$ mirror set. The methylene blue measurements were made at 655 nm and a range of concentrations from ~40 pM to ~200 pM and these data shows a linear dependence of the absorbance on the concentration. Data were only collected for the linear part to enable the determination of the limit of detection. Three replicate measurements were made at each concentration and the error bars for each concentration represent the standard deviation of the measurements. An error-weighted regression through the linear part of the plot yields a straight line (equation of the line is given in fig. 5.8) with the correlation coefficient R = 0.992 and a 1σ error limit for the intercept of 2.7×10^{-3}. The LOD can be calculated from the value of the 3σ error limit on the intercept, which produced a concentration of 12 pM. The limit of quantification (LOQ) can also be

determined from the 10σ error limit on the intercept and yields a concentration of 41 pM.

5.2.2. Sudan Black

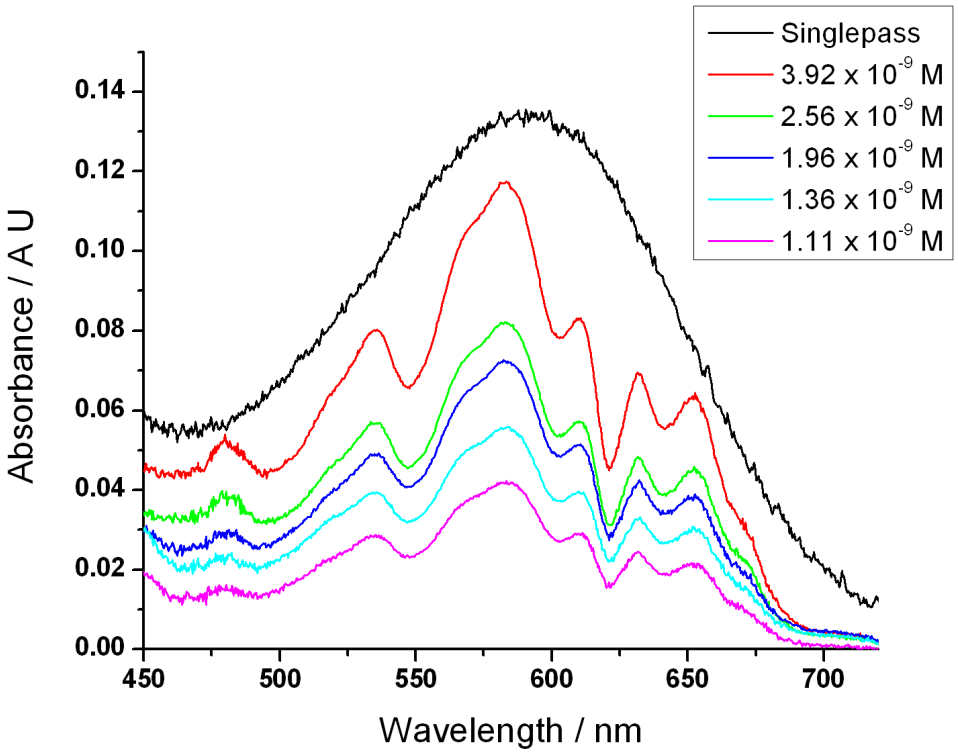

Figure 5.9: The BBCEAS spectrum of sudan black in acetonitrile in the range 450–700 nm. (Obtained with the white LED and the $R \geq 0.99$ mirror set. A scaled single-pass spectrum of sudan black is also shown)

Figure 5.9 shows representative absorption spectra recorded over a ~250 nm wavelength range in a single measurement for sudan black using the white LED and the $R \geq 0.99$ mirror set. When compared to the scaled single pass measurement, background absorption due to the solvent can be observed at ~ 550 nm and ~620nm, whilst the other ripples were caused by the variation in the reflectivity profile of the $R \geq 0.99$ mirror set.

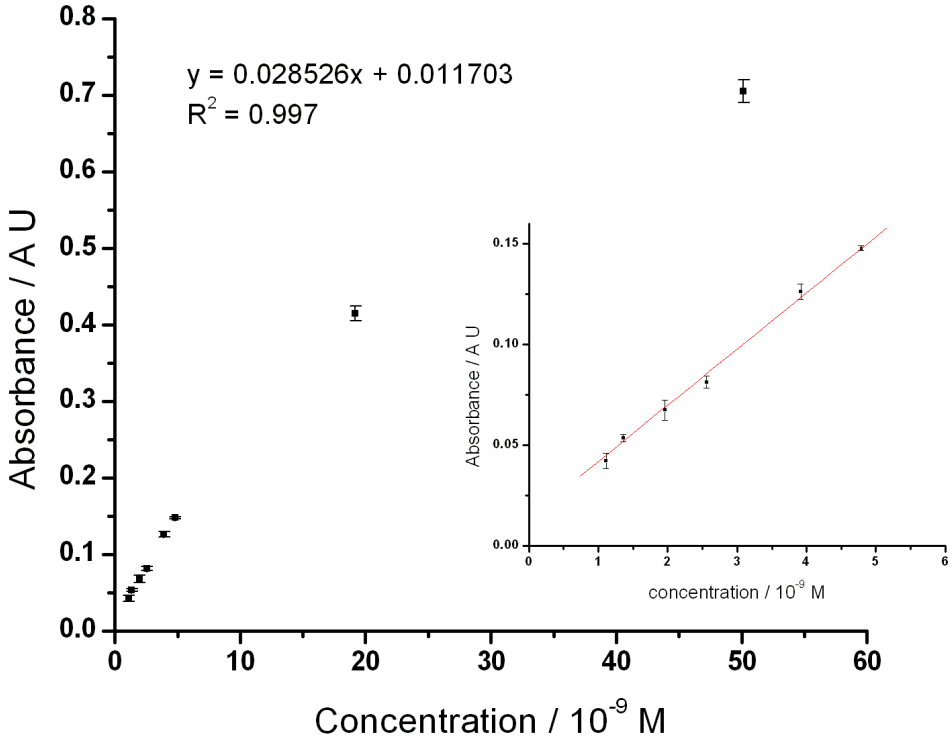

Figure 5.10: An absorbance versus concentration plot for sudan black.
(Concentration range ~ 1 nM to ~ 50 nM, obtained using the white LED and the R ≥ 0.99 mirror set. The inset shows the measurements in the linear range from ~1 nM to ~5 nM. The error bars represent the 1σ error limit of three replicate measurements at each concentration. The equation on the diagram refers to an error-weighted linear fit to the measurements shown in the insert)

Figure 5.10 shows plots of absorbance versus concentration for sudan black. The sudan black measurements were made at 584 nm and a range of concentrations from ~1 nM to ~50 nM. Three replicate measurements were made at each concentration and the error bars for each concentration represent the standard deviation of the measurements. The plot can be broken into two parts. These data in the inset shows measurements in the range ~1 nM to ~5 nM, which show a linear dependence of the absorbance on the concentration. The measurements at higher concentrations, up to ~50 nM were nonlinear. An error-weighted regression through the linear part of the plot yields a straight line (equation of the line is given in fig. 5.10) with the correlation coefficient R^2 = 0.997 and a 1σ error limit for the intercept of 2.1 x 10^{-3}. The LOD can be calculated from the value of the 3σ error limit on the intercept, which produces a

concentration of 156 pM. The limit of quantification (LOQ) can also be determined from the 10σ error limit on the intercept and yields a concentration of 521 pM. At absorbance values above ~0.2 the plot in fig. 5.10 is no longer linear with respect to increasing concentration, but measurements of absorbance values of up to ~ 0.7 were made without significantly visible increases in the 1σ error limit on three replicate measurements.

5.3. Discussion

Results have been obtained for liquid phase BBCEAS measurements in a 20 cm cavity with the analytes methylene blue and sudan black dissolved in acetonitrile. This represents the first time that BBCEAS has been applied to liquid phase analytes in such a long pathlength cavity. The main figures of merit obtained were values of the *CEF*, the α_{min}, and also the LODs by two independent methods. These are discussed after initial comments on some of the experimental challenges presented by this study and the general applicability of the technique. This is followed by a comparison with previous cavity studies in which the mirrors were in direct contact with the liquid phase analytes, and finally some suggestions as to how the experimental setup could be improved are made.

The motivation for making this study arose from trying to make ultra sensitive absorption measurements on liquid phase analytes using BBCEAS. The previous study in a 2 mm cuvette (chapter three), suggested that major improvements would arise from the hundred fold increase in base pathlength and also the lack of a cuvette in the cavity should lead to lower background interface scattering and absorption losses, which would allow improvements in the sensitivity with higher reflectivity mirrors. These improvements have been largely realised, but the experimental difficulties raised by the solvents proved something of a surprise. Hallock *et al.* [6] had hinted at the problems raised by the choice of solvent and had made suggestions for measurements in the 620 – 670 nm range, but no information was given for measurements at shorter wavelengths. Our preliminary studies with a range of solvents showed that absorptions due to high overtone CH and OH stretches either precluded their

use in measurements beyond 600 nm or introduced restrictions for the wavelength range in which the maximum number of passes could be achieved. The long effective pathlength of ~16 m with the $R \geq 0.99$ mirror set also accentuated differences in the transmission of the solvents at other wavelengths. It is recommended to use the highest purity spectrophotometric grade solvent that can be afforded. Acetonitrile which was the solvent chosen for use in this study had significant absorptions at ~620 nm and ~550 nm due to the 5^{th} and 6^{th} CH overtones. The widths of the absorptions were ~20 and ~30 nm respectively. This represents at least ~20% of the visible spectrum (400 – 700 nm) where it will be difficult to obtain a large number of passes. The higher CH overtones (e.g. 7^{th} overtone at ~475 nm) should get progressively weaker but will have a greater effect if higher reflectivity mirrors are used. The applicability of this technique is consequently limited for those analytes where the peak absorption coincides with the CH overtones. However, most liquid phase analytes which absorb in the visible, have broad absorption spectra with peak widths >50 nm, and even if the BBCEAS spectra are distorted by solvent absorptions the technique can still be usefully applied.

The *CEF* values obtained with the $R \geq 0.99$ mirror set for methylene blue (*CEF* = 78) and sudan black (*CEF* = 82) are approximately the same. The small difference is most probably due to the variation in reflectivity profile of the mirror set, as a function of wavelength. Comparing these values with those obtained using the 2 mm cuvette, one can see that the best value obtained in that study (*CEF* = 52, with the $R \geq 0.99$ mirror set) is significantly lower, which is good evidence to show that as expected, the background cavity losses are considerably reduced in this study. This is further confirmed when comparing the *CEF* values obtained using the higher reflectivity $R \geq 0.999$ mirror set. For the 2 mm cuvette study the highest *CEF* value was only 104, that is, only a twofold increase in the number of passes on increasing the mirror reflectivity tenfold, which was attributed to the limiting interface losses from the cuvette. For the present study, measurements with the $R \geq 0.999$ mirror set were made on methylene blue and a *CEF* value of 429 was obtained. This is a ~5.5 fold increase in the number of passes on increasing the mirror reflectivity tenfold. However, it is still lower than what would be expected from gas-phase

measurements, for which the number of passes is given by $(1 - R)^{-1}$ [6]. That is, $R \geq 0.999$ mirrors should result in ≥1000 passes. This however, assumes that background scattering and absorption losses are insignificant, also the stated reflectivity of mirrors is quoted for contact with air. When the mirrors are in contact with a liquid the actual reflectivity can decrease significantly, especially for higher reflectivity mirrors.

The sensitivity of the BBCEAS measurements as determined by the α_{min} value has been calculated for all the measurements in this study. For the experiments on methylene blue and sudan black with the $R \geq 0.99$ mirror set values of 4.4×10^{-7} and 3.4×10^{-7} cm^{-1} have been obtained. The difference in the values arises from the fact that the spectral intensity of the white LED used for these measurements was significantly higher at 584 nm (the peak absorption wavelength for sudan black) than at 655 nm (the peak absorption wavelength for methylene blue). Consequently shorter integration times could be used for the sudan black measurements, which resulted in lower levels of dark noise from the CCD detector and thus a lower α_{min} value. Comparing these values with those obtained from the 2 mm cuvette it can be seen that the current values for the $R \geq 0.99$ mirror set, are approximately one hundredfold better, which is what one might expect given that the base pathlength is 100 times longer, and the *CEF* values are slightly higher. However, the lower background losses in the 20 cm cavity allowed these values to be obtained with a white LED, whilst the best values with the 2 mm cuvette required the use of a higher intensity red LED. If the best values with the white LED in the 2 mm cuvette are compared, then the present values are approximately 500 times better. The differences increase to a factor of approximately 1400, when the measurements with the $R \geq 0.999$ mirror set and the red LED are compared. The greater losses in the 2 mm cuvette setup, resulted in far worse α_{min} values than obtained with the $R \geq 0.99$ mirror set, whilst in the 20 cm cell the lower cavity losses allowed a ~5.5 fold increase in the number of passes, which compensated for the increased noise from a longer integration time and actually resulted in a small improvement in the α_{min} value compared to the $R \geq 0.99$ mirror set.

The LOD for all the analytes has been calculated by two independent methods. The spectral method used the α_{min} value calculated from the 10 successive absorption spectra (see chapter 3.2), whilst the regression method obtained the LOD from the error limit on the intercept of a plot of absorbance versus concentration, and knowledge of the effective pathlength of measurement and molar extinction coefficient of the analyte. It is clear that the LOD values obtained by the regression method are substantially higher than those obtained by the spectral method. Initially this difference appeared puzzling as the regression method involved three replicate measurements at each concentration which have should in principle led to a more accurate value than the spectral method which essentially was obtained from one measurement. However on further investigation it appeared that the replicate measurements introduced a new source of error due to the mechanical stability of the optical cavity. Emptying and refilling the cavity resulted in small changes in the cavity alignment leading to small changes in the measured absorbance. It was not possible to adjust the cavity mirrors to get exactly the same cavity alignment for each replicate measurement and thus this variation becomes the limiting factor in obtaining the LOD by the regression method. We would suggest that the LODs obtained by the spectral method are a fairer indication of what is achievable with the BBCEAS setup.

The linear dynamic range for the BBCEAS measurements were nearly two orders of magnitude for the experiments carried out using the $R \geq 0.99$ mirror sets. For larger absorbance values, the response became non linear as shown in figure 5.6 and 5.10, but in principle could still be quantified using a calibration curve. The nonlinear behaviour at higher concentrations was attributed to the increasing absorbance of the analyte, resulting in lower number of passes and subsequently a reduction in the effective pathlength.

For the moderately broad absorptions of methylene blue in figure 5, spectral distortion can be observed at ~620 nm from background solvent absorption. For broad absorptions such as that of sudan black in figure 5.9, spectral distortion is present at ~550 nm and ~620 nm from background solvent absorption, whilst the other spectral distortions arise from the mirror reflectivity profile. The single-pass spectrum of sudan black is by comparison broad and featureless. These spectral distortions could in principle be corrected by

knowledge of the form of the reflectivity profile of the mirrors either from the manufacturer's data sheet or from independent CRDS measurements, along with accurate measurement of the background absorption of common solvents. A simpler procedure could be to obtain the form of the reflectivity and background absorption profile by taking the ratio of the BBCEAS spectrum of a broad absorber in a given solvent, to the single-pass spectrum and using those data to correct all other spectra.

Table 5.2: A comparison between this study and previous selected liquid-phase cavity studies as a function of technique, the mirror reflectivity, base pathlength, the wavelength of measurement, the lowest value of α_{min}, the minimum LOD for an analyte, and the molar extinction coefficient ε for that analyte

Study	Technique	Mirror reflectivity	Base path length (cm)	Wavelength (nm)	α_{min} (cm^{-1})	LOD (M)	ε (M^{-1} cm^{-1})
This work	BBCEAS	0.999	20	655	2.8×10^{-7}	4.6×10^{-12}	7.9×10^{4}
Hallock *et al.* [6]	CRDS	0.9998	21	620-670	1×10^{-6}	$\sim 1 \times 10^{-11}$	1×10^{5}
Hallock *et al.* [5]	CRDS	0.9998	23	655	3.3×10^{-7}	-	-
Bahnev *et al.* [7]	CRDS	0.9998	0.2	532	1.6×10^{-4}	2.5×10^{-9}	5.4×10^{4}
van der Sneppen *et al.* [3]	CRDS	0.99996	0.2	532	1.0×10^{-5}	1.5×10^{-8}	1.4×10^{4}
van der Sneppen *et al.* [3]	CRDS	0.9995	0.2	355	5.0×10^{-5}	7.5×10^{-8}	1.02×10^{4}
McGarvey *et al.* [8]	CEAS	0.99998	0.175	783	3×10^{-6}	2×10^{-10}	6×10^{4}

Table 5.2 summarises some of the figures of merit from this study such as lowest value of α_{min} obtained, the lowest LOD obtained, and the molar absorption coefficient for the particular analyte. These are compared with corresponding data where available, from the small number of reported previous liquid phase cavity studies where the analyte was in direct contact with the cavity mirrors. Comparing with the results from this study, it can be observed that the mirror reflectivities used in the previous studies were generally much higher. The best figures of merit for this study were obtained with the $R \geq 0.999$ mirror set but the values obtained with the $R \geq 0.99$ mirror set were only slightly worse. The lowest α_{min} value obtained in this study is 2.8 x 10^{-7} cm^{-1} which is the lowest reported value to date for a liquid phase measurement, making these the most sensitive liquid phase absorption measurement reported. It should be pointed out that α_{min} is directly proportional to the base pathlength, and at 20 cm the base pathlength used in this study is amongst the longest used to date. It is most similar to those used in previous studies by Hallock *et al*. [5] and it is with these studies that closest comparison should be made. The first study by Hallock *et al.* [6] made CRDS measurements in a 21 cm base pathlength cell. A wide range of analytes were apparently studied but firm figures such as range of concentrations used were only given for copper acetate dissolved in acetonitrile. The sensitivity of the experimental setup was determined from a calibration plot of absorbance versus concentration and also considering the standard deviation in the ring down time as a function of time in a sample of pure acetonitrile. This led to a value of α_{min} =1 × 10^{-6} cm^{-1}, which is about four times higher than our best value and was obtained using a far more expensive experimental setup and considerably more complex experimental methodology. The second study by Hallock *et al.;* [5] used a simpler experimental setup based on cw-CRDS in a 23 cm cavity, using a cheap red laser diode. It was mainly concerned with demonstrating ultratrace kinetic measurements on methylene blue, but the sensitivity of the technique was stated to be ~3.3 × 10^{-7} cm^{-1}. This is similar to our best value and although the experimental setup is cheaper than the first study by Hallock *et al.* [6] it is still substantially more expensive than the setup used in this study as an AOM had to be used as a fast shutter to facilitate ringdown of the cavity, and fast response detection was still needed. The other studies in table 5.2 used much

shorter base pathlengths and consequently the listed α_{min} values are much higher than those obtained in this study. Table 5.2 also lists the best LOD value for the analytes studied, where available. For this study the lowest LOD of 4.6 pM, was obtained for methylene blue with the $R \geq 0.999$ mirrors. To our knowledge this represents the lowest reported LOD for a liquid phase absorption measurement. Hallock *et al.* [6] state that LODs of 10 pM could be achieved with their experimental setup for strong absorbers with molar extinction coefficients of 1×10^5 M cm^{-1} but no actual measurements on suitable analytes were reported. The second Hallock *et al.;* study [5] did not report a LOD for their kinetic measurements on methylene blue, whilst the other studies in table 5.2 have much higher reported LODs as a result of much shorter base pathlengths.

One advantage of the BBCEAS experiments as shown in figure 5.5 and 5.9 is that experiments can be made over a wide wavelength range in a single measurement, usually limited by the bandwidth of the cavity mirrors used or the bandwidth of the light source. The measurements on methylene blue and sudan black with the white LED and the $R \geq 0.99$ mirrors covered a wavelength range of ~150 nm and ~250 nm respectively. This allows the full spectral profile of the analyte to be obtained in a single measurement. By comparison the previous liquid phase cavity studies listed in table 5.2, were predominantly CRDS measurements and were carried out at a single wavelength.

Although this study has demonstrated the most sensitive liquid phase absorption measurements to date, it is possible to improve the experimental setup in several ways. The simplest method for improving the sensitivity of the measurements would be to increase the base pathlength of the cavity. This would however also increase the volume of the cavity and make it less suitable for analytes which were only available in small quantities. This disadvantage could be addressed by using narrower diameter tubing to form the cavity, although this would make alignment of the cavity more difficult.

Further improvements could be achieved either through changing the CCD spectrograph used and/or increasing the intensity of light transmitted through the cavity. As noted earlier, the uncooled CCD detector used in this study suffered from large amounts of dark noise at longer integration times, resulting in poorer than expected results. A thermoelectrically cooled CCD

detector operating at ~-70^{o}C would largely eliminate this problem but would cost in the region of £10000 to implement. This would mainly benefit the measurements with the $R \geq 0.999$ mirror set, as these required integration times of ~2.5 s in the current study. Assuming that the α_{min} values scale with the *CEF* values if dark noise is no longer a factor, one would expect α_{min} values in the region of 6×10^{-8} cm^{-1} which would lead to a LOD for methylene blue of 990 fM.

A cheaper alternative could be to use a higher intensity light source. Already more powerful 5W white LED light sources are available for only a small increase in price. Provided this extra photon flux could be collimated into the cavity this would lead to shorter integration times being used and thus less dark noise. A similar result would be achieved if more efficient collimation of the light source and alignment of the cavity to create greater cavity transmission were possible.

A final method for improving the sensitivity of the measurements would be to use higher reflectivity cavity mirrors to increase the number of passes through the cavity and thus the effective pathlength. These would only be effective in regions removed from background solvent absorptions. Analysis of the results from Hallock *et al.* [6], show they achieved ~3000 passes in their study with $R \geq 0.9998$ mirrors, which is about seven times greater than that achieved in this study. The use of higher reflectivity mirrors would however reduce the transmission through the cavity and so would have to be implemented with some of the other improvements suggested above, to be fully effective. It would also be advisable to use mirrors where the design specification takes into account the direct contact between the analyte and the mirrors.

The applicability of the BBCEAS technique would benefit from extension into both the UV and near infrared (NIR) regions as a greater number of analytes could potentially be studied. This would require the use of high reflectivity mirror sets which covered the UV and NIR regions as well as suitable light sources. The background solvent absorption would be stronger in the NIR as lower CH and OH overtone vibrations are present in this region, whilst measurements in the UV region would be hindered by the onset of electronic transitions in the solvent, but these potential problems may well provide an

alternative use for this technique, as a sensitive means for studying weak absorptions in solvents.

5.4. Conclusions

A simple, low cost experimental setup, based on BBCEAS in a 20 cm cavity in which the solvent was in direct contact with the cavity mirrors, has been demonstrated on the analytes sudan black and methylene blue, dissolved in acetonitrile. The experimental methodology was simple and similar to conventional UV-visible absorption spectroscopy. Background solvent absorptions due to the 5^{th} and 6^{th} overtone CH stretch, resulted in significant distortion of the absorption spectra around 620 and 550 nm respectively, and resulted in some restrictions on the choice of analytes. Measurements were made with a white LED and the $R \geq 0.99$ mirror set on sudan black (between 450 and 700 nm) and methylene blue (between 550 and 700 nm), whilst the use of a red LED also allowed measurements on methylene blue (between 635 and 670 nm) with the higher reflectivity $R \geq 0.999$ mirror set. In the wavelength regions removed from the solvent absorptions the cavity losses were much lower than the previous measurements with the 2 mm cuvette, and with the $R \geq 0.999$ mirror set, a *CEF* value of 429 was achieved, indicating the number of passes was no longer restricted by background cavity losses. The sensitivity of the experiments was determined through calculation of the minimum detectable change in the absorption coefficient, α_{min}. The best value of 2.8×10^{-7} cm^{-1} was obtained with the $R \geq 0.999$ mirror set, although this value was restricted by dark noise from the long integration time needed, and was only marginally better than the figures obtained with the $R \geq 0.99$ mirror set. Nevertheless, in comparison to previous studies, this value represents the most sensitive liquid phase absorption reported to date. Likewise, the best LOD value for methylene blue of 4.6 pM is to our knowledge, the lowest recorded detection limit for a liquid phase absorption measurement. Improvements to the experimental setup could be made through the use of a thermoelectrically cooled CCD detector which produces lower levels of dark noise at long integration times, a higher intensity light source, better cavity alignment and the use of higher reflectivity cavity mirrors.

5.5. References

[1] Venables, D. S. Environmental science technology, 40 (2006) 6758.

[2] Venables, D. S. Proceedings of SPIE--the international society for optical engineering, 5826 (2005) 202.

[3] van der Sneppen, L.; Wiskerke, A.; Ariese, F.; Gooijer, C.; Ubachs, W. Analytica Chimica Acta, 558 (2006) 2.

[4] van der Sneppen, L., Ariese, F.; Gooijer, C.; Ubachs, W. Journal of Chromatography A, 1148 (2007) 184.

[5] Hallock, A. J.; Berman, E. S. F.; Zare, R. N. Applied Spectroscopy, 57 (2003) 571.

[6] Hallock, A. J. Analytical chemistry, 74 (2002) 1741.

[7] Bahnev, B.; van der Sneppen, L.; Wiskerke, A. E.; Ariese, F.; Gooijer, C.; Ubachs, W. Analytical Chemistry, 77 (2005) 1188.

[8] McGarvey, T. Optics express, 14 (2006) 10441.

Chapter Six

6.0. Discrimination of teas based on total luminescence and pattern recognition

The main aim of this work was to develop a novel application of total luminescence spectroscopy to discriminate between several types of teas objectively. Firstly teas from geographically different regions were investigated. Following this, teas from similar region in Sri Lanka was discriminated using pattern recognition on total luminescence data collected.

This chapter begins with a brief history on tea, description of its constituents and a review of previous studies which have attempted to classify tea. A description of the principles of fluorescence detection is also given, followed by an explanation of principal component analysis, the pattern recognition technique used in this study.

Tea is the most widely consumed non alcoholic beverage in the world aside from water [1, 2] with an annual production of 1.8 million tonnes of dry leaves. It is estimated that somewhere between 18 and 20 billion 6 oz. cups of tea are drunk daily on our planet [3, 4]. According to Chinese mythology, tea was first discovered accidentally in China in 2737 BC when tea leaves fell in boiling water and Emperor Shen Nung enjoyed the resulting dark liquid. Since 3000 BC tea has been consumed for its medicinal properties.

Tea is usually made from the tender leaves of two varieties of the plant Camellia Sinensis. It is grown in about 30 countries but is consumed worldwide, although at greatly varying levels. Tea is extensively cultivated in China, Japan, Assam, Java, Bengal, Ceylon, Sicily, Portugal, Brazil and Jamaica. Botanically tea is a tree, but for commercial farming it is grown as a bonsai, by repeated pruning and clipping, with a usual life span of over 100 years. Tea bushes take about 7 years to reach maturity, but are ready for commercial plucking in 5 years and the yield is high during the first 30 to 50 years. The quality is subjected to the climatic influences and it is also dependent on soil, growing

environment, culture and manufacturing conditions, size of ground tea leaves and infusion preparation [5-8].

6.1. Classification of tea

Tea is generally classified as white, Green, Oolong, and Black depending on the amount of fermentation it has undergone and also based on the apparent colour.

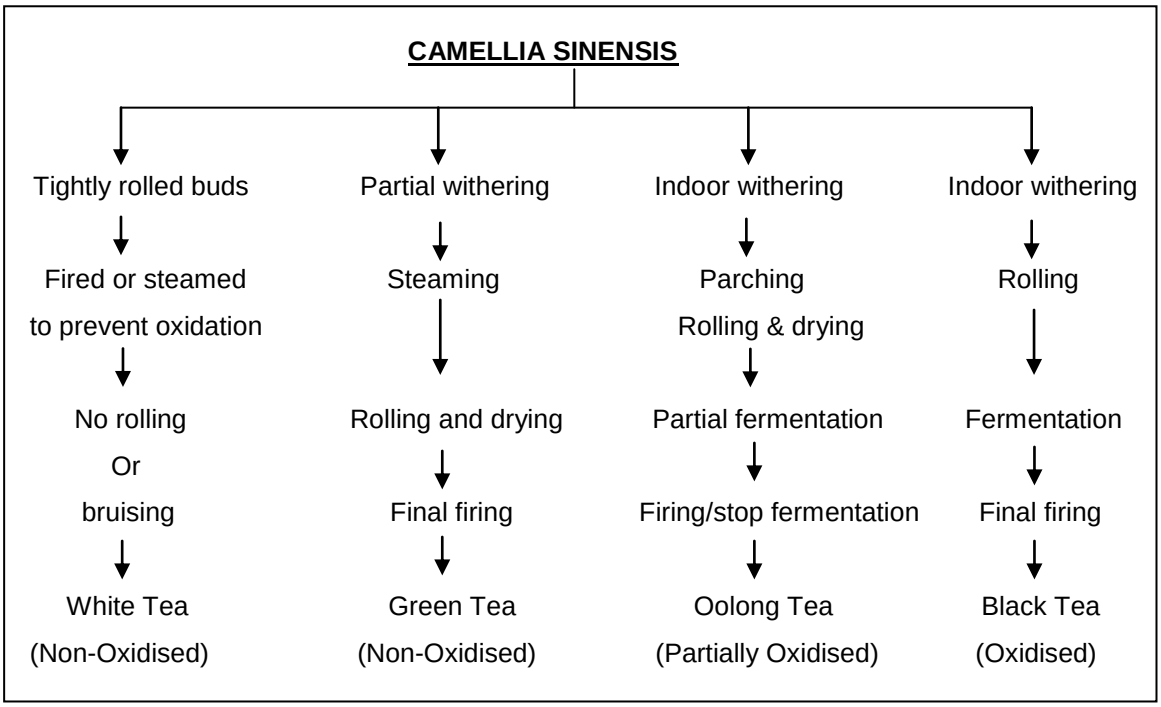

Figure 6.1: Classification of tea according to their processing techniques.

White tea is made from just the tightly rolled buds and does not undergo any oxidation or fermentation process. In order to prevent enzymatic oxidation the buds are immediately fired or steamed and then air dried (withered). The dried buds have silver like appearance and white tea is also known as Silver Needle.

Green tea is made by inactivating the fresh tender leaves, either by firing or steaming them to prevent the enzymatic oxidation of catechins. Processed products are generally described as roasted green tea and steamed green tea. The common name for green tea is Sencha.

Oolong tea also known as brown tea is prepared by firing the leaves shortly after rolling and drying the leaves. It is partially fired and then steamed. The

firing process ends the fermentation process. Hence Oolong tea is called as semi fermented tea. Its characteristics are found to be in between black and green tea.

Black tea is made by a fermentation process during which simple polyphenols are oxidised, giving black tea its astringent flavour. Fermentation is stopped by drying (firing) the leaf with hot dry air. The process deactivates the enzymes and reduces the moisture content to 2- 4 %. Before the firing process the taste is harsh and metallic, but the subsequent combination of polyphenols with leaf proteins decreases the astringency. Leaves can be processed as orthodox or CTC (Cut, Tear and Curl). CTC production accelerates fermentation and gives a higher cuppage (almost twice) for the same quantity of tea and produces a stronger liquor [6, 20].

Researchers have endeavoured to develop methods for classifying different types of teas. Teas has been classified according to their metal content [2, 21, 22][15], chemical composition and colour difference [23], Volatile components [24], Physico chemical properties [25], infrared spectroscopy [26], and also using an electronic nose [27] and electronic tongue [28].

In the manufacturing of tea, the human senses (Tea tasters) of smell and sight are used as important tools for quality diagnosis. Sensory evaluation can be subjective, but with careful design of a scoring system and rigorous training of the assessors, the evaluation can become more objective. However this remains an expensive option. Costly and time consuming instrumentations that require trained personnel have been used for the determination of odour, colour and taste. These include methods such as gas chromatography/mass spectrometry (GC-MS), high performance liquid chromatography (HPLC), colour difference meters, inductively coupled plasma atomic emission spectrometry (ICP-AES) and inductively coupled plasma mass spectrometry (ICP-MS). As a result there has been an effort to investigate devices or instrumental methods for more objective and inexpensive analysis of tea that do not require specialist technicians. Fluorescence spectroscopy is a well established simple, fast, accurate and non destructive technique and this study represents the first reported use of this technique for the classification of teas.

6.2. Consumption of tea

Black tea is more common in the western countries and it was brought to Europe during the second half of the seventeenth century, while Green tea is most common in Asian countries like China, Japan and Taiwan. Black teas mostly come from plantation in Africa, India, Sri Lanka and Indonesia whilst Green teas come from countries in the Far East such as China and Japan. India is the largest producer and consumer in the world. Being an agricultural commodity, the quality of tea is very sensitive to weather conditions whilst labour costs usually account for about 60 % of the total cost of production.

6.2.1. Quality of tea

Tea quality mainly depends on the variety of leaf, growing environment, manufacturing; particular size of ground tea leaves and infusion preparation, also its quality is measured on the basis of liquor, aroma (flavour) and leaf appearance. The best teas are produced at altitudes of 1000 to 2000 m, because tea plants grow more slowly in cooler air and the leaves yield a better flavour. High quality tea is made from the young shoots consisting of the bud and the first two leaves. The consumers of tea generally perceive quality differences on the attributes of taste, pungency, strength, freshness, colour, brightness, briskness and packing. One of the most popular forms of value addition is selling branded tea. This involves blending of many varieties of tea to maintain the consistency of taste and the blend is reached when tea taster samples hundreds of liquors. Tea tasting is a highly specialised occupation, where the tea tasters differentiate between the various flavours of tea and help to brand the varieties according to quality [6-8].

6.2.2. Chemical constituents of tea responsible for taste

Tea leaf, in common with all plant leaf matter, contains enzymes, biochemical intermediates, carbohydrates, protein, lipids, and structural elements normally associated with plant growth and photosynthesis. In addition, tea leaf is distinguished by its remarkable content of methylxathines and polyphenols. These two groups of compounds are predominantly responsible for those unique properties of tea that account for its popularity as beverage. The most important chemical constituent that influences the taste and flavour in tea infusions are polyphenols, flavonols, caffeine, sugars, organic acids, amino acids and volatile flavour compounds. Phenolic compounds of tea such as theaflavins and thearubignins are very important from an intrinsic quality point of view and constitute 60% of the total water-soluble constituents of black tea. Moreover they are responsible for the major organoleptic properties of colour, brightness (bright orange/red tone) and astringency [7, 9-11]. Tea catechins (Flavonols)- Epigallocatechin gallate (EGCE) , Epigallocatechin (EGC), Epicatechin (EC) etc., are colourless, water soluble compounds which impart bitterness and astringency to green tea infusion. Green Tea leaves are rich in polyphenolic compounds that belong to the flavonoid group. Flavonoids are compounds whose structure is based on the flavone structure as shown in figure 6.2 [6]

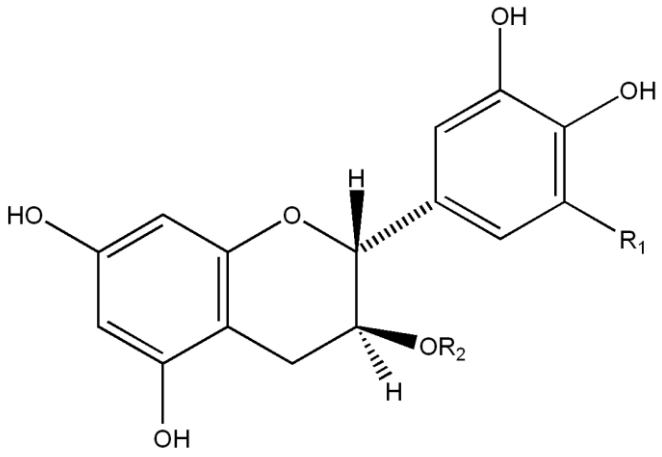

$R_1 = H,\ R_2 = H$ Catechin
$R_1 = OH,\ R_2 = H$ Gallocatechin (GC)
$R_1 = OH,\ R_2 = galate$ Epigallocatechin gallate (EGCG)

Figure 6.2: The structure of common flavonoids (Catechins).

Almost all the characteristics of manufactured tea including taste, colour and aroma are associated directly or indirectly with the modification of catechins. During black tea manufacture catechins decrease is associated with the increase of monoterpene alcohols. Degalloation from ester catechins to non-ester catechins results in bitterness and astringency of green tea [12-14].

Other important constituents are theine (caffeine), varying in commercial specimens from 2.5 – 5.5% of the dry matter of tea leaves. Caffeine is responsible for the briskness. Large quantities of tannic acid, identical with gallotannic acid, from 7 to 21 per cent; gallic acid, oxalic acid, and quercetin, Kossel (1888) found theophylline in tea extract, a compound which was similar to theobromine. The biosynthesis of these two compounds involves methylation of hypoxanthine or xanthine which forms caffeine. The chemicals observed by Rochleder and Kossel show the interest in tea analysis already present in the late nineteenth century [15].

Green tea contains more tannic acid than black tea, which is prepared from the same lot of fresh leaves. Hence it can be concluded that it decomposes during fermentation. The amount of theine is practically the same in both. Theine was discovered in tea 1827, and found to be identical with caffeine in 1838. The strength of tea is not necessarily proportionate to the amount of theine present. David Hooper [16] determined the tannin in 65 specimens of India and Ceylon teas, and found them to vary from 10 to 21 per cent; the finest grades contained the most tannin. The quality or strength of tea is determined by the proportion of theine to total tannin, including that, which is altered in the fermentation process. In the finest teas, the proportion of theine is large [17, 18].

6.2.3. Chemical constituents and biochemistry

Many volatile have been detected in green tea, but about 30 of them have been identified, including benzyl, phenylmethyl alcohols, hexenol, linalool, geraniol and methyl salicylate as the main constituents. The first major classification of flavour compounds could be by its volatility or how easily the compound evaporates in air. A single compound can evoke many different flavour characteristics, but normally arouses one type of response from one type of

receptor in the nose. An overview of flavour chemicals in green tea is shown in Table 6.1.

Table 6.1: Volatile compounds classes and sensory characteristics of green tea.
(A VFC data report, 1999 [1, 5, 8, 19])

CHEMICAL CLASSES	SENSORY CHARACTER	EXAMPLES
Acids	Urine, sweat, rancid, sweaty, rancid butter, sour	Benzoic acid, Octanoic acid, Pentanoic acid, Butanoic acid, 2-Methyl propanoic acid, Acetic acid.
Alcohols	Bitter, Medicinal, Piney, Caramel, geranium, Sweet.	Linalool, Methanol, α – Terpineol, Benzyl alcohol, Cadinol, 1, 5-Octadien-3-ol.
Aldehydes	Fruity, Green, Oxidised, Sweet, Soapy, Almond.	Acetaldehyde, Hexanal, Decanal, Vanilin, Nonanal, Benzaldehyde.
Bases	Popcorn, nutty, earthy, pea.	2,6 dimethyl pyrazine, Methylpyrazine, Indole, Ethylpyrazine, Ethyl amine.
Esters	Fruity	Dibutylphthalate, Benzyl acetate, Methyl jasmonate.
Hydrocarbons	Naphthalene, (Alkanes are usually odourless)	Tar
Ketones	Almond, Pungent, Mushroom, Geranium, Butter.	Acetophenone, Alpha-Ionone, 1-Octen-3-one, Teaspirone, Jasmone.
Maillard reaction products	Brown, Burnt, Caramel, Earthy.	Pyrazine(s), Pyridine, Furans.
Phenolics	Medicinal, Smokey.	Phenol(s), Thymol, Anethole.
Terpenoids	Citrus, Piney.	Limonene, Pinene.

With the invention of gas chromatography many volatile compounds have been identified. Identification and quantification of flavour chemicals cannot be the sole objective of the modern day flavour chemists, as gas chromatography analysis does not establish the contribution of individual volatile compounds to flavour. It has also been found that, large peaks on the

chromatogram do not necessarily correlate to flavour. Hydrocarbons like long chain alkanes are sometime present in high quantity in green tea, but often show weak aromas. The hydrocarbons are quite helpful in bringing the flavours to the nose as they acts as solvents and combine with other flavour compounds and form azeotropic mixtures that evaporate easily. In green tea, aldehydes like hex-2-enal (Figure 6.3) impart the green flavour, whereas benzaldehyde imparts a strong almond flavour.

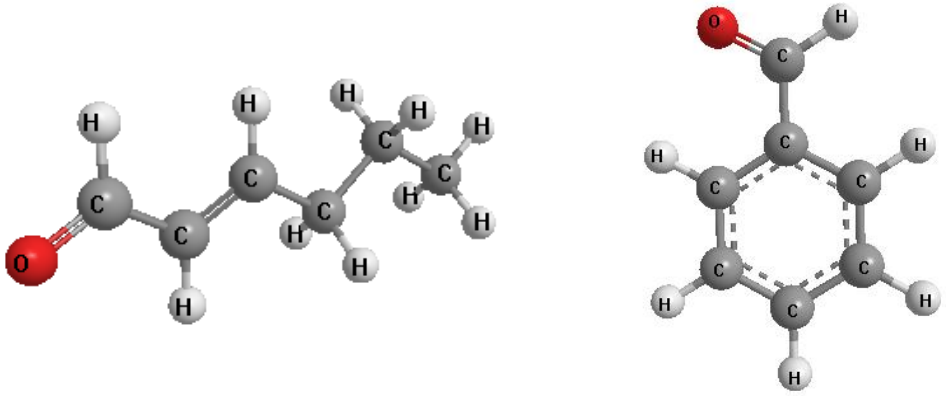

Figure 6.3: Structure of hex-2-enal (green flavour) and benzaldehyde (almond flavour)

Alcohol has an odour threshold higher than corresponding aldehydes, hence they are normally less important to flavour profiles. Aldehydes and ketones are converted to alcohols on prolonged storage. Benzyl alcohol imparts a nice caramel aroma to tea and 1, 5-octadien-3-ol produces a sweet flavour and linalool (Figure 6.4) has a bitter flavour.

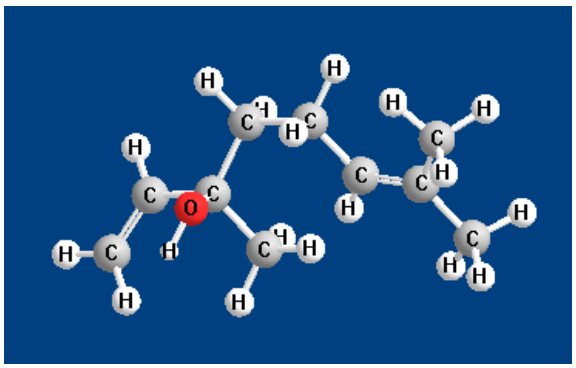

Figure 6.4: Structure of linalool (bitter flavour)

6.2.4. Thermal formation of aroma compounds in tea

In 1948 Ketrovich and Tokareva [19] showed that at high temperature aldehydes are produced by the interaction of amino acids and sugars and in 1962 Popov and Skobeleva [19] also observed the formation of carbonyl compounds on oxidation of amino acids by tea catechins at temperatures of about 70 to 95 ^{0}C. They also reported an increase in aldehydes, when green tea was exposed to a temperature of 70 ^{0}C. Before thermal treatment the amount of tea aldehydes was found to be 4.84 ppm, but after heating for 4 hours and 6 hours the amount of aldehydes were 6.31 ppm and 7.05 ppm respectively. They also showed that when phenylalanine and tea catechins were reacted at 70 ^{0}C a rose flavour was detected [19]. Formation of flavour compounds from the oxidative degradation of beta-carotene in tea fermentation was shown by Mikhail *et al* (1986) [19] and illustrated in figure 6.5.

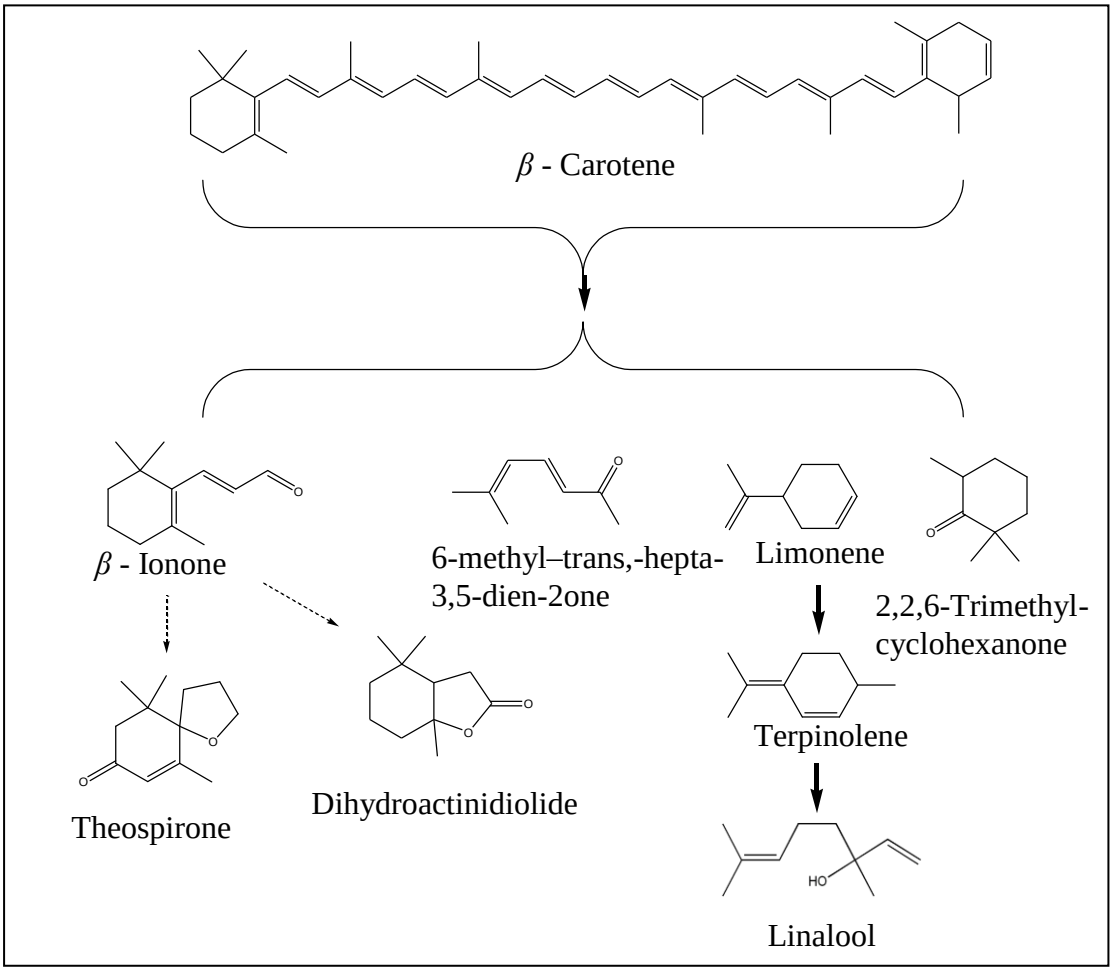

Figure 6.5: Oxidative degradation of carotenes during tea fermentation.

6.3. Fluorescence and Total luminescence spectroscopy

Fluorescence can be described as an optical phenomenon, in which a molecule absorbs a high-energy photon, and re-emits it typically as a lower energy (longer wavelength) photon. Usually the photon is absorbed in the ultraviolet and emitted (luminescence) in the visible range of the electromagnetic spectrum. Unlike absorption spectroscopy, fluorescence spectroscopy is not a universal technique as only a fraction of analytes contain energy levels which firstly are fluorescent and also are accessible at convenient wavelengths for qualitative and quantitative analytical purposes. However, the sensitivity of fluorescence based detection is typically several orders of magnitude greater than conventional absorption spectroscopy.

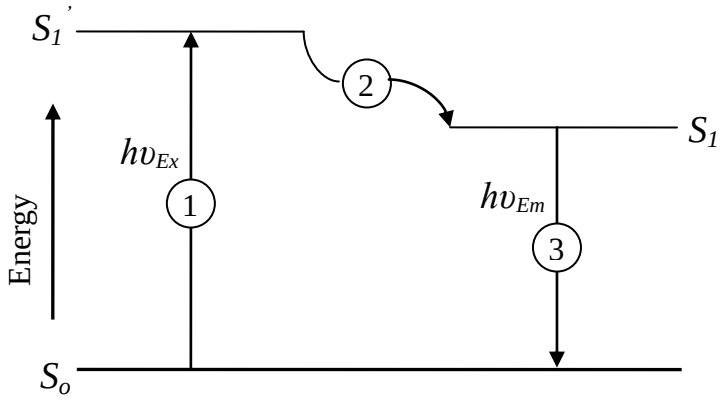

Figure 6.6: A Jablonski diagram

Fluorescence activity in a hypothetical material can be schematically illustrated by the three stages of the classical Jablonski diagram shown in figure 6.6. In the first stage a photon of energy $h\upsilon_{Ex}$ is supplied by an external source such as an incandescent lamp or a laser and absorbed by the fluorophore, creating an excited electronic singlet state S_1'. In the second stage, the excited state exists for a short time (1 – 10 ns) during which, the fluorophore undergoes conformational changes and is also subjected to interactions with the molecular environment. The two important consequences of these processes are, firstly the energy of S_1' is partially dissipated, yielding a relaxed singlet excited state

S_1 from which fluorescence emission originates. Secondly, not all the molecule initially excited by absorption of stage 1 returns to the ground state S_o , by fluorescence emission. Other processes such as collisional quenching, fluorescence resonance energy transfer (FRET) and intersystem crossing may also depopulate the excited state. The third stage consist of a photon of energy $h\upsilon_{Em}$ being emitted, returning the fluorophore to its ground state S_o. As a result of the vibrational relaxation of the excited state, the energy of this photon is lower, and therefore of a longer wavelength, than the excited photon $h\upsilon_{Ex}$. The difference in energy or wavelength represented by ($h\upsilon_{Ex}$ - $h\upsilon_{Ex}$) is called the Stokes shift. The Stokes shift is fundamental to the application of fluorescence as a sensitive analytical technique as it allows emission photons to be detected against effectively a zero background, isolated from the excitation photons in the wavelength domain. In contrast as described in chapter two, absorption spectroscopy requires measurement of small changes in the intensity of the transmitted light relative to high levels of incident light levels at the same wavelength.

The fluorescence quantum yield, $\Phi_{F,}$ which is the ratio of the number of fluorescence photons emitted (Stage 3) to the number of photon absorbed (Stage 2), is a measure of the relative extent to which these processes occur.

The following equations and derivations (equations 6.1 to 6.6) has been adapted from Schulman's book on "Molecular Luminescence spectroscopy" [29] and describes the process of total luminescence spectroscopy.

The quantum yield is expressed by the following equation;

$$\phi_F = \frac{k_f}{k_f + k_d} \tag{6.1}$$

Where; k_f is the rate of fluorescence and k_d is the rate of the competing deactivation processes.

If the intensity of the incident light, I_o is known, then the intensity of light that is absorbed, I , can be calculated using the Beer-Lambert law;

$$I = I_o \left(1 - 10^{-\varepsilon c l}\right) \tag{6.2}$$

The fluorescence intensity, I_F, can be derived by combining equation 6.1 and 6.2 for a fluorophore at a set excitation (λ_i) and emission wavelength (λ_i)
Assuming $I_o(\lambda_i)$ is the intensity of excitation at wavelength λ_i and $\gamma(\lambda_i)$ is the fraction of I_F at wavelength λ_i.

$$I_{Fij} = \ln(10)\, cI_o(\lambda_i)\, l\varepsilon\phi_F \gamma(\lambda_j) \tag{6.3}$$

Total luminescence spectroscopy (TLS) is a multi dimensional technique that involves simultaneous acquisition of multiple excitation and emission wavelengths in order to increase the method selectivity. If the experimental fluorescence excitation spectrum is $x(\lambda_i)$ and the experimental fluorescence emission spectrum is $y(\lambda_i)$, and if I_{Fij} is measured for numerous wavelengths, the total luminescence spectrum can be represented by equation 6.4 for numerous wavelengths.

$$I_F = cx(\lambda_i)y(\lambda_j) \tag{6.4}$$

The TLS can be represented in terms of a matrix with vectors, X = $x(\lambda i)$ and Y = $y(\lambda_j)$, where equation 6.4 can be expressed as;

$$I_F = cXY^T \tag{6.5}$$

Plotting fluorescence intensity as a combined function of excitation and emission wavelength is known as the excitation emission matrix (EEM). If there are i components, equation 6.5 may be expanded on the condition that none of the mixture components interact.

$$I_F = \sum I_{Fi} = \sum c_i\, X_i\, Y_i^T \tag{6.6}$$

The excitation emission matrix can be used as a fingerprint for a single or a mixture of fluorescent components as they provide multidimensional fluorescence intensity information for both the emission and excitation wavelengths. The distinctive shapes of EEMs may be visually examined or

combined with pattern recognition for qualitative and quantitative measurements.

6.3.1. Principal Components Analysis with TLS.

Pattern recognition is commonly used with fluorescence spectra especially in interpreting EEMs with multiple components due to the large amount of data involved. As the TLS of tea is related to the content of polyphenols and flavanoids, and these compounds are responsible for the major organoleptic properties, it is proposed that TLS could be used as a measure of quality for tea. It is further proposed that rather than calibrate the TLS data to quantify individual components and then relate these concentrations to organoleptic quality; it might be possible to relate the data more directly to quality using statistical methods such as principal component analysis (PCA).

PCA is a statistical tool commonly used for unsupervised (i.e. no prior knowledge is assumed of the data) classification of multivariate data. The main aim of PCA is to reduce the dimensionality of the data so that it may be examined in lower dimensional space. This method allows natural clustering of the data to be observed as well as providing an insight into how effectively a pattern recognition system could classify the data. PCA works by finding a new set of axis, principal components (PC), which are linear combinations of the combinations of the original variables.

$$Y_1 = a_1 X_1 + a_2 X_2 + \ldots\ldots\ldots a_n X_n$$

$$Y_2 = a_{21} X_1 + a_{22} X_2 + \ldots\ldots\ldots a2_n X_n \qquad (6.7)$$

Where; Y_x - Principal component x; X_x – original variable x; a_x – Coefficient x.

The coefficients are chosen in such as way that each new variable is uncorrelated with the others. The PCs also are chosen so that they account for the maximum variation in the data. The components are calculated so that the principal component PC1 accounts for the largest variance, the second principal component PC2 accounts for the next largest variance and so on. Usually the

first three principal components will account for ≥ 85% of the variation of the data. The natural clustering of multidimensional data can be displayed either in a three dimensional plot with the first 3 principal component or a two dimensional plot with just the first two principal components PC1 and PC2. Several applications of PCA may be found in the literature with respect to establishing the difference between dissimilar teas using quality control data [30], trace metal contents [2, 31], colour [3], volatile components [23], and organic components [26].

In this study, TLS has been used as a fingerprint, and pattern recognition applied to these fingerprints has allowed the discrimination of different types of teas. TLS is a non-invasive technique where the sample is subjected only to excitation light and has been used successfully for many varied applications such as discrimination of fuels [32], water monitoring [33] and classification of oils [34].

6.4. Total luminescence spectroscopy and measurement procedures for geographically different teas.

Total luminescence measurements were carried out using a Hitachi F- 2000 (Tokyo, Japan) spectrofluorimeter, with a quartz cell (VWR, Leicestershire, UK) of 10 mm pathlength. The apparatus was remotely operated using the F3D software (Hitachi) on a PC connected via an RS232 port. The light source was a long life 150 W xenon lamp with ozone self dissociation function. The wavelength scan rate and the band pass were maintained at 1200 nm/min and 10 nm respectively.

Seven different types of Tea were used in this study. Three leaf teas; Assam (Sainsbury), Kenya (Sainsbury), Ceylon (Tea Pucker pure Ceylon tea) and four PET bottled Japanese Tea; Black Tea (Kirin Beverages), Oolong tea (Suntory), Green tea (Ito – En Beverages), Houji tea (Ito – En Beverages). The Japanese teas were kindly donated by the GEN foundation (London, UK).
Water purified by reverse osmosis, was used throughout.

6.4.1. Preparation of leaf tea samples for fluorescence analysis (Assam, Kenya and Ceylon).

Tea samples (0.5 g) were weighed and transferred into 60ml brown glass bottles. Hot water (80 ^{o}C, 30 ml) was added to each bottle by means of a pipette. The tea was allowed to simmer for 5 min and the liquor was then filtered through Whatman® No 1 filter papers (125mm diameter). The filtration process removed tea particles that produced scattering of the incident excitation light. The filtrate was collected and stored in brown glass flask for 15 min to allow the brew to cool to room temperature before being analysed using the fluorimeter. This sample procedure was repeated for each tea sample.

6.4.2. Preparation of bottled tea for fluorescence analysis.

The bottled teas were used without further filtration. It was found that they did not contain any particles that might interfere with the fluorescence analysis, as they are filtered during the manufacturing process. The bottled teas available for this study were found to be too concentrated as self quenching was observed when the EEMs were recorded. Hence the teas were diluted two fold with reverse osmosis purified water and then stored in brown glass bottles before analysis with the fluorimeter, as this produced an active concentration similar to that of the leaf infusion.

6.4.3. Total luminescence analysis.

The diluted solutions were placed in the 10 mm pathlength quartz cuvette and the total luminescence measurement was carried out using the fluorimeter. The temperature of the samples was recorded before each run, hence ensuring that they were at room temperature. The excitation wavelength was set from 250 to 590 nm with an interval of 20nm. The emission was set from 300 to 700 nm with an interval of 5nm. The contour interval was set at 10nm.

6.4.4. Statistical analysis

These data were standardised using Minitab version 14 (Minitab Inc, State College PA 16801-3008, USA). The 3D EEMs were constructed and the PCA was carried out using Unscrambler Version 9 (CAMEO Software Inc, Woodbridge,USA).

6.5. Results and discussions

The total luminescence spectra were recorded for the different teas. Residual excitation peaks were observed in the EEMs for excitation wavelengths at 20 nm intervals between 350 and 590 nm and emission wavelengths at 5 nm intervals between 340 and 605 nm.

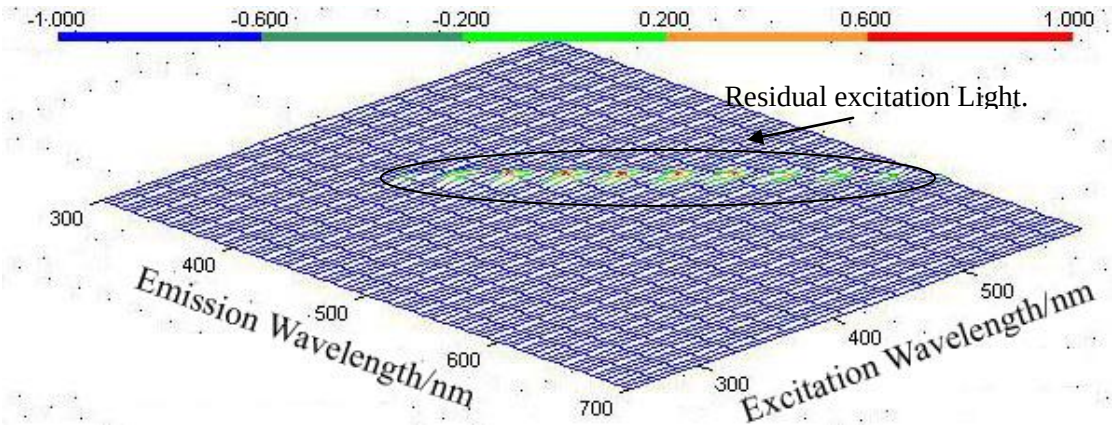

Figure 6.7: EEM of bottled black tea

Figure. 6.7, shows the EEM of Japanese black tea. It can be observed that because the residual excitation peaks have a relatively high intensity, the fluorescence from the tea is masked.

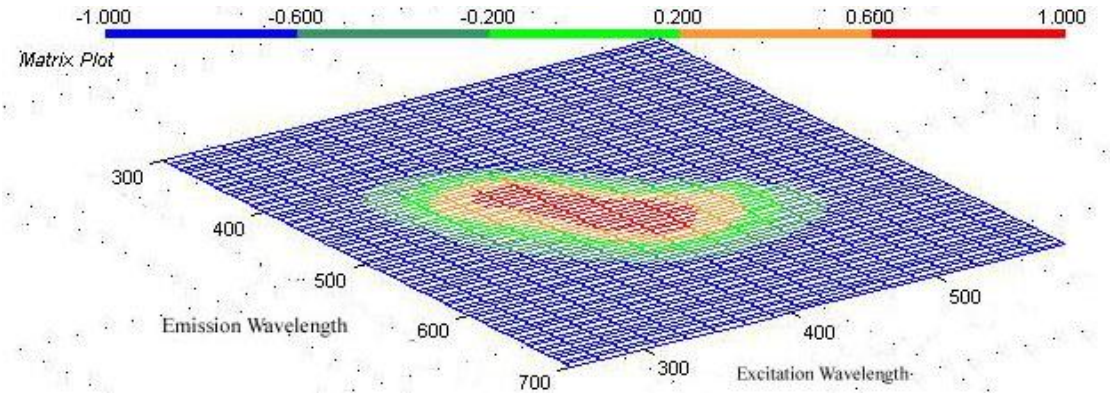

Figure 6.8: EEM of bottled Japanese black tea with the residual excitation light removed.

The residual excitation peaks were manually removed using excel from all the data collected and Figure. 6.8, shows the EEM of the same Japanese tea that was used to produce the EEM of in figure.6.7, but without the excitation peaks. The TLS data collected were standardized from 1 to -1 using Minitab 14. Hence the highest peak was given a score of 1 and the lowest peak a score of -1. This process was carried out in order to standardise all samples according to the proportion of the chemicals responsible for luminescence in the teas. The standardisation process reduced problems due to slight variations in infusion strength, and was also less difficult than trying to standardise infusion strengths.

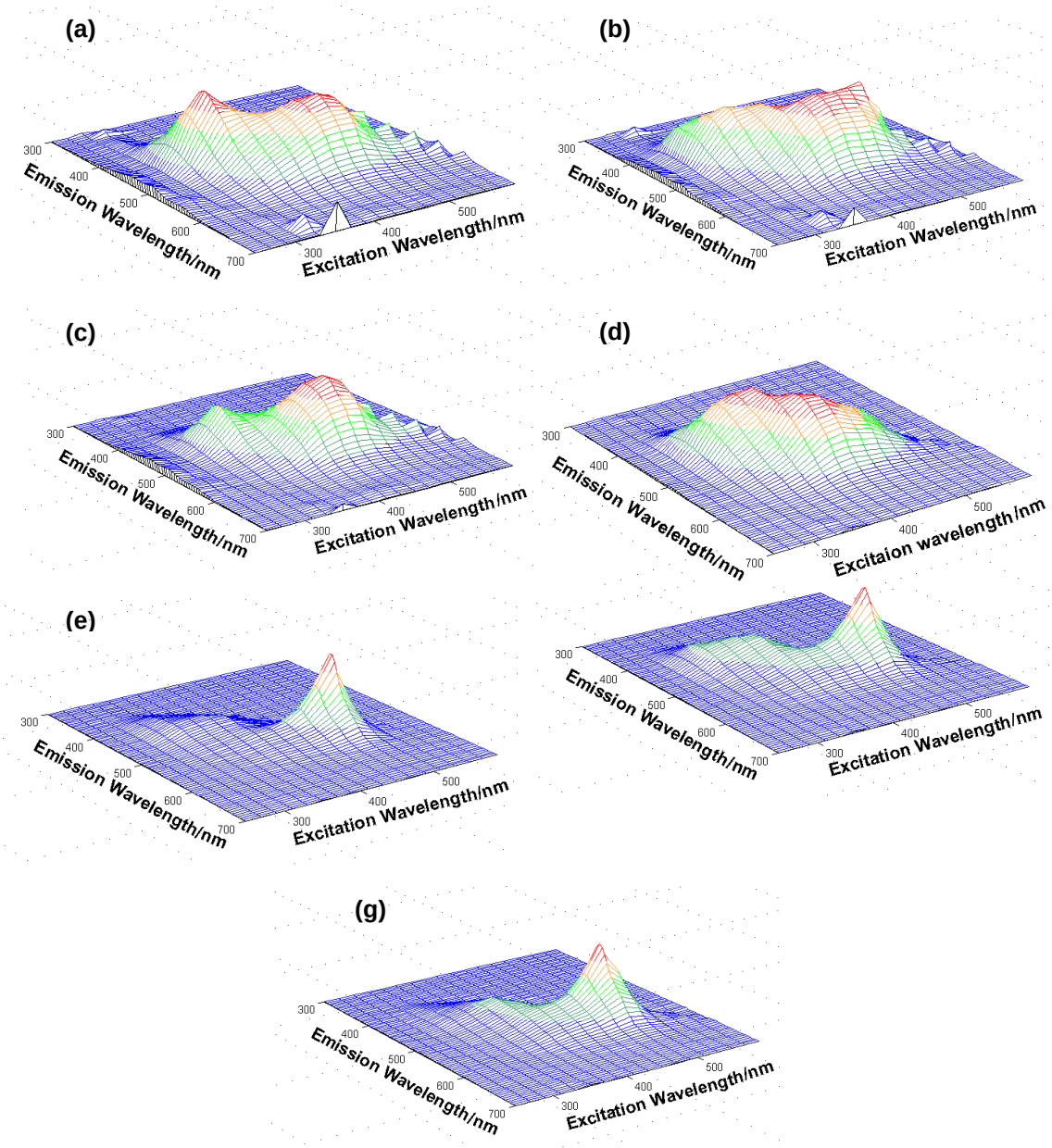

Figure 6.9: Excitation-emission matrices of (a) Assam tea, (b) Ceylon tea (c) Kenya tea (d) Japanese Black tea (e) Japanese green tea (f) Japanese Houji tea (g) Japanese Oolong tea..

Figure 6.9 shows the EEMs for the standardized data. The x axis represents the emission wavelength and the y axis represents the excitation wavelength, while the z axis represents the fluorescence intensity. The TLS of the Black teas are shown in figure 6.9 (a) to (d).The 3D fluorescence spectra show different emission spectra for the different type of teas. The distinct shapes can be visually analyzed for discrimination between Assam, Kenya and Japanese Black tea as they have completely different patterns. However, the small difference between Assam and Kenya tea is less obvious apart from the difference in intensity. Therefore a statistical method can be applied to discriminate between the teas. The statistical method will also be useful if small changes in fluorescence produced during blending or adulteration of tea is being investigated

The TLS of the bottled Japanese teas are shown in figure 6.9. (e) to (g).The 3D fluorescence spectra show different emission spectrum for the different type of teas. The small differences between Green, Houji and Oolong tea are less obvious. A PCA was performed on these data from the 7 different types of tea and Figure. 6.10 shows the resulting PCA scores plot. It can be seen that the seven tea groups occupy seven regions within the variance space.

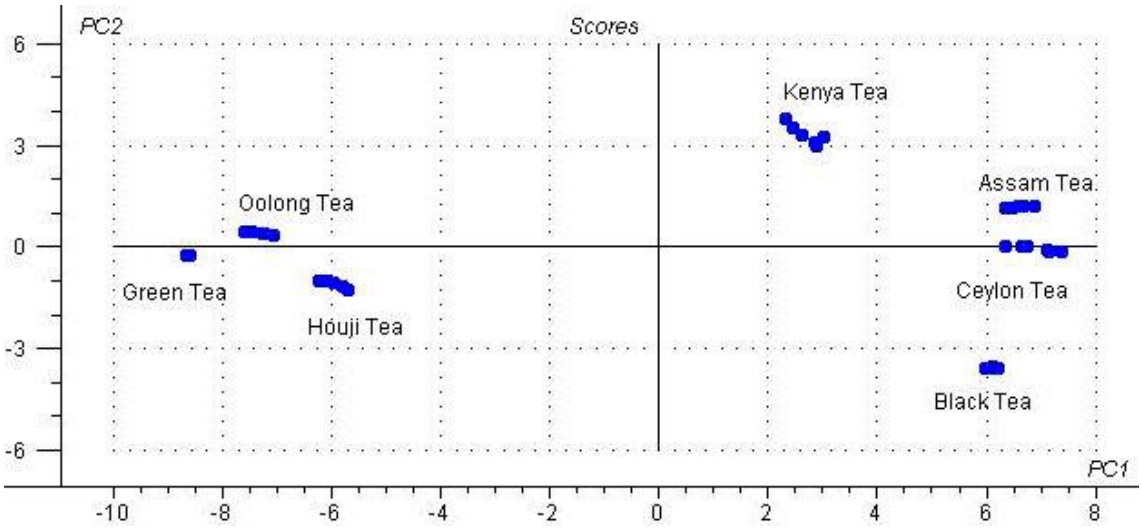

Figure 6.10: PCA scores plot from the TLS of the seven varieties of teas.

Thus the different teas (Oolong, Green, Houji, Kenya, Assam, Ceylon and Black) are sufficiently separate, without any classification errors. In the first principal component (PC1) the Black teas shows positive scores in contrast to unfermented teas which are found on the left. The Black teas are found on the right quadrants with Kenya tea on the top (positive score for PC1 and positive score for PC2), Japanese Black tea on the bottom right (positive score for PC1 and negative score for PC2) and Assam and Ceylon in the mid right portion (positive score for PC1) of the variance space. In the first principal component (PC1) the Black teas (Kenya, Assam, Ceylon, Japanese PET black tea) shows positive scores in contrast to unfermented teas (Green, Oolong and Houji Tea) which are found on the left quadrant. Oolong tea showed a positive score for both PC's whereas Green tea and Houji tea showed negative score for both PC's. According to the results obtained PCA provides very good discrimination between the different classes of tea.

According to the statistical analysis Green, Houji and Oolong tea are different from Black teas. This can be explained by the fact that Green tea is unoxidised, Brown teas (Oolong tea and Houji tea) are not fully oxidized whilst Black tea is fully oxidized. The Black teas show a broader emission spectrum due to the formation of more compounds during the Malliard's reaction. The data from the PCA plot would potentially be a useful tool in the tea industry for discriminating between different types of teas and also as a monitoring tool for the processing of tea.

6.6. The application of total luminescence spectroscopy to discriminate between geographically similar teas

Although the discrimination of the seven different types of teas demonstrated in the last section was promising, in many ways it was not a challenging problem as some of the teas could be discriminated merely by visual inspection. It was therefore decided to try and apply the method to the far more difficult task of discriminating between geographically similar teas. Black teas from a total of 15 different plantation estates in Sri Lanka were used in this study. These are listed in table 6.2. Black tea is classified according to the size of the leaves and the origin of the tea. The elevation of the estate where the tea is grown has a big influence on the quality of the tea and this is also listed in table 6.2. Tea grows from sea level up to approximately 2400 metres above sea level. All teas used in this research were Black teas harvested in Sri Lanka.

Table 6.2: Elevation and region of the Sri Lankan Black teas

TEA	ELEVATION (M)	REGION
Karavita	0-300	Low Country
Berbeula	0-300	Low Country
Neluwa	508	Malwatta Valley
Kenilworth	625	Mid Country
Aislaby	1219-1372	Malwatta Valley
Poonagalla	1230	Bandarawela
Highforest	1252	Udapussellewa
Mattakelle	1430	Dimbula, Lindula/ Talawakelle
Naya Bedda	-	Bandarawela
Diyagama west	1510	Dimbula, Lindula/ Talawakelle
Powysland	-	Dimbula, Lindula/ Talawakelle
Glenore	1524	Bandarawela
Loinorngroup	1800	Bogawantalawa
St. James	>1200	Malwatta Valley
Agarapathi	-	-
Kellie Bedde	>1200	Uva
Uva Highland	>1200	Malwatta Valley
Pedro estate	>1200	Nuwara Eliya

Total luminescence measurements were carried out using the same spectrofluorimeter apparatus described in section 6.3. The wavelength scan rate and the band pass were maintained at 1200 nm/min and 10 nm respectively.

6.6.1. Alternative preparation of leaf tea samples for fluorescence analysis

A more efficient means of sample preparation was later on adopted for the geographically similar teas as the initial experiments carried out on 9 teas (Aislaby, Diyagama west, Highforest, Karavita, Kenliworth, Loinorngroup, Mattakelle, Pedro estate, Poonagalle) showed that the simple sample preparation described in section 6.3.1 did not yield good discrimination between the different types of Sri Lankan Black teas. Figure 6.11 illustrates a schematic diagram of the Soxhlet apparatus which was used for solvent extraction of the tea samples.

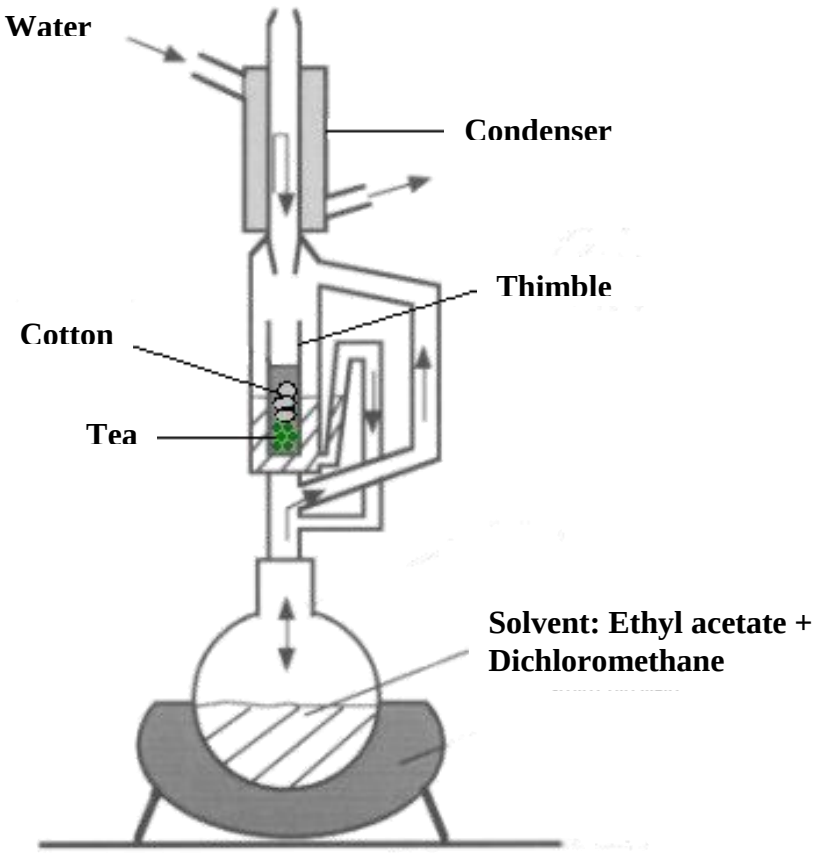

Figure 6.11: Soxhlet apparatus for solvent extraction.

Tea samples (1.0 g) were weighed and transferred into a thimble, covered with glass wool and placed in the Soxhlet apparatus. 75 ml of ethyl acetate (Fisher Scientific, UK) was added to 75 ml of dichloromethane (Fisher Scientific, UK) in a 250 ml round bottom flask. The extraction was carried out for 45 minutes at a temperature of 78 ^{o}C. After extraction, the content of the round bottom flask was evaporated to dryness in a steam rotary evaporator Rotavapor ®, Buchi, CH). The content of the flask was then dissolved in 10 ml water and stored in a brown bottle prior to fluorescence analysis.

6.6.2. Total luminescence analysis and statistical analysis

The total luminescence analysis was initially carried out using the same conditions as in section 6.3.3 and the residual excitation peaks were removed as described in section 6.5. These data collected were standardised and the PCA was carried out using Minitab version 14 (Minitab Inc, State College PA 16801-3008,USA).

6.7. Results and discussions.

The total luminescence spectra were recorded initially for nine different Sri Lankan Black teas. Residual excitation peaks were observed in the EEMs for excitation and they were removed as described in section 6.5. A PCA was carried out on the data from the different type Sri Lankan Black teas and Figure. 6.12 represents the PCA scores loading plot and shows the observed correlation between the teas. The inset in Figure 6.12 is the 3D PCA representation of the total luminescence data of the different teas.

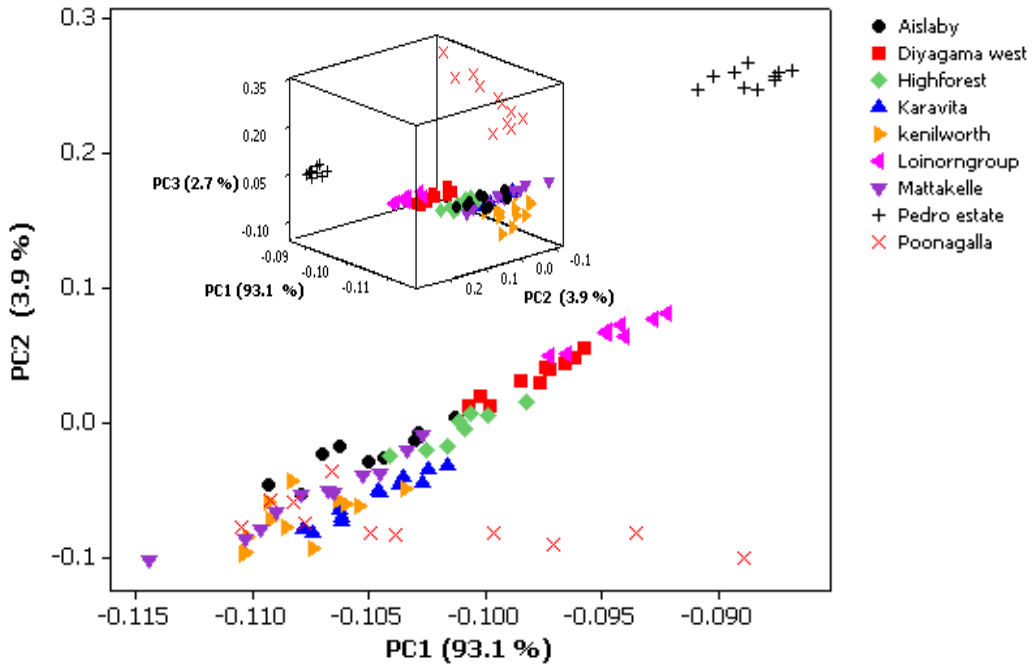

Figure 6.12: PCA scores loading plot for total luminescence of Sri Lankan Black teas.

It can be seen from the loading plot that Pedro estate tea is different from the other teas and the other teas overlap each other. However when the first 3 PCs are utilised the 3D PCA scores plot shows that Poonagalle and Pedro estate were uncorrelated to the other teas and this correlates with the fact that these two teas are from different regions namely Bandarawela and Nuwara eliya respectively. Due to the poor visual separation in the PCA loading plot, a new sample preparation method was adopted as described in section 6.6.1, to

maximise the extraction of polyphenols and other compounds that fluoresced. This technique was then applied to 11 different Sri Lankan Black teas, namely Agarapathi, Aislaby, Berbeula, Glenore, Kellie Bedda, Naya Bedda, Neluwa, Poonagalle, Powysland, St James, Uva Highland.

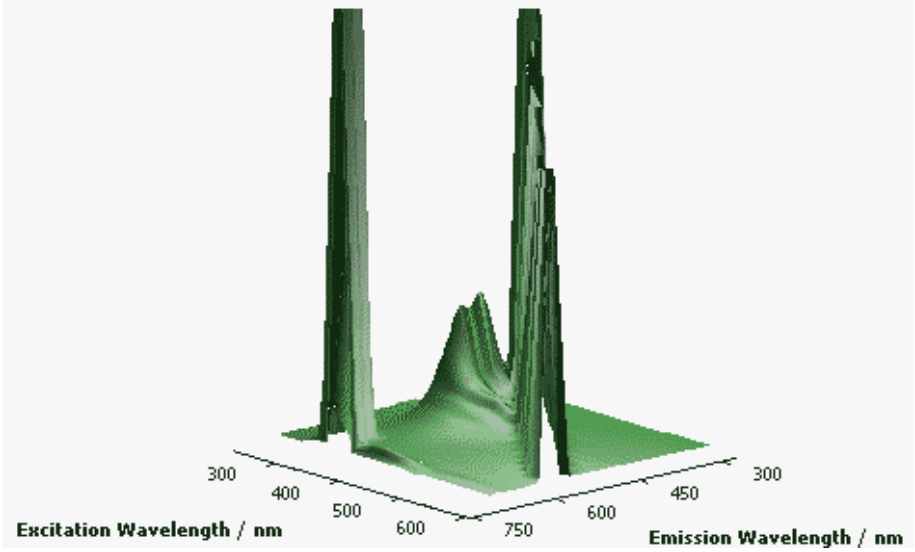

Figure 6.13: Excitation-emission matrices of Poonagalle tea prepared as described in section 6.4.1.

The total luminescence data (EEM) of a Poonagalle tea sample prepared according to section 6.4.1 is shown in figure 6.13. When this EEM is compared to that produced from sample extracted using the method described in section 6.6.1. (figure 6.14), it can be seen that the latter does not contain residual excitation peaks and has a higher intensity of total luminescence.

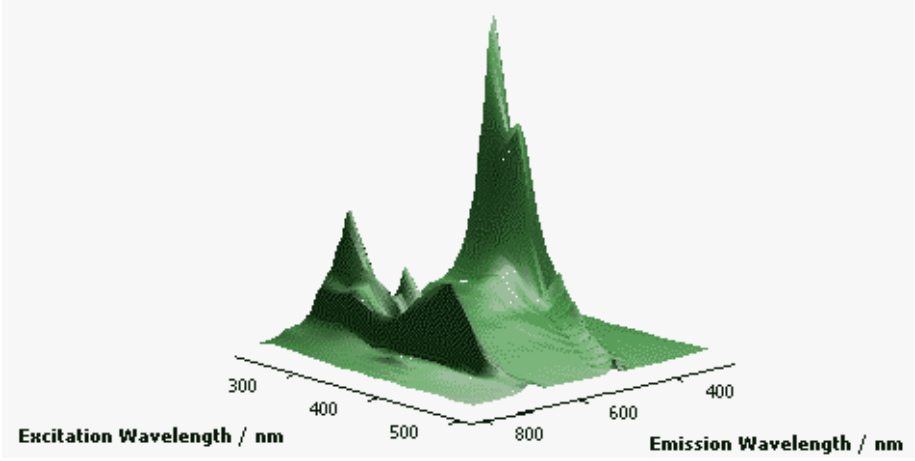

Figure 6.14: Excitation-emission matrices of Poonagalle tea prepared as described in section 6.6.1.

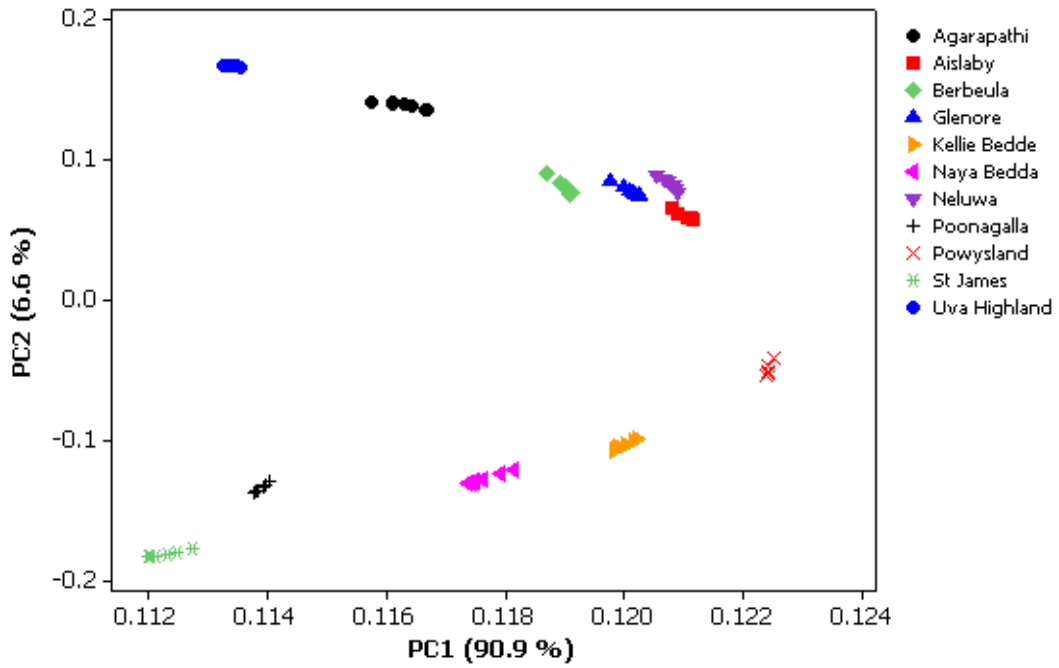

Figure 6.15: PCA scores plot for total luminescence of Sri Lankan Black teas prepared according to section 6.6.1

The resulting PCA loading plot from the Sri Lankan teas prepared according to section 6.6.1 is shown in figure 6.15. As in the case of all previous PCA plots, these data were normalised by autoscaling. The plot shows an excellent result as all the eleven Sri Lankan teas are visually separable when the first two PCs are utilised. As we are compressing a large data set with many variables to a few latent dimensions in a new variance space, the variations between samples can be observed and drift in replicate data sets can also be identified. Previous studies have also used PCA as a technique to visualise drift in large data sets [35, 36, 37].

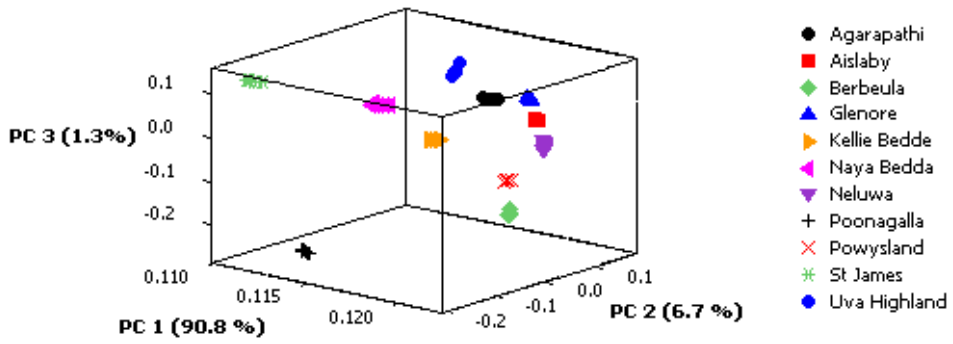

Figure 6.16: 3D PCA plot for total luminescence of Sri Lankan Black teas prepared according to section 6.6.1.

The 3D PCA scores plot in figure 6.16 shows an even better separation of all eleven teas. Although the 3rd PC in the data only represents 1.3 % of the variance in the data, by allowing the axes to be observed from a different perspective a visual separation of all the groups is possible. As described by Pardo *et al.* [35] the first PC displays the highest percentage of the total variance and has most information about drift in the data sets. Therefore, when the 3rd PC is used it can be observed in figure 6.16 that the drift in replicate data is reduced.

Previous studies have attempted to discriminate between teas. Herrador *et al*. [38], graded Green, Black and Oolong tea according to their metal content using inductive coupled plasma atomic emission spectroscopy. The sample preparation was over 2 hours and consisted of digestion with concentrated acids. Applying PCA on their data set did not result in a neat separation of the three classes of tea and they suggest that this behaviour indicates that tea classes could not be separable when using classification techniques such as linear discriminant analysis (LDA). A complex data analysis technique, artificial neural networks trained by back propagation of errors (BP-ANN) was used to enable excellent classification. Fernandez *et al*. [21] applied PCA to multi-element data obtained from three kinds of tea beverages, i.e. infusions, instant and soft drinks. Only separation between soft drinks and the rest of the samples was achieved. A supervised pattern recognition technique was required to

achieve a recognition ability of 94.6%. Liu *et al*. [39] reported the discrimination of three categories of tea (Black, Green and Oolong) based on their content of cellulose, hemicelluloses, lignin, polyphenols, caffeine and amino acids. Excellent discrimination between the different categories of tea was visualised by plotting the first two principal components, although clear distinction between varieties in each category was not achieved.

This work on the application of PCA to total luminescence data from teas has laid the foundation for further work which will be required to develop a cheap, robust and objective apparatus for discrimination between different types and quality of tea. More data would be required to apply robust pattern recognition techniques such as LDA which would result in quantitative classification of the teas. This objective device could be further correlated with sensory analysis by trained tea tasters. The TLS data has been shown to allow discrimination of teas (both geographically similar and dissimilar) but it is unlikely that all the TLS data points collected are needed. It is more likely that much of the data is redundant as only a maximum of 3 PCs were required for good visual discrimination. Therefore it would be useful to apply data reduction techniques to select the most significant data points. This would allow reduced analysis time and may improve the classification of the teas.

The information obtained from the optimisation of data collection (after data reduction) could be used with a cheap LED based EEM fluorescence spectrometer similar to that developed by Hart and Jiji [40], to develop an LED based optical array. The device would make use of a series of LEDs to cover the excitation wavelength range from the UV through to the visible spectrum. The data reduction process would be used to identify the most important excitation wavelengths. The resultant fluorescence light could be detected using a compact CCD spectrograph similar to that used in chapter 3, 4 and 5. An even simpler detector array could be made from a series of selective photodiodes chosen to be sensitive to the wavelengths identified to be most important for classification from data reduction. An alternative simple fluorimeter could be constructed by using a filter wheel in front of a broadband excitation source such as a tungsten halogen lamp in conjunction with a similar filter wheel in front of a photodiode detector.

6.8. Conclusion

Discrimination between several types of teas has been achieved by applying a simple visualisation technique (PCA) to geographically similar and dissimilar teas, based on data collected by total luminescence spectroscopy. Initially the ability to discriminate between seven types of teas from Africa, India, Sri Lanka and Japan was investigated. Seven well separated groups were visualised in the first two principal components. Some structuring in the plots related to the variety of the teas investigated. This technique could be applied as an objective tool in the tea industry to achieve the right blend of teas and also as a monitoring tool in the tea industry. The second part of this study explored the ability to discriminate eleven teas from Sri Lanka. Preliminary experiments on tea samples prepared by normal infusion did allow good discrimination between the varieties of tea. After a solvent extraction technique was applied to prepare the tea samples, clear separation could be achieved and well separated groups were observed in the PCA plot. Further work is required to develop more quantitative classification of the tea and to construct a simple apparatus for discrimination between classes of teas. The device could be potentially useful to tea manufacturers as they currently have to use trained tea tasters who can only make subjective judgements.

6.9. References

[1] Harbowy, M. E.; Balentine, D. A. Crit. Rev. Plant Sci., 16 (1997) 415.

[2] Fernández-Cáceres, P. L.; Martín, M. J.; Pablos, F.; González, A. G. Journal of Agricultural and Food Chemistry, 49 (2001) 4775.

[3] Weisburger, J. H. Cancer Letters, 114 (1997) 315.

[4] International Tea Committee, Annual Bulletin of Statistics (1990) .

[5] Ramadurai, N. Planters Chronical (2000) 537.

[6] Ponce, E.; Taylor, A. J. Flavour Chemistry of Ethnic Foods (1997) 197.

[7] Astill, C.; Birch, M. R.; Dacombe, C.; Humphrey, P. G.; Martin, P. T. Journal of Agricultural and Food Chemistry, 49 (2001) 5340.

[8] Englehardt, U. Caffeinated Beverages Symp, 219th Am Chem Soc Meet (1999) 111.

[9] Larger, P.J.; Jones, A.D.; Dacombe, C. Journal of Chromatography A, 799 (1998) 309.

[10] Bonoli, M.; Colabufalo, P.; Pelillo, M.; Toschi, T. G.; Lercker, G. Journal of Agricultural and Food Chemistry, 51 (2003) 1141.

[11] Obanda, M.; Owuor, P. O.; Mang'oka, R.; Kavoi, M. M. Food Chemistry, 85 (2004) 163.

[12] T. Miyazawa, K. Nakagawa, Bioscience, Biotechnology and Biochemistry, 62 (1998) 829.

[13] Yang, C. S.; Wang, Z. Journal of the National Cancer Institute, 85 (1993) 1038.

[14] Wang, H.; Provan, G. J.; Helliwell, K. Trends in Food Science and Technology, 11 (2000) 152.

[15] Andersson, H. C.; Hallström, H.; Kihlman, B. A. Intake of caffeine and other methylxanthines during pregnancy and risk for adverse effects in pregnant women and their foetuses, Nordic Council of Ministers, ISBN 92-893-1098-7 (2005) .

[16] Felter, W. H.; Lloyd, U. J. http://www.henriettesherbal.com/eclectic/kings/camellia-sine.html, accessed 02/12/2008.

[17] Roberts, E. A. H.; Smith, R. F. The Analyst, 86 (1961) 94.

[18] Takino, Y.; Imagawa, H.; Horikawa, H.; Tanaka, A. Agric. Biol. Chem., 28 (1964) 64.

[19] Mikhail, A.; Bokuchava, Skobeleva, N. I.; (Eds) Morton I. D. and Macleod, A. J. Food Flavours: Part B, Elsevier Science, Amsterdam, 1986, p. 49.

[20] Kawakami, M.; Ganguly, S. N.; Banerjee, J.; Kobayashi, A. Journal of Agricultural and Food Chemistry, 43 (1995) 200.

[21] Fernández, P. L.; Pablos, F.; Martín, M. J.; González, A. G. Food Chemistry, 76 (2002) 483.

[22] Liang, Y.; Lu, J.; Zhang, L.; Wu, S.; Wu, Y. Food Chemistry, 80 (2003) 283.

[23] Togari, N.; Kobayashi, A.; Aishima, T. Food Res. Int., 28 (1995) 495.

[24] Borse, B. B.; Rao, L. J. M.; Nagalakshmi, S.; Krishnamurthy, N. Food Chemistry, 79 (2002) 419.

[25] Budínová, G.; Vlác□il, D.; Mestek, O.; Volka, K. Talanta, 47 (1998) 255.

[26] Dutta, R.; Hines, E. L. Gardner, J. W.; Kashwan, K. R.; Bhuyan, M. Sensors and Actuators, B: Chemical, 94 (2003) 228.

[27] Ivarsson, P.; Holmin, S.; Ho□jer, N.; Krantz-Ru□lcker, C.; Winquist, F. Sensors and Actuators, B: Chemical, 76 (2001) 449.

[28] Pecore, S.; Kellen, L. Food Quality and Preference, 13 (2002) 369.

[29] Schulman, G. S. (Ed.), Molecular Luminescence spectroscopy Methods and applications: Part 1, John Wiley & Sons, USA, 1985, p. 826.

[30] Tzouros N.E., Arvanitoyannis, I. S. Critical Reviews in Food Science and Nutrition, 41 (2001) 287.

[31] Moreda-Piñeiro, A.; Fisher, A.; Hill, S. J. Journal of Food Composition and Analysis, 16 (2003) 195.

[32] Patra, D.; Sireesha, L. K.; Mishra, A. K. Indian Journal of Chemistry - Section A Inorganic, Physical, Theoretical and Analytical Chemistry, 40 (2001) 374.

[33] Baker, A. Water Research, 36 (2002) 189.

[34] Scott, S. M.; James, D.; Ali, Z.; O'Hare, W.T;. Rowell, F. J. Analyst, 128 (2003) 966.

[35] Pardo, M.; Niederjaufner, G.; Benussi, G., Comini, E.; Faglia, G.; Sberveglieri, G.; Holmberg, M.; Lundstrom, I. Sensors and Actuators, B: Chemical, 69 (2000) 397.

[36] Holmin, S.; Krantz-Ru□lcker, C.; Lundstro□m, I.; Winquist, F. Measurement Science and Technology, 12 (2001) 1348.

[37] Hui, D.; Jun-Hua, L.; Zhong-Ru, S. Sensors and Actuators, B: Chemical, 96 (2003) 354.

[38] Herrador, M. A.; González, A. G. Talanta, 53 (2001) 1249.

[39] Liu, X.; van Espen, P.; Adams, F.; Yan, S. H.; Vanbelle, M. Analytica Chimica Acta, 200 (1987) 421.

[40] Hart, S. J.; JiJi, R. D. Analyst, 127 (2002) 1693.

.

Chapter Seven

7.0. An optical ammonia sensor based on fluorescence quenching of a dye immobilised in a sol gel matrix

7.1. Introduction

Fluorescence spectroscopy, as described in chapter six is a highly sensitive technique for the quantitative and qualitative detection of suitable species with limits of detection in the parts per trillion (ppt) being reported for state of the art measurements [1]. Amongst the species commonly studied using fluorescence detection are gaseous atmospheric pollutants such as NO_2 and NO (through chemiluminescence) and also SO_2. The standard method for fluorescence detection involves the measurement of emitted photons from a fluorescent species, against a 'zero background'.

A related method can be used for species which cause a decrease in the fluorescence intensity of a fluorescent compound with increasing concentration. This is known as fluorescence quenching. Demas *et al.* described quenching of a reporter, M by an analyte, Q by the following processes;

Photon absorption $\mathrm{M} + h\nu \rightarrow {}^*\mathrm{M}$

Luminescence ${}^*\mathrm{M} \rightarrow \mathrm{M} + h\nu$

Nonradiative decay ${}^*\mathrm{M} \rightarrow \mathrm{M} + \Delta$

Dynamic quenching ${}^*\mathrm{M} + \mathrm{Q} \rightarrow \mathrm{M} + \mathrm{Q}$

A more rapid depletion of the excited state, detected as either a decrease in steady state fluorescence or a shorter fluorescence lifetime is observed in the presence of a quencher. Quenching can be described as either dynamic or

static. A variety of processes such as excited state reactions, energy transfer, complex formation, and collisional encounters can result in quenching. Dynamic quenching is the result of collisional encounters between the quencher and the fluorophore whereas static quenching is due to formation of a nonfluorescent complex [2, 3]. The optical properties (i.e. high optical density or turbidity) of a sample can also be responsible for decrease in fluorescence intensity. This is generally described as 'trivial quenching' and contains little molecular information. Dynamic quenching occurs when an excited fluorophore interacts with an atom or molecule that can facilitate non-radiative transitions to the ground state as shown in figure 7.1.

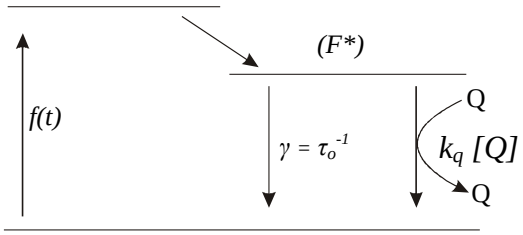

Figure 7.1: Schematic of dynamic quenching [4] (where; *f(t)* is the constant excitation function, γ is the decay rate of the fluorophore in the absence of the quencher, K_q is the bimolecular quenching constant)

Dynamic quenching of fluorescence intensity can be described by the Stern-Volmer equation [5].

$$\frac{F_o}{F} = 1 + K_q\tau_o\,[Q] = 1 + K_{SV}\,[Q] \qquad (7.1)$$

The equation can be derived by describing the fluorescence intensity of a fluorophore in the presence or absence of a quencher. The fluorescence intensity for a fluorophore is directly proportional to its concentration in the excited state, [*F**]. When under constant illumination a steady state population of fluorophores is established and the rate of change in fluorescence intensity is zero i.e.

$$\frac{d[F^*]}{dt} = 0 \qquad (7.2)$$

In the presence and absence of quencher, the rate of change in the concentration of fluorophores in the excited state can be expressed by the following equations;

$$\frac{d[F^*]}{dt} = f(t) - \gamma\,[F]_0 = 0 \qquad (7.3)$$

$$\frac{d[F^*]}{dt} = f(t) - (\gamma + K_q\,[Q])\,[F] = 0 \qquad (7.4)$$

Where, *f(t)* is the constant excitation function, and γ is the decay rate of the fluorophore in the absence of the quencher i.e. $\gamma = \tau_o^{-1}$. $K_q[Q]$ is the additional decay rate in the presence of quencher and K_q is generally referred to as the bimolecular quenching constant. F and F_o are the fluorescence intensities in the presence and absence of the quencher respectively. [Q] is the concentration of the quencher. Dividing equation 7.3 by 7.4 gives the Stern-Volmer equation.

$$\frac{F_O}{F} = \frac{\gamma + K_q[Q]}{\gamma} = 1 + K_q\,\tau_o[Q] = 1 + K_{SV}\,[Q] \qquad (7.5)$$

Where, τ_o is the fluorescence lifetime of the fluorophore in the absence of the quencher. $K_q\ \tau_o$ can also be expressed as K_{SV}, the Stern-Volmer quenching constant

In static quenching the fluorescence quenching take place by the formation of a ground state non-fluorescent complex. When this complex absorbs light, it immediately returns to the fundamental ground state without emission of photons. A schematic of static quenching is represented in figure 7.2.

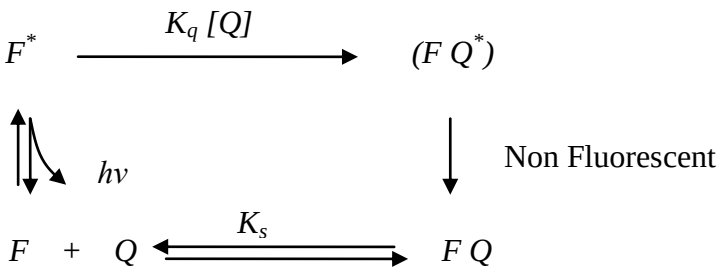

Figure 7.2: Schematic of collisional quenching [4] where; F^* is the excited state, K_q is the bimolecular quenching constant, K_s is the complex formation association constant, Q is the quencher.

Static quenching can be described by the following equation.

$$\frac{F_0}{F} = 1 + K_s\,[Q] \tag{7.6}$$

Where; F and F_o are the fluorescence intensities in the presence and absence of the quencher respectively. [Q] is the concentration of the quencher. K_s is the association constant for complex formation and described by [3]

$$K_s = \frac{[F-Q]}{[F][Q]} = \frac{[F]_0 - [F]}{[F][Q]} = \frac{[F_0]}{[F][Q]} - \frac{1}{[Q]} \tag{7.7}$$

$[F - Q]$ is the concentration of the non-fluorescent complex. $[F]$ is the concentration of uncomplexed fluorophore and $[F_0]$ is the total concentration of fluorophore. It can be observed from equation 7.1 and 7.6 that the dependence of fluorescence intensities for static quenching appears identical to dynamic quenching, but it should be noted that the quenching constant is the association constant for complex formation. The absorption profile of a fluorophore can be use to discriminate between static and dynamic quenching. During static quenching the absorption profile changes while it doesn't for dynamic quenching. A fluorescence lifetime measurement is normally the best method to discriminate between static and dynamic quenching. During static quenching a fraction of the fluorophore is removed as it becomes non fluorescent while the other fraction still shows the same lifetime and hence a change in fluorescence lifetime is not observed. Whereas in dynamic quenching the fluorescence lifetime is proportional to the change in fluorescence intensity [5, 6].

The main aim of this work was to develop and investigate an optical sensor for the detection of ammonia gas, based on fluorescence quenching of a novel dye, 9 aminoacridine hydrochloride (9 AAH) ($C_{13}H_{10}N_2 \cdot HCl$) immobilised in a suitable sol gel matrix.

Firstly a working prototype using standard macro scale optical components was demonstrated. Following this, a simpler and lower cost optical sensor was developed and tested. This chapter begins by describing the role of gaseous ammonia in the natural environment and reviewing previous studies

which have attempted to measure ammonia gas. A description of the novel fluorescent dye is given, followed by optimisation of the sol gel process used to immobilise the fluorescent dye. The development and measurements performed with the initial prototype optical sensor are then described followed by the development and measurements obtained with the simplified optical sensor.

7.1.1. The role of ammonia and its detection

Ammonia gas is naturally present in the atmosphere, although anthropogenic sources now account for most of its presence. It is an airborne pollutant largely emitted directly or indirectly by activities such as agriculture, the fertilizer industry, industrial combustion processes, petrol vehicles fitted with catalytic converters and industrial coolants. The best estimate according to Defra (Department for Environment, Food and Rural Affairs) of the total emission in the UK for 2000 was 0.32 Tg [7]. Agriculture was identified as the major contributor of ammonia to the atmosphere. Most of the ammonia emitted from agricultural sources is from livestock production (mainly cattle farming), with the rest coming from fertilizers and crops. Non-agricultural sources account for around 0.05–0.06 Tg of ammonia. A wide range of non-agricultural sources contribute to ammonia emissions in the UK, including pets; wild animals; sewage sludge; industrial and combustion processes; and petrol vehicles fitted with catalytic converters.

In order to protect sensitive habitats the UK has signed a number of international agreements to reduce ammonia emissions. Total UK ammonia emissions (excluding natural emissions from wild animals and humans) fell overall by 18 per cent between 1990 and 2006 to 0.315 Tg . This compares with the target for 2.01 of 0.297 Tg under the UNECE Gothenburg Protocol and the EU National Emissions Ceiling Directive. Emissions in 2006 were similar to those in 2005 [7]. Ammonia is a primary irritant to humans and the recommended threshold limit for human exposure is set at a concentration of 25 ppm [8, 9]. The gas is released mainly during naturally occurring processes, i.e. the breakdown of the urea excreted by farm livestock and other mammals or of the uric acid excreted by birds. Ammonia is very soluble in water and readily

reacts with other substances in the atmosphere to form ammonium compounds such as ammonium sulphate and nitrate. Figure 7.3 shows a schematic representation of the nitrogen cycle [10].

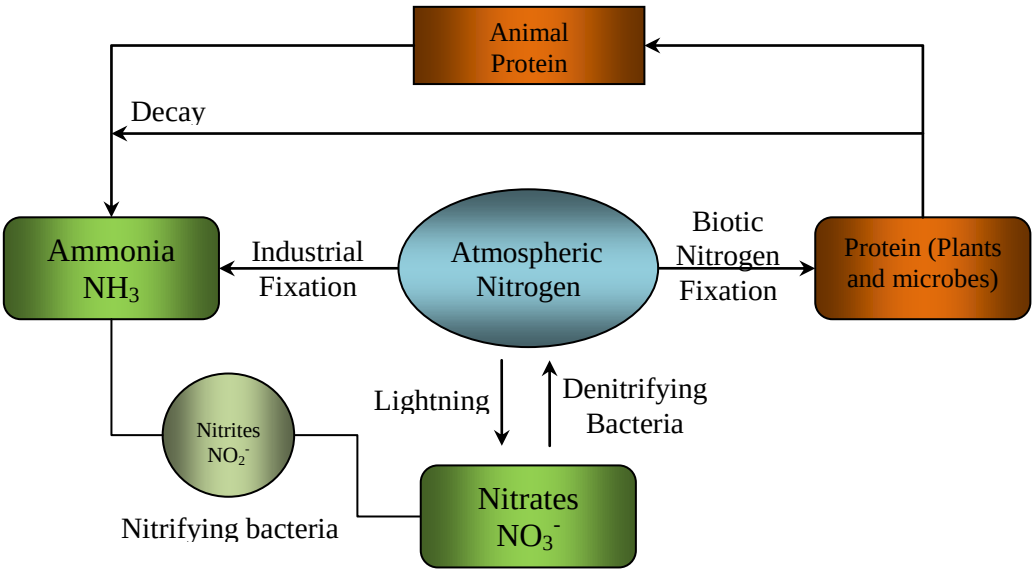

Figure 7.3: A schematic of the Nitrogen cycle.

Three major classes of current ammonia sources are nitrogen fixation, ammonification and combustion. The contribution of nitrogen fixation to the worldwide ammonia emission is estimated to be 1.0 Tg / year. A larger source is ammonification, a series of metabolic activities that decompose organic nitrogen such as manure from agriculture and wildlife or leaves and is responsible for producing 20 – 35 Tg/year. The third source combustion from chemical plants and motor vehicles accounts for 2.1-8.1 Tg/year [11].

Ammonia has profound effects on natural ecosystems [10]. Ammonia is a source of nitrogen and can increase soil fertility and hence damage ecosystems which have naturally low levels of soil nitrogen. Deposition of acidifying pollutants such as ammonium compounds and nitrogen oxides have a range of detrimental effects such as [12]:

- Increased acidity of freshwaters which leads to the loss aquatic organisms.
- Increased acidity of soils which alters the soil chemistry and can leave terrestrial ecosystems vulnerable to drought, disease and insect attack.

- Increased levels of harmful metals in drinking water (leaching of ammonium salts).
- Excessive nutrient enrichment of natural ecosystems from deposition of the nitrogen-containing atmospheric pollutants NO_x and NH_3.
- Ammonia emissions are also associated with secondary particulate formation (ammonium sulphates and ammonium nitrates) and thus have implications for human health and climate change.

Background ammonia levels in the natural environment can be very low, down to sub-ppb concentration levels. To monitor atmospheric ammonia levels accurate detectors with detection limit of 1 ppb or lower are required. Whereas, near intensive farming areas, ammonia concentrations are considerably higher and hence detectors in the sensitivity range of about 10 ppm are required [13, 14].

Ammonia is also produced naturally by the human body. There is a need for monitoring breath ammonia level as it can be a fast diagnostic method for biological conditions such as disturbed urea balance (kidney disorder) and/or ulcers caused by *Helicobactor pylori* stomach bacterial infection. Sensors that are able to measure down to 50 ppb level of ammonia in exhaled air would be required for breath analysis [11]. Another area where the medical community is interested in monitoring levels of ammonia is in sport medicine. Ammonia can diffuse out of the blood into the lungs when the ammonia levels become higher than the ammonia levels in the air. The expired ammonia levels can increase exponentially with increasing workload. Thus a sensor capable of making measurements in the range 0.1 to 10 ppm is needed [11].

Hence to meet the increasing demand for methods suitable for continuous monitoring of ammonia, a variety of sensors have been developed. Most are based on electrochemical and optical transduction. Many spectroscopic studies have been carried out in the past on ammonia detection using absorption [14-17] fluorescence [9, 18] and infrared spectroscopy [11].

Cavity enhanced absorption spectroscopy (CEAS) has recently been used to qualify and quantify ammonia gas [19-22]. Kassi *et al.;* [23] have reported limit of detection of 14 ppb for ammonia in volcanic gases. This work demonstrated the first in-situ application of GaSb diode lasers, capable of room temperature operation in the 2–2.7 μm range. The sensor showed little

interference from water vapour and carbon dioxide and in this spectral region several important atmospheric and volcanic trace gases showed strong absorption lines. Peeters *et al.;* [24] developed a compact open path optical ammonia detector based on CEAS. A tunable external cavity diode laser operating at 1.5 μm was used. Low ammonia concentration was measured in air at atmospheric pressure and the limit of detection achieved was 100 ppb, with a fast response time of few seconds.

Conventionally ammonia is quantified using potentiometric sensors. A potentiometric sensor is an electrochemical sensor whose output gives an electromotive force (e.m.f). The e.m.f is generated by the exchange process of elemental charge taking place at the interfaces between an electronic and ionic conductor. There are a few potentiometric sensors that have been developed for ammonium ion and ammonia gas. The diffused gas causes a change in the pH within the aqueous layer in contact with the electrode surface. The potentiometric sensors have major drawbacks such as slow response time and interference from other volatile and non volatile acids and bases. These sensors are not suitable for analysis of blood ammonia at pH 7.4 [25, 26]. Conductometric gas sensors have been used for the detection of ammonia using a sensitive layer (i.e. ZnO, SnO_2 or CuBr) [27]. These types of gas sensors show a lack of selectivity because the gas detection mechanism is quite unspecific and generally any type of reducing gas is detected.

Ammonia has also been quantified using a quartz crystal micro balance [28]. *Ali et al.* [29] reported the detection of gaseous ammonia with a piezoelectric quartz crystal coated with pyridoxine hydrochloride, the ammonia was thermally desorbed onto the crystal from a tungsten oxide coated cylindrical denuder tube. The linear dynamic range was 3.1 to 8.2 μg L^{-1}.

The sample constituents can easily poison currently available sensors as they generally work on changes in pH. These limitations have led researchers to extend their effort to develop optically based ammonia sensors that have high sensitivity, fast response time and remote controllability [11]. A range of optical sensors have been described in the literature that exploits the interaction of ammonia vapour with a pH dependent dye material, which experiences a colour change [11, 30, 31].

Optical methods have always played a major role in different fields of analytical chemistry. Chemical and biochemical species have been quantified using optical methods such a colorimetry, photometry and spot tests. The history of optical sensors can be traced back to the pH indicator strips which were pH sensitive indicators immobilised on cellulose. Bergman [32] was the first to exploit the quenching effect of oxygen on the fluorescence of polyaromatic hydrocarbons. His instrument consisted of a UV light source, a sensing layer, a flow through chamber and a photocell at the opposite wall of the chamber. Optical sensors offer many other advantages such as electromagnetic immunity and electrical isolation. They are also lightweight, low cost, robust and rugged.

In general, these sensors work by monitoring the absorption, phosphorescence or fluorescence characteristics of an indicator dye in a suitable matrix. Ammonia interacts with the indicator dye causing a change in the absorbance or emission spectrum, which is monitored using a suitable detector [33-38]. There are also some ammonia sensors based on evanescent absorption and optical wave-guide phenomena that have been reported in the literature [15, 39, 40].

7.1.2. Properties of 9 AAH

The sensor used in this study exploits the effect of ammonia quenching the fluorescence intensity of 9 amino acridine hydrochloride (9 AAH) ($C_{13}H_{10}N_2 \cdot HCl$) immobilised in a xerogel using tetramethylorthosilicate as the primary alkoxide precursor. 9 AAH has previously found use in biochemistry as a DNA intercalator, antibacterial agent, topical antiseptic for humans and an anticancer drug [41-44]. It has earlier been studied in solution [44, 45]. At higher concentrations, it undergoes excimer formation at room temperature and exhibits a dimer–excimer equilibrium at low temperatures [46].

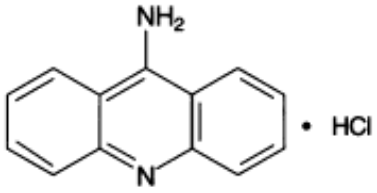

Figure 7.4: Molecular structure of 9 AAH **($C_{13}H_{10}N_2 \cdot HCl$)**

As shown in figure 7.5 9 AAH was found to fluoresce at the same wavelength when in different matrices such as ethanol, water and sol gel. Hence showing the same wavelength profile in sol gel as compared to 9 AAH in ethanol

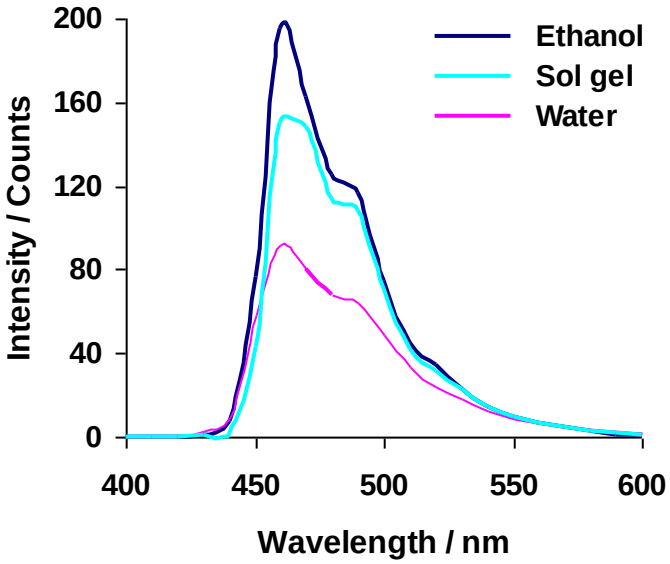

Figure 7.5: Fluorescence spectrum of 9 AAH in water, ethanol and sol gel.

Only one previous study has attempted to use the fluorescence quenching of 9 AAH for the detection of ammonia. Ali and co workers [9] (a member of the PhD supervision team) first reported the fluorescence quenching of 9 AAH in the solution phase by NH_3. This study indicated that 9 AAH would be an attractive candidate as a sensor dye. Furthermore the fluorescence showed little or no interference from acidic gases, such as SO_2, HCl, and H_2S. These findings directly led to the choice of 9 AAH as the sensor material which would be immobilised in a sol gel matrix and used for the detection of gas phase ammonia.

7.1.3. Choice of sol gel matrix

A sol gel matrix was chosen as it has a unique chemistry which is suitable for incorporating a fluorophore into porous inorganic glass hosts and allows the analyte to be evenly distributed into the matrix. Out of the three most common immobilisation techniques [47] the encapsulation method showed advantages over the adsorption and covalent binding methods and was used in this study. The reagents trapped in the matrix usually do not leach out or only leach out very slowly when an appropriate entrapment procedure is used for the encapsulation method. The sol gel matrix can be prepared at low temperature (xerogel), shows good mechanical and chemical resistance and also allows one to control the pore size and thickness of the films [47, 48]. Immobilisation in a sol gel matrix has further advantages of chemical inertness, porosity, low cost, photochemical stability, and transparency for optical measurement [49].

In 1984 Avnir *et al*. [48] first demonstrated the incorporation of a dye within a sol gel matrix, but it was not until the early 1990s that this dye encapsulation technique was used for the development of an optical sensor [50]. In recent years the use of sol gels has become increasingly popular in the field of sensor research [30, 50-54].

7.1.4. The sol gel process

As described by Trinkel *et al.* [55] (part of the Wolfbeis group) critical parameters in ammonia sensing or gas sensing in general are the permeability and permeation selectivity of the matrix used. The ability to trap organic and bio-organic molecules in organic oxides through the sol gel process was first introduced in 1984 [56], which opened the road to a whole new class of materials and intense activity in many laboratories. The sol gel process may be used to produce thin glasses that have well defined optical and physical characteristics. The sol gel process is a method that may be used to synthesize thin glass films from silicon alkoxide precursors at room temperature. A sol is any colloidal system with dispersed phase of droplet or particles, usually 10µm – 1nm in size in a continuous phase which can be composed of solids, liquids

and gases, that is to say, colloidal suspension of solid particles in a liquid. The solid particles in the colloidal phase are stable due to short-range forces such as van der Waals attraction and surface charges. A gel is defined as a substance that contains a continuous solid skeleton enclosing a continuous liquid phase. Gels consist of continuous solid and fluid phases of colloidal dimensions. The sol gel process is a name given to the hydrolysis and polycondensation of organic compounds to form ceramic materials. In the sol gel process, a sol of a given precursor is prepared, which then undergoes some chemical & physical changes, grows in size and forms a gel. This gel when dried under suitable temperature conditions yields the product [57].

A particular example of the sol gel process involves the reaction of tetramethylorthosilicate (TMOS) with ethanol and water. During sol gel processing a one phase solution (i.e. TMOS) undergoes a transition to a rigid two phase system of solid silica and solvent filled pores.

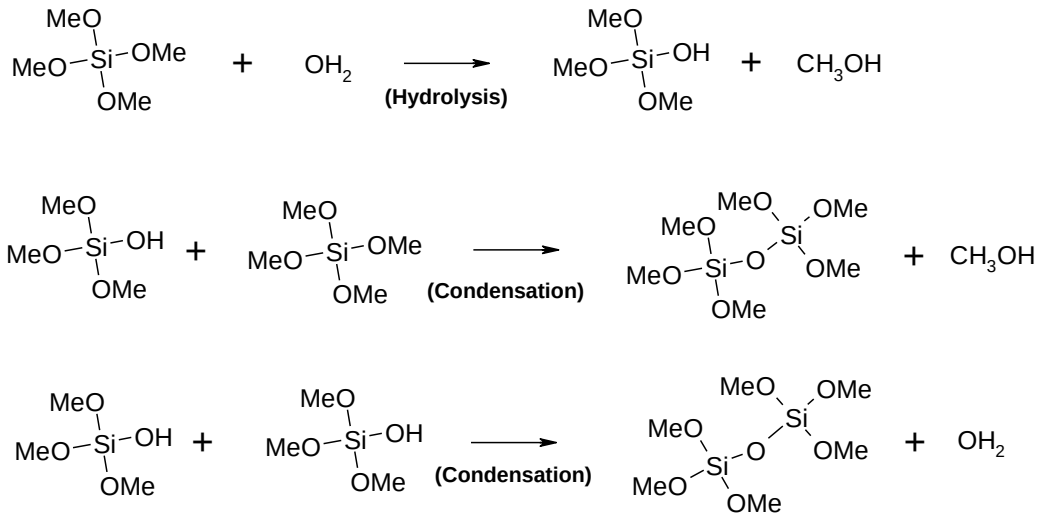

Figure 7.6: Some of the reactions which occur in the sol gel process

Hydrolysis occurs when TMOS and water are mixed together in ethanol or any other mutual solvent. The reaction is called hydrolysis, because a hydroxyl ion becomes attached to the metal atom, as shown in the reaction in figure 7.6. The partially hydrolysed alkoxides give either one or two silanols that reacts with another silanol or ethoxy group forming a condensed polymer of silica with elimination of water and ethanol respectively [54].

Gels dried under atmospheric pressure and at temperature close to room temperature are normally referred to as xerogels. These are the result of gentle drying to avoid cracking associated with the very low permeability of the solid network [53].

Lobnik *et al.* [58] reported a sensor system for dissolved ammonia using tetramethylorthosilicate (TMOS) and diphenyldimethylorthosilicate (Diph-DiMOS) as the alkoxides. The sensor showed high permeability to ammonia, impermeability to protons and good photostability. The doped sol gel was prepared by magnetically stirring a mixture of aminofluoroscein, TMOS and ethanol before hydrochloric acid catalyst was added. The spectrum was found to be similar to that shown by the dye in solution.

7.2. Investigation of xerogel materials

Metal alkoxides are popular precursors for sol gel processing; due to their reactivity they tend to undergo hydrolysis and polycondensation reactions to produce highly condensed and branched network polymers. The networking depends on the functionality of the metal. Silicon (Si) with coordination number of 4, forms highly branched networks. The starting materials used in the preparation of the sol gels are usually inorganic metal salts or organometallic compounds such as metal alkoxides. In a sol gel process, the precursor undergoes reactions to form a colloidal suspension (i.e. sol). Further processing of the "sol" allows one to make glass type materials in different forms. Thin films for sensor applications are produced on a piece of substrate (for example glass) by spin-coating or dip-coating.

7.2.1. Materials and methodology

The choice of sol gel matrix for immobilisation of the sensing material required some consideration as early studies had noted problems due to cracking of the thin films [59]. On the other hand recent studies have also demonstrated that not only is it possible to develop suitable techniques for sol gel materials but rather simple processes are normally enough to yield high quality films [51, 60]. The quality of the sol gel is crucial in the preparation of an optical sensor. If the sensing material is granular or has cracks, this will alter its optical properties and affect the sensitivity and response time of the sensing layer. Therefore twelve types of xerogels were prepared in a systematic manner, to assess which would be the best one for use in the optical sensor. The sol gels films were characterised and the best ones had the least cracks, showed greatest optical clarity and highest fluorescence intensity. The alkoxides used for the preparation of the different sol gels were tetramethoxysilane (TMOS) (Sigma Aldrich, UK), methyltriethoxysilane (MTES) (Sigma Aldrich, UK), dimethoxydimethylsilane (DDMS) (Sigma Aldrich, UK), phenyltriethoxysilane (PTES) (Fluka, Switzerland) and octyltriethoxysilane (OTES) (Fluka, Switzerland).

Xerogels were synthesised using the method described below. The method was modified for different xerogel processing by changing the alkoxides ratio in the step shown in figure 7.7.

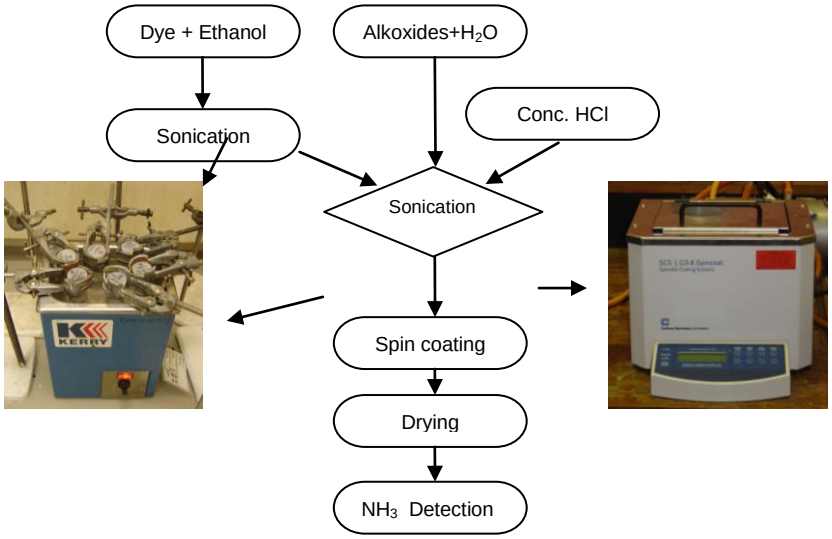

Figure 7.7: Schematic outlining the sol gel processing used in this study.

Figure 7.7 is a schematic representation of the sol gel process. A typical sol gel preparation was carried out as follows; 0.10g of 9 aminoacridine hydrochloride (9 AAH) (Sigma Aldrich) was added to 25 ml of ethanol (Fisher Scientific, UK) and was placed in an ultrasonic bath (Kerry, UK) for rapid dissolution of the dye. 1.0g of alkoxide was added to 0.40g of distilled water and 2.5 ml of ethanol and 9 AAH mixture. All compounds were inserted in a sample bottle and 2 drops of hydrochloric acid (HCl) was added. The solution was sonicated for 1 hour. The dye doped sol gels were spin coated (2000 rpm for 30 sec) onto the glass sides. Prior to coating, the glass slides (76 x 26x 0.8 mm) were cleaned according to a modified version of the protocol used by Lobnik *et al.;* [58].The glass slides were washed with piranha solution (1:1 mixture of conc. Nitric acid : Hydrogen peroxide (35%)), activated in concentrated nitric acid for 12 hr, washed with deionised water and ethanol and dried at 100 ^{0}C for 2 hours. Coated slides were dried at room temperature in a desiccator for at least one week before they were used for sensing. The reaction conditions i.e. high acidity, low water content and long drying time were chosen so that the sol gels produced would have low leaching rates of the immobilised dye [61].

7.2.2 Results and discussions

The sol gel films produced by varying the ratios of the alkoxides (TMOS, PTEOS, MTEOS, OTEOS and DDMS) were studied using a scanning electron microscopy (SEM) (JEOL JSM-35C). The thicknesses of the films were found to be approximately 200 nm when measured by the SEM. The response time of the sol gel based sensor is usually limited by diffusion, which in turn is dependent on various parameters such as sizes of pores, thickness of the film, size and concentration of the analyte [62]. Hence the xerogel was spun at a high speed to produce a thin sensing layer.

As summarised in Table 7.1, the SEM pictures illustrated that out of the 12 different types of xerogel synthesised only those synthesised with a 50% mixture of TMOS and 50% PTEOS, MTEOS or OTEOS produced uniform crack free sol gels films.

Table 7.1: Ratio of alkoxide precursors used for sol gel processing and their respective physical appearance.

TMOS	PTEOS (1)	MTEOS (2)	OTEOS (3)	DDMS (4)
25 %	Cracks	Cracks	Cracks	Granular
50 %	**Uniform**	**Uniform**	**Uniform**	Granular
75 %	Non uniform	Non uniform	Non uniform	Granular

The sol gel produced by mixing varying ratios of TMOS to DDMS all produced granular film whereas the films with 25% of PTEOS, MTEOS and OTEOS had cracks and sol gel films with 75% of additives were non uniform with some crystallisation. Figure 7.8 shows representative SEM pictures of the different sol gel films produced.

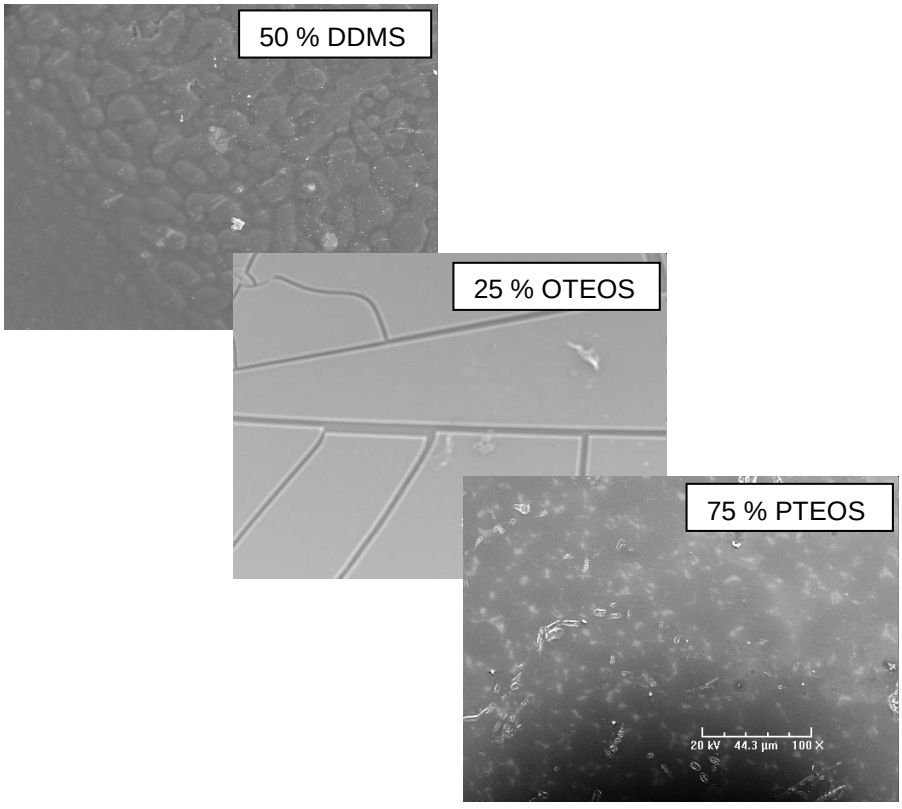

Figure 7.8: SEM pictures of representative sol gel films.

The effect of cleaning the glass slides was also investigated by spin coating sol gel mixtures that produced uniform coating on a clean and also on normal uncleaned glass slides. As observed in figure 7.9 the slides that had undergone the cleaning regime produced better quality sol gel films. The matrix used for immobilisation of 9 AAH was therefore the 50% OTEOS xerogel as it gave the best film in terms of optical clarity and was crack free.

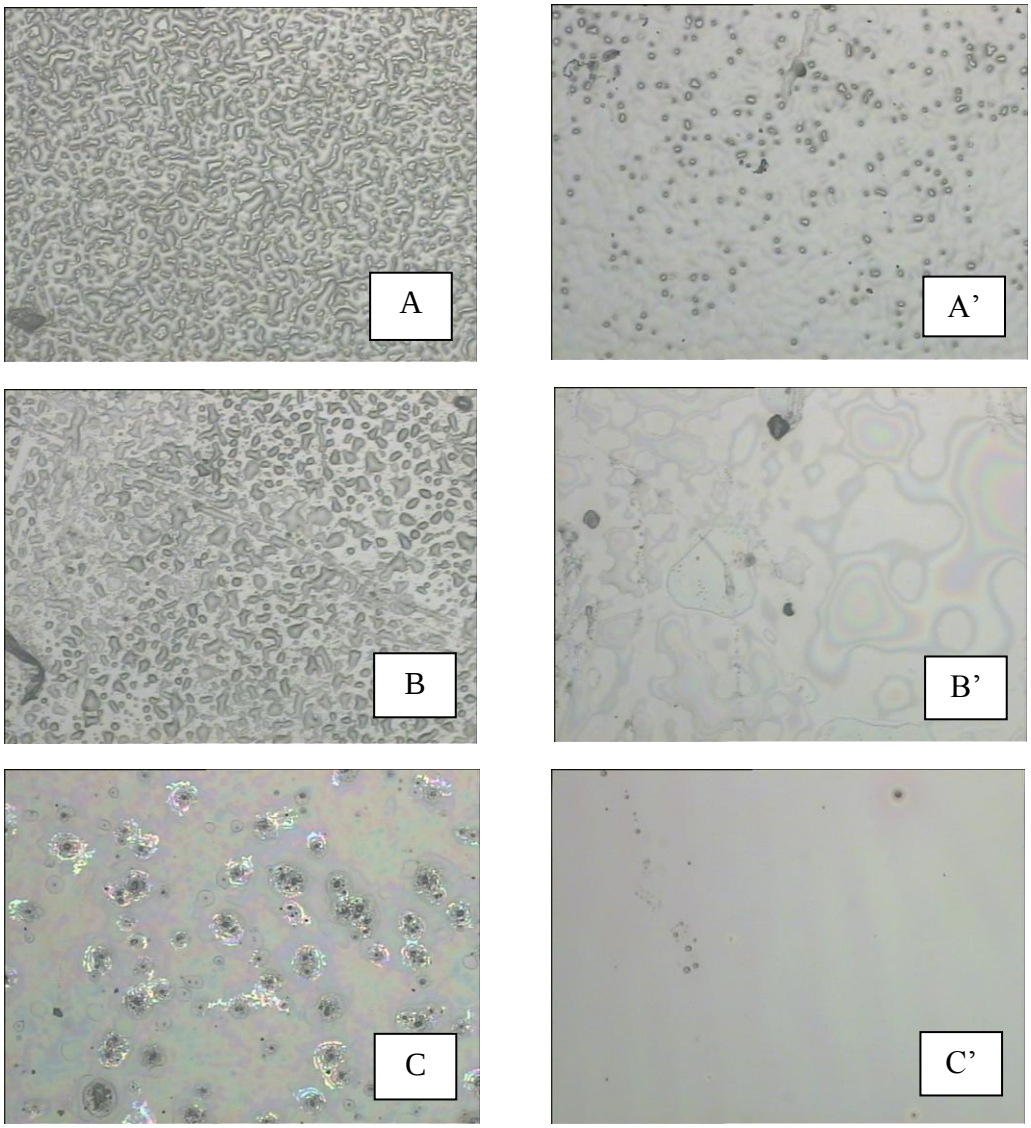

Figure 7.9: SEM pictures of xerogel coated slide. A – 50% PTEOS on uncleaned slide, A' - 50% PTEOS on cleaned slide; B – 50% MTEOS on uncleaned slide, B' - 50% MTEOS on cleaned slide; C - 50% OTEOS on uncleaned slide, C' - 50% OTEOS on cleaned slide

7.3. Measurement procedures for the initial prototype

Preliminary measurements on the optical sensor were performed using a prototype experimental setup, consisting of an excitation source, the optical sensor and a fluorescence detector. The choice of instrumentation was largely dictated by what was then readily available in the laboratory. It was planned that the results obtained with this prototype experimental setup would allow a simpler and more robust sensor to be designed at a later stage.

7.3.1. Materials

Tetra methyl orthosilicate, 98% (Sigma Aldrich), 9 aminoacridine hydrochloride (9 AAH), 98% (Sigma Aldrich), Hydrochloric acid (Fisher Scientific), Nitric acid (Fisher Scientific), Sulphuric acid (Fisher Scientific), Sodium hydroxide (Sigma Aldrich), Ethanol (Fisher Scientific), Nitrogen balanced ammonia gas at a certified concentration of 95.2 ppm was obtained from BOC, Hydrogen sulphide (BDH), Sulphur dioxide (BDH), Nitrogen gas (Air product). Deionised water was used thought out.

7.3.2. The experimental setup

Fluorescence measurements were performed with an Avantes fiberoptic spectrometer (AVS 2000) as the detector. The lamp output from a Hitachi F-2000 spectrofluorimeter was used as the light source.

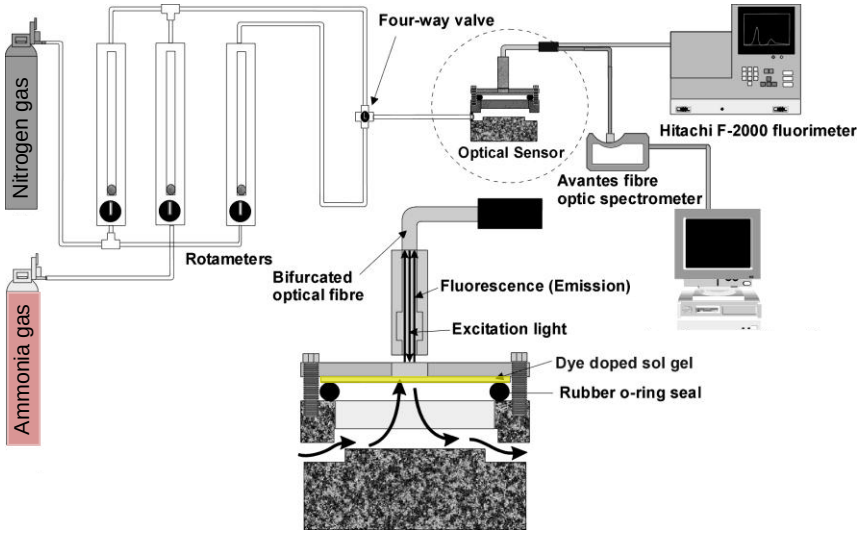

Figure 7.10: A schematic of the optical sensor setup.

A schematic of the experimental setup is shown in figure 7.10 the sensor system was coupled to a Hitachi F-2000 spectrofluorimeter by a bifurcated optical fibre. The xenon lamp of the spectrofluorimeter was used as the excitation light source to illuminate the dye doped sol gel which was spin coated onto the glass slide. The gas chamber was micro machined in aluminium. The sensing slide was placed over the gas chamber and a rubber 'O' ring provided a sufficient gas tight seal. The resultant fluorescence was directed into the second arm of the bifurcated optical fibre and detected by a compact UV-visible spectrometer (Avantes AVS2000). The spectrometer was connected to a personal computer and controlled through the Avasoft program. The excitation wavelength was set at 410 nm as it was found that this produced the most intense fluorescence at the detection wavelength 494 nm.

The gas flow was controlled by a series of rotameters (Supelco Inc). A certified mixture of ammonia gas (95.2 ppm ammonia in nitrogen (BOC)) was used for subsequent experiments. Different concentrations of ammonia were

produced by dilution of the standard ammonia gas with a separate controllable flow of nitrogen gas (Air product, UK). The steps in a typical experiment were as follows. Firstly nitrogen gas was allowed to flow through the system for 15 min and a 'blank' background fluorescence reading was recorded using the UV-visible spectrometer. Then a given concentration of ammonia gas was passed through the sensor and the subsequent fluorescence quenched spectrum was recorded. The concentration of the ammonia gas flowing through the sensor was changed by varying the flowrate of the certified ammonia gas with respect to the separate nitrogen flow whilst keeping the total flowrate at a constant 100 ml min^{-1}. This allowed concentrations of ammonia in the range ~5-100 ppm to be achieved. Typically measurements at six to nine different concentrations were made for each experiment. A linear regression through a Stern-Volmer plot of these data allowed the Stern-Volmer constant (K_{sv}) and the limit of detection (LOD) to be determined.

7.3.3. Results and discussions

Quenching of the fluorescence intensity was observed on exposure of the dye doped sol gel to different concentration of ammonia as shown in figure 7.11.

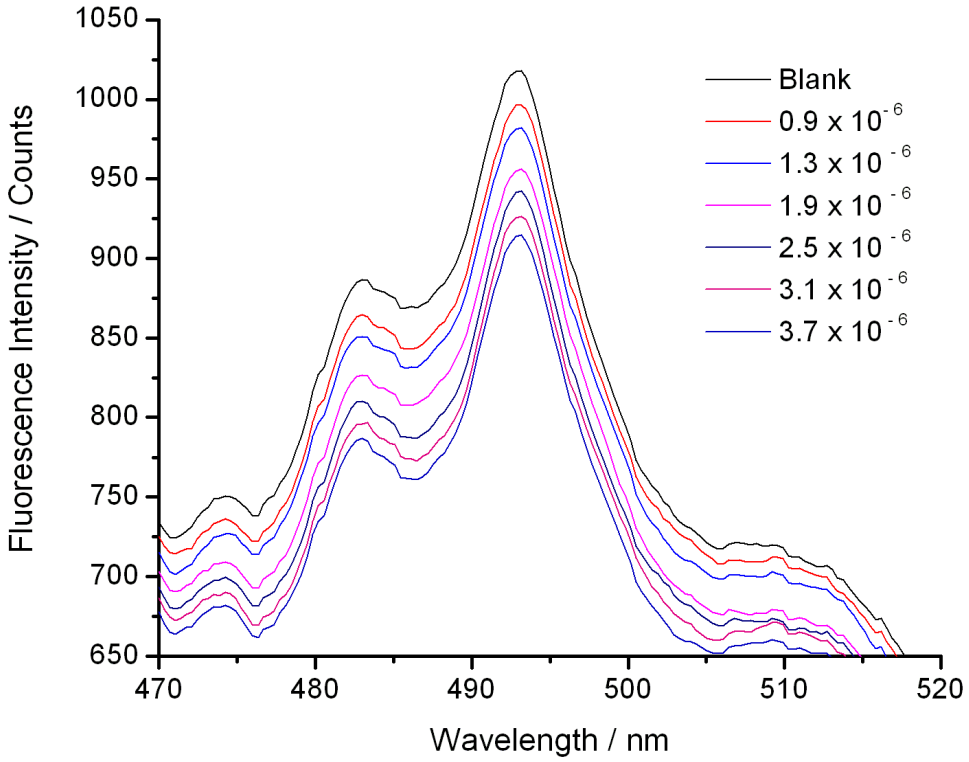

Figure 7.11: Fluorescence quenching of the dye doped sol gel on exposure to concentration of ammonia in the range 0 – 3.7 $\times 10^{-6}$ M (0 – 63 ppm). Some spectra were omitted for clarity, the full data set can be found in figure 7.12.

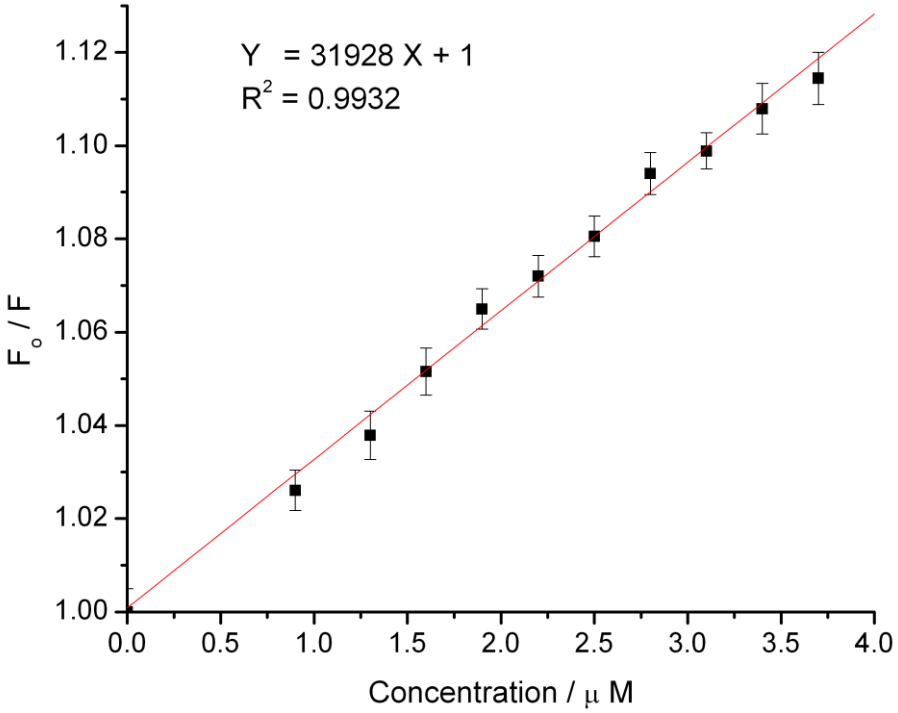

Figure 7.12: A Stern-Volmer plot of the fluorescence quenched data

Figure 7.12 shows the Stern-Volmer plot for the fluorescence quenching of the dye by ammonia at 494 nm. The error bars represent the 1σ error limit of six replicate measurements at each concentration. The equation on the diagram refers to an error-weighted linear fit to the measurements of the line with the correlation coefficient, R^2 = 0.9932 and a 1σ error limit for the intercept of 3 x 10^{-4}. The K_{sv} value for 9 aminoacridine hydrochloride in the sol gel matrix was found to be 3.2 x 10^4 M^{-1}. The LOD can be calculated from the value of the 3σ error limit on the intercept, and produces a concentration of 238 nM (~ 4 ppm).The limit of quantification (LOQ) can also be determined from the 10σ error limit on the intercept and yields a concentration of 793 nM (~13 ppm).

7.3.4. Effect of acidic gases

Generally most optical based ammonia sensors utilise fluorophores whose fluorescence are altered with a change in pH. These sensors have low selectivity as charged species such as protons and other interfering compounds usually affect the fluorescence intensity of the fluorophores. The effects of acidic gases were investigated by flowing different concentration of the gases hydrogen sulphide (BDH) and sulphur dioxide (Air product) through the sensor and recording the resultant fluorescence intensity. The concentrations of the acidic gases were diluted down with nitrogen using a series of rotameters. Sulphur dioxide and hydrogen sulphide concentration were determined by collecting the gas in sodium hydroxide solution and back titrating with sulphuric acid. The fluorescence was detected and recorded using the same optical setup described earlier.

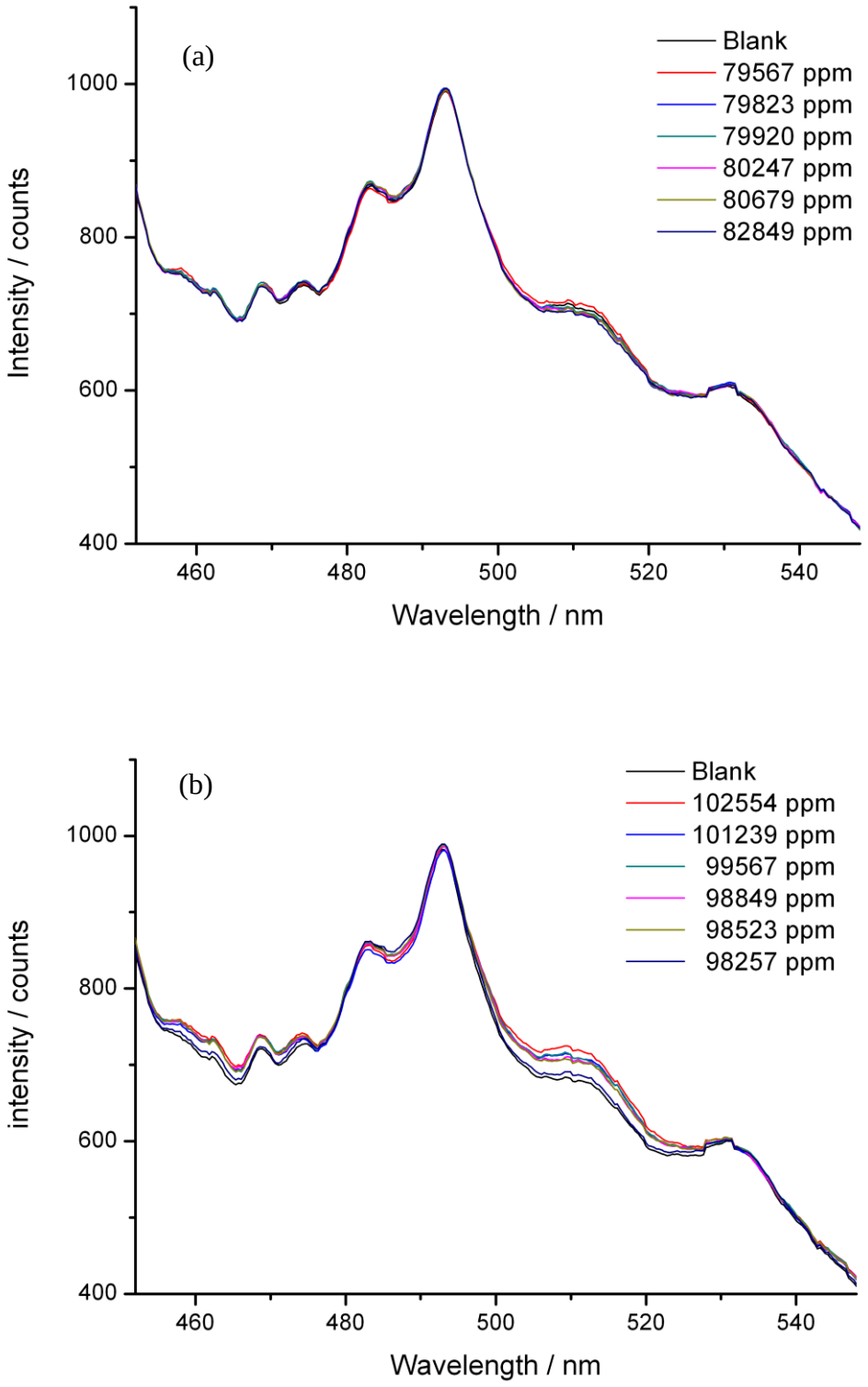

Figure 7.13: The effect of high concentrations of (a) HCl and (b) SO_2 on the fluorescence intensity of the sensor

The concentrations of the acidic gases were about 1000 times greater than that of the target analyte and yet no quenching of the fluorescence intensity at 494 nm was observed. This provided good evidence that the sensor was highly selective to ammonia and was not affected by acidic gases. Other basic analytes could theoretically interfere with the sensor, but as ammonia is the most significant basic gas in the atmosphere [63] the effect of other basic gases was not studied.

7.4. Measurement procedures for small scale prototype

7.4.1. Optimisation of the waveguide sensor

The fibre optic sensor described in 7.3.2 had limitations due to the arrangement of the optical setup and the low Stokes shift of the fluorescent dye 9 AAH [45]. The detection of fluorescence at 90^{o} to the sensing layer resulted in a large amount of background signal from the excitation source. The small difference between the excitation and emission wavelengths made it difficult to spectrally discriminate between the two. To overcome these limitations a simpler optical setup based on a waveguide sensor, and using an LED excitation source was developed. The principle of the waveguide sensor is based on a fraction of the fluorescence from the sensing layer penetrating the glass slide below at an angle greater than the critical angle and thus undergoing total internal reflection along the glass slide and exiting from the edge of the slide at a particular angle. This provides some spatial discrimination against the excitation light which exits the slide at a slightly different angle. A simple empirical experiment was carried out to determine the ideal detection angle for the fluorescence exiting the sensing layer.

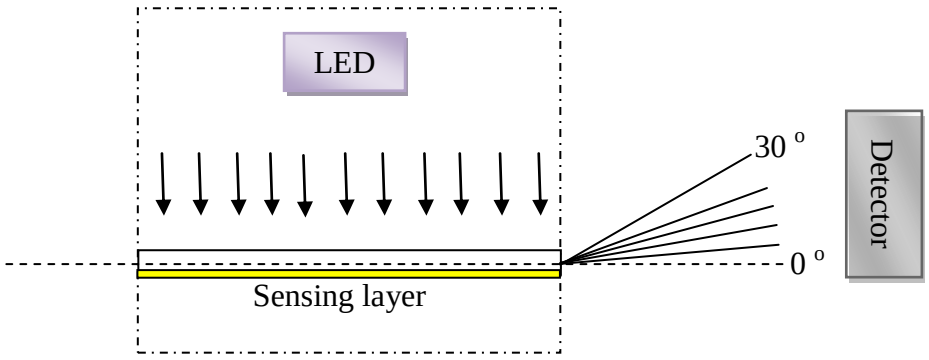

Figure 7.14: Schematic of setup to determine the best angle for the detection of maximum fluorescence intensity exiting the substrate layer.

A schematic of the setup used to determine the 'magic angle' at which the maximum fluorescence intensity leaves the substrate layer is shown in figure 7.14. The fluorophore was illuminated at right angle using a 5 mm diameter blue LED (ETG Corporation, USA) with a peak emission wavelength of 410 nm. The emitted fluorescence exiting the substrate was collected by an optical fibre coupled to a compact CCD spectrophotometer (Avantes AVS2000). The data acquisition was carried out using the Ocean Optics software.

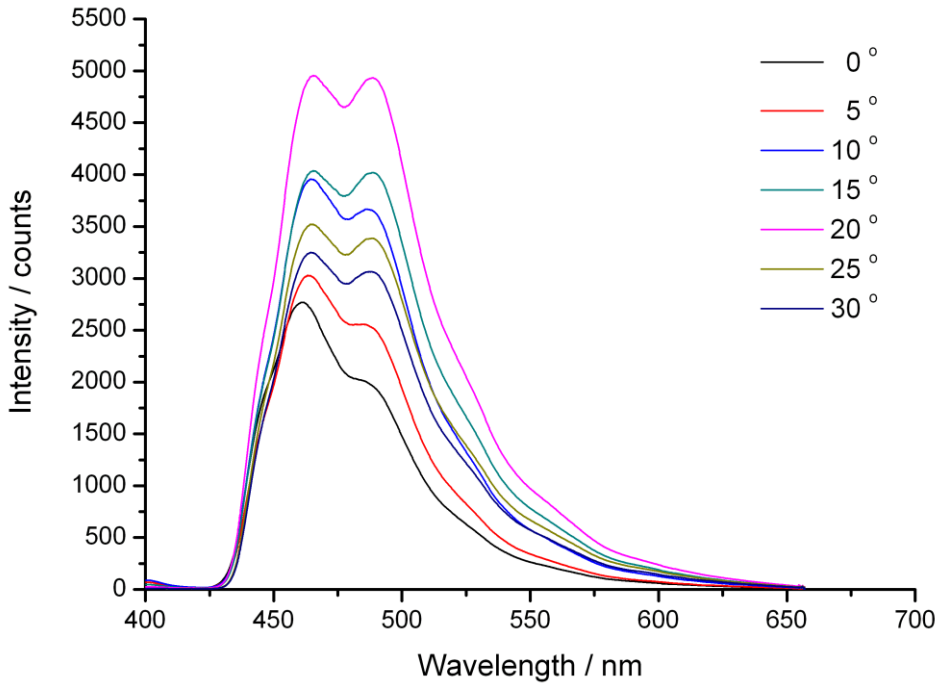

Figure 7.15: Fluorescence intensity at 0^{o}, 5^{o}, 10^{o}, 15^{o}, 20^{o}, 25^{o} and 30^{o}

Figure 7.15, shows the fluorescence intensity collected at 0, 5, 10, 15 20, 25, 30 degrees from the edge of the substrate. The optimum geometry of the detector was empirically assessed by varying the angle at which maximum intensity of the fluorescence exited the edge of the glass slide. Light exiting the sensing layer at 20 degrees was found to have the highest intensity and was therefore chosen as the best angle for the subsequent development of the ammonia sensor.

7.4.2. The dual channel optical sensor

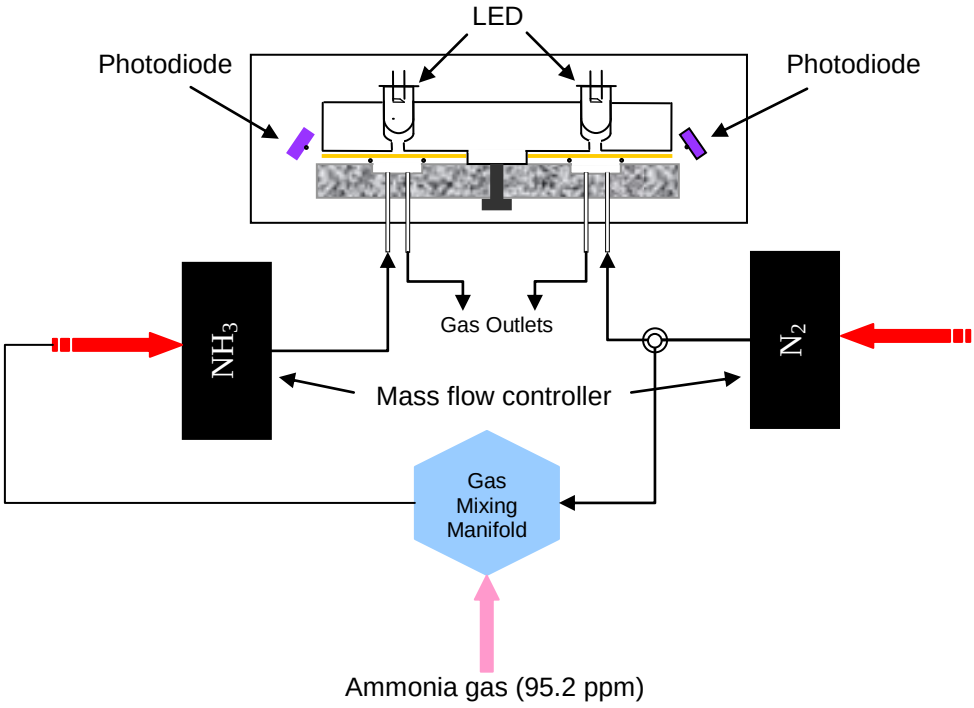

Figure 7.16: A schematic of the dual channel optical sensor

The next stage of development involved simplifying the detection setup by replacing the CCD spectrometer with a photodiode and also using a referencing system to improve the sensitivity of the sensor. Figure 7.16 shows a schematic of the dual channel optical sensor. The system consisted of two sensing chambers equipped with two glass slides coated with the dye doped sol gel. One of the sensing chambers served as the reference channel for the

measurements, allowing for temperature compensation during acquisition time of the sensor. The sensing layer was illuminated at right angles using a 5 mm blue LED (ETG Corporation, USA) with a peak emission wavelength of 410 nm. The fluorescence signal was detected using a selective photodiode (EPIGAP EPD-520). The associated electronics consisted of a microprocessor interfaced to an analog-digital converter as described in figure 7.17.

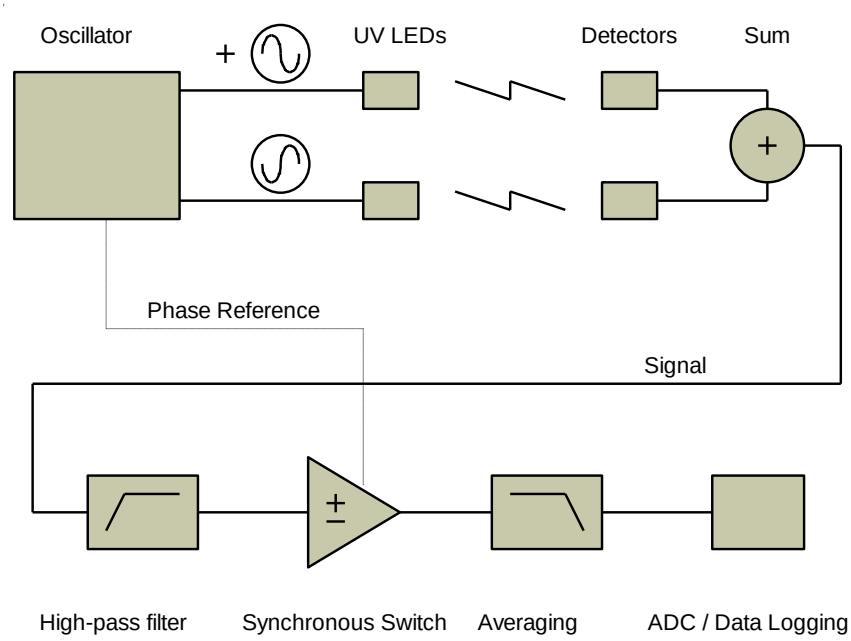

Figure 7.17: A Block diagram of the electronic design for the dual channel sensor.

To improve the sensitivity and stability of the optical measurement, a dual channel differential system was designed along with a lock-in amplifier based on a AD698 universal LVDT signal conditioner (Analog devices, USA). This included a stable sinewave oscillator with complementary outputs, two synchronous demodulators and a ratiometric circuit which gave an output dependant on the ratio of two signals. For maximum sensitivity the difference between the two channels was measured, rather than the ratio. To simplify the subtraction, a non conventional arrangement was devised where the cells were illuminated by complementary (out-of-phase) sinewaves and the output from the detectors was added rather than subtracted. The ratiometric feature of the AD698 was still used; the oscillator signal fed it through a phase shift network adjusted to compensate for phase shifts in the rest of the system, and ensured that any amplitude variation in the oscillator signal was compensated.

The optical sensor was linked to a gas dilution system with flow controllers (Brooks® instruments, Holland) and a computer for data collection and analysis. Nitrogen gas (BOC) was used as the dilution gas. The concentration and flow of the ammonia gas and nitrogen gas were precisely controlled by two mass flow controllers, which were plugged into a control unit (MFC, Brooks® instrument, The Netherlands). The concentration of ammonia gas in the measuring chamber was varied by mixing different level of ammonia gas with nitrogen in a gas line. The concentration of ammonia (in ppm) was defined as the ratio of the pressure of ammonia gas to the total pressure of ammonia and nitrogen gases. The gas pressure was monitored using 10 and 1000 torr range capacitance manometers (Baratron®, US) from MKS instruments. The ammonia concentration was varied between 5ppm and 95.2 ppm. Concentrations lower than 5ppm could not be measured reliably due to experimental setup limitations, associated with the gas mixing capability in the gas manifold.

After inserting the dye sensing layer on top of the gas chamber, nitrogen gas, was introduced into the measuring chamber. When the detector output was constant for 1 minute, ammonia gas was introduced into the system and the interaction between ammonia gas and the 9 AAH doped sol gel film led to a change in the output signal. Ammonia gas was passed over the sensor for nine minutes for each measurement as this was the maximum amount the mixing container could handle. After each measurement the sensor was purged by passing pure nitrogen gas through the gas chamber for 5 minutes which caused the detector output to return to baseline levels.

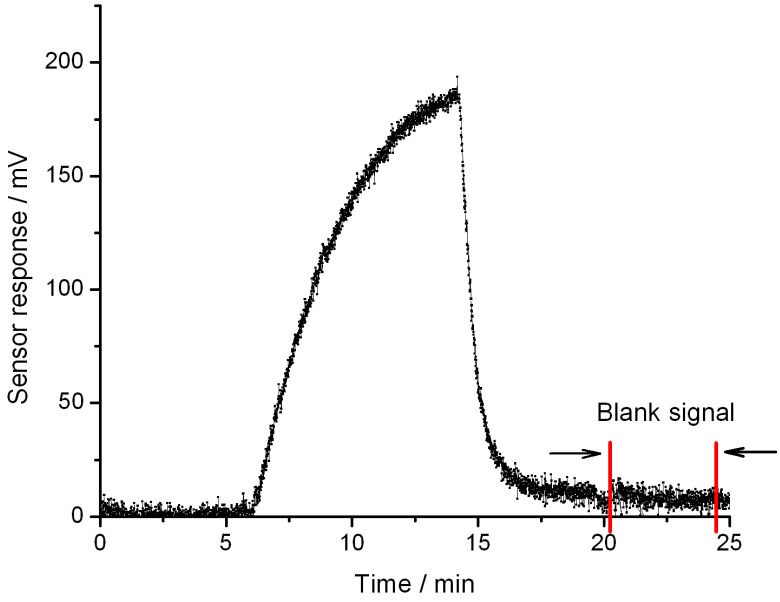

Figure 7.18: Sensor response with 38 ppm ammonia

The sensor response for an ammonia concentration of 38 ppm is shown in figure 7.18. The standard deviation of the blank signal was used to calculate the minimum detectable concentration of ammonia.

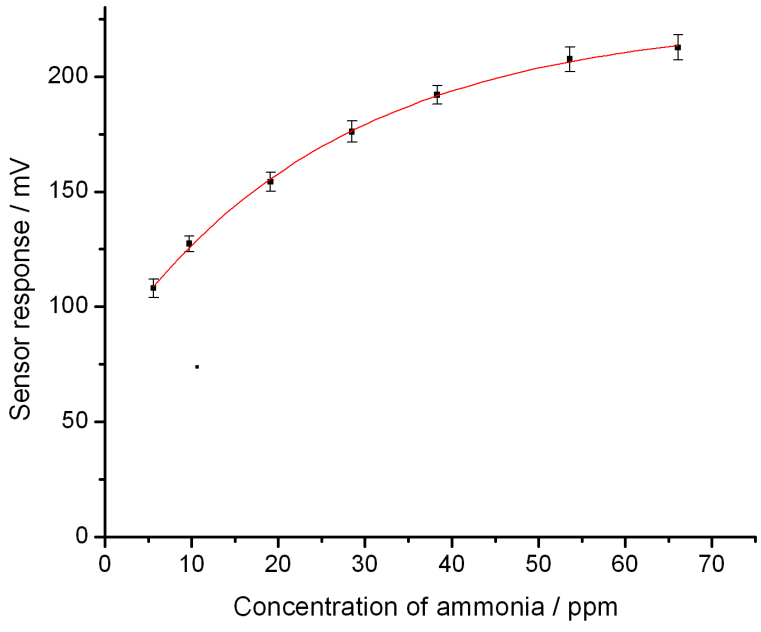

Figure 7.19: The response of the sensor to ammonia gas in the range 5 – 70 ppm

Figure 7.19 shows shows a plot of the response of the sensor as a function of increasing ammonia concentration. The non-linear behaviour may reflect the combined response of 9 AAH molecules accessible to ammonia and those, in the densified region of the support sol gel structure, which are not. Figure 7.19 also suggests that the sensor shows highest sensitivity at concentrations lower than 5 ppm as the slope of the curve is steeper. It is also possible that the response might become linear at lower concentrations. Unfortunately as mentioned previously the gas handling setup did not allow concentrations of ammonia lower than 5 ppm to be reliably generated. The standard deviation of the blank signal for all the measurements was found to be on average 1.6 % of the maximum total change in signal. The minimal detectable concentration calculated from the average standard deviation of the blank signal was 387 ppb.

7.4.3. Discussion and Further Work

Although further development work is required, this work shows the great potential of the sol gel approach for the fabrication of ammonia sensors. The sol gel approach enables sensor fabrication in a simple manner for a range of configurations. It has been tested for gaseous ammonia monitoring and possibly could be extended to monitoring of ammonia in solution.

Ammonia has widespread use in several sectors, the main uses being industrial refrigeration systems, fertilisers, explosives and chemicals production. Ammonia is also generated in agriculture, farming and is evolved in catalysed combustion processes in heat and power generation. Table 7.2 summarises the requirement for ammonia sensors with regards to their application, limit of detection, response time and the temperature at which they will be used. The detection of ammonia gas is traditionally performed by potentiometric sensors within a laboratory and such static sampling devices have significant limitations such as high consumption of the analyte, high expense, and require the presence of an experienced operator [16]. Ammonia sensing devices for atmospheric monitoring, farming and vehicles emission includes infrared gas analysers. These commercially available instruments, although sensitive, are nevertheless expensive, bulky and have certain restrictions in terms of reproducibility, stability, sensitivity and selectivity [16].

Table 7.2: Summary of current requirements in ammonia gas sensing

Applications	Detection methods	Detection limit range required	Response Time required	Temperature range	Authors
Monitoring of atmospheric ammonia	Electrochemical Catalytic metal Photoacoustic spectroscopy Open path IR analyser	0.1 ppb to ~ 200 ppm	Minutes	0 – 40 ^{o} C	Erisman,J.W *et al.;* [64] Barrett et al.; [65] Winquist, F *et al.;* [66] Huszár,Helga *et al.;* [13] Cao,W et al.; [16] Malins,C *et al.;* [15]
Livestock inventory	Absorption Spectroscopy Open path IR analyser	1 to 35 ppm	Minutes	10 – 40 ^{o} C	Mount *et al.*; [14] Ni,J.Q *et al. ;* [67]
Vehicles emission	FTIR spectroscopy	4 – 200 mg / min	Seconds	Up to 300 ^{o} C	Durbin,T.D *et al.*; [68]
Exhaust gases	Selective catalytic reaction Electrical resistance	1 – 100 ppm	Seconds	up to 600 ^{o} C	Moos,R. *et al.*; [69] Xu,C.N *et al.;* [52]
Chemical industry	Electroconducting polymer	20 - 1000 ppm	Minutes	up to 500 ^{o} C	De La Hoz,R.E *et al. ;* [70] Kukla,A.L. *et al. ;* [71]
Breath Analysis / Medical applications	Potentiometric	50 – 2000 ppb	Minutes	20 – 40 ^{o} C	Ament,W *et al.;* [72] Kearney,D.J *et al.;* [73]

The U.S. Occupational Safety and Health Administration (OSHA) has set a maximum exposure time of 15 min to ammonia levels of 35 ppm in the air and an 8 h exposure limit of 25 ppm. The equipment and setup cost for current methods can be around £600 for small animal establishments and more than £13000 for large animal buildings [67]. Our dual channel sensor system would comparatively be much cheaper to manufacture due to the low cost of LEDs, photodiodes and other associated electronic components.

Malins *et al.* [15] developed a reversible personal ammonia sensor for the industrial environment that used a pH sensitive dye. The sensitivity was in the 5 – 100 ppm range with a response time of around 2 minutes. The drawback of this sensor was that it was not very selective and was based on absorption measurements which are comparatively less sensitive than fluorescence measurements. Other such sensors have been developed by Cao *et al*. [16] their sensor had a linear dynamic range from 10 to 1000 ppm with a response time of 10 seconds. The developed sensor system compared favourably well with the personal ammonia sensor as it was reversible and had a similar working range.

Catalytic oxide materials are widely used for ammonia gas sensing membranes due to their good sensitivity and fast response time. The drawback of these sensors is that reaction energy needs to be supplied by heating the sensor to high temperatures [74]. Potentiometric detection based ammonia measurement in air has been carried out by West *et al.;* [75] using a sensor based on an ionophore, with a range between 2 ppb and 100 ppm and a response time up to ~ 4 minutes. Traditional ammonia sensors such as electrochemical and semiconductor detectors; have serious drawbacks in terms of selectivity, lifetime and functional safety in explosive environments [11].

Given the requirements for ammonia gas sensing, the optical sensor developed in this study could be used as a sensor for ammonia detection in farming and the industrial environment as it has a working range in the low ppm levels and a response time in minutes. The fluorescent dye 9 AAH used for ammonia sensing is selective to ammonia and does not act as a pH sensitive dye as its fluorescence intensity is not affected by acidic gases. Other types of basic gases may interfere, but are found at very low (ppb) levels in the atmosphere [76]. The study by Calderon *et al.;* [77] estimated the total amine

concentration to be 160 – 2800 pmol m^{-3} in southern Sweden. The sensor could also find application in areas such as refrigeration plants as at temperatures below freezing, the vapour pressure of any gaseous amines from deterioration of foodstuffs would be negligible [15]. The small size and flexibility of the sensor design would make it ideal as a tool for onsite measurements. The optical fibre setup can easily transmit chemical information between the spectrometer and a remote sample. A fibre optic sensor would be suitable for monitoring environmental hazards including either hostile or not easily accessible events. Optical fibres are relatively insensitive to sources of noise, such as radioactivity and electric fields, and signals acquired with optical fibres are much less prone to environmental interferences than those transmitted through electrical wires.

The limitations of dye based sensors are mainly due to the sensitivity of their response to temperature [16]. The dual channel sensor setup described in section 7.4.2 is able to overcome temperature drifts and noise due to the electronics as all measurements are made in comparison to a reference measurement. The selectivity could be improved with membranes such as metal phosphonate thin films, which may offer a route to better gas selectivity [78]. The sensitivity of the sensor could be increased by applying phase sensitive detection. This reduces background noise. In order to improve the response time of the waveguide ammonia sensor, the effect of elevated ambient temperatures could be thoroughly investigated, as previous studies have shown this to have a positive effect [16].

Ammonia is also produced in small quantities by the human body. The normal level can be altered as a result of kidney disorder or ulcer, where urea conversion leads to presence of ammonia in breath. A measurement of ammonia in exhaled air at the 50-100 ppb level would allow fast and non-invasive diagnostics. The small scale prototype currently has a minimum detection limit in the high ppb range and with implementation of the further work suggested, a non invasive sensor could be developed for use in the medical diagnostics sector.

7.4.4. Conclusions

An optical sensor for the detection of ammonia gas has been developed in several stages. The operation of the sensor depends on the fluorescence quenching of the dye 9 AAH immobilised in a sol gel matrix. Initial experiments on a large scale prototype were used to identify the best formulation which produced a crack free xerogel matrix. These experiments also showed that the sensor response was not affected by the presence of acidic gases such as HCl and SO_2. The second stage involved simplifying the optical setup and redesigning the optical sensor to function as a waveguide sensor, which reduced the background contribution from the excitation source. The final stage consisted of further simplification of the detection setup and the use of dual channel monitoring to improve the sensitivity of the sensor. Measurements using diluted mixtures of ammonia gas in the range 5 -70 ppm showed that the response of the sensor was nonlinear, with the sensitivity increasing at lower concentrations. The measurement of the baseline noise allowed the LOD to be estimated at ~400 ppb. In its current form the sensor is a simple, lightweight and low cost device which would be suitable for use in farming and industrial applications. However, modifications to the method of detection may allow the sensitivity to be improved to the 50 ppb level which may make it suitable for medical diagnostics.

7.5. References

[1] Nagl, S.; Schaeferling, M.; Wolfbeis, O. S. Microchimica Acta, 151 (2005) 1.

[2] Albani, J. R. Principles and Applications of Fluorescence Spectroscopy, Blackwell, UK, 2007, p. 255.

[3] Lakowicz, J. R. Principles of Fluorescence Spectroscopy, Kluwer Academic/Plenum, New York, 1999, p. 698.

[4] Lakowicz, J. R. Principles of Fluorescence Spectroscopy, Springer, US, 2006, p. 954.

[5] Lakowicz, J. R. Principles of Fluorescence Spectroscopy, Plenum Press, New York, 1983, p. 258.

[6] Albani, J. R. Structure and Dynamics of Macromolecules: Absorption and Fluorescence Studies, Elsevier Science, Amsterdam, 2004, p. 141.

[7] Derfa, http://users.rcn.com/jkimball.ma.ultranet/BiologyPages/ N/Nitrogen Cycle.html. (accessed 23/08/2008)

[8] C□ağlar, P.; Narayanaswamy, R. The Analyst, 112 (1987) 1285.

[9] Sharma, A.; Ali, Z.; Higgins, I. J. Proceedings of SPIE - The International Society for Optical Engineering, 1637 (1992) 107.

[10] http://users.rcn.com/jkimball.ma.ultranet/BiologyPages/ N/Nitrogen Cycle.html (accessed on 20/03/2007).

[11] Timmer, B.; Olthuis, W.; Van Den Berg, A. Sensors and Actuators, B: Chemical, 107 (2005) 666.

[12] Shialis, T.; Reis, S.; Searl, A. Ammonia damage costs. Final report. London, Entec UK Ltd., (2007) p. 26.

[13] Huszár, H.; Pogány, A.; Bozóki, Z.; Mohácsi, Á, Horváth, L.; Szabó, G. Sensors and Actuators B: Chemical, 134 (2008) 1027.

[14] Mount, G. H.; Rumburg, B.; Havig, J.; Lamb, B.; Westberg, H.; Yonge, D.; Johnson, K.; Kincaid, R. Atmospheric Environment, 36 (2002) 1799.

[15] Malins, C.; Doyle, A.; MacCraith, B. D.; Kvasnik, F.; Landl, M.; S□imon, P.; Kalvoda, L.; Lukas□, R.; Pufler, K.; Babusík, I. Journal of Environmental Monitoring, 1 (1999) 417.

[16] Cao, W.; Duan, Y. Sensors and Actuators, B: Chemical, 110 (2005) 252.

[17] Yagodina, O. V.; Nikolskaya, E. B. Analytica Chimica Acta, 385 (1999) 137.

[18] Buckley, S. G. Applied Optics, 37 (1998) 8382.

[19] Vasudev, R. Applied Physics B: Lasers and Optics, 87 (2007) 163.

[20] Thorpe, M. J.; Moll, K. D.; Jones, J. R.; Safdi, B. J. Science, 311 (2006) 1595.

[21] Berden, G.; Peeters, R.; Meijer, G. Chemical Physics Letters, 307 (1999) 131.

[22] O'Leary, D. M.; Orphal, J.; Ruth, A. A.; Heitmann, U.; Chelin, P.; Fellows, C. E. Journal of Quantitative Spectroscopy and Radiative Transfer, 109 (2008) 1004.

[23] Kassi, S.; Chenevier, M.; Gianfrani, L. ; Salhi, A.; Rouillard, Y.; Ouvrard, A.; Romanini, D. Optics Express, 14 (2006) 11442.

[24] Peeters, R. Chemical Physics Letters, 337 (2001) 231.

[25] Meyerhoff, M. E.; Robins, R. H. Analytical Chemistry, 52 (1980) 2383.

[26] Meyerhoff, M. E. Analytical Chemistry, 52 (1980) 1532.

[27] Bendahan, M.; Lauque, P.; Seguin, J.; Aguir, K.; Knauth, P. Sensors and Actuators, B: Chemical, 95 (2003) 170.

[28] Rechenbach, T.; Schramm, U.; Boeker, P.; Horner, G.; Roesky, C. E. O.; Trepte, J.; Winter, S.; Pollex, R.; Bargon, J.; Weber, E.; Schulze Lammers, P. Sensors and Actuators, B: Chemical, 57 (1999) 255.

[29] Ali, Z.; Thomas, C. L. P.; Alder, J. F.; Marshall, G. B. The Analyst, 117 (1992) 899.

[30] Wolfbeis, O. S. Analytical Chemistry, 78 (2006) 3859.

[31] Nivens, D. A.; Schiza, M. V.; Angel, S. M. Talanta, 58 (2002) 543.

[32] Bergman, I. Nature, 218 (1968) 396.

[33] Grady, T.; Butler, T.; MacCraith, B. D.; Diamond, D.; McKervey, M. A. Analyst, 122 (1997) 803.

[34] Jin, Z.; Su, Y.; Duan, Y. Sensors and Actuators, B: Chemical, 72 (2001) 75.

[35] Ismail, F.; Malins, C.; Goddard, N.J. Analyst, 127 (2002) 253.

[36] Landl, M.; Simon, P.; Kvasnik, F. Sensors and Actuators, B: Chemical, 51 (1998) 114.

[37] S□imon, P.; Landl, M.; Breza, M.; Kvasnik, F. Sensors and Actuators, B: Chemical, 90 (2003) 9.

[38] Scorsone, E.; Christie, S.; Persaud, K.; Simon, P.; Kvasnik, F. Proceedings of SPIE - The International Society for Optical Engineering, 4829 II (2003) 978.

[39] Yimit, A.; Itoh, K.; Murabayashi, M. Sensors and Actuators, B: Chemical, 88 (2003) 239.

[40] Malins, C.; Butler, T. M.; MacCraith, B. D. Thin Solid Films, 368 (2000) 105.

[41] Wirth, M.; Buchardt, O.; Koch, T.; Nielsen, P. E.; Nordén, B. Journal of the American Chemical Society, 110 (1988) 932.

[42] Wainwright, M. Journal of Antimicrobial Chemotherapy, 47 (2001) 1.

[43] Morrissey, R. E.; Lamb J. C.; Morris, R. W.; Chapin, R. E.; Gulati, D. K.; Heindel, J. Fundamental and Applied Toxicology, 13 (1989) 747.

[44] Gangola, P.; Joshi, N. B.; Pant, D. D. Chemical Physics Letters, 80 (1981) 418.

[45] Pant, D. D.; Joshi, G. C.; Tripathi, H. B.; Pramana, 27 (1986) 161.

[46] Gangola, P.; Joshi, N. B.; Pant, D. D. Chemical Physics Letters, 80 (1981) 418.

[47] Levy, D.; Reisfeld, R.; Avnir, D. Chemical Physics Letters, 109 (1984) 593.

[48] Avnir, D.; Levy, D.; Reisfeld, R. Journal of Physical Chemistry, 88 (1984) 5956.

[49] Kandimalla, V.; Tripathi, V. S.; Ju, H. Critical Reviews in Analytical Chemistry, 36 (2006) 73.

[50] MacCraith, B. D.; McDonagh, C. M.; O'Keeffe, G.; McEvoy, A. K.; Butler, T.; Sheridan, F. R. Sensors and Actuators, B: Chemical, B29 (1995) 51.

[51] Mitzi, D. B. Chemistry of Materials, 13 (2001) 3283.

[52] Xu, C. N.; Miura, N.; Ishida, Y.; Matsuda, K.; Yamazoe, N. Sensors and Actuators B: Chemical, 65 (2000) 163.

[53] J. Phalippou, http://www.solgel.com/articles/June00/phalip/introsolgel.htm, (accessed 01/12/2008).

[54] Hu, M. Z.; Zielke, J. T.; Byers, C. H.; Lin, J. S.; Harris, M. T. Journal of Materials Science, 35 (2000) 1957.

[55] Trinkel, M.; Trettnak, W.; Reininger, F.; Benes, R.; O'Leary, P.; Wolfbeis, O. S. Analytica Chimica Acta, 320 (1996) 235.

[56] Bein, T. (Ed.), Supramolecular Architecture: Synthetic Control in Thin Films and Solids, ACS, Washington, D. C., 1992.

[57] Binner, J. Advanced Ceramics Report, 1990 (1990) 13.

[58] Lobnik, A.; Wolfbeis, O. S. Sensors and Actuators B: Chemical, 51 (1998) 203.

[59] Innocenzi, P.; Abdirashid, M. O.; Guglielmi, M. Journal of Sol-Gel Science and Technology, 3 (1994) 47.

[60] Jerónimo, P. C. A.; Araújo, A. N.; Conceic□ão M.; Montenegro, B. S. M. Talanta, 72 (2007) 13.

[61] Aharonson, N.; Altstein, M.; Avidan, G.; Avnir, D.; Bronshtein, A.; Lewis, A.; Liberman, K.; Ottolenghi, M.; Polevaya, Y.; Rottman, C.; Samuel, J.; Shalom, S.; Strinkovski, A.; Turniansky, A. Materials Research Society Symposium - Proceedings, 346 (1994) 519.

[62] Lee, J.E.; Saavedra, S. S. Analytica Chimica Acta, 285 (1994) 265.

[63] Trinkel, M.; Trettnak, W.; Reininger, F.; Benes, R.; Leary, P. O.; Wolfbeis, O. S. Int. J. Environ. Anal. Chem., 67 (1997) 237.

[64] Erisman, J. W.; Otjes, R.; Hensen, A.; Jongejan, P.; Van Den Bulk, P.; Khlystov, A.; Mo□ls, H.; Slanina, S. Atmospheric Environment, 35 (2001) 1913.

[65] Barrett, K. Atmospheric Environment, 32 (1998) 381.

[66] Winquist, F.; Spetz, A.; Lundström, I.; Danielsson, B. Analytica Chimica Acta, 164 (1984) 127.

[67] Ni, J.; Heber, .A. J. Advances in Agronomy, 98 (2008) 201.

[68] Durbin, T. D.; Wilson, R. D.; Norbeck, J. M.; Miller, J. W.; Huai, T.; Rhee, S. H. Atmospheric Environment, 36 (2002) 1475.

[69] Moos, R.; Mu□ller, R.; Plog, C.; Knezevic, A.; Leye, H.; Irion, E.; Braun, T.; Marquardt, K.; Binder, K. Sensors and Actuators, B: Chemical, 83 (2002) 181.

[70] De La Hoz, R. E.; Schlueter, D. P.; Rom, W. N. American Journal of Industrial Medicine, 29 (1996) 209.

[71] Kukla, A. L.; Shirshov, Y. M.; Piletsky, S. A. Sensors and Actuators, B: Chemical, 37 (1996) 135.

[72] Ament, W.; Huizenga, J. R.; Kort, E.; Van Der Mark, T. W.; Grevink, R. G.; Verkerke, G. J. International Journal of Sports Medicine, 20 (1999) 71.

[73] Kearney, D. J.; Hubbard, T.; Putnam, D. Digestive Diseases and Sciences, 47 (2002) 2523.

[74] Lee, Y.; Song, K.; Huh, J.; Chung, W.; Lee, D. Sensors and Actuators B: Chemical, 108 (2005) 292.

[75] West, S. J.; Ozawa, S.; Seiler, K.; Tan, S. S. S.; Simon, W. Analytical Chemistry, 64 (1992) 533.

[76] Oberg, K. I.; Hodyss, R.; Beauchamp, J. L. Sensors and Actuators, B: Chemical, 115 (2006) 79.

[77] Calderón, S. M.; Poor, N. D.; Campbell, S. W. Atmospheric Environment, 41 (2007) 4281.

[78] Brousseau, L. C.; Aoki, K.; Yang, H. C.; Mallouk, T. E. Interfacial Design and Chemical Sensing, American Chemical Society (ACS), Symposium Series 561, American Chemical Society, US, 1994, p. 60.

Chapter Eight

8.0. General Conclusions

Three general areas of new applications of optical analytical techniques have been investigated in this thesis. Firstly innovative application of broadband cavity enhanced absorption spectroscopy (BBCEAS) to the detection of liquid phase analytes has been demonstrated. Secondly the use of total luminescence spectroscopy to discriminate between different types of teas has been investigated. Finally an optical gas sensor has been developed which is based on ammonia gas quenching the fluorescence intensity of a dye immobilised in a sol gel matrix.

This thesis initially investigated BBCEAS measurements in a 2 mm cuvette as a means of sensitive liquid phase analysis. It has been shown that a low cost setup could be used to achieve sensitivities similar to those previously obtained using substantially more expensive cavity based experimental setups [1]. Four analytes namely Ho^{3+}, brilliant blue-R, sudan black and coumarin 334 were investigated in the appropriate wavelengths range of the visible part of the electromagnetic spectrum from 400 – 700 nm. Measurements on Ho^{3+} and sudan black with the white LED and the $R \geq 0.99$ mirrors covered a broad wavelength range of ~250 nm and represents the largest wavelength range covered to date in a single CEAS experiment. The lowest value of the minimum detectable change in the absorption coefficient, α_{min}, obtained in this study was 5.1×10^{-5} cm^{-1} and obtained using $R \geq 0.99$ mirrors. The best LOD was obtained for the strong absorber brilliant blue-R, and was approximately 620 pM. The *CEF* values were found to generally increase with higher mirror reflectivities, although the increase was significantly less than expected in comparison with gas phase measurements. This could be attributed to relatively large scattering and absorption losses from the cuvette windows. Measurements with the $R \geq 0.99$ mirror set showed a combined cuvette and solvent losses of $\sim 1 \times 10^{-2}$ per pass, which is rather high compared with the only other comparable liquid phase BBCEAS study [2] which reported cuvette

losses of ~10^{-3} per pass and solvent losses of ~10^{-3} cm^{-1}. A linear dynamic range of measurement of about two orders of magnitude, from the LOD of ~1 x 10^{-3} AU to 0.2 AU, has been shown with a non linear behaviour at higher concentrations.

In latter experiments the BBCEAS optical setup was applied as the detection method for a home built HPLC system. A 1 cm pathlength HPLC cell with quartz windows having a nominal volume of 70 μl was used in this study. The cavity was formed by two plano-concave $R \geq 0.99$ mirrors with a bandwidth of ~420 – 670 nm. Two analytes rhodamine 6G and rhodamine B were chosen for separation by HPLC. The rationale for the choice was because they were chemically similar species with distinctive visible spectra and would co-elute in an isocratic separation. The sensitivity of the technique as determined by the best α_{min} value was 1.9 x 10^{-5} cm^{-1}. This α_{min} value was obtained using relatively low reflectivity $R \geq 0.99$ mirrors and only 45 passes through the cavity. The results obtained in this study compared surprisingly well with the previous CRDS based measurements. The most significant advantage of the current HPLC-BBCEAS study over the previous studies arose from the recording of the absorption spectrum over a range of wavelengths for each measurement. The measurements on rhodamine 6G and rhodamine B were all recorded between 450 and 600 nm, whereas previous studies only made measurements at a single wavelength. The spectral data collected was also represented in the form of a contour plot which was useful in visualising the two nearly co-eluting analytes. The LOD values for the two analytes studied indicated that the HPLC-BBCEAS setup was between 54 and 77 times more sensitive than a commercial Perkin Elmer HPLC system.

The final application of BBCEAS in this thesis was to a significantly longer 20 cm pathlength cell where the mirrors were in direct contact with the liquid phase analyte. Hallock *et al.* [3] reported that careful choice of solvent should to be made as many of the common ones showed strong absorptions in the 620 – 670 nm regions. In this study it was found that acetonitrile offered the greatest transparency over the largest wavelength range with the $R \geq 0.99$ mirrors, and consequently was chosen as the solvent for subsequent measurements. The experiments were carried out using different cavity mirrors

($R \geq 0.99$ & $R \geq 0.999$ mirrors). The *CEF* values obtained with the $R \geq 0.99$ mirror set for methylene blue (*CEF* = 78) and sudan black (*CEF* = 82) were approximately the same. Measurements with the $R \geq 0.999$ mirror set were made on methylene blue and a *CEF* value of 429 was obtained. The lowest α_{min} value obtained in this study was 2.8×10^{-7} cm^{-1} which is the lowest reported value to date for a liquid phase measurement, making this study the most sensitive liquid phase absorption measurement reported. The lowest LOD recorded was 4.6 pM, and was obtained for methylene blue with the $R \geq 0.999$ mirrors.

A novel application of total luminescence spectroscopy to discriminate between several types of teas objectively was also investigated. This work demonstrated the potential of fluorescence spectroscopy to distinguish between seven types of tea namely Oolong, Green, Houji, Kenya, Assam, Ceylon and Japanese Black tea. The EEM generated from the data collected produced distinct shapes that allowed visual discrimination between the black teas. However the small differences between the brown and green tea was less obvious. A pattern recognition technique based on PCA was applied to all the data collected and resulted in discrimination between all geographically dissimilar teas without any classification error. This study was further extended to geographically similar Black teas from 11 different plantation estates in Sri Lanka. After implementation of a new solvent extraction regime, the PCA plot produced excellent results as all eleven Sri Lankan teas were visually separable without classification errors when the first two principal components were used. This work lays the foundation for further work that could lead to the development of a cheap, robust, objective sensor system to determine the quality of tea rather than using the costly subjective assessment of tea tasters.

The final part of the thesis dealt with the development of an optical sensor for the detection of ammonia gas. The operation of the sensor was based on the fluorescence quenching of the dye 9 AAH immobilised in a sol gel matrix. The matrix used for immobilisation was a 50% OTEOS 50% TMOS xerogel as it gave the best film in terms of optical clarity and was crack free compared the other 11 xerogels investigated. The limit of detection for the initial prototype was 4 ppm and it was also shown that the sensor response was not

affected by the presence of acidic gases such as HCl and SO_2. This sensor was comparable in sensitivity to the personal ammonia sensor for industrial environments developed by Malins *et al.* [4]. The final version of the sensor made use of a dual channel monitoring system to improve the sensitivity of the sensor. Measurements using diluted mixtures of ammonia gas in the range 5 - 70 ppm showed that the response of the sensor was nonlinear, with the sensitivity increasing at lower concentrations. The measurement of the baseline noise allowed the LOD to be estimated at ~400 ppb. Further development of this sensor could potentially lead to a cheap handheld portable device for the screening of several medical conditions.

8.1. References

[1] Islam, M.; Seetohul, L. N.; Ali, Z. Applied Spectroscopy, 61 (2007) 649.

[2] Fiedler, S. E. Review of scientific instruments, 76 (2005) 1.

[3] Hallock, A. J. Analytical chemistry, 74 (2002) 1741.

[4] Malins, C.; Doyle, A.; MacCraith, B. D.; Kvasnik, F.; Landl, M.; Šimon, P.; Kalvoda, L.; Lukaš, R.; Pufler, K.; Babusík, I. Journal of Environmental Monitoring, 1 (1999) 417.

Appendix A

Macro modules for data sorting (Macro developed with considerable help from Dr Simon Scott)

```
Sub FileOpener(pfilename As String, pcount As Integer)
' FileOpener Macro, Opens data file, copies data in worksheet
Dim pname As String
    Workbooks.OpenText filename:=pfilename _
      , Origin:=437, StartRow:=1, DataType:=xlDelimited, TextQualifier:= _
      xlDoubleQuote, ConsecutiveDelimiter:=False, Tab:=True,
Semicolon:=False, _
      Comma:=False, Space:=False, Other:=False, FieldInfo:=Array(1, 1), _
      TrailingMinusNumbers:=True
   pname = Application.ActiveWorkbook.Name
   Windows("SpectDataRipper.xls").Activate
'   Range("I3:N228").Select
'   Application.CutCopyMode = False
  ' Call SetBackcolour(pname)
   Call copyMacro(pname, "SpectrometerData.xls", pcount)
  ' Call ChartPlotMacro(pname)
   Windows(pname).Activate
'  pname = Replace(pname, ".txt", ".xls")  ' Change file type from text to Excel
'  ChDir "..\Test"
'  ActiveWorkbook.SaveAs Filename:=pname, FileFormat:=xlExcel9795, _
'      Password:="", WriteResPassword:="", ReadOnlyRecommended:=False, _
'      CreateBackup:=False
'   ActiveWorkbook.Close
  Application.CutCopyMode = False
  ActiveWindow.Close SaveChanges:=False
```

```
End Sub
Option Explicit
' Insert and remove custom menu into a workbook
Sub createCustomMenus()
  ' Create Custom Menus in Workbook
  Dim cbc As CommandBarControl
  Set cbc = Application.CommandBars("Worksheet menu
bar").FindControl(Type:=msoControlPopup, Tag:="SimonCustomMenu")
  If Not cbc Is Nothing Then cbc.Delete
  createPopup
End Sub
Sub deleteCustomMenus()
  ' Delete the Custom Menus
  Dim cbc As CommandBarControl
  Set cbc = Application.CommandBars("Worksheet menu
bar").FindControl(Type:=msoControlPopup, Tag:="SimonCustomMenu")
  If Not cbc Is Nothing Then cbc.Delete
End Sub
Sub createPopup()
  ' create a custom popup control on the main menu bar
  Dim cbpop As CommandBarControl
  Dim cbctl As CommandBarControl
  Set cbpop = Application.CommandBars("Worksheet Menu
Bar").Controls.Add(Type:=msoControlPopup, Temporary:=True)
  With cbpop
     .Caption = "&Nitin's Data Manipulation"
     .Tag = "SimonCustomMenu"
     .Visible = True
  End With
  ' Add a menu item (since there is no sub-menu then this is a ControlButton)
  Set cbctl = cbpop.Controls.Add(Type:=msoControlButton, Temporary:=True)
  With cbctl
     .Caption = "Fi&le Chooser"  ' user visible caption
     .Tag = "SimonCustomMenu"   ' internal tag for identification
```

```
    .OnAction = "ChooseDirAndFiles" ' run this macro when clicked
    .Parameter = "ThisWorkbook"  ' to pass this on
    .Visible = True
    .Enabled = True
  End With
  Set cbctl = cbpop.Controls.Add(Type:=msoControlButton, Temporary:=True)
  With cbctl
    .Caption = "About"  ' user visible caption
    .BeginGroup = True  ' put a separator line above this menu item
    .Tag = "SimonCustomMenu"   ' internal tag for identification
    .OnAction = "showAbout" ' run this macro when clicked
    .Parameter = "ThisWorkbook"  ' to pass this on
    .Visible = True
    .Enabled = True
  End With
End Sub
'---------------------------------------------------------------------
'Run this code only once, will create the directory dialog!
Sub dialog_creator()
   DialogSheets.Add
   ActiveSheet.Name = "Directory Switcher"
   Set DLG = DialogSheets("Directory Switcher")
   With DLG.DialogFrame
     .Left = 0
     .Top = 0
     .Caption = "Directory Switcher"
     .Height = 215
     .Width = 202
   End With
   DLG.Labels.Add Top:=25, Left:=20, Width:=160, Height:=15
   With DLG.Labels(1)
     .Name = "Path_String"
     .Caption = CurDir()
   End With
```

```
DLG.Labels.Add Top:=21, Left:=199.5, Width:=160, Height:=33
With DLG.Labels(2)
   .Name = "instructions"
   .Caption = "Double click an entry to select it. " & _
    "Select the ""..."" to ascend one level"
End With
DLG.Buttons.Add Left:=310, Top:=100, Width:=60, Height:=15
Set dfltbtn = DLG.Buttons(3)
With dfltbtn
   .Caption = "Don't click!"
   .OnAction = "GoToIt"
   .DismissButton = False
   .DefaultButton = True
End With
DLG.ListBoxes.Add Left:=20, Top:=45, Width:=160, Height:=100
Set lb = DLG.ListBoxes(1)
lb.Name = "SwitcherLB"
DLG.Buttons.Add Left:=21, Top:=156.75, Width:=157.5, Height:=15.75
Set drvchgr = DLG.Buttons(4)
drvchgr.Caption = "Change Drive"
drvchgr.Name = "Drvchanger"
drvchgr.OnAction = "DrvSwitcher"
Set OKbtn = DLG.DrawingObjects("Button 2")
With OKbtn
  .Left = 21
  .Top = 177.75
  .Name = "OKButton"
  .OnAction = "Dismiss_Click"
End With
Set Cnclbtn = DLG.DrawingObjects("Button 3")
With Cnclbtn
   .Left = 126
   .Top = 177.75
   .Name = "CancelButton"
```

```
      .OnAction = "Dismiss_Click"
   End With
End Sub
Option Explicit
' This module contains the code to run and control
' the dialogs that select the files for processing.
Dim KeepShowing As Boolean
Dim StartDirect As String
Dim DirList As String
Dim ChoiceDir As String
Dim DLG As DialogSheet
Public drv As String * 1
Sub ChooseDirAndFiles()
  ' show the file dialog to run the macro set (everything is run from this dialog)
  dlgFiles.Show
End Sub
Sub showAbout()
 ' show About Dialog
 dlgAbout.Show vbModal
End Sub
' Do not call any of the macros below directly
'---------------------------------------------------------------------
'This procedure runs Directory Dialog (called from the File Dialog)
Sub Master()
   KeepShowing = True
   StartDirect = CurDir()
   ChoiceDir = StartDirect
   InitializeTheList
   Showit
End Sub
Sub InitializeTheList()
   'dimension the object variable for the dialog
   Set DLG = DialogSheets("Directory Switcher")
   'make the label show where you are now
```

```
  DLG.Labels("Path_String").Text = CurDir()
  'clear out the list box on the dialog
  DLG.ListBoxes("SwitcherLB").RemoveAllItems
  'if the chosen directory is the root directory
  If Len(ChoiceDir) = 3 Then
    'this returns only directories to the list
     DirList = Dir(ChoiceDir & "*", vbDirectory) '
  Else
    'append a "\" to the list and then get the directories there
    DirList = Dir(ChoiceDir & "\*", vbDirectory) '
  End If
  'Use a loop to recall the dir function as long as there are
  'directories at this level.
  Do While Len(DirList) > 0
     Select Case DirList
     Case Is = "."
     'doing nothing jumps the code to the end select
     Case Is = ".."
     'doing nothing jumps the code to the end select
     Case Else
     Dim analysis As Integer
     'bitwise comparison analyzes if the file is a directory
     analysis = GetAttr(DirList) And vbDirectory
     'if it IS a directory,
        If analysis > 0 Then
        'jump to the endif statement below
        Else
           'otherwise force the code to the end of the loop
           GoTo endlooper
        End If
     End Select
  'add dirlist to the list
  DLG.ListBoxes("SwitcherLB").AddItem DirList
endlooper:
```

```
    'look for the next file
    DirList = Dir()
    'return to the top of the do loop
    Loop
End Sub
Sub Showit()
    'show the dialog within a loop which repeats until the KeepShowing
    'variable is set to false (see the Dismiss_Click procedure)
    Do While KeepShowing = True
        'if the user clicked OK then
        If DLG.Show = True Then
        'do nothing special
        Else
            'If the user clicked cancel, return the current directory
            'to the one that was there before starting this procedure.
            ChDir (StartDirect)
        End If
      'return to the top of the loop
    Loop
End Sub
Sub GoToIt()
    'This is called by the default button (labeled "Don't click") which
    'is not shown within the dialog frame.
    Dim childtofind As String
    'childtofind holds the value of which choice was made from the list
    childtofind = DLG.ListBoxes(1). _
        List(DLG.ListBoxes(1).ListIndex)
    'if the current directory is the root
    If Len(CurDir()) > 3 Then
        'append a "\" character to it before changing directories
        ChDir (CurDir() & "\" & childtofind)
    Else
        'just concatenate the choice made with the current directory
        'and switch to it
```

```
      ChDir (CurDir() & childtofind)
    End If
    'refresh the value of the choicedir variable for evaluation in the _
    'initializing procedure
    ChoiceDir = CurDir()
    InitializeTheList
End Sub
Sub Dismiss_Click()
    'this is called by the OK and cancel buttons
    KeepShowing = False
End Sub
Sub DrvSwitcher()
    'enable an escape route
    Application.EnableCancelKey = xlInterrupt
    'error handler
    On Error GoTo oops
    'assign value to drv
    drv = Left(InputBox(prompt:="Enter a valid drive letter:", _
    Default:=Left(CurDir(), 1), _
    Title:="Choose another drive"), 1)
    'Check to see if Cancel was pressed
    If Trim(drv) = "" Then Exit Sub
    'change drive to drv. If an error occurs, it will be here
    ChDrive drv
    'update the choicedir variable for evaluation during the
    'initialize the list routine
    ChoiceDir = CurDir() 'this added to debug problem drive switching
    InitializeTheList
    'if no errors encountered, relinquish control to the calling _
    procedure
    Exit Sub
    'In case the drive letter you entered is invalid, this will handle
    'the error
oops:
```

```
    MsgBox "The drive you have entered is invalid." & Chr(13) & _
    "Please enter a valid drive."
    'A second chance
    drv = Left(InputBox(prompt:="Enter a valid drive letter:", _
       Default:=Left(CurDir(), 1), _
       Title:="Choose another drive"), 1)
    'return to the line after where the error occurred (most likely
    'the line above where choicedir is reassigned its value before
    'calling initialize the list)
    Resume Next
End Sub
```